University of Iowa
Iowa Research Online

Theses and Dissertations

Spring 2013

Environmental fate of endocrine disrupting growth promoters used in cattle production

Shen Qu
University of Iowa

ENVIRONMENTAL FATE OF ENDOCRINE DISRUPTING GROWTH

PROMOTERS USED IN CATTLE PRODUCTION

by

Shen Qu

An Abstract

Of a thesis submitted in partial fulfillment of the requirements
for the degree of Doctor of Philosophy in
Civil and Environmental Engineering
in the Graduate College of
The University of Iowa

May 2013

Thesis Supervisor: Professor David M. Cwiertny

ABSTRACT

Trenbolone acetate (TBA), melengestrol acetate (MGA) and zeranol are synthetic growth promoters extensively used in animal husbandry, yet despite occurrence in water and soil little is known about their environmental fate. The work provides some of the first details related to the persistence and mobility of these synthetic growth promoters and their metabolites (SGPM) in natural aquatic systems.

In sunlit surface waters, results suggest that the families of TBA (including 17β-trenbolone, 17α-trenbolone and trendione) and MGA (also melengestrol) will readily undergo direct photolysis with half-lives between ~0.25-1 h in both natural and simulated sunlight. In contrast, zeranol, β-zearalanol and zearalanone only degrade via indirect photolysis pathways mediated by dissolved organic matter. Their transformation is attributable primarily to hydroxyl radical and triplet DOM at neutral pH values, whereas the contribution of singlet oxygen becomes greater in more alkaline waters. An observed pH-dependence for rates of indirect photolysis suggests these photooxidants react primarily with the monodeprotonated form of zeranol, as well as its metabolites.

Given their high rates of direct phototransformation, close attention was paid to elucidating the photoproducts for the TBA family. Generally, all metabolites of TBA photodegrade primarily to a species hydroxylated at the C12 position of the steroid ring. While this 12-hydroxy trenbolone species is photostable, it can hydrolyzes to di- and tri-hydroxy products. Most notably, however, it is also prone to dehydration, which results in the regeneration of the TBA metabolite from which it was derived. This dehydration pathway can be acid- and base-catalyzed, but it also occurs to an appreciable extent at neutral pH. It is also temperature dependent, with greatest rates of parent metabolite regeneration at higher temperature. Consequently, the rapid rate of photolysis for TBA metabolites observed in daylight is followed by photoproduct-to-parent reversion mechanism in the dark indicating they will be far more persistent than currently realized.

In soil systems, all SGPMs exhibit a high affinity for organic rich soil (e.g., peat), consistent with an important role for hydrophobic interactions in governing their uptake. However, the extent and reversibility of sorption in such systems is not predictable from common metrics for compound hydrophobicity (e.g., octanol-water partitioning coefficients), suggesting that specific chemical interactions also influence uptake. In model soils systems with lower organic carbon content (1-6% w/w), sorption occurs in parallel with transformation reactions that are mediated by the inorganic phases present. In suspensions of model metal oxides (e.g., SiO_2, MnO_2 and the iron oxide ferrihydrite), SGPM decay is observed, presumably from either hydrolysis or oxidation, although reaction products were not identifiable. Thus, in soil systems, especially those with moderate to low organic carbon content, most SGPMs will primarily undergo transformation rather than sorption.

Results from this work can be used to more accurately predict the fate of synthetic steroid growth promoters in agriculturally impacted water and soil. This information will be critical for assessing the totality of the risks posed to ecosystem health by this emerging pollutant class.

Abstract Approved: _____

Thesis Supervisor

_____

Title and Department

_____

Date

ENVIRONMENTAL FATE OF ENDOCRINE DISRUPTING GROWTH

PROMOTERS USED IN CATTLE PRODUCTION

by

Shen Qu

A thesis submitted in partial fulfillment of the requirements
for degree of Doctor of Philosophy in
Civil and Environmental Engineering
in the Graduate College of
The University of Iowa

May 2013

Thesis Supervisor: Professor David M. Cwiertny

Graduate College
The University of Iowa
Iowa City, Iowa

CERTIFICATE OF APPROVAL

_____

PH.D. THESIS

_____

This is to certify that the Ph.D. thesis of

Shen Qu

has been approved by the Examining Committee
for the thesis requirement for the Ph.D. degree in Civil and Environmental
Engineering at the May 2013 graduation.

Thesis Committee: _____
                        David M. Cwiertny, Thesis Supervisor

                   _____
                        Dana W. Kolpin

                   _____
                        Nandita Basu

                   _____
                        Gene F.Parkin

                   _____
                        Keri C. Hornbuckle

This dissertation is dedicated to my dearest grandmother, Xingyu Li, grandfather, Zhenji Zuo, my mother, Huifen Zuo, my father, Bo Qu and my husband, Cong Zhou. Thank you for all of your love, support, and sacrifice throughout my life.

兹将本论文献给我最亲爱的姥姥李兴玉，姥爷左振基，母亲左惠芬，父亲曲波和爱人周聪。感谢你们给予我的爱，支持与奉献。

ACKNOWLEDGMENTS

It has been a long journey for me to finish my PhD thesis. I first started in the lab at the University of California, Riverside and transferred with my advisor to the University of Iowa. I got a challenging project and have been through a lot of difficult but interesting questions. I am lucky that I obtained help from a lot of people. One of the joys of completion is to thank all the friends and family who have helped and supported me along this long but fulfilling road.

I would like to express my sincere gratitude to my advisor, Dr. David M. Cwiertny, without whose support the completion of this PhD dissertation would be impossible. He is always smart on explaining the results from my experiments and leads me to the right direction to answer the research questions. Although we are among the first to study a new group of emerging contaminants, which results in a lot of unexpected problems, he always motivates me and guides me to find the right way. He not only tells me how to do things but enlightens me to think and solve the problems by myself which allows me to enhance my skills on solving problems as a scientist. Moreover, he also taught me a lot on how to present my scientific results which allowed me to improve my skills on interpreting and presenting data.

Some professors have been very kind enough to extend their help at various phases of this research, and I do hereby acknowledge all of them. I would like to thank our collaborator, Dr. Edward P. Kolodziej at the University of Nevada, Reno, for his valuable contribution on this project, especially on the products analysis. I also want to thank Dr. Douglas Latch at Seattle University for his insightful opinions on photolysis, Dr. Daniel Schlenk at University of California, Riverside for contribution on toxicity study, Dr. James B. Gloer at University of Iowa for NMR analysis and Dr. Jonas Baltrusaitis at University of Iowa for computational analysis on products.

I am also thankful to my thesis committees, Dr. Sharon Walker, Dr. Mark R. Matsumoto, Dr. Jay Gan and Dr. Wilfred Chen at University of California, Riverside and Dr. Keri C. Hornbuckle, Dr. Gene F. Parkin, Dr. Dana W. Kolpin and Dr. Nandita Basu at University of Iowa. My committee at UC Riverside gave me a lot of valuable ideas and suggestions when I defended my thesis proposal. The insightful opinions and questions from my committee at University of Iowa helped me to improve my final thesis.

I appreciate the help, discussion and encouragement from my colleagues, also my friends, Dr. Yang Xie, Caylyn Lanzl, Rebekah Oulton, Edgard Verdugo and Dr. Danmeng Shuai. We share the accomplishment and bitter of our research. And thank you for their coordination on use of the instruments. I also got a lot of help from my friends in both UC Riverside and University of Iowa. I would like to thank Jacob Lanphere, Ying Han, Yi Liang, Matthew D. Tarnoff, Dr. Yue Wang, Dr. Liyan Jin for their help on my research work and encouragement on my PhD life.

I would like to take this opportunity to thank all the great staff members who help me a lot at both UC Riverside and University of Iowa. I also appreciate the funding source from USDA Agriculture Food Research Initiative (AFRI) Water and Watersheds grant (#2010-65102-20425) to support all my research.

Most importantly, I would like to thank my family for their endless support and encouragement. My mother, Huifen Zuo and my father Bo Qu always encourage me to face the hurdles in both my research work and daily life. Without their unconditional support it would be impossible for me to come to the United States to pursue my PhD degree. Last but not least, I would like to thank my husband, Cong Zhou. We met at the beginning of my PhD life, he accompanied me all the way through my 5 years PhD. I share my happiness and bitter with him and he was always supportive.

ABSTRACT

Trenbolone acetate (TBA), melengestrol acetate (MGA) and zeranol are synthetic growth promoters extensively used in animal husbandry, yet despite occurrence in water and soil little is known about their environmental fate. The work provides some of the first details related to the persistence and mobility of these synthetic growth promoters and their metabolites (SGPM) in natural aquatic systems. Here, laboratory experimental studies explore their tendency to undergo phototransformation in surface waters and their interaction with soil via sorption or mineral-promoted reactions.

In sunlit surface waters, results suggest that the families of TBA (including 17β-trenbolone, 17α-trenbolone and trendione) and MGA (including melengestrol) will readily undergo direct photolysis. They exhibit half-lives between ~0.25-1 h in both natural and simulated sunlight that were largely insensitive to environmental variables (e.g., temperature, pH and cosolutes). In contrast, zeranol, β-zearalanol and zearalanone only degrade via indirect photolysis pathways mediated by dissolved organic matter. Their transformation is attributable primarily to hydroxyl radical and triplet DOM at neutral pH values, whereas the contribution of singlet oxygen becomes greater in more alkaline waters. An observed pH-dependence for rates of indirect photolysis suggests these photooxidants react primarily with the monodeprotonated form of zeranol, as well as its metabolites.

Given their high rates of direct phototransformation, close attention was paid to elucidating the photoproducts for the TBA family. Generally, all metabolites of TBA photodegrade primarily to a species hydroxylated at the C12 position of the steroid ring. While this 12-hydroxy trenbolone species is photostable, it can hydrolyzes to di- and tri-hydroxy products. Most notably, however, it is also prone to dehydration, which results in the regeneration of the TBA metabolite from which it was derived. This dehydration pathway can be acid- and base-catalyzed, but it also occurs to an appreciable extent at

neutral pH. It is also temperature dependent, with greatest rates of parent metabolite regeneration at higher temperature. Consequently, the rapid rate of photolysis for TBA metabolites observed in daylight is followed by photoproduct-to-parent reversion mechanism in the dark. This phenomenon has broad and important implications for the fate of TBA metabolites in surface waters. Generally, they will be far more persistent than currently realized, and their concentration will exhibit, pH, diurnal and seasonal dependencies.

In soil systems, all SGPMs exhibit a high affinity for organic rich soil (e.g., peat), consistent with an important role for hydrophobic interactions in governing their uptake. However, the extent and reversibility of sorption in such systems is not predictable from common metrics for compound hydrophobicity (e.g., octanol-water partitioning coefficients), suggesting that specific chemical interactions also influence uptake. In model soils systems with lower organic carbon content (1-6% w/w), sorption occurs in parallel with transformation reactions that are mediated by the inorganic phases present. In suspensions of model metal oxides (e.g., SiO_2, MnO_2 and the iron oxide ferrihydrite), SGPM decay is observed, presumably from either hydrolysis or oxidation, although reaction products were not identifiable. Thus, in soil systems, especially those with moderate to low organic carbon content, most SGPMs will primarily undergo transformation rather than sorption.

Results from this work can be used to more accurately predict the fate of synthetic steroid growth promoters in agriculturally impacted water and soil. This information will be critical for assessing the totality of the risks posed to ecosystem health by this emerging pollutant class.

TABLE OF CONTENTS

LIST OF TABLES

LIST OF FIGURES

Figure

CHAPTER I. INTRODUCTION

1.1   Sources, occurrence and impact of hormones

in natural waters

In recent years, improved methods of analysis have led to the discovery of a new generation of pollutants in surface waters. These include pharmaceuticals, personal care products and hormones [1-4]. In particular, the presence of hormones has attracted much attention due to potential risks associated with their biological activity. Most sex hormones are steroids, which share a characteristic base structure of a four-ring network consisting of three cyclohexane rings and one cyclopentane ring [5]. Steroids are further subdivided based upon their function. Estrogens, such as 17β-estradiol (Figure 1-1), are the main sex hormones in women, and an essential part of a woman's reproductive process [6, 7]. Androgens including testosterone (Figure 1-1) stimulate or control the development and maintenance of masculine characteristics in vertebrates [6, 7]. Progestins such as progesterone (Figure 1-1) affect progestational activity and are involved in the female menstrual cycle [6, 7]. Besides the naturally produced hormones such as those mentioned above, synthetic hormones also exist, such

17β-estradiol   Testosterone   Progesterone   17α-Ethinyl
                                                                 estradiol
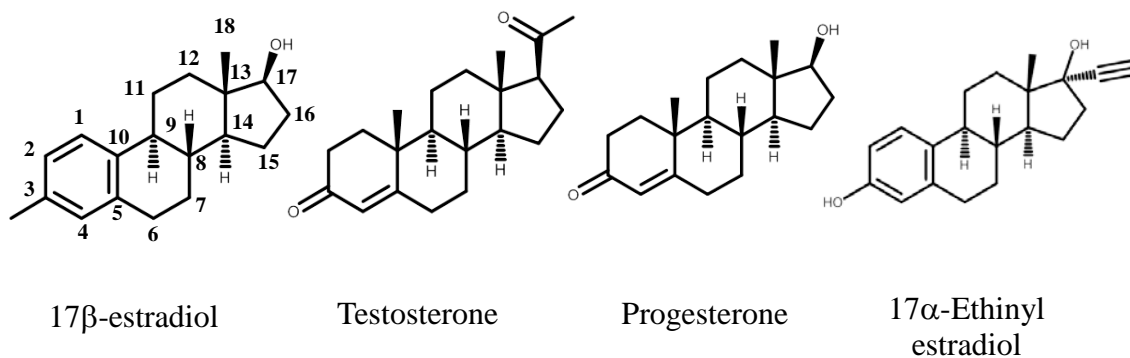
Figure 1-1. Structures of several steroidal hormones

as 17α-ethinylestradiol (EE2), a synthetic estrogen that is the active agent in the birth control pill.

In terms of environmental occurrence, estrogenic hormones are a great concern because they are among the most frequently detected in natural waters, with typical concentrations ranging from 10 to several hundreds of ng/L [4, 8]. In a noteworthy nation-wide survey, water samples were taken from 139 streams across 30 states between 1999 and 2000. Several natural hormones including 17α-and 17β-estradiol were detected with maximum concentrations of 0.16 and 0.019 µg/L, respectively [4]. It is commonly believed that a major source of many of these emerging micropollutants (also referred to as chemicals of emerging concern (CECs)) is effluent from municipal wastewater operations [9-15]. Hormones are naturally produced and excreted in waste by humans and animals, while synthetic hormones including ethinyl estradiol (EE2) are often prescribed for medicinal purposes and subsequently excreted after metabolism. Accordingly, these species are expected to be present in sewage and wastewater treatment plant influent, and if not removed during these processes will enter into the environment as effluent discharge.

Another important source of hormones is animal agriculture operations [12, 16, 17]. Rivers receiving effluents from cattle feedlots have been found to contain sufficient levels of hormonally active agents, which include both hormones naturally produced by cattle as well as agents dosed to animals to promote growth and meat production. Over 4 tons of total androgens were estimated to be excreted into the environment by cattle, pigs, sheep and chickens in 2000 alone [18]. These hormones of agricultural origin can enter the surface and groundwater via runoff from feedlots waste and through the application of animal wastes (manure and urine) to soils as fertilizers [12, 16, 17].

Growing concern over hormones in the environment is linked to their potential to induce a variety of adverse health effects in aquatic organisms and human bodies exposed to these compounds. Interest in the ability of steroid hormones to impact water quality

and ecosystem health began in the 1990s when scientists in the United Kingdom reported the presence of feminized male fish in wastewater-impacted rivers [19-21]. Most hormones are recognized endocrine disrupting compounds (EDCs), which are defined as species that can interact with and alter the physiological function of the endocrine system in living organisms [7]. Numerous reports of endocrine disruption in aquatic organisms exposed to municipal wastewater effluent and agriculture runoff indicate that steroidal hormones can have substantial and detrimental impacts on ecosystem health [12, 19, 20, 22-27]. Most notably, exposure to natural and synthetic estrogens has been shown to alter the reproductive potential of some wild fish populations [19]. Harries et al. placed male trout at various distances downstream of an effluent entry point to serve as biomarkers of estrogen exposure in rivers in the United Kingdom. They found that the male trout placed near the effluent entry showed female characteristics, suggesting that effluents of sewage treatment works are estrogenic to fish [20]. Although this result may be caused by estrogen-mimicking chemicals, it is also possible the observations were induced by natural and synthetic estrogens in the discharge.

It is also important to note that exposure to even low concentrations of steroids can be very significant. Kidd et al. dosed an entire lake with 5 ng/L of the synthetic estrogen ethinyl estradiol (EE2) and subsequently observed widespread disruption in reproductive output and fecundity in fathead minnows [23]. In fact, the fathead minnow population was driven to extinction over a 3 year exposure period due to the reproductive failures which indicated a severe adverse impact of steroid exposure on fecundity. Therefore, endocrine disruption due to steroid exposure has the potential to substantially reduce or even eliminate populations of sensitive species because the steroids decrease the ability of these populations to replace themselves.

1.2   Use of growth promoters in animal agriculture

Several steroidal hormones are used currently as growth promoters in animal husbandry in the U.S. for the sake of meat production. These growth promoters improve feed efficiency, rates of weight gain and relative proportions of muscle and fat [7, 12]. In animal agriculture, hormones produced naturally by the animal are referred to as "endogenous" hormones, whereas additional "exogenous" hormones, which can be either natural or synthetic in nature, are administered via ear implants. Indeed, nearly all cattle used for meat production receive exogenous hormones as growth promoters at low dose levels through pellets implanted in their ears [26, 28]. Balter, for example, estimated that ~90-97% of beef cattle in the U.S. are implanted with exogenous, steroids, most of which are synthetic steroids [29].

The U.S. Food and Drug Administration (USFDA) has approved three synthetic hormones for growth promotion in cattle and sheep raised for meat production [30, 31]. These are zeranol (commercially available in Zeraplix), a resorcyl lactone that is a non-steroidal estrogen, trenbolone acetate (TBA) (commercially available in Revalor), an androgenic steroid, and the progestin melengestrol acetate (MGA) (commercially available in Heifermax500)(see Figure 1-2) [30]. Their relatively high intravenously administered doses are 36-72 mg/implant, 140-200 mg/implant and 0.5 mg/day for zeranol, trenbolone acetate and melengestrol acetate, respectively [12, 28]. Once applied to animals, some of these growth promoters can be excreted unmetabolized, although most mass is excreted as various metabolites. In studies with heifers using radiolabeled TBA, 80% of the intravenously administered dose (based on radioactivity) was excreted in bile within 24 h, but all was metabolized; 17α-trenbolone (17α-TBOH; 33% of excreted radioactivity) was the dominant metabolite, while 17β-trenbolone (17 β - TBOH; 0.9%) and trendione (1.2%) appeared in smaller quantities [32]. For MGA, about 10-17% of the administered dose was excreted in feces unmetabolized [33], where

once in the environment it may hydrolyze at slightly basic pH (~8 or 9) to melengestrol [34]. Zeranol (25 mg/d) dosed to heifers yielded 2-5 µg/L of unmetabolized zeranol in urine, with β-zearalanol (2-5 µg/L) and zearalanone (0.1-0.5 µg/L) metabolites also observed [35]. The three synthetic growth promoters and their major biological metabolites described above will be heretofore referred to as SGPMs.

1.3   Environmental occurrence and

associated risks of SGPMs

The three growth promoters mentioned above, as well as their major metabolites, have been frequently detected in surface waters and soil near animal agriculture operations on the order of 10-100 ng/L and 1-100 ng/g level, respectively [16, 17, 24, 36-38]. Durhan et al. detected 17α- and 17β-TBOH at concentrations ranging between 10-120 ng/L near a cattle feedlot discharge point in Ohio [37]. The 17α- and 17β-TBOH were detected in 6 samples and 2 samples, respectively, in a total of 9 samples from discharge sites. TBA metabolites were detected at 1.7 ng/g in liquid manure and 5-75 ng/g in solid manure while MGA was detected at 0.3-8 ng/g in solid manure [17]. Bartlet-Hunt et al. also detected up to 55 ± 22 ng/g 17α-TBOH and 65 ± 0.4 ng/g MGA in fresh manure and feedlot surface soils[36]. Kolok et al. investigated the presence of several natural and synthetic steroids in the Elkhorn River of Nebraska, with MGA being detected at all six sampling sites at detectable concentration. Zeranol has been observed at ng/L levels in water bodies impacted by sewage discharges [24, 38].

The detection of these compounds in natural waters and soil raises concern over potential health risks. 17β-TBOH and 17α-TBOH are potent androgens in fish and mammals even at ng/L level [37, 39]. In particular, 17β-TBOH is a known reproductive toxicant in fish; tests have shown significant reductions on fecundity of fathead minnow due to exposure to 17β-TBOH at concentration larger than 27 ng/L [22]. Moreover,
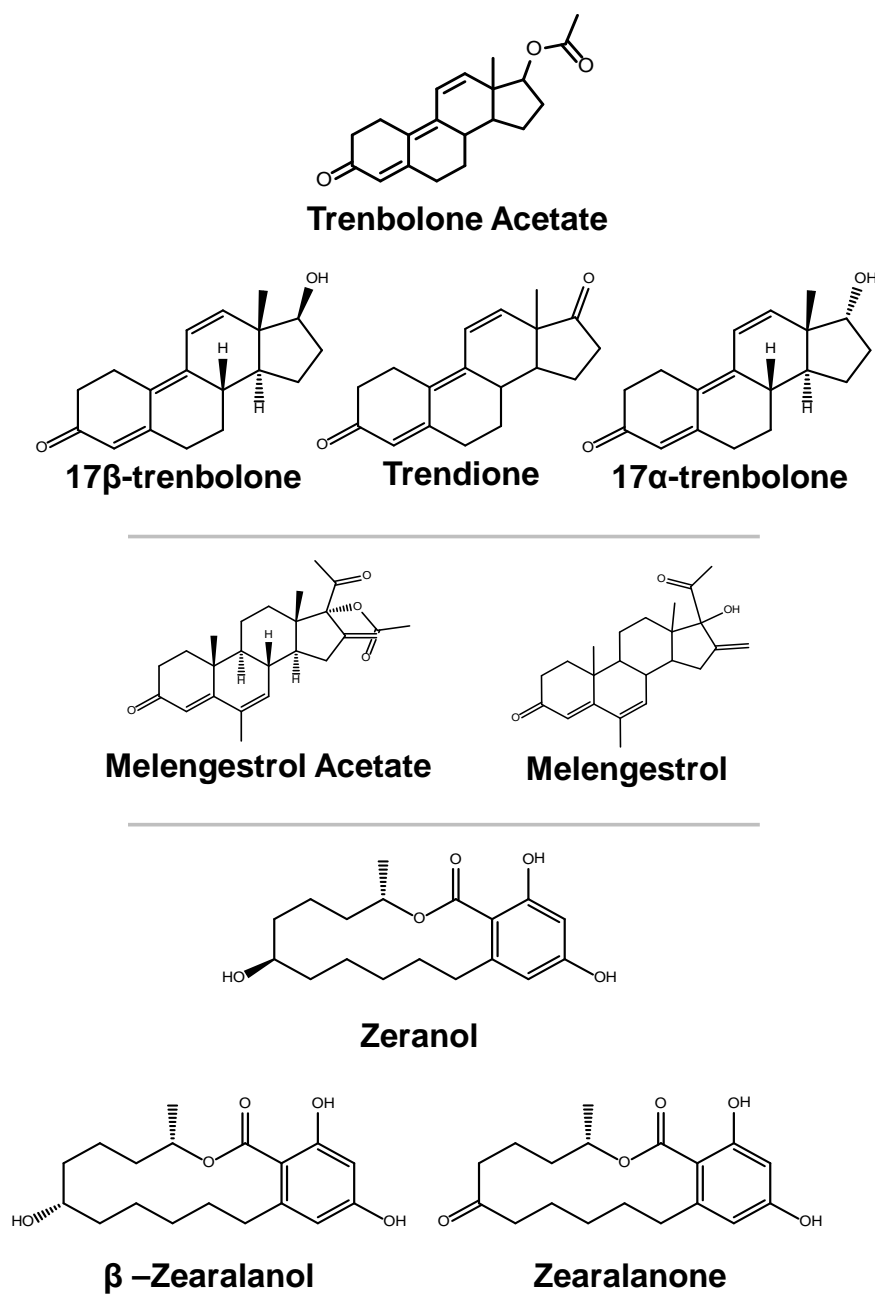
Figure 1-2. Structures of synthetic growth promoters and their metabolites (SGPMs) considered herein.

affinity of 17β-TBOH and 17α-TBOH for the human androgen receptor has also been reported [40]. Similarly, MGA is toxic to fish even at ng/L level [24], and potentially hazardous to humans at a dose of 0.7 mg due to its adverse effect on female physiological functions [41]. Estrogenic zeranol has raised concerns over the potential risks to human health because exposure to excess estrogen may be linked to human breast and uterine cancer [30].

Because environmental exposure to very low levels of SGPMs has been linked to significant adverse health effects in aquatic organisms [22], the mass of SGPMs implanted in a single animal potentially can affect a large volume of receiving water. For example, about 200 mg of TBA is contained in cattle ear implants, which will form about 170 mg of active 17β-TBOH *in vivo* [28]. Although the fraction of TBA excreted in animals varies, an estimate of 10% excretion yields a concentration of 28 ng/L of 17β-TBOH in 600,000 L of receiving water, neglecting degradation and sorption. Thus, implantation of one cow has the potential to produce harmful levels of 17β -TBOH in over a half of a million liters of water.

1.4   Current understanding of growth
promoter environmental fate

The presence and adverse effects on ecosystem of selected SGPMs are certain but their fate and transport in the natural environment is poorly understood. There are several possible natural attenuation processes for SGPMs. In addition to dilution in SGPM-free natural water, environmental processes such as photolysis, biodegradation, sorption and abiotic chemical transformations are likely to significantly reduce SGPM concentrations. Possible pathways of SGPMs attenuation in the natural environment are illustrated in Figure 1-3. This research focuses on the photolysis, sorption and abiotic chemical transformation of SGPMs. Current research and important data gaps associated with each of these processes are summarized below:
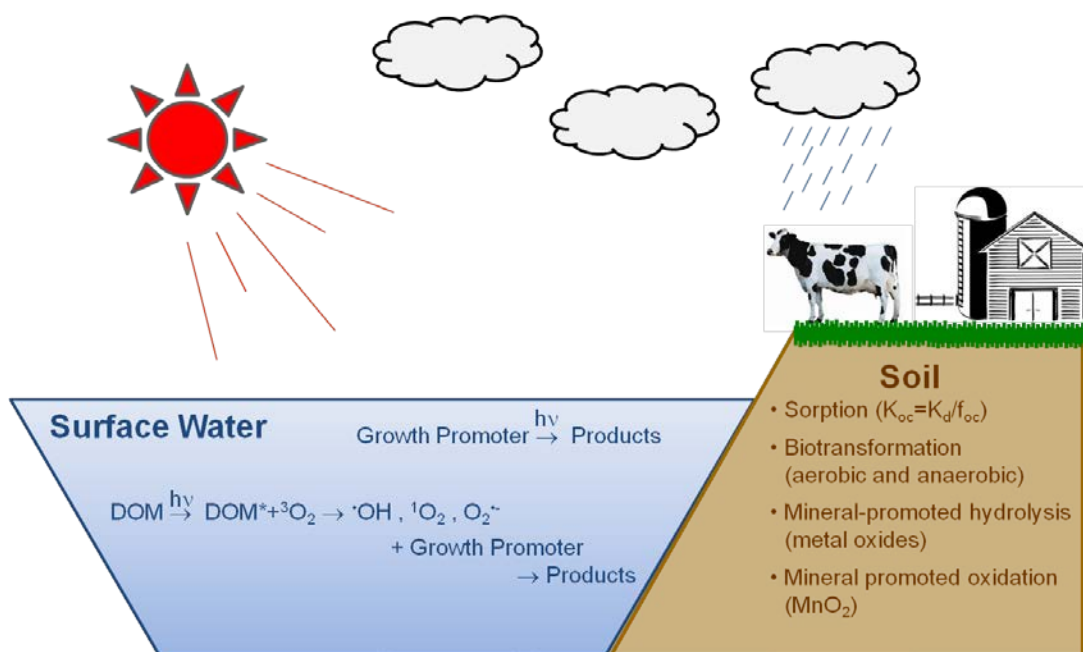
Figure 1-3. Potential environmental pathways of SGPMs

Photodegradation

Photodegradation, or photolysis, can occur by two pathways referred to as direct and indirect photolysis [42]. In direct photolysis, molecules directly absorb light energy causing bond cleavage or rearrangement. In indirect photolysis, light is absorbed by a chromophore such as dissolved organic matter (DOM), which then transfers the light energy to another species. When O_2 is the species receiving the energy, as is often the case in most aerobic environments such as surface waters, reactive oxygen species (ROS) are produced. Common ROS in natural waters include hydroxyl radical ($^\bullet OH$), singlet oxygen ($^1O_2$), superoxide ($O_2^{\bullet-}$) and hydrogen peroxide (H_2O_2). After their production, these highly reactive photooxidants can react with a range of organic micropollutants in water and lead to chemical transformation [42]. It is also recognized that triplet excited

states of dissolved organic matter (^{3}DOM*) can function as photooxidants by reacting directly with micropollutants rather than with O_2 [43].

For SGPMs photolysis, little information is available regarding reaction rates and products, as well as key environmental variables that influence this process. Van der Merwe and Pieterse indicated that the concentration of 17β-TBOH in bovine urine decreased over 2 days exposure to sunlight whereas the concentrations of zeranol did not change [44]. However, they only studied these two SGPMs in urine, and no data were obtained in water. Most information regarding SGPM photolysis in aquatic systems comes from the manufacture's environmental assessment reports [34, 45, 46]. The photodegradation of 17α-TBOH, TBA and MGA were investigated in quartz tubes with exposure to sunlight by their manufacturers. They were all susceptible to direct photolysis with half-lives of several hours. TBA exhibited a half-life of 1.1-2.5 h which was fairly stable between pH 5-9, whereas 17α-TBOH exhibited half-lives of 12.6 h, 3.1 h and 3.3 h and pH 5, 7 and 9, respectively. As 17α-TBOH has no ionizable functional groups, such that the longer half-life at pH 5 was attributed to cloudy weather and limited sunlight in the pH 5 experiments [34, 46]. In another study, 17β-TBOH was found to be degraded with exposure to single 254 nm UV light but no data were reported with respect to sunlight [47]. These reports are limited, however, in that they are generally restricted to parent compound only, and information related to metabolites and the identity of transformation products remains unknown. Furthermore, these studies only consider direct photolysis, whereas indirect photolysis, which can also be important in natural waters, was ignored.

Based on the structures of SGPMs and the limited amount of previous photolysis data, metabolites of TBA and MGA are expected to readily undergo both direct photolysis due to the presence of their conjugated π-bond systems. Notably, we expect the 4,9,11-triene structure to make the trenbolone family of compounds to be especially prone to direct phototransformation. On the other hand, indirect photolysis pathways can

reasonably be expected to dominate for zeranol and its metabolites. The zeranol family possesses aromatic moieties that will exhibit absorption maxima outside the solar spectrum, resulting in photostability consistent with the earlier report of Van der Merwe and Pieterse [44]. However, the phenolic moieties present in zeranol should be reactivity toward most ROS as well as triplet excited state DOM.

Sorption and Abiotic Soil Processes

Early studies on SGPM sorption were primarily limited to select species (e.g., MGA and 17β-TBOH), generally neglected sorption tendencies of major metabolites, and often failed to clearly differentiate between sorption and biodegradation. For example, Schiffer et al. [48] used a column study with aggregated soil materials to examine the transport of 17β-TBOH and MGA. They found that although column breakthrough was fast, only small amounts of 17β-TBOH and MGA were detected in the column effluent. They interpreted this observation as evidence for both compounds exhibiting very high affinity for soil organic matter present in their column, with high levels of retardation in the upper portion of the soil column. They concluded that in natural systems, the retardation for these compounds would be high and result in low mobility in subsurface environments [48]. A major shortcoming of this work, however, was that the potential for biodegradation was not considered. Thus, loss of 17β-TBOH and MGA could have been attributed to either irreversible uptake onto soil organic matter (presumably via hydrophobic interactions) or via biologically mediated transformation. Similarly, a study by Lee et al. reported values of $\log K_{oc}$ for 17β-TBOH [12], where K_{oc} is the standard soil-water partitioning coefficient, K_d, normalized to the soil organic matter content [42]. Again, no attempt was made to control biodegradation in their sorption studies, thereby limiting the value of their reported partitioning coefficient.

More recently, efforts have been made to better address the possible contribution of biotransformation such that metrics of SGPM sorption could be more accurately

measured. For example, Khan et al. explored the sorption isotherms of 17α-TBOH, 17β-TBOH and TBO on 5 autoclaved-sterilized soils with organic carbon content ranging from 0.48%-7.5%. They observed linear isotherms for all three compounds on the 5 soils with the distribution coefficient (K_d) proportional to soil organic carbon content [49]. So the author suggested that the hydrophobic interaction was the dominant force driving the uptake of the three trenbolone compounds, although other interactions such as H-bonding involving the phenol or ketone groups may also contribute to the sorption of some hormones given the poor correlation between logKow and K_d values [49]. A similar trend for sorption was also observed in another recent study. Card et al. developed sorption isotherms of several endocrine disrupting compounds including 17α-TBOH, 17β-TBOH, TBO, MGA and zeranol with three agriculture soils with organic matter contents ranging from 1.1%-7.7% (by mass) [50]. They reported logK_{oc} and K_{ow} values measured experimentally, as well as sorption isotherms collected on each model soil. To account for possible biotransformation, these studies employed autoclaving for soil sterilization, and also constructed sorption isotherms based on the mass of SGPM recovered via extraction of equilibrated soils with organic solvents (e.g., methanol). Using this approach, they found that sorption isotherms were generally linear for most solute-soil combinations and that K_d values were well correlated with the soil organic carbon content (i.e., %OC), similar to the correlation that was also previously reported for 17α-TBOH, 17β-TBOH and TBO by Khan et al. [49].

Nevertheless, questions still remain about some fundamental aspects of SGPM partitioning in soil systems. While the work of Card et al. and Khan et al. proposed that hydrophobic interactions were primarily responsible for uptake, other results from the same laboratory [51], which considered the uptake of 17α-TBOH,17β-TBOH and TBO onto humic acids, proposed a different driving force for adsorption. Specifically, Qiao et al. suggested that specific interactions rather than hydrophobic partitioning (as would be expected for correlations with soil organic carbon content) dictated sorption [51]. Thus,

questions persist as to what characteristics of the SGPM and soil are truly most critical for sorption. Another factor yet to be addressed is that nearly all prior studies with SGPMs [48-50, 52, 53] have failed to consider whether sorption is reversible. This detail is necessary for predicting the extent to which sorption will affect SGPM mobility as they are transported through soil systems.

A final factor that has yet to merit any research focus is the possibility that inorganic phases present in soil may also influence the fate of SGPMs. While inorganic mineral phases could potentially function as sorbents, particularly when electrostatic interactions or surface complexation are important routes for uptake, they may also be able to promote various transformation reactions. For example, melengestrol acetate and the zeranol family of compounds have hydrolyzable ester functionalities. Also, resonance resulting from 4,9,11-triene structure in the trenbolone family of compounds yields several carbon centers that are electron deficient and may also be prone to attack by nucleophiles under certain conditions. Although hydrolysis is reported to be slow at near-neutral pH values for these compounds [34, 45, 46], metal oxides commonly found in soil are known to catalyze hydrolysis reactions via the formation of surface complexes that are more prone to attack by H_2O or OH^- than the freely dissolved molecule. In addition to hydrolysis, manganese and iron oxides minerals can also oxidize a wide range of organic compounds including species such as estrone, 17β-estradiol and estradiol, which have similar structure moieties to SGPMs [54, 55]. Currently, however, studies have yet to consider a role for metal catalyzed hydrolysis and oxidation for SGPMs, and thus such pathways merit consideration.

1.5   Overview and Thesis Organization

The overall objective of this research is to determine the environmental persistence of SGPMs used in animal agriculture. We propose that a thorough understanding of the dominant natural sinks for SGPMs, as well as an appreciation for

the associated reaction mechanisms and end products, will allow us to better predict their lifetime in aquatic environments and assess the risks they pose to ecosystem and human health. From current research, we lack reliable data regarding such processes thereby limiting our understanding of their environmental persistence and impact.

This work contains three chapters of original research investigating the fate of SGPMs in natural environment. We hypothesize that based on their structures and chemical properties, SGPMs will undergo a variety of natural attenuation processes including transformation via direct and indirect photolysis, sorption to soil organic matter, and mineral-promoted hydrolysis and oxidation. These processes are explored in the subsequent chapters.

The work in Chapter 2 aims to evaluate the rates and mechanistic pathways for the photolysis of SGPMs in sunlit surface water, and the impact of common aquatic chemical variables (e.g., temperature, pH and co-solutes) on these processes. Specifically, we consider the direct photolysis of trenbolone and MGA family compounds, which we identify as the major phototransformation pathway for these species, and indirect photolysis of zeranol and its metabolites. Zeranol indirect photolysis is investigated in systems with several model humic and fulvic acids as representative organic matter present in surface water, and the specific photogenerated oxidants responsible for transformation are explored through the use of selective photochemical probe and quencher compounds. Also in Chapter 2, we provide a preliminary assessment of the photoproducts generated from the direct photolysis of compounds from the TBA and MGA families, and these products are further elaborated on in Appendix A.

Chapter 3 explores the long-term stability of photoproducts generated via the direct photolysis of TBA metabolites and presents a unique and potentially transformative result with implications for the long-term persistence of these species in surface waters. We show that the dominant phototransformation product for 17β-TBOH, 17α-TBOH and TBO is a hydroxylated species at the C12 position (position number

labeled in Figure 1-1). This 12-hydroxy variant of trenbolone was found to be unstable, and prone to dehydration, resulting in the regeneration of the parent species from which was derived. In essence, we show that the direct photolysis of TBA metabolites is largely reversible, resulting in clear light-dark (e.g, day-night) cycling in the persistence of the metabolite. Environmental factors controlling the rate of this dehydration reaction responsible for the regeneration of parent metabolite, most notably pH and temperature, are also explored and the environmental implications of this result are discussed.

Chapter 4 aims to determine the timescale as well as the extent for SGPMs sorption on soils and identify the soil components (e.g., inorganic mineral phases or organic matter) responsible for SGPM soil-water partitioning. Several model soils with a range of soil organic carbon content were used to investigate the correlation between SGPMs sorption and organic matter, and thus address the relative importance of hydrophobic interactions in governing the soil-water partitioning within and across families of SGPMs. As interactions between SGPMs and inorganic phases in soils has merited essentially no prior attention in the literature despite the high probably of surface promoted hydrolysis and redox reactions, Chapter 4 also focuses on the fate of SGPMs in suspensions of selected metal oxides (the iron oxide ferrihydrite, SiO_2 and MnO_2) that are naturally abundant in soil. Collectively, results from Chapter 4 help to establish the relative importance of hydrophobic partitioning into soil organic matter and inorganic mineral promoted transformation reactions when considering the fate of SGPMs in aqueous subsurface systems.

1.6   Expected Outcomes

Results from this work will provide quantitative rate information that can be used to predict the half-lives of SGPMs in aquatic and soil environments. Companion work conducted in collaboration at the University of Nevada, Reno will determine the rates and extent of aerobic and anaerobic biodegradation of SGPMs, thus providing a complete

understanding of their environmental fate due to both biotic and abiotic processes. Emphasis in all experiments has been placed on determining the relative stability of parent compounds relative to their dominant metabolites, as well as identifying major products of all transformation reactions. This focus will help us better predict which forms of these compounds are most likely to persist in aquatic environments, and thereby guide future toxicological investigations as to their impact on ecosystem and human health. We expect to obtain a comprehensive, quantitative understanding for the fate and transport of SGPMs in natural aquatic and soil environments. The direct and indirect photolysis rates, mechanistic pathways, and photolysis end products can help us develop an improved model for predicting SGPM persistence in surface waters impacted by agricultural run-off. From the sorption studies, partitioning coefficients for each SGPM can be used to predict the mobility of SGPMs in soil and subsurface systems. To date, mineral-catalyzed hydrolysis and surface-mediated oxidation of SGPMs has yet to be documented. The results from abiotic transformation will be the first to show the importance of such pathways in controlling SGPM persistence in soils. Collectively, the outcomes of this project will help to better predict the fate and transport of SGPMs in the natural environment and better assess the risks these emerging contaminants pose on ecosystem health.

CHAPTER II. PHOTOTRANSFORMATION RATES AND

MECHANISMS FOR SYNTHETIC HORMONE GROWTH

PROMOTERS USED IN ANIMAL AGRICULTURE[1]

2.1 Abstract[1]

Trenbolone acetate, melengestrol acetate, and zeranol are synthetic hormones extensively used as growth promoters in animal agriculture, yet despite occurrence in water and soil little is known about their environmental fate. Here, we establish the time scales and mechanisms by which these synthetic growth promoters and their metabolites (SGPMs) undergo phototransformation in sunlit surface waters. The families of trenbolone acetate (including 17β-trenbolone, 17α-trenbolone and trendione) and melengestrol acetate (including melengestrol) readily undergo direct photolysis, exhibiting half-lives between ~0.25-1 h in both natural and simulated sunlight that were largely insensitive to solution variables (e.g., pH, temperature and cosolutes). Direct photolysis yielded products that not only are more photostable but also maintain their steroidal ring structure and therefore may retain some biological activity. In contrast, zeranol, β-zearalanol and zearalanone only exhibited reactivity in irradiated solutions of model humic and fulvic acids as well as nitrate, and rates of indirect photolysis increased steadily from pH 7 to 9. Use of selective probe and quencher compounds suggest hydroxyl radical and triplet state dissolved organic matter are responsible for zeranol family decay at neutral pH, although singlet oxygen contributes modestly in more alkaline waters. This observed pH-dependence appears to result from photooxidants reacting primarily with the monodeprotonated form of zeranol (pKa values of 8.44 and 11.42). This investigation provides the first characterization of the fate of this emerging

---

pollutant class in sunlit surface waters, and prioritizes future efforts on the identity, fate
and biological impact of their more persistent phototransformation products.

2.2   Introduction

Growth promoters are used extensively in animal agriculture to improve feed
efficiency, weight gain, and muscle-to-fat ratio [12, 31, 56, 57]. They include natural and
synthetic hormones, and it is estimated that over 97% of U.S. beef cattle receive such
supplements [29]. A particularly potent subset of growth promoters are the anabolic
synthetic hormones, of which the U.S. Food and Drug Administration has approved three
for use in cattle and sheep raised for meat production [30]. These are trenbolone acetate
(TBA), an androgenic steroid with anabolic potency 8-to-10-fold greater than
testosterone propionate [58], the progestin melengestrol acetate (MGA) with activity in
cattle 125-fold greater than progesterone [59], and zeranol, a non-steroidal, resorcyl
lactone derived from the mycotoxin zearalenone, which functions as an estrogen (Table
2-1).

After application, some of these growth promoters can be excreted
unmetabolized, although most mass is excreted as various metabolites. In studies with
heifers using radiolabeled TBA, 80% of the intravenously administered dose (based on
radioactivity) was excreted in bile within 24 h, but all was metabolized; 17α-trenbolone
(17α-TB; 33% of excreted radioactivity) was the dominant metabolite, while 17β-
trenbolone (17β-TB; 0.9%), which represents the biologically active form of TBA, and
trendione (1.2%) appeared in smaller quantities [32]. For MGA, about 10-17% of the
administered dose was excreted in feces unmetabolized [33], where once in the
environment it may hydrolyze at slightly basic pH (~8 or 9) to melengestrol [34]. Zeranol
(25 mg/d) dosed to heifers yielded 2-5 µg/L of unmetabolized zeranol in urine, with β-
zearalanol (2-5 µg/L) and zearalanone (0.1-0.5 µg/L) metabolites also observed [35].

Because of their widespread application, their high administered dose (e.g., 36-72 mg/implant, 140-200 mg/implant and 0.5 mg/day for zeranol, trenbolone acetate and melengestrol acetate, respectively) [12, 28] and the large number of cattle receiving implants annually, the discharge of synthetic growth promoters and their metabolites (hereafter SGPMs) into the environment is a certainty. Indeed, there are a growing number of reports of their occurrence in surface waters and soil near animal agriculture operations on the order of 10-100 ng/L and 1-100 ng/kg level, respectively [16, 17, 24, 36-38], raising concerns over potential ecosystem health risks because of their anabolic potency [22, 24, 30, 37, 39-41]. For example, Ankley *et al.* reported that 17α- and 17β-trenbolone are reproductive toxicants in fish that result in decreased fecundity in the female fathead minnow at 10-30 ng/L concentrations [22, 39].

Given the limited information available on their persistence in surface waters, assessing the ecosystem impacts of this emerging pollutant class remains challenging. Photolysis likely represents a major attenuation pathway for SGPMs, yet little information exists about the rates, mechanisms, and products of photolysis, as well as how solution variables (e.g., pH and cosolutes) influence these processes. Outside of limited data for the photolysis of 17β-trenbolone and zeranol in cattle urine [44] and the decay of 17β-trenbolone with 254 nm light during simulated UV treatment [47], most information on SGPM photolysis comes from the manufacturer's environmental assessment report produced at the time of the chemical's market introduction [34, 45, 46]. These reports indicate the possibility of direct photoreaction for TBA and MGA, but fundamental details about these photoreactions were not rigorously explored. For example, these reports only considered direct photolysis (i.e., absorption of light to break or rearrange bonds within the chemical structure) and ignored the potential importance of indirect photolysis pathways (i.e., light is first absorbed by another chromophore that then initiates reaction via energy transfer to another species). Furthermore, these reports

rarely considered metabolite photoactivity, and these may be the species most likely encountered in surface waters.

The overall objective of this study is to establish the time scales and dominant mechanism of photolysis for the suite of nine SGPMs in Table 1. In batch photoreactors using both natural and simulated sunlight, we identify those species prone to direct photolysis and quantify their half-lives ($t_{1/2}$ values) and quantum yields (Φ values) for this process. Indirect photolysis was probed using a suite of model humic and fulvic acids as sources of possible reactive entities including reactive oxygen species (ROS) and triplet state DOM (^{3}DOM*). The specific species responsible for indirect photolysis were then assessed using standard probe compounds to quantify steady-state concentrations of transient ROS in our photoreactors, as well as through the use of selective quenchers to suppress the activity of specific ROS toward SGPMs. We explore the effects of common environmental variables (e.g. temperature, pH, co-solutes) on these processes, and compare the rates and pathways observed in model laboratory systems to results obtained using two natural water samples with varying levels of dissolved organic carbon (DOC). Finally, we provide an initial description of transformation products generated via direct photolysis, but a more detailed treatment of these transformation products will be provided in a future study.

Table 2-1. Structures of synthetic growth promoters and their metabolites (SGPMs) considered herein.
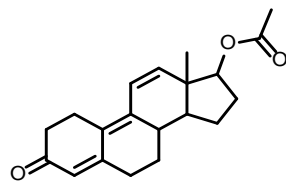
Trenbolone Acetate
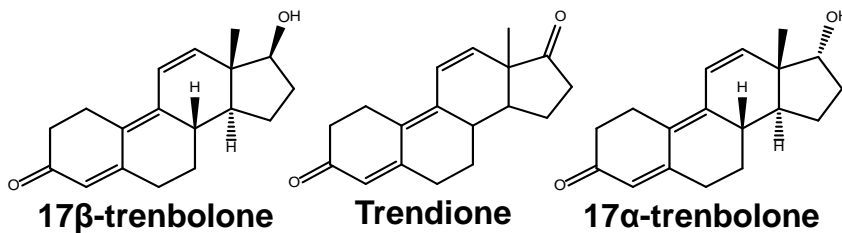
17β-trenbolone   **Trendione**   **17α-trenbolone**
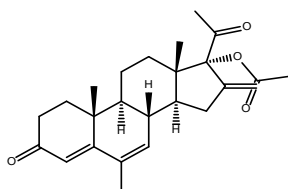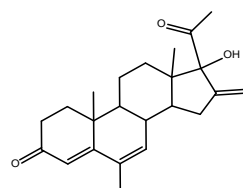
Melengestrol Acetate   **Melengestrol**
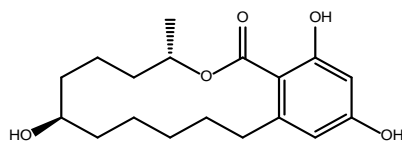
Zeranol
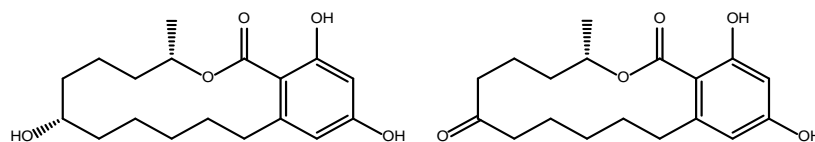
β –Zearalanol   **Zearalanone**

2.3   Experimental Methods

<u>Reagents</u>

Unless noted, all chemicals were reagent grade or better and were used as received. Synthetic growth promoters and their metabolites (SGPMs) were acquired from commercial sources including trenbolone acetate (Steraloids, >99%), 17β-trenbolone (Sigma-Aldrich,> 95%), 17α-trenbolone (Cerilliant, 99%), trendione (Steraloids, >99%), melengestrol acetate (Sigma-Aldrich, 96%), melengestrol (Steraloids Inc., 99%), zeranol (Sigma-Aldrich, 97%), β-zeralanol (Sigma-Aldrich, 97%) and zearalanone (Sigma-Aldrich, 97%). All SGPMs were acquired from commercial sources, of high purity, and used as received. We note that because TBA is not typically excreted unmetabolized [32], it was included in only a select number of experiments to compare its behavior to that of its major metabolites.

A 5 mM phosphate buffer prepared from potassium phosphate (Fisher, 99%) was used in most photochemical experiments (pH 7.0 and 7.5). A limited number of experiments conducted between pH 8-9 utilized 5 mM buffer prepared from boric acid (Sigma-Aldrich). Stock solutions of SGPM also were prepared in 5 mM phosphate buffer or deionized water. Deuterium oxide (Sigma-Aldrich, 99% D), sodium azide (Fisher, 99%), sodium formate (Sigma-Aldrich, 99%), isoprene (Sigma-Aldrich, >99%), catalase (Sigma-Aldrich, 99%) and superoxide dismutase (Sigma-Aldrich, 99%) were used to explore the reactive species participating in indirect photolysis experiments. Several models of dissolved organic matter were also used including Fluka humic acid (FHA) and several materials acquired from the International Humic Substance Society (IHSS; St. Paul, MN) including Elliott soil humic acid (ESHA), Leonardite humic acid (LHA), Suwanee River humic acid (SRHA) and Suwanee River fulvic acid (SRFA). Potassium oxalate (Fisher, 99%) and ammonium ferric sulfate dodecahydrate (Fisher, 99%) were used for chemical actinometry to measure photon rate, and quantum yield measurements

used p-nitroanisol (PNA; Acros Organics, 99+ %) and pyridine (PYR; Acros Organics, 99+ %).

Phenol (Sigma-Aldrich, >99%), 4-chlorobenzoic acid (Sigma-Aldrich, 99%) and benzoic acid (Sigma-Aldrich, ≥99.5%) were explored as probes to measure the steady-state concentration of hydroxyl radical (•OH) in irradiated suspensions of dissolved organic matter. A DPD reagent solution prepared from N,N-diethyl-p-phenylene-ammonium sulfate (Acros Organics; 97%) and a POD reagent solution from horseradish peroxidase (Sigma-Aldrich) were used for colorimetric measurement of hydrogen peroxide (H_2O_2) concentrations. Rose Bengal (Sigma Aldrich; >99%), methylene blue (Sigma-Aldrich; dye content ≥ 82%) and Erythrosin B (Acros Organics) were used as singlet oxygen sensitizers while H_2O_2 (30 wt. % in H_2O; Sigma-Aldrich) and ferrous chloride (Fisher) were used in Fenton's reaction to generate •OH. Furfuryl alcohol (Acros Organics; 98%) and acetophenone (Acros Organics; 99%) were used in competition kinetic experiments to quantify the rate coefficients for SGPM reaction with singlet oxygen ($^1O_2$) and •OH, respectively. All solutions were prepared in deionized water (Millipore, Q-Grad2).

<u>Preparation of Aqueous SGPM Stock Solutions</u>

To avoid any influence of methanol in photochemical batch experiments, only aqueous stock solutions of SGPMs were used. Aqueous stocks of each SGPM were prepared by dissolving a known mass of parent compound in 5 mM phosphate buffer or DI water while mixing overnight. To remove any residual undissolved solid, the solution was then filtered via a 0.2 µm PTFE syringe-driven filter. A sample of the filtrate was then analyzed via HPLC as described below to determine its concentration, which was quantified via comparison to an external calibration curve generated with aqueous SGPM samples prepared from stock solutions in methanol. The remainder of the filtrate was

then diluted with phosphate buffer as needed to achieve the desired starting concentration in photochemical batch experiments.

Direct Photolysis Experiments

Rates and products of direct photolysis were explored using both simulated and natural sunlight. The majority of experiments were conducted using a commercially available 450 W Xenon arc lamp (Newport Corporation). The light was first passed through a water filter to remove IR radiation, reflected off a 90° full reflectance beam turning mirror, and then passed through an AM 1.5 filter and a 305 nm long-pass filter to generate a spectrum of light more closely resembling that available at earth's surface. Photon rates were measured by chemical actinometry using ferrioxalate [60] , yielding a photon flux of 3.9×10^{-4} photons/m^2/sec (6.5×10^{-28} einsteins/m^2/sec) when normalized to the incident area of the photoreactor.

Unless noted, all photochemical experiments were conducted in a water-jacketed, borosilicate photoreactor (37 mm inner diameter $\times$ 67 mm depth for a nominal volume of ~50 mL; Chemglass), whose contents were mixed via magnetic stirrer and stir plate during all experiments. Experiments used 20 mL of SGPM solutions in 5 mM phosphate buffer (prepared as described in the previous section), with the majority conducted at pH 7.0 and 25 °C. The system temperature was held constant via recirculating water bath. Upon irradiation, aliquots of solution (~1 mL) were withdrawn at periodic intervals and transferred to a 2.5 mL amber autosampler vial for subsequent analysis via HPLC with photodiode array detector (HPLC-DAD) or LC with detection via tandem mass spectrometry (LC/MS/MS). Typical initial concentrations in photolysis experiments were 1-10 μM (on the order of ~0.3-30 mg/L). Although these concentrations are greater than those previously reported in surface waters, they were necessary to facilitate HPLC-DAD analysis, which is the method best suited for processing the large number of samples generated in our kinetic studies. We note that a possible risk of working at these

relatively high concentrations is that self-quenching or self-screening could affect the degradation rates and quantum yields reported herein. However, a limited number of experiments conducted at environmentally relevant conditions (~nM levels) for a subsequent study yielded comparable reactivity to that observed herein. Thus, we do not believe these phenomena to be significant in our more concentrated systems. When possible experiments were conducted in triplicate, but limitations in the amount of certain chemicals arising from their cost sometimes resulted in fewer replicates. Control experiments were conducted with each SGPM in dark (i.e., not irradiated) systems.

Experiments with simulated sunlight also explored the effect of common environmental variables on SGPM photolysis. The variables included temperature (10°C), pH (5, 7, 9), and the presence of cosolutes. Cosolutes were considered across environmentally relevant concentrations and included bicarbonate (HCO_3^-, up to 30 mg/L HCO_3^-), nitrate (NO_3^-, up to 50 mg/L NO_3^-), phosphate [up to 125 µg/L as P using a DI water background (i.e., without phosphate buffer)] and dissolved organic matter (up to 50 mg/L of Elliott soil humic acid, Leonardite humic acid, and Fluka humic acid).

A subset of experiments examined direct photolysis via natural sunlight. Experiments were conducted in duplicate using solutions irradiated by incident sunlight over the months of June to September in Riverside, California (latitude: 34° N, longitude: 117° W, temperature = 28 ± 3 °C). Reactors were constructed and sampled as described previously for simulated sunlight, although experiments with sunlight were only conducted at pH 7.0 and a water bath rather than recirculating system was used to maintain a near constant temperature. For these experiments, the quantum yield (Φ values) was measured via the method of Leifer [61] using the binary actinometer PNA/pyridine of Dulin and Mill [62] as detailed in the following description.

Chemical Actinometry with Ferrioxalate in Simulated

and Natural Sunlight Experiments

Equal volumes of 0.02 M ammonium ferric sulfate dodecahydrate and 0.06 M potassium oxalate monohydrate (both in 0.1N H_2SO_4) were mixed in the dark [63] . After illumination, samples were taken every minute to measure Fe^{2+} production. The product Fe^{2+} was analyzed by first adding 200 μL of 1 g/L 1,10-phenanthroline followed by 200 μL of 100 g/L of an ammonium acetate buffer. The entire sample was then allowed to sit in the dark for 1 h prior to absorbance measurements on a UV-visible spectrophotometer (at λ=510 nm) [64]. The rate of Fe^{2+} production based on the increase in concentration over time was then converted to a photon rate according the procedures outlined by Goldstein and Rabani [63].

<div align="center">

Quantum Yield Measurements for

Direct Photolysis in Natural Sunlight

</div>

The quantum yield (Φ) of a photochemical reaction describes the moles of reactant transformed per moles of photons absorbed [61]. Following the approach of Leifer, an environmental quantum yield, representing the average value of Φ over the wavelengths at which a specific SGPM absorbs sunlight, was calculated using equation 1:

$$\phi_{dc} = \left(\frac{k_{dc}}{k_{da}}\right)\left\{\frac{\sum_\lambda \epsilon_{\lambda a} L_\lambda}{\sum_\lambda \epsilon_{\lambda c} L_\lambda}\right\} \phi_{da} \quad (2-1)$$

where ϕ_{da} and ϕ_{dc} are the quantum yield of the actinometer and test chemical, respectively; k_{da} and k_{dc} are the rate constant for the actinometer and the test chemical, respectively; $\epsilon_{\lambda a}$ and $\epsilon_{\lambda c}$ are the molar absorptivity of the actinometer and the test chemical, respectively; and L_λ is the solar irradiance with units of millieinsteins·cm^{-2}day^{-1}. Solar irradiance (i.e., values of sunlight intensity at wavelength λ) was obtained from Appendix A in the text of Leifer [61]. Specifically, the values of L_λ used in quantum yield calculations were obtained from Table A-7 for L_λ values at 30° N latitude during the summer because all experiments were conducted in Riverside, CA (33°N) during summer time.

Chemical actinometry was performed using the binary actinometer PNA/pyridine described by Dulin and Mill.[62] For PNA, the ϕ_{da} value is reported to be

$$\phi_{da} = 0.437[PYR] + 0.000282 \quad (2-2)$$

and was thus determined from the known experimental molar concentration of pyridine ([PYR]). The actinometer half-life was adjusted by varying the ratio of PNA to pyridine such that it was comparable to the half-life of each SGPM. Rates of photolysis were determined by measuring the disappearance of the SGPM and PNA. The molar extinction coefficients were determined from measured UV/Vis spectra of each SGPM and the actinometer at known aqueous concentrations.

<u>Indirect Photolysis Experiments</u>

For indirect photolysis, experiments were conducted with irradiated solutions of model dissolved organic matter (DOM). Experiments used simulated sunlight in an identical reactor to that described for direct photolysis studies. Humic acids (HA) and fulvic acids (FA) obtained from commercial sources included Fluka humic acid (FHA), Elliott soil humic acid (ESHA), Leonardite humic acid (LHA), Suwanee River humic acid (SRHA) and Suwanee River fulvic acid (SRFA). Stock solutions (~200 mg/L) were prepared by dissolving known masses of each HA and FA into deionized water adjusted to pH 12 using 5 M NaOH. The mixture was then adjusted to pH 7 using 5 M HCl, and subsequently diluted to produce the concentration utilized in photolysis experiments (1-10 mg/L).

Complementary experiments with each HA and FA were conducted in the absence of SGPMs to quantify the steady-state concentration of select ROS generated upon irradiation using probe compounds [e.g., phenol for hydroxyl radical ($^\bullet$OH) and furfuryl alcohol for singlet oxygen ($^1O_2$)]. Details on these methods are provided in the following section. The role of each ROS in SGPM transformation was assessed using selective quenchers including either formate or isopropanol (50-100 mM) for $^\bullet$OH,

sodium azide (10 mM) for $^1O_2$, superoxide dismutase (2 U/ml) for superoxide, and catalase (200 U/ml) for H_2O_2. Isoprene (0.1% v/v) was also used to assess involvement of triplet state DOM (^{3}DOM*). A subset of experiments was conducted in D_2O to probe further the role of $^1O_2$, whereas some were also conducted in deoxygenated systems to examine reaction pathways not involving ROS. Experiments with zeranol were also conducted as a function of pH, using 5 mM phosphate buffer at pH 7.0 and 7.5, while higher pH values (8.0-9.0) used a 5 mM borate buffer. Finally, for select SGPMs, we explored the second-order rate coefficients for reaction with $^1O_2$ and $^•OH$ as quantified via the procedures described in the following section.

<div align="center">

Measurement of ROS in Irradiated Solutions

of Humic and Fulvic Acids

</div>

Phenol and furfuryl alcohol (FFA) were used as probes for $^•OH$ and $^1O_2$, respectively. Modeling the loss of each probe using exponential decay, the steady-state concentrations of $^•OH$ and $^1O_2$ were calculated from the measured pseudo-first order rate coefficient (i.e., k_{obs} value) and the known second order rate coefficient for the reaction between the ROS and probe (i.e., $k_{phenol/•OH} = 1.4 \times 10^{10}$ $M^{-1}s^{-1}$ and $k_{FFA/1O2} = 1.2 \times 10^8$ $M^{-1}s^{-1}$)[65],[66]. We note that for measurement of $^•OH$, other probe compounds were explored including *para*-chlorobenzoic acid ($k_{•OH} = 5 \times 10^9$ $M^{-1}s^{-1}$)[67] and benzoic acid ($k_{•OH} = 2.1 \pm 0.3 \times 10^9$ $M^{-1}s^{-1}$) [68]. However, their order of magnitude smaller second-order rate constants for reaction with $^•OH$ relative to phenol, made accurate measurement of $^•OH$ difficult over reasonable experimental timescales in irradiated HA and FA solutions.

Concentrations of H_2O_2 were measured colorimetrically [69]. DPD reagent was prepared weekly by dissolving 0.1 g of N,N-diethyl-1,4-phenylenediammonium sulfate (DPD) in 10 mL 0.1 N H_2SO_4 and stored in the dark at 5°C. POD reagent was prepared weekly by dissolving 10 mg peroxidase product from horseradish in 10 mL of Millipore water and stored in the dark at 5°C. For analysis, a 900 μL aliquot of sample was mixed

with 100 µL of 25 mM phosphate buffer (pH 6), 15 µL of DPD reagent and 15 µL of POD reagent. Absorbance was measured at 551 nm and resulting H_2O_2 concentration was determined via a calibration curve generated with known standards of H_2O_2.

Assessing the Involvement of Different ROS

in Zeranol Indirect Photolysis

The potential role of each ROS in zeranol transformation was assessed using selective quenchers. Quenchers included sodium formate and isopropanol (50-100 mM) for $^{\bullet}OH$, sodium azide (10 mM) for $^1O_2$, superoxide dismutase (2 U/ml) for superoxide, catalase (200 U/ml) for H_2O_2 and isoprene (0.1% v/v) for triplet state DOM ($^3DOM^*$). If the addition of excess quencher inhibited SGPM transformation, the corresponding entity was assumed to participate in degradation. The contribution of singlet oxygen was also evaluated in solutions with D_2O, which stabilizes and thus promotes the reactivity of singlet oxygen. Thus, enhanced rate of SGPM decay in D_2O would be evidence of the involvement of $^1O_2$. Experiments were typically conducted in pure D_2O, although experiments with natural water samples utilized a 50:50 v/v mixture of D_2O and the water sample. A small number of experiments also were conducted in deoxygenated systems using a custom photoreactor with a removable top fitted with a quartz window. When sealed, the contents of the reactor could be kept free of O_2 by applying an overpressure of nitrogen. Further, all solutions in the sealed reactor were first purged with N_2 to eliminate dissolved O_2. Experiments conducted in the absence of O_2 helped to differentiate between $^3DOM^*$ and ROS in SGPM transformation; decay in the absence of molecular oxygen supports direct reaction with excited state DOM.

Competition Kinetics Experiments with Zeranol

The second-order rate coefficient for zeranol reaction with $^1O_2$ was estimated in a photochemical system at pH 7 (5 mM phosphate buffer) containing 2 µM Rose Bengal as

a singlet oxygen sensitizer. Briefly, the rate of zeranol transformation (~7 µM initial concentration) was measured relative to that of FFA (initial concentration of 100 µM), a compound whose reactivity toward $^1O_2$ is well characterized ($k_{FFA/1O2} = 1.2 \times 10^8$ $M^{-1}s^{-1}$) [66]. The second-order rate constant could then be calculated according to equation 3

$$k_{\text{zeranol}/1O2} = \frac{\ln(\frac{[Z_t]}{[Z_0]})}{\ln(\frac{[FFA_t]}{[FFA_0]})} k_{\text{ FFA}/1O2} \qquad (2-3)$$

where $k_{\text{zeranol}/1O2}$ is the rate constant for the reaction between zeranol and singlet oxygen, and $k_{FFA/1O2}$ is the established rate constant for the reaction between furfuryl alcohol and singlet oxygen. We note that near equivalent values for the second-order rate coefficient between zeranol and $^1O_2$ were obtained if alternative sensitizers (e.g., methylene blue and Erythrosin B)[70] were used, indicating that $^1O_2$, and not sensitized Rose Bengal, was involved in zeranol transformation.

The second order rate coefficient for reaction with hydroxyl radical was measured by using the Fenton reaction to generate $^\bullet OH$ at pH 3. In the absence of light, 60µM of $FeCl_2$ was combined with an equivalent concentration of H_2O_2 and a dilute solution of zeranol (~ 7 µM) so as to achieve pseudo-first-order decay, at least initially. Rates of zeranol loss were compared to acetophenone ($k_{/acetophenone/\bullet OH} = 5.9 \times 10^9$ $M^{-1}s^{-1}$) [71] via equation 4

$$k_{\text{zeranol}/\bullet OH} = \frac{\ln(\frac{[Z_t]}{[Z_0]})}{\ln(\frac{[A_t]}{[A_0]})} k_{\text{acetophenone}/\bullet OH} \qquad (2-4)$$

where $k_{\text{zeranol}/\bullet OH}$ is the rate constant for the reaction between zeranol and hydroxyl radical, and $k_{\text{acetophenone}/\bullet OH}$ is the rate constant for the reaction between acetophenone and hydroxyl radical.

Experiments in Natural Water Samples

Water samples from a runoff-impacted creek and agricultural return water collected in an irrigation canal in the Yuba River watershed (Browns Valley, CA) were also used in photolysis experiments. Immediately after collection, samples were passed through a 0.2 μm PTFE filter under vacuum. The pH of these water samples were between pH 6.8 and 7.0, and by TOC analysis the dissolved organic carbon (DOC) contents for the creek and agricultural return water were 50 mg/L and 6 mg/L, respectively. Other characteristics of this surface water were not measured (e.g., alkalinity and nitrate), but we expect such constituents to be present at relatively low levels because the samples were collected in winter and thus likely diluted by the seasonal rain. Photolysis experiments with these waters were conducted according to the aforementioned procedures, and dark control experiments were conducted to evaluate the possibility of alternative loss processes.

Analytical Methods

Samples were analyzed on a 1200 Series Agilent HPLC-DAD equipped with an Eclipse XBD-C18 column (4.6 × 150 mm, 5 μm particle size) using methods for SGPMs adapted from previous studies [7, 48, 72, 73]. Photoproducts were examined via high resolution LC-MS/MS analysis conducted with a Paradigm Multi-Dimensional Liquid Chromatography (MDLC) instrument (Michrom Bioresources, Auburn, CA) equipped with a Genesis Lightning C-18 4μm particle 200Å pore size (2.1 x 100 mm) column (Grace Davison). Eluted compounds were analyzed using an LTQ-Orbitrap XL (ThermoElectron, Bremen Germany) detector equipped with an Ion Max source (ThermoElectron) using Xcalibur v 2.0.7 software for data processing.

Analysis of trenbolone family members used a mobile phase of 50:50 acetonitrile (ACN):H_2O, a flow rate of 1 mL/min, an injection volume of 25 μl and a 350 nm detection wavelength [7]. Analysis of melengestrol family members used a mobile phase

of 60:40 ACN:H$_2$O, a flow rate 1 mL/min, an injection volume of 25 µl and a 300 nm detection wavelength [48]. Analysis of α-zearalanol and β-zearalanol used a mobile phase of 60:40 methanol (MeOH):H$_2$O, a flow rate 1.5 mL/min, an injection volume of 20 µl and a 210 nm detection wavelength [72], whereas zearalanone analysis used a mobile phase of 8:46:46 MeOH:H$_2$O:ACN [73], a flow rate 1 mL/min, an injection volume of 25 µl and a 210 nm detection wavelength.

For measurement of steady-state ROS concentrations and reaction rate coefficients with zeranol, analysis of phenol used a mobile phase of 65:35 1 mM sodium acetate at pH 3:ACN, a flow rate 0.75 ml/min, an injection volume of 20 µl and a 254 nm detection wavelength. Analysis of FFA used a mobile phase of 45:55 MeOH:H$_2$O, a flow rate 0.75 mL/min, an injection volume of 20 µl and a detection wavelength of 210 nm. Acetophenone was analyzed with a mobile phase of 50:50 5 mM phosphate buffer at pH3:MeOH, a flow rate 1 mL/min, an injection volume of 25 µl and a 254 nm detection wavelength.

High resolution LC-MS/MS analysis was used to identify products generated in photoreactors. Photoproducts were first separated on a Paradigm Multi-Dimensional Liquid Chromatography (MDLC) instrument (Michrom Bioresources, Auburn, CA) using a Genesis Lightning C-18 4µm particle 200Å pore size (2.1 x 100 mm) column (Grace Davison). Eluent flow rate was 600 µL/min and the solvent gradient ranged from 25% B to 72% B over 18 min, followed by 100% B for 1 min, for a 25 minute total run time. Solvent A was 0.1% acetic acid in water and solvent B contained 0.1% acetic acid in ACN. Eluted compounds were analyzed using an LTQ-Orbitrap XL (ThermoElectron, Bremen Germany) detector equipped with an Ion Max source (ThermoElectron) using Xcalibur v 2.0.7 software for data processing. The MS was operated in data-dependent mode switching between Orbitrap-MS for high resolution full scan data and LTQ-MS/MS for low resolution tandem mass spectrometry fragmentation data. Full scan spectra (m/z 100–350) were acquired in the positive ion mode with resolution of 100,000

in profile mode. The three most intense data-dependent peaks at each analysis interval were subjected to MS/MS using collision-induced dissociation with a minimum signal of 5,000, isolation width of 3.0 amu, and normalized collision energy of 35.0%. Ions already selected were dynamically excluded for 30 seconds after a repeat count of 2 with a repeat duration of 10 seconds. Also, during each sampling scan, all ions of m/z 271.17 and 269.15, representing 17α- or 17β-TBOH parents and TBO respectively, were subjected to MS/MS analysis using collision-induced dissociation with a normalized collision energy of 35.0% and an isolation width of 3.0 amu.

2.4   Results and Discussion

Direct Photolysis of SGPMs with

Simulated and Natural Sunlight

Concentration profiles for SGPMs as a function of irradiation time with natural and simulated sunlight are shown in Figure 2-1. All SGPMs except the zeranol family were prone to direct photolysis at pH 7. For the TBA and MGA families, the loss followed exponential decay, allowing first-order rate coefficients and corresponding $t_{1/2}$ values (Table 2-2) for direct photolysis to be quantified from semi-log plots of concentration versus time. Direct photolysis was rapid for the TBA and MGA families, producing $t_{1/2}$ values between ~0.25-1 h in simulated light (Figure 2-1a and Table 2-2). The TBA family was slightly, but consistently, more reactive than melengestrol acetate and melengestrol, which exhibited nearly identical photolysis rates. Within the TBA family, 17β-trenbolone and TBA photolyzed at nearly equivalent rates, which were slightly albeit significantly faster than those observed for trendione and 17α-trenbolone. SGPM decay in natural sunlight (Figure 2-1b) closely mirrored behavior observed with simulated light. Although TBA metabolites still exhibited greater reactivity than melengestrol acetate and melengestrol in sunlight, the reactivity difference was not as pronounced as with simulated light, presumably from minor differences in the irradiance

spectra of the two light sources (see Figure 2-2). Notably in all dark controls, SGPM concentrations were stable, confirming that no other transformation pathways occurred over these time scales.

These observed trends in direct photolysis can be rationalized by the relative light absorbance and photochemical quantum yields for each family of SGPMs. In Figure 2-1c, UV/vis absorbance spectra for each SGPM are compared to the solar irradiance available at the earth's surface, in which overlap between SGPM absorbance and available light energy is necessary for direct photoreaction. Within a family of compounds, absorbance spectra are nearly identical. All TBA family members exhibit absorbance maxima in the UV-A region at approximately 350 nm, characteristic of their conjugated 4,9,11 triene π-bond system, with secondary maxima near 240 nm. The MGA family exhibited a single absorbance maximum at 298 nm, a shift toward lower wavelengths relative to TBA and its metabolites because of their lower degree of π-bond conjugation. This in turn produces a lesser degree of overlap with the solar spectrum than compared to the TBA family. This result is most easily seen via plots of the spectral overlap integral for each species (Figure 2-3), which represents the product of the compound's molar absorptivity (ε_λ) and the light intensity (L_λ), both as a function of wavelength. In contrast, zeranol and its metabolites possess primary absorbance maxima near 254 nm, characteristic of their aromatic moiety, although a small amount of absorbance is measureable above 300 nm. Such limited absorption of the zeranol family within the solar spectrum likely contributes to their stability upon irradiation.
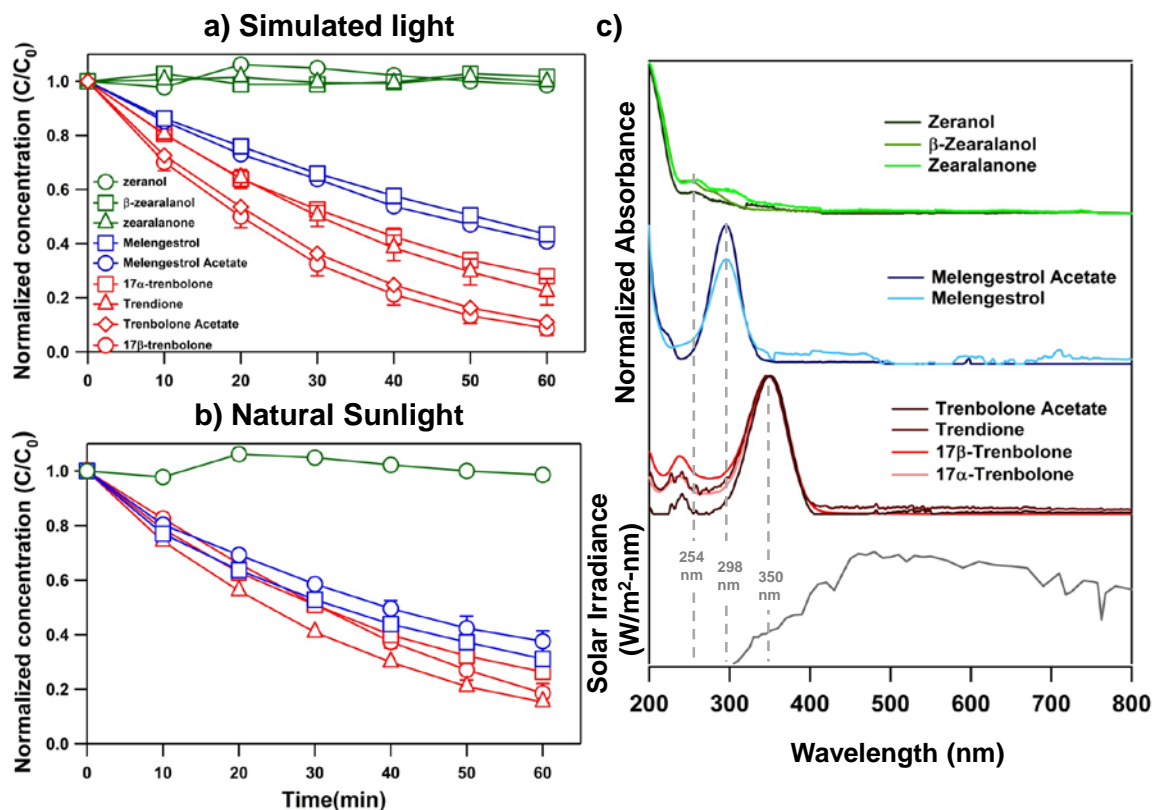
Figure 2-1. Concentration profiles of SGPMs as a function of irradiation by (a) simulated sunlight and (b) natural sunlight in 5 mM phosphate buffer at pH 7. Only a subset of SGPMs was considered in natural sunlight to verify trends and time scales observed with the simulated light source. (c) UV-visible light absorption spectra collected for all SGPMs in Milli-Q water. Noted in panel c are the primary absorbance maxima for each compound class, and the solar irradiance available at the earth's surface is provided for comparison (ASTM reference spectra G173-03). Uncertainties represent one standard deviation of at least duplicate experiments. If uncertainties are not visible, they are smaller than the symbol.

Table 2-2. Half-lives ($t_{1/2}$ values) and quantum yields (Φ) for SGPMs found to undergo direct photolysis at pH 7.0. Also provided are $t_{1/2}$ values measured for zeranol and its metabolites in irradiated solutions of Elliot Soil Humic Acid (ESHA) at pH 7.0.

Direct Photolysis

SGPM	$t_{1/2}$ values (min)[a]		Direct photolysis rate constant (min^{-1})		Quantum yield (Φ)[b] x10^3
	Simulated Sunlight	_Natural Sunlight_	_Simulated Sunlight_	_Natural Sunlight_	
Trenbolone acetate	18.7 ± 1.2	NM[c]	0.037 ± 0.002	NM	NM
17β-trenbolone	16.9 ± 1.0	24.7 ± 3.2	0.041 ± 0.003	0.0280 ± 0.004	1.58 ± 0.16
17α-trenbolone	32.5 ± 0.8	31.1 ± 0.8	0.213 ± 0.0005	0.0223 ± 0.0006	1.49 ± 0.11
Trendione	27.3 ± 1.6	22.1 ± 0.8	0.0254 ± 0.0015	0.0314 ± 0.0012	3.1 ± 0.4
Melengestrol Acetate	46.3 ± 1.5	42.7 ± 3.3	0.0150 ± 0.0005	0.0162 ± 0.0013	4.9 ± 0.5
Melengestrol	50.4 ± 1.0	36.4 ± 2.8	0.0137 ± 0.0003	0.0198 ± 0.0015	7.8 ± 0.5

Indirect Photolysis

	$t_{1/2}$ values in 5 mg/L ESHA (hours)[d]
Zeranol	3.24 ± 0.14
β –Zearalanol	4.1 ± 0.8
Zearalanone	4.8 ± 0.2

[a]Photon rates measured via chemical actinometry with ferrioxalate were 4x10^{-7} photons/sec for simulated sunlight generated with a Xe arc lamp and ranged between 2-5x10^{-7} photons/sec over the course of experiments with natural sunlight (conducted between June-September in Riverside, CA). Uncertainties represent one standard deviation from at least duplicate experiments. [b]Reported only for natural sunlight. Uncertainties represent 95% confidence intervals from regression analysis shown in Figure 2-2. [c]Not measured because trenbolone acetate is not excreted in an unmetabolized form. [d]Uncertainties represent 95% confidence intervals from regression analysis of semi-log plots of concentration versus time for data shown in Figure 2-4.
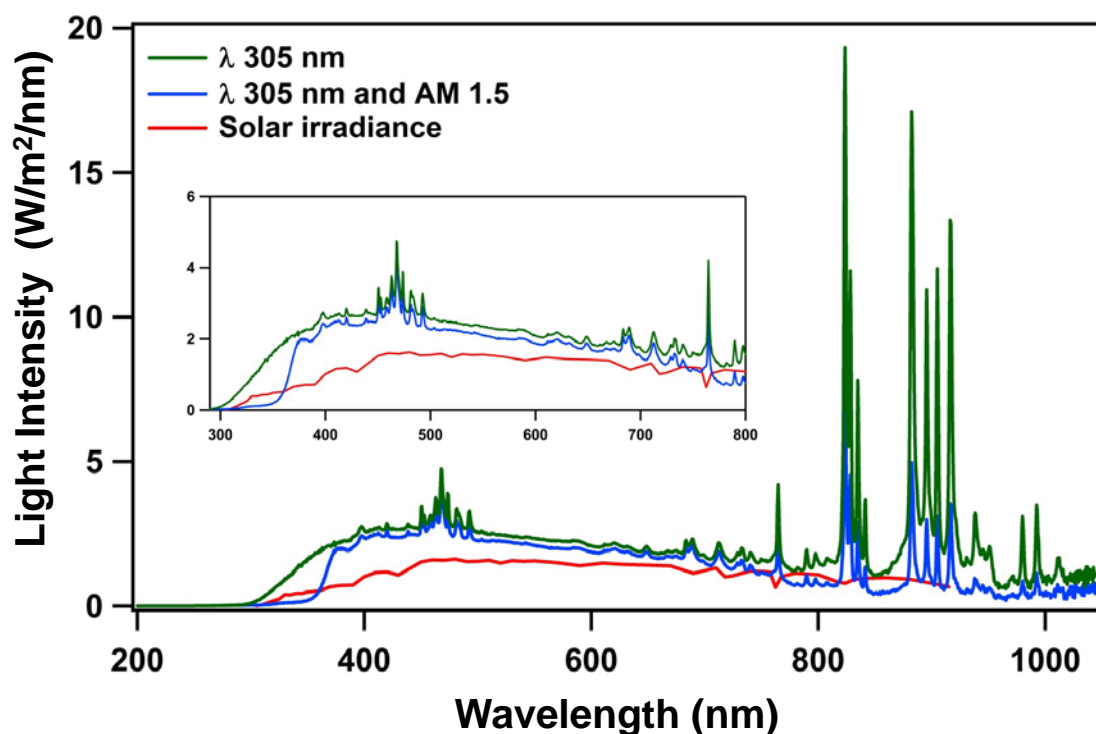
Figure 2-2. Spectral output for the commercially available 450 W Xenon arc lamp (Newport Corporation) used in experiments with simulated sunlight. The inset shows a close-up of the light within the region from 300-800 nm. The spectral outputs demonstrate the impact of the optical filters used in our experiments. Light in all experiments was passed through a 305 nm long pass filter and an AM 1.5 filter, the influence of which is shown. Data were collected using an ILT950 Spectroradiometer System from International Light Technologies (Peabody, MA). For comparison, the solar irradiance available at the earth's surface is provided in red (ASTM reference spectra G173-03).

Quantum yields measured in natural sunlight (Table 2-2 and Figure 2-4) were slightly greater for melengestrol acetate ($\sim 5 \times 10^{-3}$) and melengestrol ($\sim 8 \times 10^{-3}$) than for the trenbolone metabolites (ranging from $1.5 - 3 \times 10^{-3}$). We have assumed that these quantum yields are independent of wavelength, and we are unable to report a quantum yield for zeranol family compounds due to their lack of direct photoreactivity, even over longer irradiation timescales (≥ 6 h). For 17β-trenbolone, the quantum yield measured herein is similar to that reported by Gryglik et al. [47], who reported a quantum yield for 17β-trenbolone of 2.9 (± 0.2) $\times 10^{-3}$ at 254 nm. The greater quantum yields for melengestrol acetate and melengestrol help to explain minimal difference in photoactivity relative to TBA metabolites, which absorb light over a greater portion of the available solar spectrum.

These Φ values are comparable to those reported for other natural and synthetic steroids. For example, in work with the natural androgen testosterone, Vulliet et al. [74] reported a quantum yield of 2.4×10^{-3} at 313 nm. Another reasonable comparison is to estrone, a metabolite of 17β-estradiol also prone to direct photolysis. Working with a solar simulator, Lin and Reinhard [75] measured a quantum yield for estrone of 2.96×10^{-2}, roughly twice the largest Φ value measured herein for melengestrol. Therefore, it appears the TBA and MGA families exhibit photoefficiencies that are at best equivalent to other classes of steroid hormones. However, due to their greater extent of overlap with the solar spectrum, they tend to exhibit half-lives (< 1 h) that are considerably shorter than previously observed for the direct photolysis of most natural and synthetic estrogens (between 5-40 hour in DI water) [75] and testosterone (~ 5 hour with irradiation 313 nm light) [74].

Additional experiments were conducted with 17β-trenbolone and MGA to examine the influence of solution composition on direct photolysis rates. Essentially, rates of 17β-trenbolone transformation were invariant across a broad range of temperature (10-25°C), pH (5, 7, 9), and co-solute concentrations including
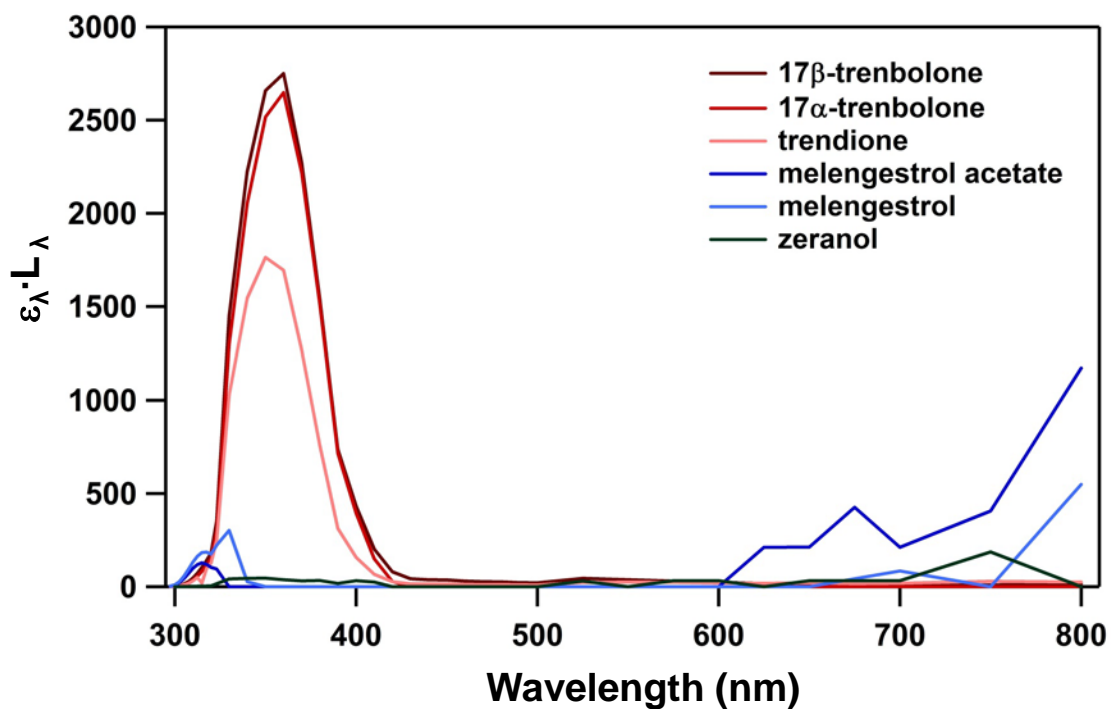
Figure 2-3. The spectral overlap integral, calculated from the product of the molar absorptivity (ε_λ) and the light intensity (L_λ) as a function of wavelength, for most of the SGPMs considered in the current investigation. The integral was calculated as part of the procedures described above for measuring the quantum yield for the direct photolysis of each compound in natural sunlight.
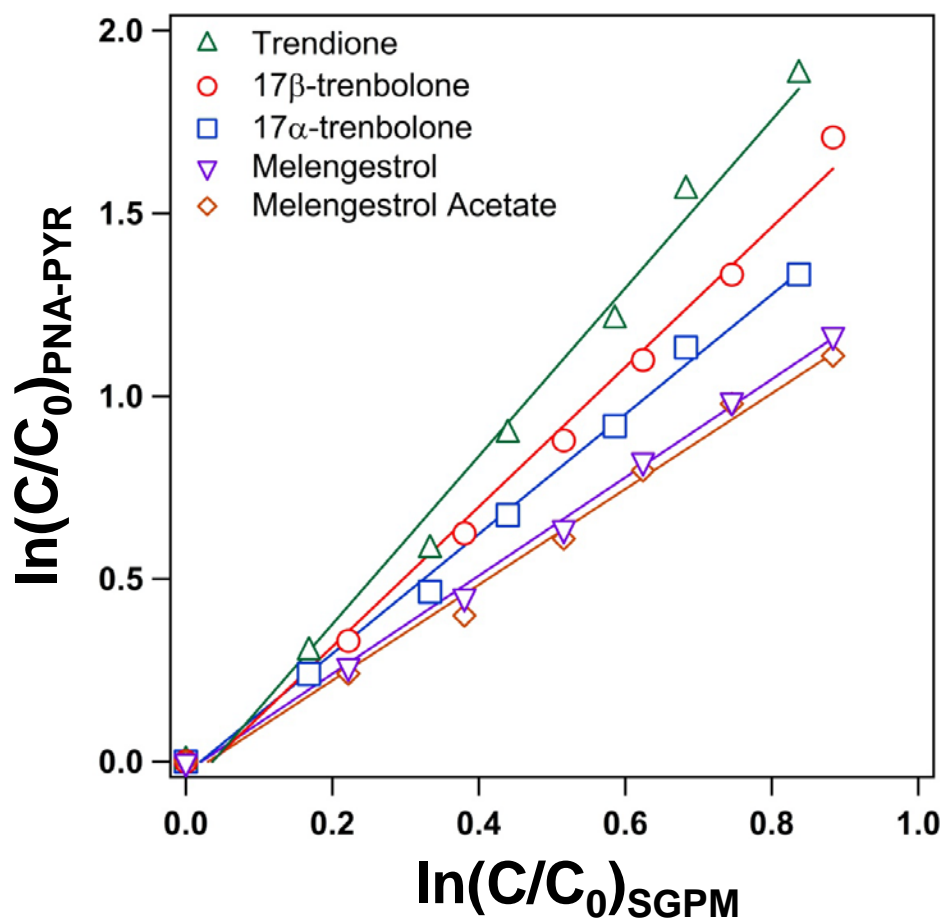
Figure 2-4. Plots of the natural log of the normalized concentration of the binary actinometer PNA/PYR versus the natural log of the normalized concentration of SGPMs prone to direct photolysis upon exposure to natural sunlight. The slopes from these plots were used to calculate quantum yields of SGPMs with natural sunlight (i.e., the slope of each line represents $\frac{k_{dc}}{k_{da}}$ in equation 1). The initial concentration of the actinometer and SGPMs was ~10μM. Experiments with SGPMs were conducted at pH 7 using 5 mM phosphate buffer whereas photolysis of PNA-PYR was studied in DI water.

HCO_3^- (up to 30 mg/L as HCO_3^-), NO_3^- (up to 20 mg/L as NO_3^-), and phosphate (up to 125 µg/L as P) (Figure 2-5). As shown in Figure 2-5, the rate of 17β-trenbolone photolysis was essentially invariant over the range of aquatic variables considered. The only instance of inhibition was observed at a very high concentration (50 mg/L) of Fluka humic acid, which inhibited the transformation rate by ~30%. The extent of inhibition observed agrees well with that expected from the screening factors calculated for 17β-trenbolone in DOM-containing systems (please see below). Notably, the presence of model organic matter (ESHA, LHA, and FHA ranging from 0-50 mg/L) exhibited neither a positive (e.g., production of photochemically reactive species) nor a substantially negative (e.g., light screening to inhibit direct photolysis) impact over the range of concentrations considered. For 17β-TB, rates of photolysis were essentially invariant up to 10 mg/L of ESHA or LHA, and even 50 mg/L of FHA only inhibited the rate of photolysis by ~30% (Figure 2-5f). MGA was slightly more prone to inhibition, exhibiting a comparable ~35% decrease in direct photolysis rate at 10 mg/L of ESHA (Figure 2-6). These rate decreases appear primarily attributable to light screening, as estimated screening factors agree well with the decrease in k_{obs} values observed in organic matter containing systems. Accordingly, the greater inhibition of MGA photolysis is thereby attributable to the larger degree of humic and fulvic acid absorbance (Figure 2-7) at its maximum absorbance wavelength (~300 nm) relative to that for 17β-trenbolone (~350 nm). As expected, absorbance exhibited by these model HA and FA solutions increases with decreasing wavelength. Nevertheless, based on measured half-lives in both natural and simulated light (Table 2-2) and the negligible to minor influence exerted by most common aquatic variables (Figure 2-5 and 2-6), direct photolysis appears to be the dominant loss process in most sunlit surface waters for the TBA and MGA families, both of which are unlikely to persist for more than a few hours due to their propensity for direct photolysis.
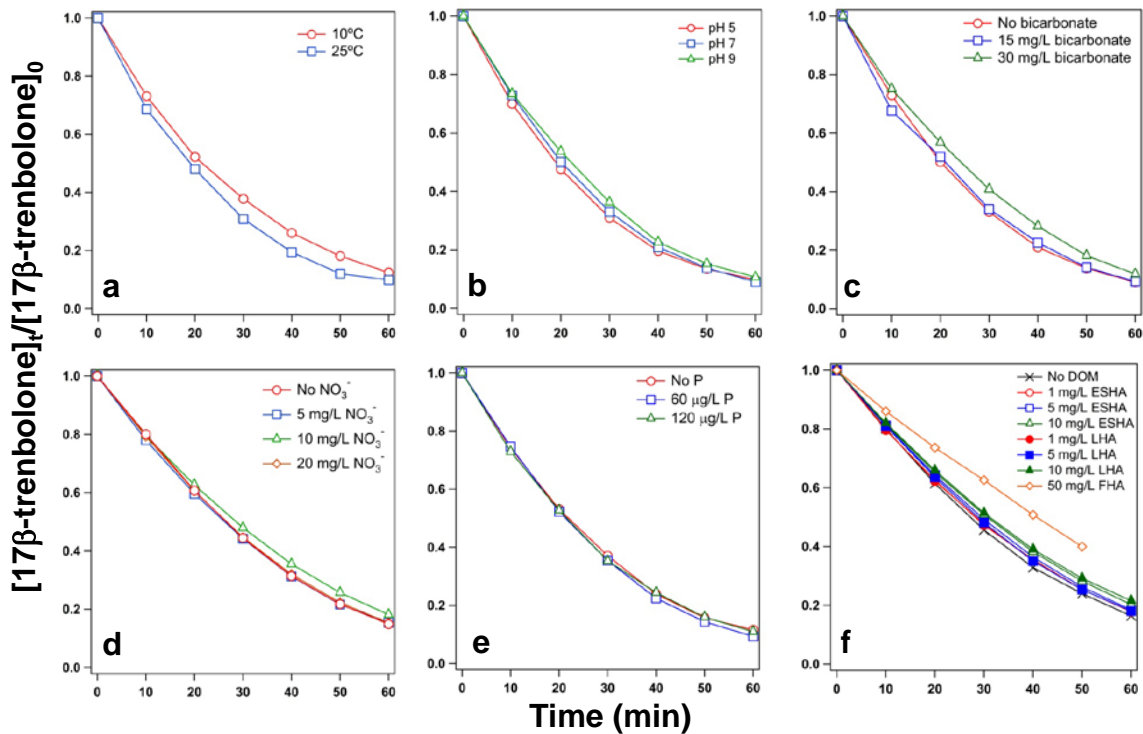
Figure 2-5. Effect of several common aquatic variables on the direct photolysis of 17β-trenbolone exposed to simulated sunlight. The variables explored include (a) temperature (10 and 25 °C) (b) pH (5, 7, and 9) (c) bicarbonate (15 and 30 mg/L at HCO_3^-) (d) Nitrate (5, 15, and 20 mg/L as NO_3^-) (e) Phosphorus (62 and 124 µg/L as P) (f) DOM (1, 5, and 10 mg/L of Elliot Soil humic acid and Leonardite humic acid, as well as 50 mg/L for FHA). In all experiments, the initial concentration of 17β-trenbolone is ~10µM. Experiments were conducted in 5 mM phosphate buffer, except for experiments examining the effect of dissolved phosphate concentrations, which were conducted in DI water adjusted to and maintained at pH 7 with dilute acid and base.
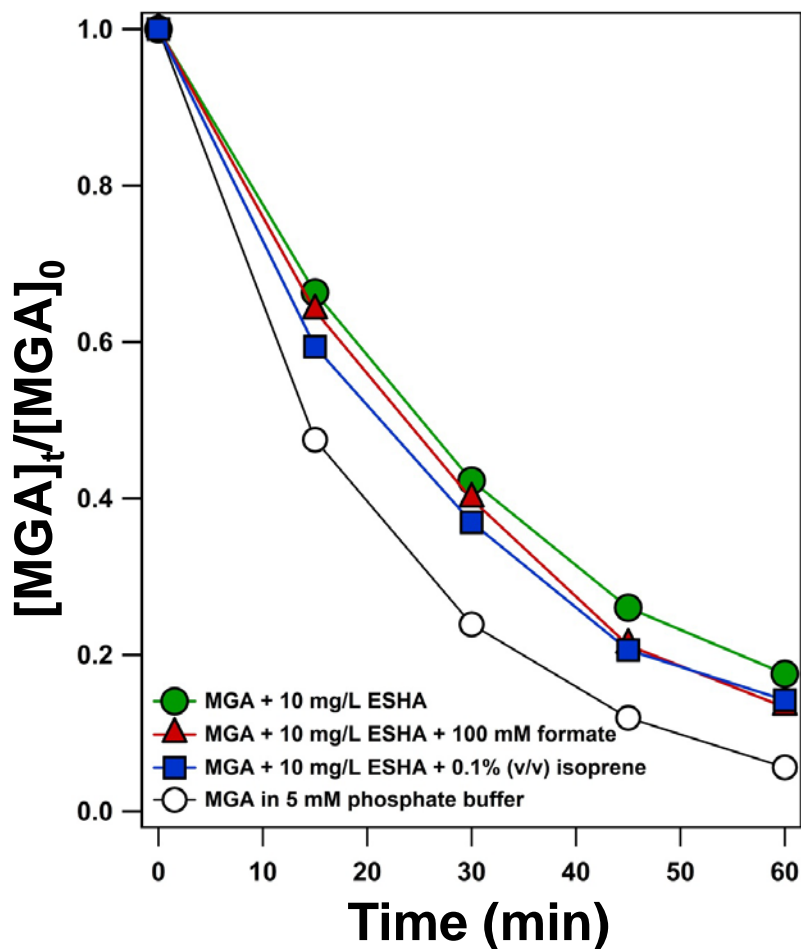
Figure 2-6. Inhibition of MGA direct photolysis arising from the presence of 10 mg/L ESHA. The rate of MGA photolysis decreased by roughly 30% in the presence of ESHA, a value that agrees well with the screening factors estimated for direct photolysis of 2.5 μM of MGA in a 10 mg/L solution of ESHA (please see discussion above). The extent of inhibition was not influenced by the presence of potential scavengers for photogenerated oxidants such as triplet DOM or hydroxyl radical. Experiments were conducted in 5 mM phosphate buffer at pH 7.0.
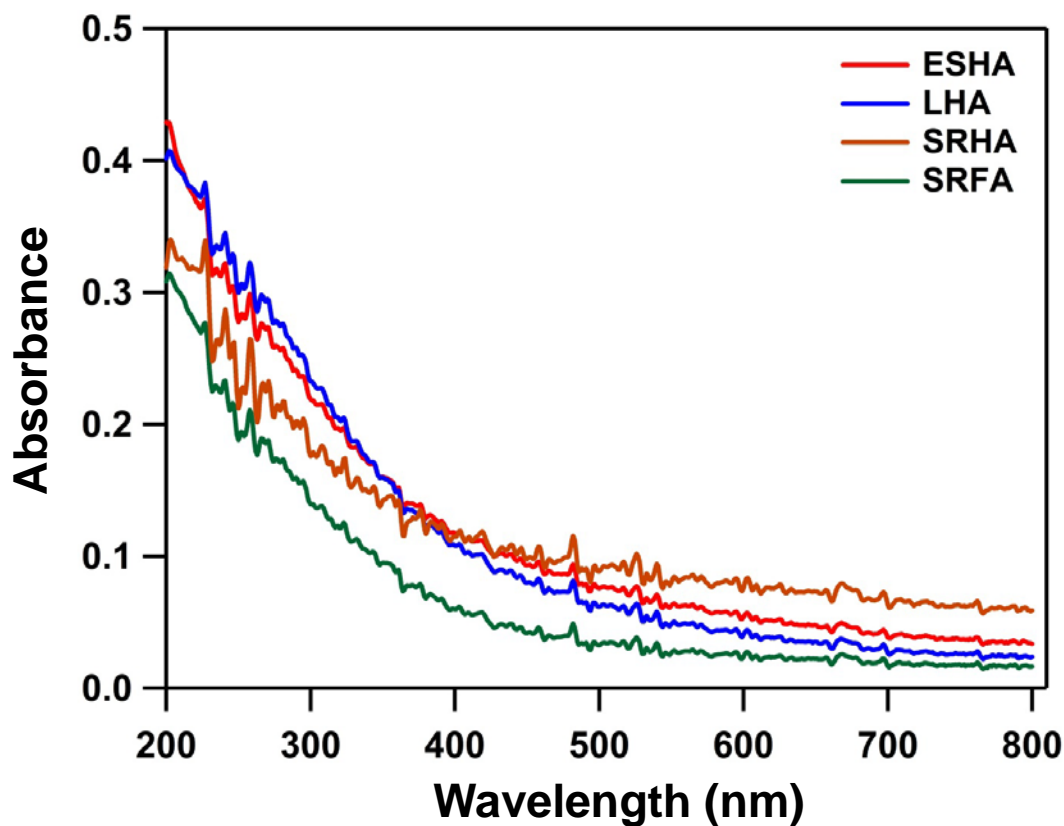
Figure 2-7. Absorbance scans for 5 mg/L solutions of Elliot Soil Humic Acid (ESHA), Leonardite Humic Acid (LHA), Suwanee River Humic Acid (SRHA) and Suwanee River Fulvic Acid (SRFA) at pH 7. Solutions were prepared in 5 mM phosphate buffer, and absorbance scans were normalized relative to a blank comprised of this buffer solution.

Estimation of Light Screen Factors in

DOM-containing Solutions

Following the method from Leifer [61], we calculated light screening factors (S_λ) for the direct photolysis of 10 μM 17β-trenbolone in 10 mg/L ESHA, 10 μM 17β-trenbolone in 50 mg/L FHA, and 2.5 μM MGA in 10 mg/L ESHA (all of which are representative conditions for our experiments).

$$S_\lambda = \frac{k_{d\beta}}{k_d} = (1 - 10^{-\alpha_\lambda l})/(2.303\alpha_\lambda l) \qquad (5)$$

In equation 5, $k_{d\beta}$ is the first-order direct photoreaction rate constant in the water with dissolved organic matter and k_d is the first-order direct photoreaction rate constant in pure water. Further, l is the path length of the cell (i.e., quartz cuvette), which is 1 cm in this case for, and α_λ is the absorption coefficient of an aqueous solution at wavelength λ in the natural logarithm system which can be calculated by equation 6.

$$A_\lambda = (\alpha_\lambda + \epsilon_\lambda[C])l \qquad (6)$$

In equation 6, ϵ_λ is the molar absorptivity at wavelength λ ($M^{-1}cm^{-1}$).

We found these wavelength dependent screening factors vary between are 0.65-0.97, 0.43-0.96 and 0.79-0.99 over 300 nm to 800 nm, respectively, for the systems described above. These values agree well with the decrease in direct photolysis rate we observed experimentally in these DOM-containing systems.

Indirect Photolysis of Zeranol and

its Metabolites at Neutral pH

Although they did not undergo direct photolysis, zeranol and its metabolites were reactive in irradiated solutions of humic and fulvic acids. At pH 7.0, zeranol loss was observed in all solutions (5 mg/L) of model DOM (Figure 2-8a), with the greatest rate of decay being observed for ESHA ($t_{1/2} \sim 3$ h) while SRFA was least active ($t_{1/2} \sim 19$ h).

Comparable reactivity was also observed for β-zeralanol and zearalanone in ESHA systems (Figure 2-9 and Table 2-3), suggesting similar mechanisms of transformation across the compound class. Dark controls with all species both in irradiated systems without ESHA (i.e., direct photolysis) and in dark (i.e., non-irradiated) solutions of ESHA were stable over relevant time scales, suggesting no other loss processes occurred. As is evident, zeranol, β-zearalanol and zearalanone exhibit comparable transformation rates in the presence of ESHA, suggesting similarities in the entities, mechanisms and functionality moieties on each structure responsible for reaction. Rather, our results are most consistent with a reaction between zeranol and reactive species generated upon irradiation of DOM [e.g., reactive oxygen species (ROS) or triplet DOM (^{3}DOM*)].

Comparison of measured $t_{1/2}$ values for zeranol to the steady-state ROS concentrations in irradiated HA and FA solutions at pH 7.0 provided an initial assessment of possible photooxidant(s) responsible for attenuation. This comparison is shown in Table 2-3 for steady-state concentrations of hydroxyl radical ($[^\bullet OH]_{ss}$) and singlet oxygen ($[^1O_2]_{ss}$) in DOM solutions, concentrations that were measured in the absence of zeranol. Both $^\bullet OH$ and $^1O_2$ were quantifiable in all solutions; whereas $[^\bullet OH]_{ss}$ values were roughly constant in all systems, Table 2-3 reveals that zeranol half-lives loosely scale with $[^1O_2]_{ss}$.

Furthermore, established routes for $^\bullet OH$ and $^1O_2$ formation (i.e., the Fenton reaction and $^1O_2$ sensitizers such as Rose Bengal or Erythrosin B, respectively) revealed that both oxidants are indeed reactive toward zeranol. From competition kinetic experiments (Figure 2-10) attempting to quantify second-order rate coefficients for the reaction of each ROS with zeranol, we can estimate second-order rate coefficients for zeranol reaction with $^\bullet OH$ ($k_{zeranol/\bullet OH} = 7.40$ x $10^9 \pm 0.06$ M^{-1}s^{-1}) and $^1O_2$ ($k_{zeranol/1O2} = 1.48$ x $10^7 \pm 0.01$ M^{-1}s^{-1}). Notably, for the reaction with $^1O_2$, the use of alternative singlet oxygen sensitizers (e.g., methylene blue and Erythrosin B) yielded comparable results. These alternative sensitizers were considered because excited states of Rose Bengal can react with some compounds directly [76]. Such a reaction does not appear to be at play in

our systems with Rose Bengal and zeranol given the consistency of our results with alternative sensitizers.

However, we caution that because of the pH-dependent nature of zeranol photolysis in DOM-containing systems (see Figure 2-17 in the later section), these estimated second-order rate coefficients may be of limited value for predicting zeranol persistence in surface waters. For example, based upon measured values of $[^{\bullet}OH]_{ss}$ in ESHA systems (see Table 2-3) and the value of $k_{zeranol/\bullet OH}$ reported above, we would anticipate the $t_{1/2}$ value for zeranol reaction with $^{\bullet}OH$ to be far longer (~50 h) than was actually observed experimentally (~ 3 h). We believe this discrepancy is an indication that the monodeprotonated form of zeranol is an important, if not dominant, reactive species toward photogenerated oxidants at pH 7. The value of $k_{zeranol/\bullet OH}$ reported above was measured via the Fenton reaction at pH 3, at which it is reasonable to assume the primary reaction occurs between the fully protonated (i.e., neutral) form of zeranol with $^{\bullet}OH$. At higher pH values where the monodeprotonated (and eventually dianionic) zeranol form is prevalent, it too would likely react with $^{\bullet}OH$, and generally be expected to exhibit a higher second-order rate coefficients for this process. Similarly, the value of $k_{zeranol/1O2}$ reported above assumes all of the zeranol is in its fully protonated (i.e., neutral) form. However, our experiments with Rose Bengal were conducted at pH 7, where a very small, but potentially highly reactive, fraction of zeranol will be present in an anionic state. To more accurately predict zeranol persistence in DOM-containing systems, more work is needed to determine how values of $k_{zeranol/\bullet OH}$ and $k_{zeranol/1O2}$ (as well as for the reaction with $^{3}DOM^{*}$) vary as a function of the pH and ionization state of zeranol.

Closer examination suggests that $^{1}O_2$ is most likely not responsible for zeranol loss in our HA and FA solutions at pH 7.0. Experiments conducted in the presence of excess azide (10 mM), commonly used as a quencher for $^{1}O_2$ [77, 78], revealed no inhibition of zeranol decay relative to azide-free systems (Figure 2-8b). Similarly,

experiments conducted in pure D_2O (Figure 2-8b), in which the lifetime of $^1O_2$ is greater than in H_2O thus promoting its reactivity[79], did not exhibit enhanced rates of zeranol transformation. Additional experiments with selective quenchers provided greater insight into the species responsible for zeranol attenuation at neutral pH. Excess formate (50-100 mM) or similar radical scavenger (e.g., isopropanol) slowed zeranol decay by roughly 50% (Figure 2-8c).

Table 2-3. Hydroxyl radical and singlet oxygen steady state concentration (in M) and zeranol decay half-lives in systems of irradiated model humic and fulvic acids (at pH 7). Uncertainties represent 95% confidence intervals from linear regression analyses used in the quantification of these values.

Dissolved Organic Matter	Hydroxyl Radical ($^\bullet$OH)	Singlet Oxygen ($^1O_2$)	Zeranol Half-Life (h)
Elliott Soil Humic Acid	$(5.5 \pm 0.3) \times 10^{-16}$	$(6.70 \pm 0.13) \times 10^{-13}$	3.20 ± 0.14
Leonardite Humic Acid	$(6.0 \pm 0.8) \times 10^{-16}$	$(2.09 \pm 0.14) \times 10^{-13}$	5.6 ± 0.6
Suwannee River Humic Acid*	$(3.8 \pm 0.6) \times 10^{-16}$	$(7.55 \pm 0.71) \times 10^{-14}$	11 ± 2
Suwannee River Fulvic Acid	$(4.6 \pm 0.7) \times 10^{-16}$	$(8.32 \pm 0.38) \times 10^{-14}$	19 ± 6

*As a useful point of reference, Kohn and Nelson[80] reported steady-state concentrations of singlet oxygen and hydroxyl radical of 5×10^{-14} M and 10^{-16}, respectively, in irradiated solutions with 5 mg/L SRHA at pH 7.5. These were generated with an Oriel solar simulator equipped with a 1000 W Xe lamp as their light source. These values compare favorably with those that we measured in SRHA systems.
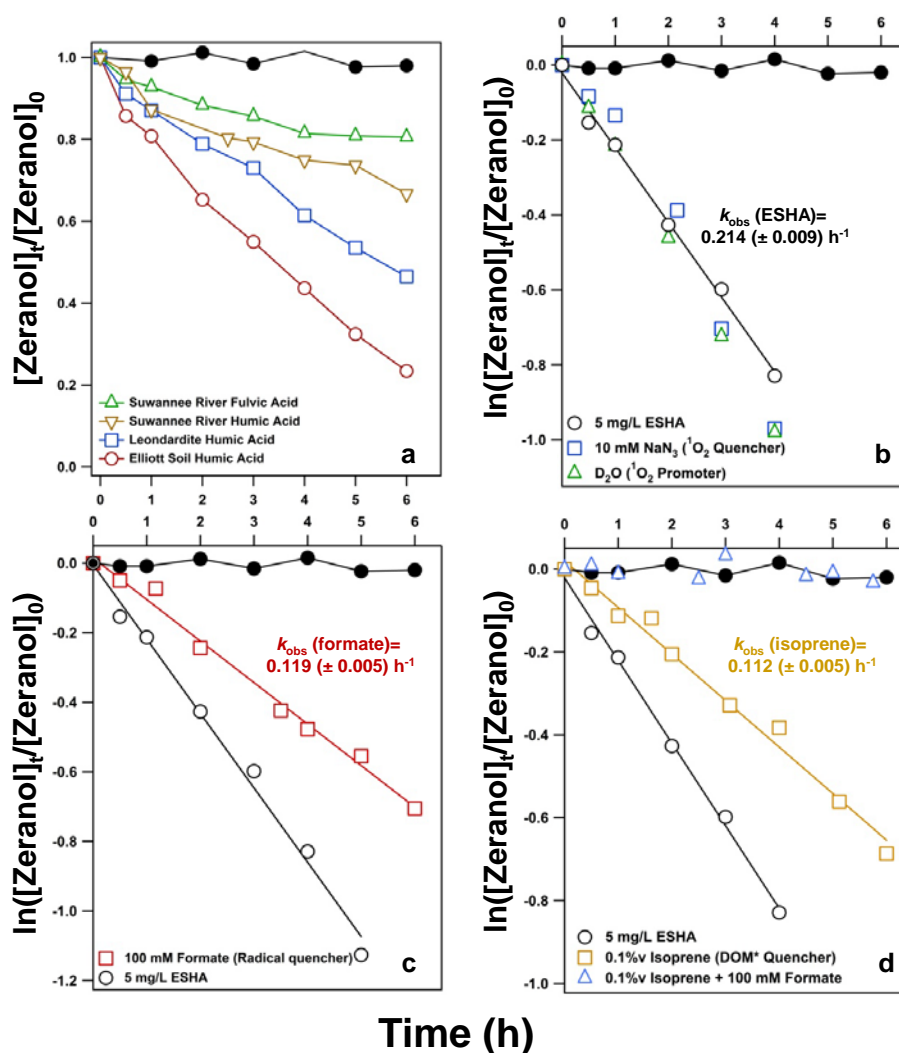
Figure 2-8. (a) Zeranol transformation in the presence of model humic acids (HA) and fulvic acids (FA) during irradiation with simulated light. Also shown are results of selective quencher experiments illustrating the effect of (b) 10 mM sodium azide (a singlet oxygen quencher) and D₂O (a singlet oxygen promoter), (c) 100 mM sodium formate (a hydroxyl radical quencher) and (d) 0.1% v/v of isoprene (a triplet state quencher) on zeranol transformation in the presence of ESHA irradiated with simulated light. Also in panel d, isoprene and formate, when added simultaneously, were able to entirely inhibit zeranol loss. In all instances, the initial concentration of zeranol was ~5μM, the concentration of each HA or FA was 5 mg/L, and the pH was maintained at pH 7 using 5 mM phosphate buffer. In panels b-d, lines represent best-fit linear regressions from which pseudo-first order rate constants for zeranol decay (k_{obs} values) were obtained. Uncertainties on k_{obs} values represent one standard deviation of the slopes obtained from linear regression analysis. Black symbols represent controls, in which zeranol was stable in both irradiated systems without model HA and FA (i.e., direct photolysis) and in dark (i.e., non-irradiated) solutions of model HA and FA.
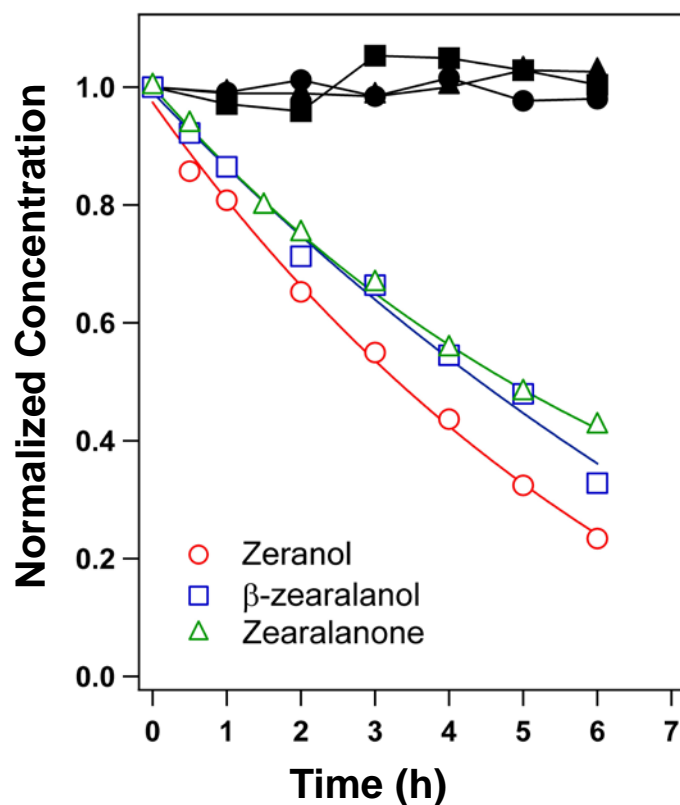
Figure 2-9. Transformation of zeranol, β-zearalanol and zearalanone in irradiated (simulated sunlight) solutions of 5 mg/L Elliot Soil humic acid (ESHA). In all instances, the initial concentration of zeranol and its metabolites was ~5 µM and the pH was maintained at 7 using a 5 mM phosphate buffer. Solid black data points represent controls, colored lines represent exponential decay model fits from which rate constants for decay and corresponding half-lives (as reported in Table 2-2) were quantified.
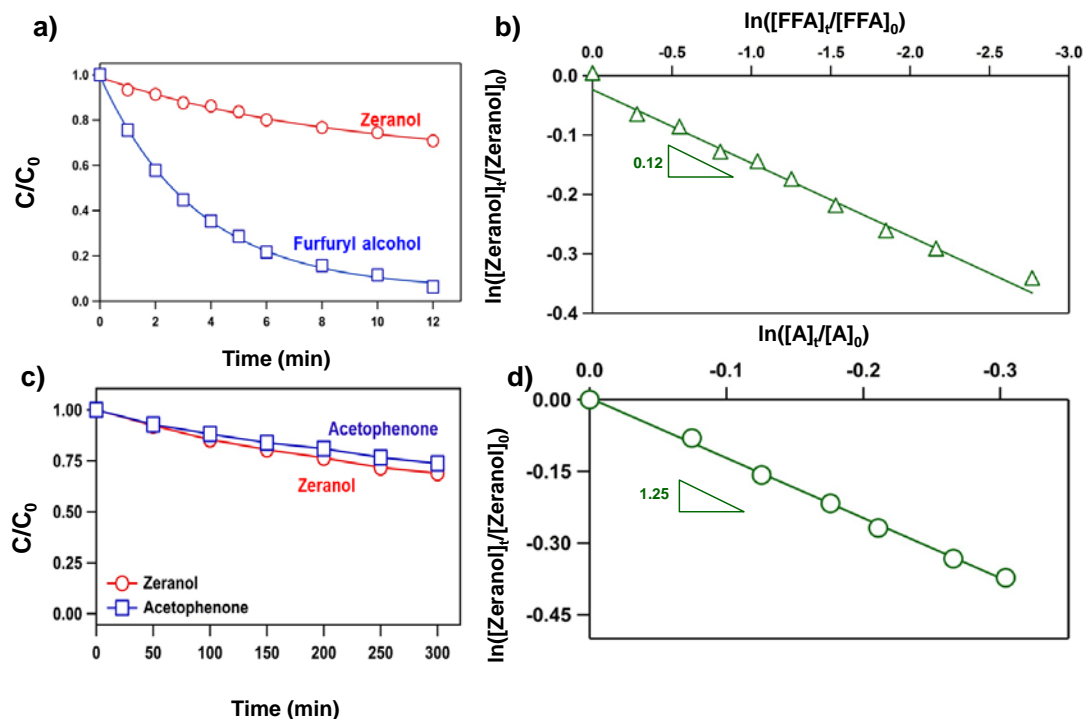
Figure 2-10. (a) Change in zeranol and furfuryl alcohol (FFA) concentration as a function of time in irradiated (simulated sunlight) solutions of 2 μM Rose Bengal at pH 7 in 5 mM phosphate buffer and (b) plots of the natural log of normalized zeranol concentration as a function of the natural log of normalized FFA concentration, the slopes of which were used in equation 3 to determine the second-order rate coefficient for zeranol reaction with singlet oxygen ($^1O_2$). (c) Change in zeranol and acetophenone (A) concentration as a function of time in pH 3 solutions containing 60 μM each of Fe^{2+} and H_2O_2 to generate hydroxyl radical ($^•OH$) via the Fenton reaction. (d) Plots of the natural log of normalized zeranol concentration as a function of the natural log of normalized acetophenone concentration, the slopes of which were used in equation 4 to determine the second-order rate coefficient for zeranol reaction with $^•OH$.

No further inhibition was observed if higher concentrations of radical scavenger were used, suggesting that $^{\bullet}OH$ contributes to some but not all of the zeranol transformation observed. Additionally, catalase, which breaks down H_2O_2, inhibited zeranol decay by a similar magnitude to that of radical scavengers (Figure 2-11). Results show that the addition of 200 U/mL catalase inhibited zeranol transformation by ~50%, consistent with H_2O_2 playing some role in zeranol transformation. Notably, H_2O_2 was unreactive toward zeranol in dark controls. We propose that the photolysis of H_2O_2 is an important route for $^{\bullet}OH$ formation in these systems, with $^{\bullet}OH$ representing one of the primary species directly responsible for zeranol transformation (see Figure 2-8 demonstrating influence of radical quenchers on rates of zeranol transformation in irradiated ESHA systems). Therefore, catalase appears to inhibit zeranol transformation by limiting H_2O_2 build up in solution, which in turn lowers the amount of $^{\bullet}OH$ available for reaction with zeranol. Further evidence in support of such a scenario was obtained with the addition of 2 U/mL superoxide dismutase (SOD) to the system, which enhanced the rate of zeranol transformation by roughly 2-fold. We believe the increase in H_2O_2 production resulting from SOD in turn enhances $^{\bullet}OH$ formation via subsequent photolysis of H_2O_2. Formation of H_2O_2 was quantifiable in irradiated DOM systems (Figure 2-12), but it was unreactive toward zeranol in dark control systems (Figure 2-13). The concentration of H_2O_2, which was determined colorimetrically via the methods described above, increased steadily over time in all systems (Figure 2-12). We note that as a result of the steadily increasing concentration of H_2O_2 observed, the values of $[^{\bullet}OH]_{ss}$ reported in Table 2-3 are best viewed as an average of the relative amount of hydroxyl radical produced in each DOM system over the timescales relevant to zeranol transformation (~6h). In actuality, the increasing concentration of H_2O_2 should in turn produce concentrations of hydroxyl radical in DOM systems that increase slightly with irradiation time. Furthermore, as shown in Figure 2-13, while stable in the dark, suggesting H_2O_2 cannot oxidize zeranol over these timescales, appreciable zeranol decay

was observed upon the irradiation of H_2O_2. Photolysis of H_2O_2 is known to generate hydroxyl radicals, and it would appear that the loss of zeranol in the irradiated H_2O_2 system results from this $^\bullet OH$ formation. Using a pseudo-first-order kinetic model for zeranol decay (i.e., exponential decay) yields a k_{obs} value of 0.18 h^{-1}. This k_{obs} value is on par with that measured in 5 mg/L ESHA systems quenched with excess isoprene (0.112 h^{-1}; see Figure 2-8). Recall, that in the presence of excess isoprene, the primary reactive photooxidant in ESHA systems is $^\bullet OH$ generated via the photolysis of H_2O_2. We believe the reasonable agreement between these k_{obs} values supports our hypothesis that photolysis of H_2O_2 is the primary route to $^\bullet OH$ formation in our ESHA systems.

Thus, the role of H_2O_2 in zeranol decay is likely linked to its photolysis, which generates $^\bullet OH$ [81]. Such a scenario is supported by experiments revealing comparable zeranol decay in irradiated systems free of DOM but containing 5 μM H_2O_2 (Figure 2-13) a concentration representative of that measured in our irradiated DOM suspensions. Also consistent with H_2O_2 photolysis as a major route to $^\bullet OH$ formation, addition of superoxide dismutase, which converts superoxide radical anion ($O_2^{\bullet-}$) into H_2O_2, enhanced the rate of zeranol decay (Figure 2-11). We attribute this enhancement to the subsequent photolysis of H_2O_2 produced via superoxide dismutase.

Evidence suggests that the remainder of zeranol transformation occurs via reaction with triplet, or excited state, DOM ($^3DOM^*$). Zeranol decay persisted in deoxygenated systems, in which ROS should not be generated at appreciable levels, which is consistent with direct reaction with $^3DOM^*$ (Figure 2-14). The observation of zeranol transformation in the absence of O_2 suggests a reaction pathway not involving reactive oxygen species (ROS), which will not be generated to appreciable extents in the absence of oxygen. However, the rate of zeranol transformation was still smaller in the O_2 free system, consistent with some contribution from ROS during zeranol transformation in O_2 containing systems. Collectively, we believe these observations agree well with the results of quencher studies that implicate hydroxyl radical and triplet

state DOM as the dominant reactive species toward zeranol. Furthermore, the presence of 0.1% v/v isoprene, commonly utilized as a triplet quencher[82, 83], inhibited zeranol decay by ~50% (Figure 2-8d), thereby accounting for the remainder of the loss we assume is not attributable to $^\bullet$OH (i.e., the amount of zeranol transformation observed in the presence of excess formate or isopropanol). Zeranol is moderately hydrophobic (reported $\log K_{ow}$ of 3.88) [50], and thus a small fraction would likely be associated with HA and FA in solution, which in turn would promote its direct reaction with ^{3}DOM*. A role for ^{3}DOM* in the photooxidation of zeranol is perhaps not surprising, as Canonica and co-workers[84, 85] have previously established that excited triplet states generated during DOM irradiation are important photooxidants for substituted phenols, which represents reasonable structural analogues for zeranol family compounds. Finally, we note that irradiated suspensions of ESHA containing both a radical (formate) and triplet (isoprene) quencher completely shut down zeranol decay over the timescales typically observed (Figure 2-8d), further supporting $^\bullet$OH and ^{3}DOM* as dominant reactive species in our systems at pH 7.

Although zeranol decay in the ESHA system was investigated most extensively, we believe •OH and ^{3}DOM* are also dominant species at play in other HA and FA systems at neutral pH. Similar experiments with quenchers and probes with Leonardite HA (Figure 2-15) were also consistent with a role for these reactive species. As shown in the figure, the use of D_2O as a $^1O_2$ promoter did not significantly enhance zeranol decay, suggesting (as was observed with ESHA and in natural water samples) that $^1O_2$ is not primarily responsible for zeranol transformation. Addition of 25 mM isopropanol as a •OH quencher inhibited the zeranol decay by ~40% while 0.1% v/v of isoprene as a ^{3}DOM* quencher inhibited the zeranol decay by about ~60%. Once again, this suggests that •OH and ^{3}DOM* are the dominant species responsible for zeranol transformation. Further, •OH and ^{3}DOM* appear to be the key players responsible for the decay of zeranol metabolites at pH 7.0. Results from experiments with zearalanone in irradiated
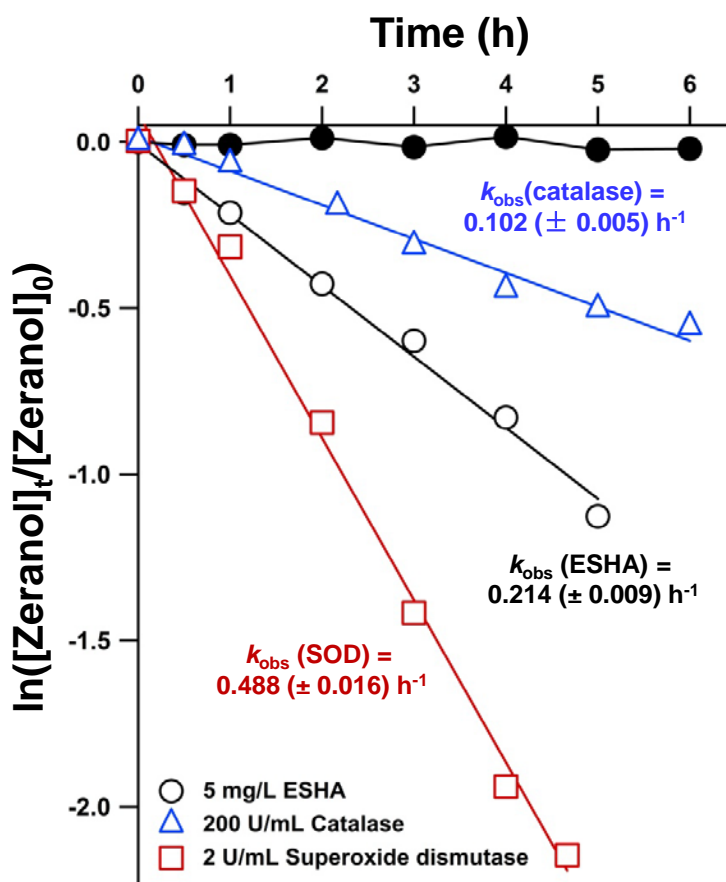
Figure 2-11. Zeranol transformation in irradiated (simulated sunlight) solutions of 5 mg/L ESHA. Also shown are the influence of catalase, a quencher for hydrogen peroxide (H_2O_2), and superoxide dismutase, which converts superoxide radical anion into H_2O_2, on the rate of zeranol transformation in this system. The initial concentration of zeranol was ~5μM and the pH was maintained at 7 using 5 mM phosphate buffer. Lines represent best-fit linear regressions from which pseudo-first order rate constants for zeranol transformation (k_{obs} values) were obtained. Uncertainties associated with k_{obs} values represent one standard deviation obtained from regression analysis.
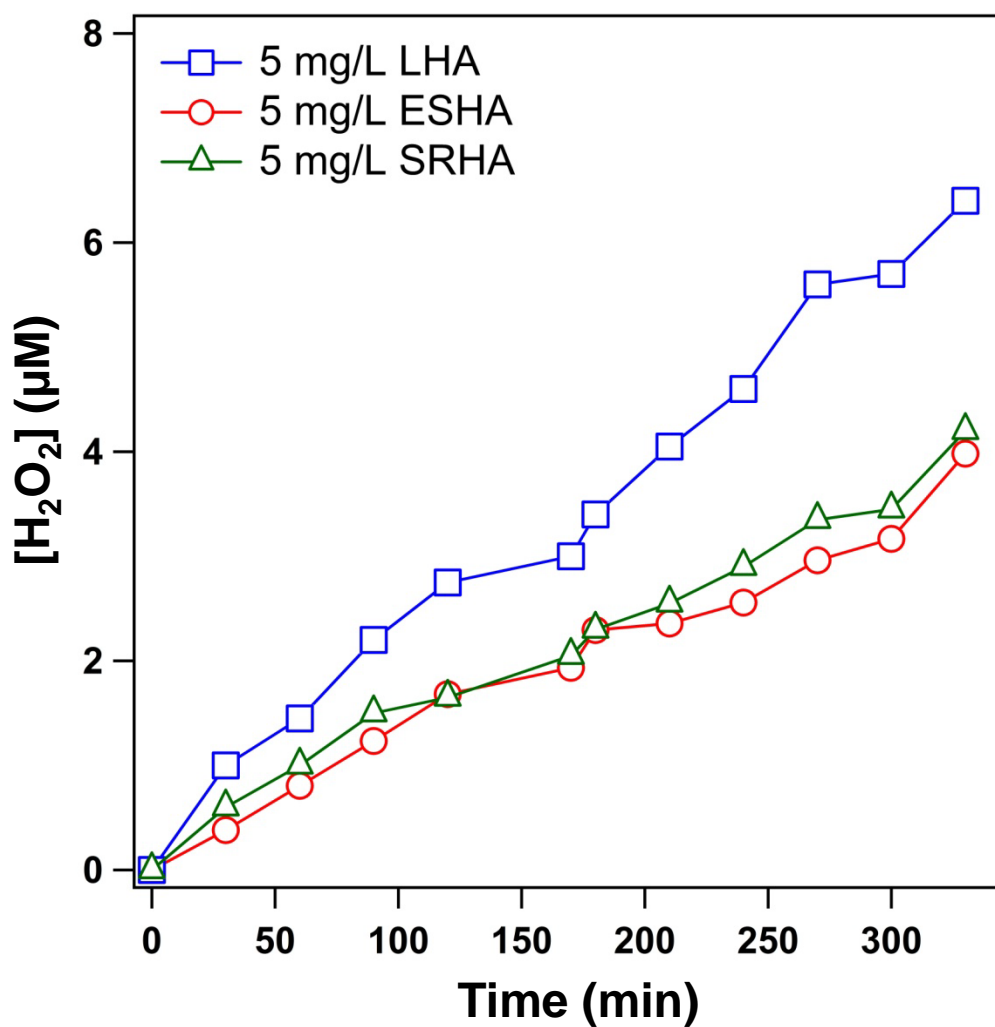
Figure 2-12. Hydrogen peroxide (H_2O_2) production over time in irradiated (simulated sunlight) solutions of Leonardite humic acid (LHA), Elliot Soil humic acid (ESHA) and Suwanee River humic acid (SRHA). Model humic acids were present at 5 mg/L and pH was maintained at 7 using a 5 mM phosphate buffer. These experimental systems did not contain any zeranol.
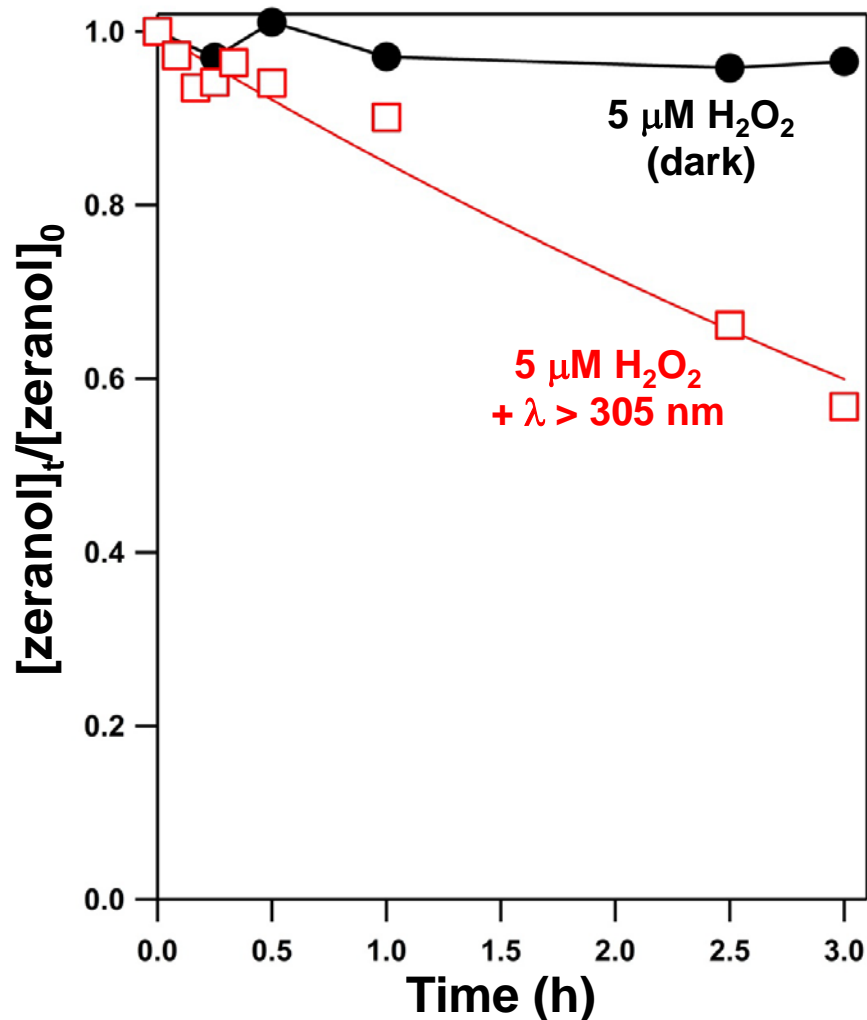
Figure 2-13. Normalized concentration of zeranol (~5 μM) as a function of time in solutions containing 5 μM H_2O_2 at pH 7 (these conditions are representative of those in our irradiated DOM suspensions; see Figure 2-12). Results are shown for H_2O_2 containing systems in the dark, as well as a solution of H_2O_2 exposed to light with $\lambda >$ 305 nm from the commercially available Xe Arc lamp.
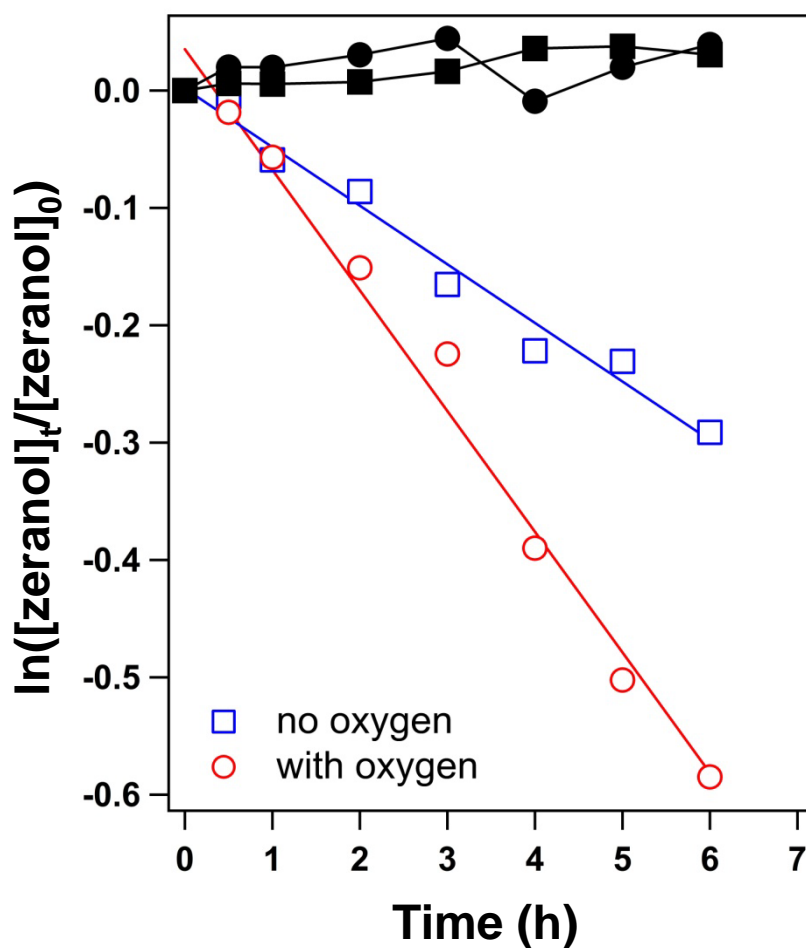
Figure 2-14. Semi-log plot of normalized zeranol concentration over time for irradiated (simulated sunlight) solutions of 5 mg/L ESHA conducted in the presence and absence of O_2. These experiments were conducted in a custom photoreactor with a screw top fitted with a quartz window, thereby allowing the O_2 level in the system to be controlled as described in the experimental section above. Experiments were conducted at pH 7 (5 mM phosphate buffer) using an initial zeranol concentration of ~5 µM. Solid black data points represent controls, in which zeranol exhibited stability both in irradiated systems without ESHA (i.e., direct photolysis) and in dark (i.e., non-irradiated) solutions of ESHA regardless of dissolved O_2 concentration.

ESHA systems at pH 7.0 containing formate and isoprene (Figure 2-16) mirror the behavior observed for zeranol. Roughly 50% of the zearalanone decay was inhibited via the addition of 100 mM formate as a hydroxyl radical quencher while about 80% of the reactivity was inhibited with the addition of 0.1% v/v isoprene as a ^{3}DOM* quencher. Isoprene and formate, when added simultaneously, were able to entirely inhibit zearalanone transformation, supportive of hydroxyl radical and ^{3}DOM* as the primary species responsible for zearalanone indirect photolysis (as was also observed for zeranol).

<div align="center">

Indirect Photolysis of Zeranol in

Slightly Alkaline Solutions

</div>

The –OH groups on zeranol have reported pKa values of 8.44 and 11.42 [45], and thus its reactivity toward photogeneraetd ROS is likely to increase as these groups deprotonate. Indeed, while zeranol remained stable in the absence of ESHA with increasing pH, its rate of transformation increased by more than one order of magnitude in the presence of ESHA (5 mg/L) as pH increased from 7.0 to 9.0 (Figure 2-17a). Based on additional studies with phenol and furfuryl alcohol, the concentration of photogenerated $^\bullet$OH and ^{1}O$_2$, respectively, did not change significantly over this pH range. Thus, this increase in reactivity is most consistent with deprotonated forms of zeranol, which become more concentrated at higher pH values, being the primary reactivity entities toward photogenerated oxidants. The inset in Figure 2-17a shows a log-log plot of the k_{obs} values for zeranol decay in irradiated ESHA suspensions measured between pH 7.0 to 9.0 as a function of the corresponding concentration of the monodeprotonated form of zeranol ([zeranol$^-$]; assuming a pK$_{a1}$ of 8.44). The slope of this log-log plot is equivalent to unity, suggesting a first-order dependence of the rate of photoreaction on the concentration of the monodeprotonated species.
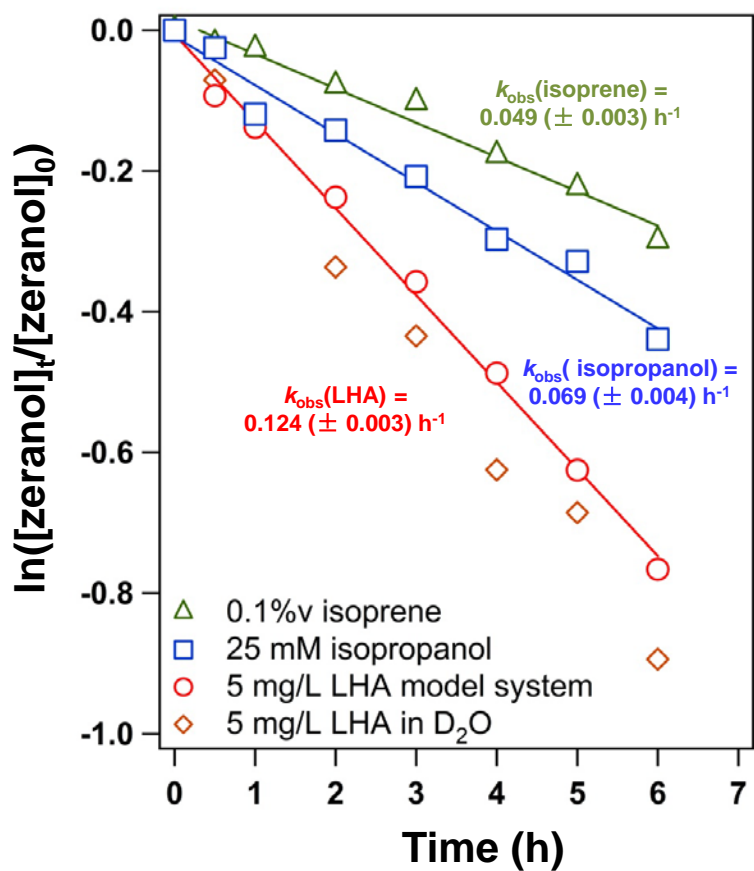
Figure 2-15. Semi-log plot of normalized zeranol concentration over time for irradiated (simulated sunlight) solutions of 5 mg/L Leonardite humic acid (LHA). Also shown is the influence of different selective quenchers and promoters on zeranol transformation rates in irradiated LHA solutions. Lines represent best-fit linear regressions from which pseudo-first order rate constants for zearalanone decay (kobs values) were obtained. Uncertainties associated with kobs values represent one standard deviation obtained from regression analysis.
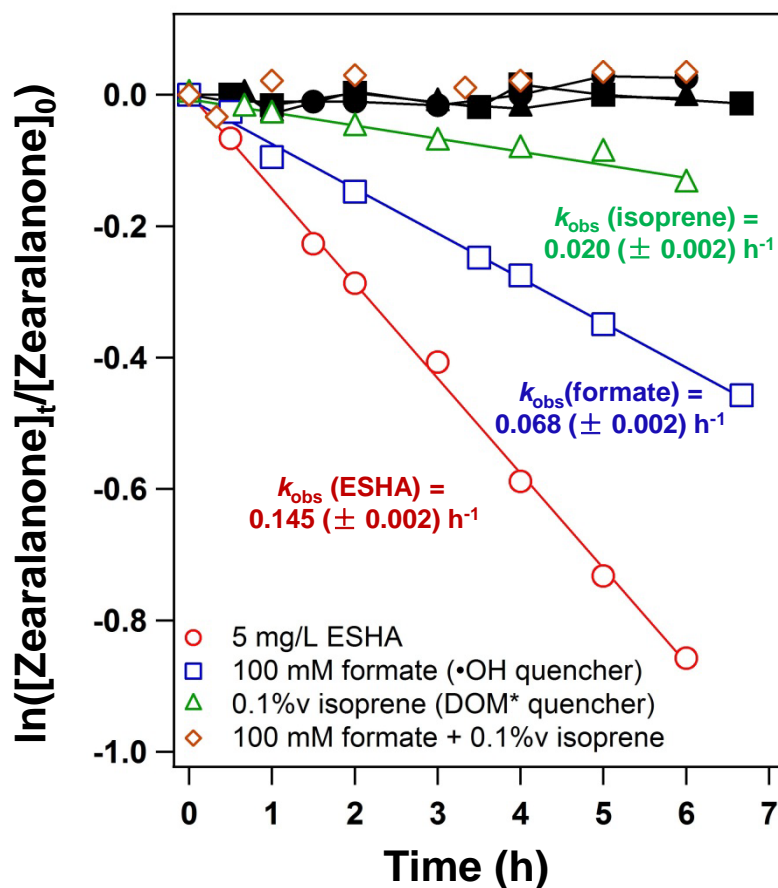
Figure 2-16. Semi-log plot of normalized zearalanone concentration over time for irradiated (simulated sunlight) solutions of 5 mg/L ESHA. Also shown is the influence of different selective quenchers on the rate of zearalanone indirect photolysis in the presence of 5 mg/L ESHA. Lines represent best-fit linear regressions from which pseudo-first order rate constants for zearalanone decay (k_{obs} values) were obtained. Uncertainties on k_{obs} values represent one standard deviation obtained from regression analysis. Solid black data points represent controls, in which zeranol exhibited stability both in irradiated systems without ESHA (i.e., direct photolysis) and in dark (i.e., non-irradiated) solutions of ESHA.
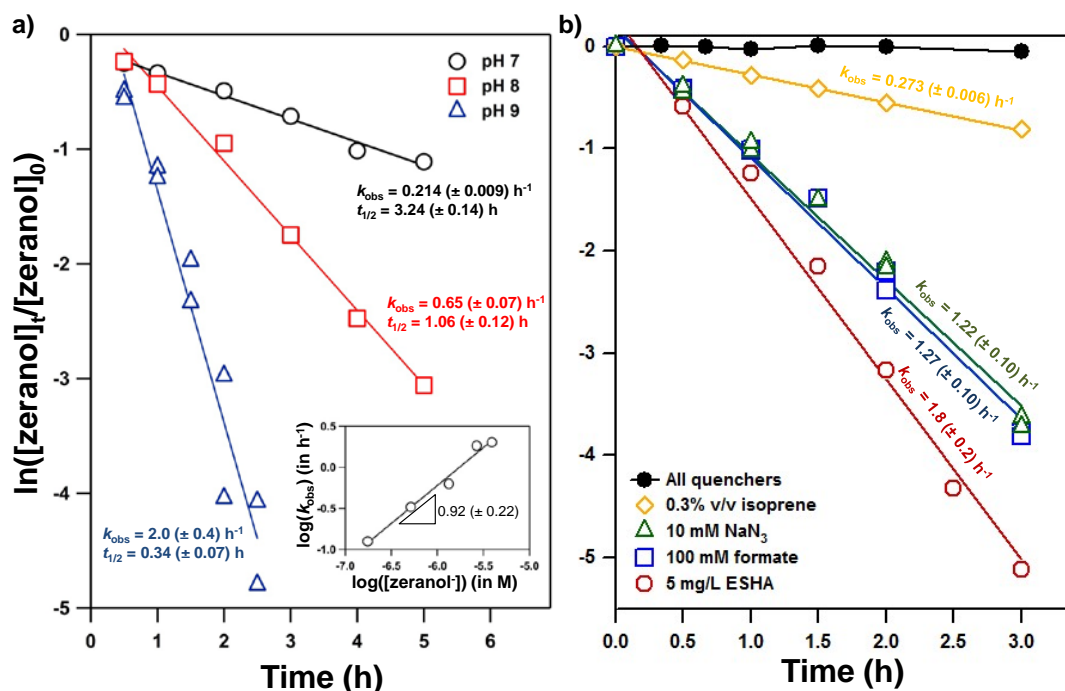
Figure 2-17. (a) Plots of the natural log of normalized zeranol concentration as a function of time in irradiated solutions of 5 mg/L of ESHA at pH 7, 8 and 9. Values of k_{obs} (with 95% confidence intervals) obtained from linear regression analyses are provided. The inset shows a log-log plot of k_{obs} values as a function of the concentration of the monodeprotonated form of zeranol ([zeranol⁻]; pK_{a1} 8.44), with a slope equivalent to unity. (b). Results of quencher experiments conducted at pH 8.5 in solutions of 5 mg/L of ESHA. Values of k_{obs} (with 95% confidence intervals) obtained from linear regression analyses are provided. Given the modest decrease observed with formate and sodium azide, results from duplicate experiments are presented to illustrate reproducibility. In all instances, the initial concentration of zeranol was ~5μM, the concentration of each HA or FA was 5 mg/L, and the pH was maintained at pH 7 and 7.5 using 5 mM phosphate buffer, while solutions at pH 8-9 were maintained with a 5 mM borate buffer.

Although $^1O_2$ does not appear to contribute to zeranol decay in our model DOM systems at pH 7.0, evidence suggest it may play a role in slightly alkaline pH waters. Additional experiments with selective quenchers at pH 8.5 suggest that $^3DOM^*$ is still a major contributor to zeranol transformation in irradiated ESHA suspensions (Figure 2-17b) based on the inhibition observed in the presence of excess isoprene (0.3% v/v). Excess formate (a radical quencher) yielded a small, but reproducible, decrease in zeranol transformation consistent with a continued role for $^\bullet OH$ at pH 8.5. Unlike at pH 7.0, the use of 10 mM sodium azide, a $^1O_2$ quencher, also resulted in a modest yet reproducible amount of inhibition. Most importantly, complete suppression of zeranol decay at pH 8.5 was only observed in systems with all three quenchers present, consistent with $^3DOM^*$, $^\bullet OH$, and $^1O_2$ all contributing to zeranol decay to some extent. Thus, while the contribution of $^1O_2$ to zeranol decay appears negligible at neutral pH, it appears to become more significant with increasing pH value. We assume this increase is because of its greater reactivity toward anionic zeranol species.

<u>Photolysis of SGPMs in Neutral pH Natural Waters</u>

Finally, additional experiments with natural water samples indicate that the phototransformation mechanism observed in model aquatic systems also occur in more complicated waters representative of agriculturally impacted ecosystems. Rates of direct photolysis for 17β-trenbolone were essentially equivalent in circumneutral pH water (pH 6.8-7.0) collected from a runoff-impacted, high DOC creek (50 mg/L) and a low DOC agricultural return water (6 mg/L). Moreover, these rates compared favorably to that measured in model systems of phosphate buffer (Figure 2-18a and 2-18b). Addition of ROS quenchers including formate and isoprene had no effect on 17β-trenbolone transformation rate, nor was the decay rate influenced when experiments were conducted in a 50:50 mixture of natural water sample and D_2O. Thus, despite the presence of relatively high DOC concentrations, indirect routes for 17β-trenbolone photolysis are

sufficiently slow relative to direct photolysis so as not to impact its persistence. We believe this to be generally true for all compounds in the TBA and MGA families.

Zeranol loss was observed upon irradiation of both natural water samples, with the greatest rate of transformation occurring in the high DOC creek water rather than the agricultural return water (Figure 2-18c and 2-18d). Rates of zeranol decay were within the range reported for 5 mg/L solutions of model humic and fulvic acids, and use of formate and isoprene as $^\bullet$OH and triplet DOM quenchers, respectively, inhibited zeranol transformation. Collectively, as was observed in model systems, results are consistent with indirect photolysis influencing the fate of zeranol in sunlit surface waters, with a prominent role for $^\bullet$OH and ^{3}DOM* in this process.

As in model systems, rates of 17β-trenbolone photolysis were essentially independent of water quality and the addition of quenchers (formate and isoprene) and promoters (50:50 water sample:D_2O) had no impact on its transformation rate. In contrast, zeranol transformation was greatest in the high DOC creek water, and the addition of isoprene and formate was able to entirely inhibit the reaction of zeranol. Again, this behavior is consistent with that observed in model systems for zeranol, supporting hydroxyl radical and triplet DOM as the primary species responsible for zeranol transformation in irradiated solutions of dissolved organic matter.

<u>Preliminary Assessment of Direct Photolysis Products</u>

Because of the relatively rapid rate of TBA and MGA family direct photolysis, information on the photoproducts generated via this process will be essential to assessing fully their impact on ecosystem health. We present an introduction to these photoproducts here, while an extensive treatment of the identity, fate and ecotoxicological impacts of these direct photoproducts is the subject of a future study.
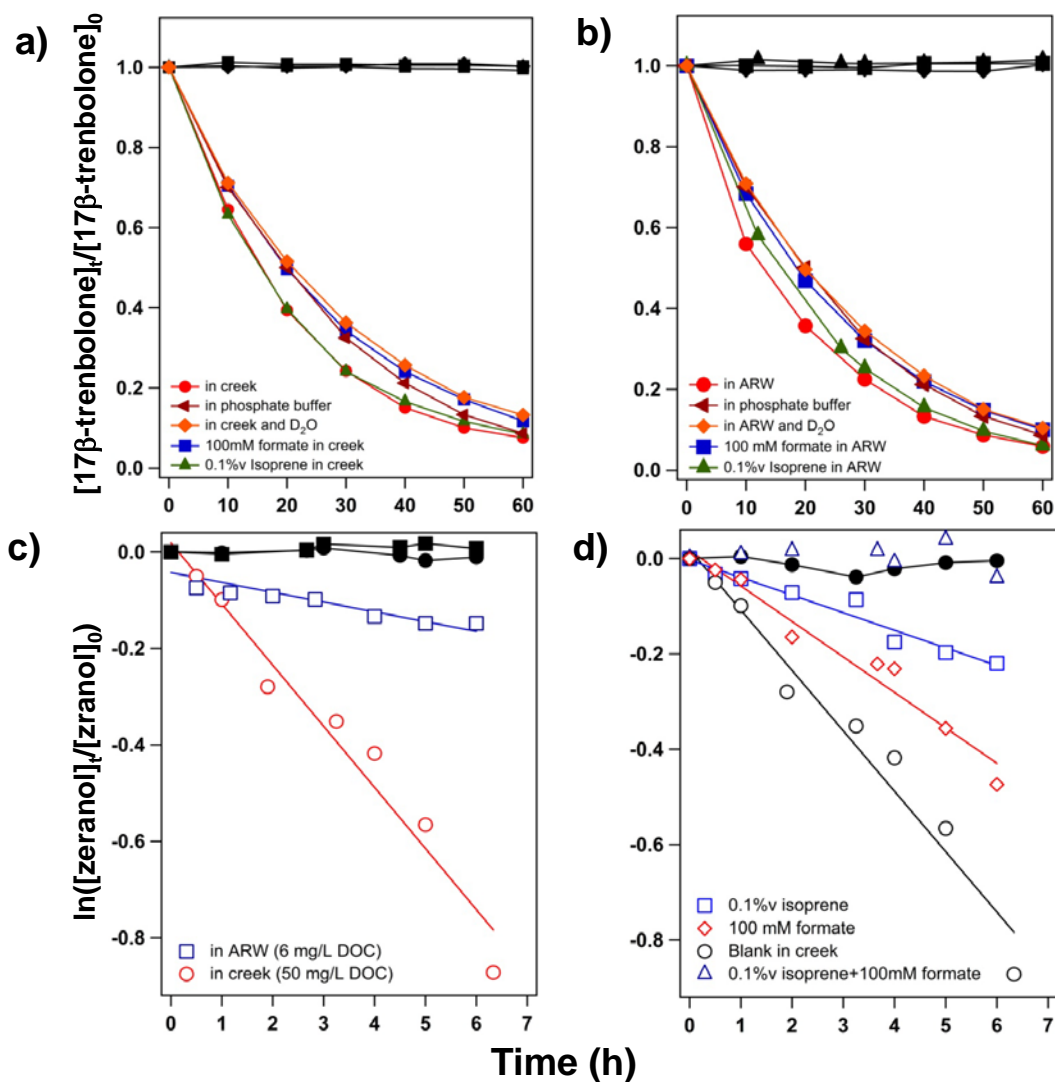
Figure 2-18. Effects of different quenchers and promoters on the rate of 17β-trenbolone direct photolysis in (a) high DOC creek water and (b) a low DOC agricultural return water (ARW) during irradiation with simulated light. For irradiation of these natural water samples with simulated sunlight, the relative rates of zeranol transformation are shown in (c) on a semi-log scale, whereas the effect of different quenchers on zeranol transformation in the high DOC creek water is presented in (d).

Within a compound class, no interspecies conversions were observed (e.g., based on comparison of known LC retention times, photolysis of 17β-trenbolone did not yield 17α-trenbolone or trendione, nor did photolysis of MGA yield melengestrol). Instead, both families of compounds photolyzed to yield mixtures of new species that are usually more polar (i.e., products elute earlier on a reverse phase LC column). Further, they exhibit primary absorption maxima at lower wavelengths outside the solar spectrum (Figure 2-19). 17β-trenbolone exhibits characteristic absorbance at 350 nm (see Figure 2-1c), and over 45 minutes, is nearly completely transformed via direct photolysis. During reaction, two new product peaks with absorbance maxima near 254 nm grow in over time. Based on the relative elution time on the reverse-phase LC column used for this analysis, these product peaks are more polar than 17β-trenbolone. Further, with maximum absorbance near 254 nm, these photoproducts will be more resistant to direct photolysis, and thus, will likely persist over longer time scales in sunlit surface waters relative to 17β-trenbolone. This is consistent with some degree of disruption to the conjugated π-bond systems characteristic to these species during photolysis. Analysis with LC/MS/MS suggests that direct photolysis yields rather modest structural transformations for these compounds, with most reaction products maintaining the steroidal ring and forming via simple hydroxyl addition (e.g., masses detected for 17β-trenbolone were m/z 289, 305, and 321, representing mono-, di-, and trihydroxy derivatives). We also cannot completely rule out the potential for photoisomerization at other stereochemical centers within TBA and MGA metabolites (e.g., methyl inversion at the C13 in TBA metabolites), as has been observed during the direct photolysis of estrone [86].

Based on these observations, photoproducts appear to be more, if not entirely, resistant to direct photolysis via sunlight, and are likely to persist in sunlit surface waters longer than the species from which they are derived. Given the slight structure modifications induced by direct photolysis, these more photoresistant products are also
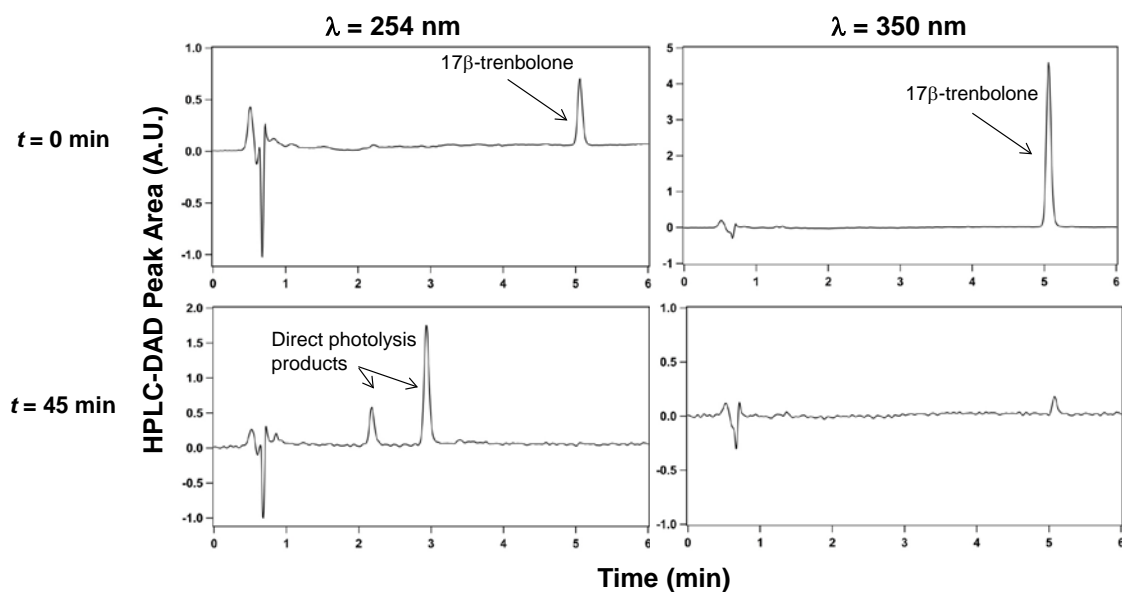
Figure 2-19. Representative LC-DAD chromatograms for samples taken during the photolysis of 17β-trenbolone. Chromatograms are shown as a function of irradiation time (0 and 45 min) and for two detection wavelengths on the DAD.

likely to retain some biochemical activity similar to their parents, the magnitude of which will be addressed in a future investigation.

2.5   Environmental Implications

This work provides some of the first evidence characterizing the persistence of synthetic hormone growth promoters in sunlit surface waters impacted by agricultural runoff. The trenbolone acetate and melengestrol acetate families, which share conjugated π-bond systems within their steroidal ring structure, are prone to direct photolysis and are likely to exhibit the least amount of persistence. They exhibit relatively short half-lives (1 hour or less), and their decay rates are largely invariant across a broad spectrum of aquatic conditions, implying that direct photolysis will be their dominant transformation mechanism in most sunlit surface waters. Indeed, relative to reports of their biotransformation in aerobic soil microcosms [87], time scales for the photolysis of TBA metabolites are considerably faster, although these transformation pathways are unlikely to compete with one another given their tendency to be localized in different environmental media. The near-constant rates of photolysis measured over the range of aquatic conditions considered may be advantageous; fate models should be able to better account for the contribution of photolysis to these species' environmental persistence.

Non-steroidal zeranol and its metabolites, which have little to no chromophoric activity within the solar spectrum, only transform via indirect photolysis. Therefore, their fate may be more difficult to predict because it will be highly dependent on the composition of the receiving water, with variables such as DOM concentration, type, and pH exerting an influence. The presence of sensitizers or other species that generate $^{\bullet}OH$ or $^1O_2$ at higher pH will shorten the lifetime of the zeranol family, whereas known scavengers (e.g., carbonate for $^{\bullet}OH$) would inhibit their indirect phototransformation. For example, we have conducted preliminary work with nitrate, another common agricultural

byproduct that photolyzes to yield $^\bullet$OH[88] (Figure 2-20), confirming its ability to facilitate zeranol transformation. A role for triplet state DOM in zeranol transformation is also noteworthy because zeranol and its metabolites are moderately hydrophobic and therefore a small fraction will be associated organic colloids in surface waters. While bound to such organic colloids they may be more recalcitrant to biotransformation, but will be highly prone to DOM-sensitized photolysis. We note that in addition to improving our understanding of zeranol and its metabolites in the environment, these insights should also prove useful in predicting the behavior of mycotoxins related to zearalenone, many of which are structurally analogous to zeranol.

Transformation has often been equated with removal and mitigation of ecological risk. However, initial evidence about the products from the direct photolysis of the TBA and MGA families suggests minor structural modifications and is most consistent with conservation of the steroid ring structure after reaction. Given the short timescales associated with phototransformation and the lower photoactivity of these product mixtures, this work emphasizes the need for detailed isolation, identification, and fate assessment for the phototransformation products of SGPMs. Such transformation products may have profound impact on ecosystem health, particularly given the anabolic potency of the parent compounds from which they are derived. In a future work, we intend to systematically explore the identity and structure of products from the photolysis of the TBA and MGA families and consider the potential ecotoxicological risks associated with their formation.
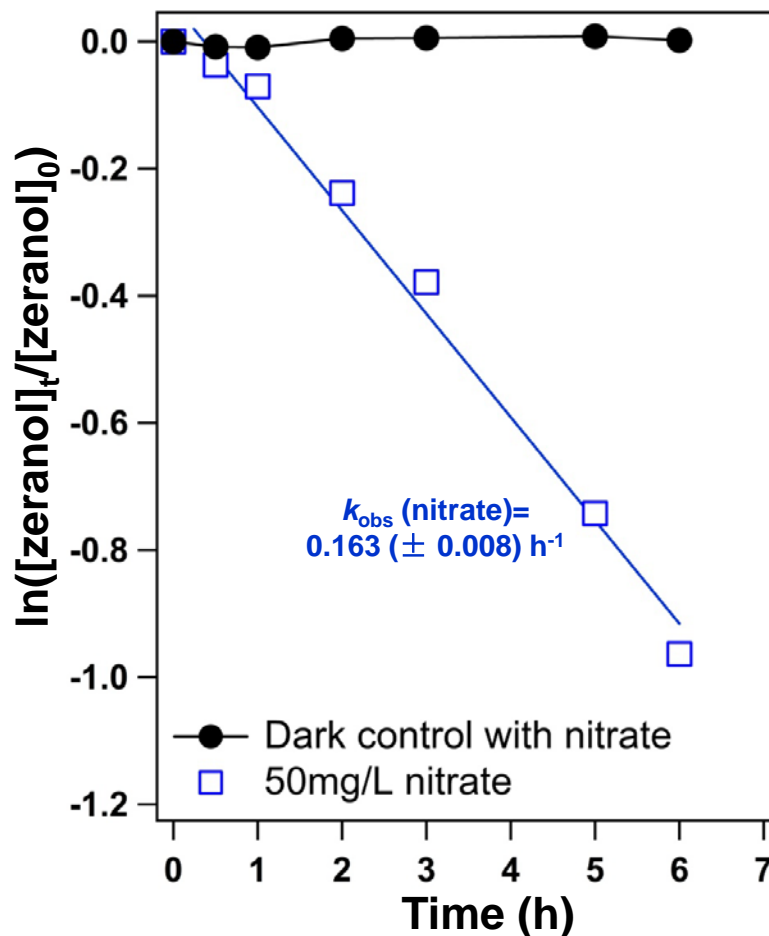
Figure 2-20. Semi-log plot of concentration as a function of time illustrating zeranol transformation in irradiated (simulated sunlight) solutions of 50 mg/L nitrate (as NO_3^-). Independent experiments with phenol as an OH radical probe indicate a $[^\bullet OH]_{ss}$ of 3.1 x 10^{-16} M in this irradiated nitrate system. Experiment was conducted at pH 7 (5 mM phosphate buffer) and using an initial zeranol concentration of ~5 μM. Data from a dark control solution of nitrate and zeranol is shown. The line represents the result of best-fit linear regression analysis, the slope of which was used to determine the pseudo-first-order rate coefficient (k_{obs} value) for zeranol transformation. The reported uncertainty represents one standard deviation for k_{obs} values resulting from linear regression analysis.

CHAPTER III. PHOTOPRODUCT-TO-PARENT REVERSION FOR
TRENBOLONE ACETATE METABOLITES: AN UNRECOGNIZED
ROUTE TO ENDOCRINE DISRUPTION IN AGRICULTURALLY
IMPACTED SURFACE WATERS?

3.1 Abstract

Previously we have shown that metabolites of trenbolone acetate (TBA), a high volume growth promoter used in animal agriculture, rapidly undergo direct photolysis to yield photproducts that are photostable but appear prone to other, non-photochemical transformation pathways. This work focuses on the long-term stability of these photoproduct mixtures, most of which are dominated by a monohydroxylated species at the C12 position on the steroid ring. Results suggest that this 12-hydroxy trenbolone species is unstable and prone to either hydrolysis, which yields higher order hydroxylated species (e.g., di- and tri-hydroxy trenbolone species), or dehydration, in which the –OH moiety is lost from the C12 position. Notably, this dehydration reaction represents a viable route by which the parent TBA metabolite can be regenerated in most surface waters, effectively making their loss via direct photolysis reversible. We attribute the unique reactivity of the primary photoproduct to the allylic nature of the –OH group at the C12 position, a functionality traditionally recognized as prone to dehydration. However, dehydration of allylic –OH groups in steroids typically only occurs under strongly acidic conditions, and it is rare, if not unprecedented, to see such a process occur so readily at neutral pH values, which we report herein. While observed for all TBA metabolites, photoproduct-to-parent reversion occurs most readily for 17α-trenbolone (17α-TBOH), allowing as much as 80-90% of the initial metabolite mass to be regenerated over several days in the dark. Consistent with known steroid chemistry, the rate of dehydration is acid-catalyzed for all metabolites, but, interestingly, base-catalyzed only for 17α-TBOH.   Dehydration is also strongly temperature dependent, occurring

most rapidly at high temperature (e.g., 35 °C). The observation of coupled photolysis and dehydration has significant implications for the fate of TBA metabolites in surface waters, causing them to be far more persistent than is currently expected based solely on consideration of their reported half-lives for direct photolysis. Consequently, we also anticipate that the occurrence and concentrations of TBA metabolites in surface waters will exhibit diurnal and seasonal cycles, as well as a dependence on surface water pH. Finally, outcomes of this work call into question the quality of all occurrence data currently available in the literature, as many aspects of sample collection, handling and processing are likely to influence the rate and extent of this dehydration reaction, thus obscuring the amount of TBA metabolites available in a sample.

3.2   Introduction

The available evidence clearly indicates that humans are discharging a wide variety of bioactive contaminants into the aquatic environment that adversely impact aquatic organisms [4, 21, 23]. Effective ecological risk assessment for these contaminants must then rely upon comprehensive knowledge of their occurrence and environmental fate, although analytical and mechanistic fate studies are often costly and time consuming. Due to these constraints, the existing paradigm for environmental risk assessment studies, including those used for regulatory purposes, often is relatively simplistic: if transformation of parent molecular structures to products is observed in the experimental system (i.e., "degradation"), risk is mostly assumed to decrease greatly and subsequent, more detailed studies are seldom necessary. In essence, pollutant degradation has historically been equated with complete removal.

Yet when considering the scope of natural and synthetic organic chemicals that may pose a threat to water resources, the universe of potential contaminant structures is exceedingly large. When transformation products (or "degradates") of these parent contaminants are also considered, this universe grows even larger still. Given their sheer

number and structural diversity, therefore, it is a near certainty that organic pollutants exist with behavior that grossly violates this traditional paradigm for environmental risk assessment. Their fate will not abide by pathways typically identified in experimental studies, and their transformation products will hold equal if not greater adverse implications for human and ecological health. As regulatory agencies grapple with establishing new mandates for next generation organic micropollutants, our emphasis must be focused on identifying these worst of the bad actors.

In the United States, 10-30 million beef cattle are implanted with the growth promoter trenbolone acetate [50, 87] which contains a 4,9,11 triene bond system highly unique among steroid structures. Upon implant dissolution, de-acetylation occurs and forms 17β-trenbolone (17β-TBOH), an androgen 5-50 times more potent than testosterone that is responsible for anabolic effects including significant weight gain in implanted cattle [89]. In the liver, 17β-TBOH is further metabolized to trendione (TBO) and 17α-trenbolone (17α-TBOH) [17, 90].

On a mass basis, trenbolone is likely the most widely produced and used synthetic steroid in the United States, although only a small fraction (8-10%) of the implant dose is excreted in manure as the bioactive metabolites 17α-TBOH, 17β-TBOH, or TBO [17]. For comparison, despite all of the research attention the synthetic contraceptive ethinyl estradiol has received, we estimate that the trenbolone metabolite mass excreted by cattle exceeds the mass excretion of ethinyl estradiol from humans by at least an order of magnitude. 17α-TBOH, the primary metabolite excreted [7], and 17β-TBOH have been detected in receiving waters impacted by animal agriculture throughout the United States [16, 37]. Though not assessed at all in the regulatory process for trenbolone, these metabolites are potent endocrine disruptors that pose a demonstrated risk to reproductive viability in exposed aquatic organisms, with 10-30 ng/L concentrations capable of significant fecundity reductions in fish [22, 25, 91]. One implant dose (*e.g.* 100 mg) can

thus contaminate over 700,000 L of water to concentrations capable of reproductive disruption.

This work is motivated by the need to evaluate the ultimate fate of TBA metabolites in surface waters. In Chapter 2 we showed that TBA metabolites readily undergo direct photolysis, with half-lives (on the order of a half hour) likely to make photolysis their dominant transformation route in surface waters. In Appendix A, we also identified the major photolysis products generated from TBA metabolites. All metabolites exhibited analogous transformation pathways in which a 12-hydroxy variant of the base trenbolone structure is the major photoproduct (Scheme 3-1).

The identification of this hydroxlyated photoproduct has substantial implications for the long-term fate of TBA metabolites in surface waters. First, –OH addition at the C12 position in the steroidal ring disrupts the 4,9,11-triene bonding structure initially present in TBA and its metabolites. This in turn shifts the absorption maximum of the photoproduct outside the solar spectrum, making it resistant to direct photolysis. Second, allylic –OH groups on steroids, such as that on the 12-hydroxy trenbolone photoproduct, are prone to acid-catalyzed dehydration reactions. For example, there are several reports of steroids with an allylic –OH group at the C3 position dehydrating to yield 3,5-dienes in the presence of moderate to strong acids [92-94]. There are also multiple reports [95, 96] in which dehydration of steroids with an allylic –OH group at the C10 position produces a steroid with an aromatic A-ring. Such acid-catalyzed pathways open the door to several unique transformations for the major photoproduct of TBA metabolites. Specifically, it is possible that dehydration of 12-hydroxy trenbolone could result in the production of the respective TBA metabolite from which it was photolytically generated.

The objective of this study is to investigate the stability of the photoproducts of TBA metabolites in water. Below, we will show that the hydroxylated photoproduct of TBA metabolites is unstable in water, readily dehydrating to yield the TBA metabolite from which it was produced. We present a series of kinetic studies establishing this

photoproduct-to-parent reversion mechanism, including a long-term study that considered the day-night cycling of trenbolone photoproducts. Furthermore, we determine the influence of system conditions (e.g., pH and temperature) on this process, and assess related implications on environmental occurrence data, fate studies, and risk assessment for aquatic organisms.

3.3   Experimental Methods

Reagents

All TBA metabolites were acquired from commercial suppliers. High purity 17β-trenbolone (Steraloids,> 99%), 17α-trenbolone (Cerilliant, 99%), and trendione (Steraloids, >99%) were used as received. Stock solutions of each TBA metabolite were prepared in reagent grade methanol (Fisher, HPLC grade) and/or deionized water (Millipore, Q-Grad2) as described in Chapter 2. A buffer prepared from potassium phosphate (Fisher, 99%) was used in most photochemical experiments, whereas a small number of experiments at higher pH used a buffer from boric acid (Sigma Aldrich, 99.5%). Hydrochloric acid (Fisher, 37%) and sodium hydroxide (Fisher, 97%) were used to adjust the pH of all solutions. Acetonitrile (Fisher, HPLC grade) was the mobile phase for HPLC analysis.

Light Source and Photoreactor Details

The majority of experiments used a commercially available 450 W Xenon arc lamp (Newport Corporation). Additional details of the source (e.g., its configuration and output) are provided in Chapter 2. Experiments were conducted in a water-jacketed borosilicate photoreactor (37 mm inner diameter × 67 mm depth for a nominal volume of ~50 mL), whose contents were mixed via magnetic stirrer and stir plate during all experiments. The system temperature was held constant via recirculating water bath. As noted, a small number of experiments utilized a Suntest CPS+ solar simulator.

Experiments conducted with the solar simulator utilized borosilicate glass beakers as a photoreactor.

Stability of TBA Metabolites and Photoproduct Mixtures

A variety of experimental systems were designed to assess the stability of photoproducts generated from the direct photolysis of TBA metabolites. Generally, these experiments coupled a period in which a solution of TBA metabolite was irradiated via simulated sunlight followed by a period in which the resulting photoproduct mixture was stored in the absence of simulated sunlight. During both the light and dark period, the concentration of the parent TBA metabolite and the products of photolysis were monitored over time. The key variables explored using this general experimental approach included the number of cycles in this light-dark sequence, so as to simulate day-night (i.e., diurnal) cycling expected in surface waters, as well as the duration, pH, and temperature of the dark period after exposure of TBA metabolites to simulated sunlight. The typical initial concentration of TBA metabolites was ~10 μM (~2.7 mg/L), although a select number of experiments were conducted at more environmentally relevant values (~420 ng/L or ~ 1.5 nM). Specific details of these different experimental approaches follow.
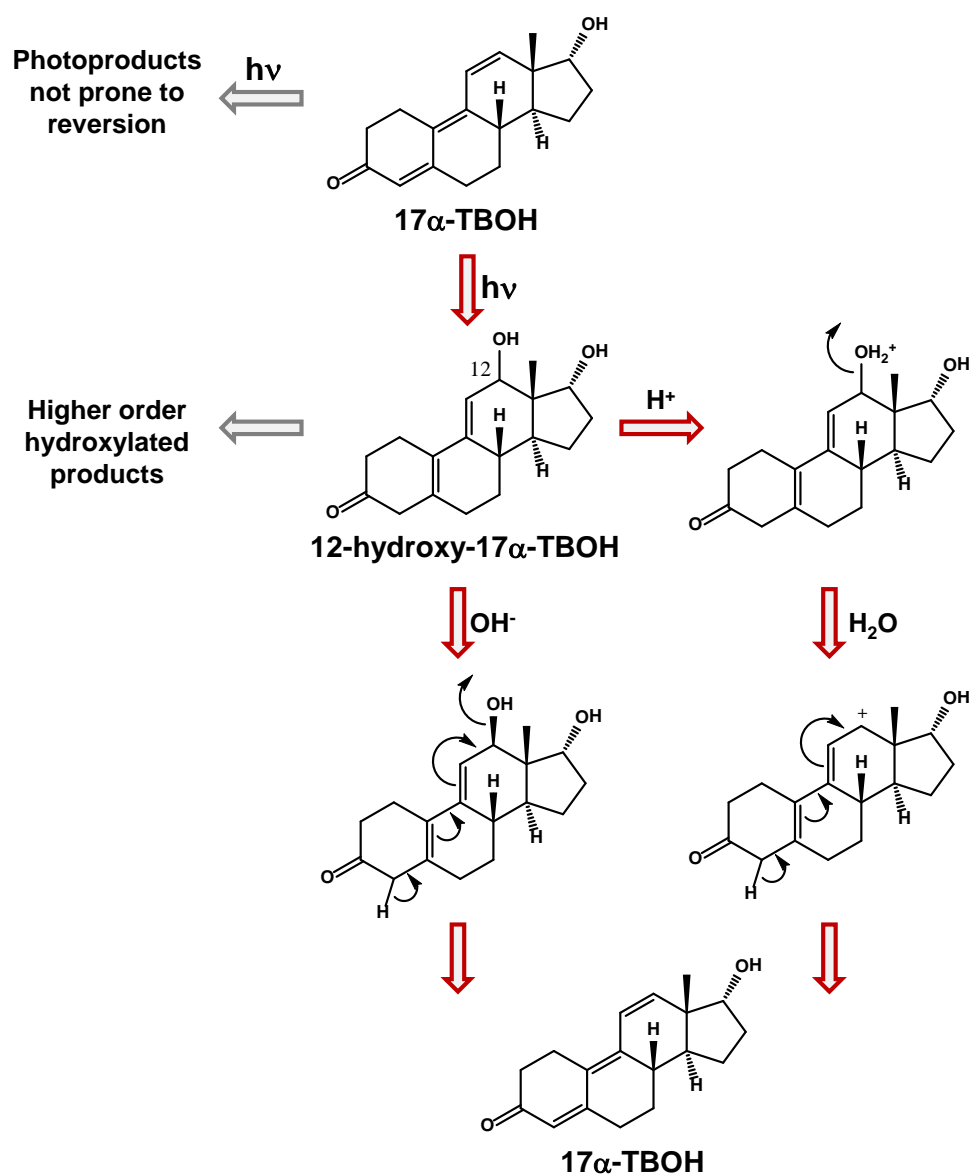
Scheme 3-1. Simplified schematic of coupled photolysis and dehydration of 17α-TBOH, which allows (via the route shown in red) the photoproduct-to-parent reversion first observed and reported herein. The scheme is shown for 17α-TBOH, whose primary photoproduct 12-hydroxy-17α-TBOH can undergo base- and acid-catalyzed dehehydration to regenerate 17α-TBOH. This reversion process also occurs appreciably at neutral pH.

Day-Night Cycling of TBA Metabolites and their Photoproducts: To monitor the long-term stability of TBA metabolites and photoproduct, experiments were designed to simulate day-night cycling. These experiments were conducted in 45 mL of 5 mM phosphate buffer to maintain pH 7. The appropriate volume of a 10 mM methanolic stock solution of the appropriate TBA metabolite was then delivered to the buffer via syringe to achieve the desired initial concentration of ~ 10 μM. The solution was then irradiated with simulated sunlight for 12 h, during which samples (~0.5 mL) were withdrawn at periodic intervals, transferred to a 2 mL amber autosampler vial, and analyzed immediately via HPLC with diode array detector (LC-DAD). After 12 h of irradiation, the photoreactor was removed from light and covered with Al foil for 12 h. During this dark period, samples (~0.5 mL) were once again withdrawn periodically and analyzed immediately via LC-DAD. This sequence of light-dark sampling was conducted over a total of 72 h, simulating a three day period of TBA metabolites in surface water.

Long-term Dark Stability of TBA Metabolite Photoproducts: Solutions (45 mL) of each TBA metabolite (~10 μM) were photolyzed for 6 h at 25 °C and pH 7, during which samples were taken for metabolite and photoproduct analysis. This duration of irradiation typically resulted in >99% of metabolite transformation. The photoreactor was then removed from light and covered with Al foil and stored for up to one week (~150 h) at 25 °C. During this extended dark period, samples (~0.5 mL) were periodically withdrawn to monitor photoproduct stability over time via LC-DAD.

Effect of Temperature on Photoproduct Stability: The influence of temperature on photoproduct stability was evaluated only for 17α-TBOH as it has the most product-to-parent reversion. A 50 mL solution of 10 μM 17α-TBOH was prepared in 5 mM phosphate buffer at pH 7 and subsequently photolyzed at 25°C. After sufficient irradiation to achieve ~99% removal, the solution was divided into four equal parts and placed in 40 mL (nominal volume) amber bottle to avoid light. The four vials were then

transferred either to a refrigerator (5°C) or a series of water baths (15°C, 25°C and 35°C) to maintain their temperature over 6 days. During this extended dark period, samples (~0.5 mL) were periodically withdrawn from each reactor to monitor photoproduct stability via LC-DAD.

Effect of pH on Photoproduct Stability: Two protocols were followed to evaluate the influence of pH on photoproduct stability. First, a subset of photolysis experiments with each TBA metabolite were conducted in DI water at 25 °C. After a period of irradiation (typically 4-6 h, over which loss of the TBA metabolite was typically ~99%) the solution for each metabolite was divided into equal parts. One volume was adjusted to pH 2 by adding 5 M HCl while the other was adjusted to pH 12 via addition of 5 M NaOH. Samples of the pH-adjusted solution (~1 mL) were then withdrawn and immediately analyzed on the LC-DAD.

The other approach involved conducting photolysis and subsequent dark stability experiments at different pH values (2, 5, 7, 9, 12) with 17α-trenbolone at 25 °C. Solutions at pH 2 were prepared using 0.01 M HCl, whereas pH 12 solutions were made from 0.01 M NaOH. For the other pH values, a 5 mM phosphate buffer was adjusted using 1 M HCl or 1 M NaOH to achieve a pH value of 5, 7, or 9. The pH in these experimental systems was monitored over time and adjusted as needed to maintain the initial pH value ($\pm$ 0.2 pH units). Photolysis experiments with 10 μM 17α-TBOH were conducted over 6 h following our standard operation and sampling procedure. After 6 h of irradiation (corresponding to ~99% 17a-TBOH removal), the solution was transferred to a 40 mL (nominal volume) amber vial to avoid further phototransformation and stored for up to 6 days at 25 °C. Over time, samples (~1 mL) were withdrawn periodically and analyzed immediately on HPLC.

TBA Metabolite and Photoproduct Stability at Environmentally Relevant Concentrations: Photolysis and dark stability experiments were also conducted with 17β-trenbolone at a more environmentally relevant initial concentration (420 ng/L or 1.5

nM). Seven identical borosilicate beakers were prepared with 100 mL of 420 ng/L 17β-TBOH in DI water. Each beaker was then photolyzed in parallel using a Suntest CPS+ solar simulator. Periodically, reactors were sacrificially sampled, in which the entire 100 mL volume was concentrated using a C18 cartridge. The cartridge was subsequently eluted with 0.5 mL of methanol, resulting in a 17β-TBOH concentration suitable for detection and analysis via LC-DAD.

<u>Analytical Methods</u>

Samples were analyzed on a 1200 Series Agilent HPLC-DAD equipped with an Eclipse XBD-C18 column (4.6×150 mm, 5 μm particle size). The analytical method adapted from Khan et al. [87] involved gradient elution with an acetonitrile (ACN):H_2O mobile phase that ramped from 25% to 72% ACN over a 13 minute period followed by re-equilibration to 25% ACN. The method employed a flow rate of 0.6 mL/min and an injection volume of 20 μL TBA metabolites were analyzed at a detection wavelength of 350 nm, whereas photoproducts were primarily analyzed at 254 nm (with some minor products also detected at 300 nm). Additional sample analysis via LC/MS/MS and NMR were conducted as described in Appendix A.

3.4   Results and Discussion

<u>Review of Photoproduct Identification</u>

As is detailed in Appendix A, all TBA metabolites exhibit analogous products of direct photolysis. Generally, each metabolite yields two primary photoproducts that are easily identifiable using LC-DAD with a detection wavelength of 254 nm. Using the LC-DAD method described above, 17β-TBOH, 17α-TBOH and TBO exhibit retention times of 4.8 min, 5.2 min and 6.2 min, respectively. All TBA metabolites are detectable via absorbance at 350 nm, characteristic of their 4,9,11-triene structure. The two primary

photoproducts exhibited retention times of 1.8 min and 2.6 min for 17β-TBOH, 3.3 min and 4.4 min for 17α-TBOH, and 3.1 min and 3.5 min for TBO.

Based upon UV/visible absorbance spectra, LC/MS/MS and NMR analysis presented in Appendix A, the major photoproduct (based on DAD response at 254 nm) has been identified as a monohydroxylated species with an –OH group on the C12 position of the steroid ring. The identity of the minor phototransformation project has not been experimentally verified, although LC/MS/MS suggests it is structurally very similar to the 12-hydroxy species. In Appendix A, we propose two possible structures for this minor product. One possibility is that it represents a well-resolved diastereomer of the 12-hydroxy species confirmed by NMR. The other option is that it is an alternative monohydroxy species. For example, we propose in Appendix A that this additional photoproduct may be hydroxylated at the C10 rather than C12 position in the steroid ring.

In subsequent experiments assessing the stability of photoproduct mixtures, attention was primarily paid to the 12-hydroxy species confirmed via complementary NMR and LC/MS/MS analysis. Stability was monitored by tracking DAD response attributable to this photoproduct over time.

<p style="text-align:center;">Initial Observations of Photoproduct-to-Parent</p>

<p style="text-align:center;">Metabolite Reversion</p>

During preliminary experiments monitoring the stability of 17α-TBOH photoproducts in the absence of light, the DAD response attributable to the two primary photoproducts (at $\lambda_{detection}$ of 254 nm) decreased over time. Unexpectedly, we also consistently observed a corresponding increase in DAD response at the detection wavelength ($\lambda_{detection}$ of 350 nm) and retention time (5.2 min) characteristic of 17α-TBOH.

Initially, we inferred this product, apparently generated from the decay of photoproducts in the absence of light, to be 17α-TBOH, the TBA metabolite from which

the photoproducts were generated. This assignment was primarily based on the agreement in LC-DAD retention time, as well as the change in absorbance maxima from near 254 nm to 350 nm, the latter of which is characteristic of the 4,9,11-triene in TBA metabolites. Thus, it appeared that the process resulting in photoproduct decay also restored the π-bond network.

As is described in greater detail below, we ultimately confirmed via complementary NMR and LC/MS/MS analysis that the species generated from photoproduct decay was indeed the respective parent TBA metabolite. Accordingly, the following experiments were intended to confirm this photoproduct-to-parent reversion mechanism and consider the implications of this process for TBA metabolite fate in surface waters. Experiments heretofore not only focus simply on photoproduct stability, but also the rate and extent to which the parent TBA metabolite was regenerated via the dark transformation reactions involving the photoproducts.

<u>Day-Night Cycling Experiments with TBA Metabolites</u>

Simulated day-night cycling experiments conducted over 72 h reveal the cyclic nature of 17α-TBOH fate in surface waters (Figure 3-1). For each day-night period, loss of 17α-TBOH during irradiation with simulated sunlight was consistently followed by a rebound in concentration during the subsequent dark period. For 17α-TBOH, dark regrowth corresponded to roughly 10% of the initial 17α-TBOH mass at 25 °C and pH 7. Furthermore, the rates of 17α-TBOH direct photolysis and regrowth were near identical in each light-dark cycle, more evidence, albeit indirect, that the species generated during the dark intervals is indeed 17α-TBOH. While data in Figure 3-1 were collected at a 17α-TBOH concentration higher than would be encountered in nature to facilitate our analysis via LC-DAD, a subset of experiments conducted at a more environmentally relevant initial concentration (~420 ng/L) revealed the same cyclic behavior (Figure 3-2).

The dark regrowth of 17α-TBOH is linked to the instability of 12-hydroxy-17α-TBOH, which is its dominant photoproduct. During day-night cycling experiments, loss of 17α-TBOH produced a corresponding growth in 12-hydroxy-17α-TBOH. More importantly, in the absence of light, decay of 12-hydroxy-17α-TBOH occurs concomitantly with 17α-TBOH regrowth, and the its decay rate in the absence of light was equivalent during each complete day-night cycle. As noted previously, the as yet unidentified additional product of 17α-TBOH photolysis (i.e., either the other 12-hydroxy-17α-TBOH diastereomer or 10-hydroxy-17α-TBOH) was formed to a more limited extent in these systems (data not shown). Although generated in much smaller quantities, based on relative DAD response, it also was not stable in the dark and could, therefore, also contribute to the regrowth of 17α-TBOH in these experiments.

The photoproduct-to-parent metabolite phenomenon is not unique to 17α-TBOH, also being observed for each of the major trenbolone metabolites (Figure 3-1b). Concentration profiles for 17β-TBOH and TBO as a function of time during day-night cycles are shown on a log-scale in Figure 3-1b. Data are shown on a log-scale because the extent of parent metabolite regrowth during the 12 h in the absence of light was considerably less (~1% of the initial system mass) for 17β-TBOH and TBO than that observed for 17α-TBOH (data for which is provided for comparison). The underlying cause for the difference is not understood, but we can speculate based upon the key species involved in the product-to-parent reversion mechanism. Although product data are not provided for 17β-TBOH and TBO in Figure 3-1, they show that the rate and extent of their dark regrowth is linked to the instability of their respective 12-hydroxy photoproduct. Specifically, it appears this primary product of direct photolysis is thermally unstable, resulting in the net formation of the corresponding parent species in the dark. Therefore, the greater extent of regrowth observed for 17α-TBOH may indicate that its 12-hydroxy photoproduct is least stable among those generated from the TBA metabolites. Alternatively, it may simply reflect that more 12-hydroxy species is

generated during direct photolysis of 17α-TBOH than is generated by photolysis of 17β-TBOH and TBO. Consistent with this latter scenario, product formation data presented in Appendix A show that 17α-TBOH does indeed result in the largest yield, based upon DAD response, of the 12-hydroxy species relative to the other TBA metabolites.

<div align="center">Extent of Photoproduct-to-Parent Metabolite Reversion</div>

<div align="center">during Extended Dark Periods</div>

In certain instances, we have found that this decay of the 12-hydroxy photoproduct can result in significant, and at times even near complete, reformation of the parent TBA metabolite. Figure 3-3 shows concentration profiles as a function of time for solutions of each TBA metabolite that were first photolyzed at pH 7 for 6 h with simulated sunlight, after which the photoproduct mixture was stored in the dark at room temperature (25 °C) for nearly 90 h. Such a scenario simulates their initial occurrence in the photic zone of a surface body followed by subsequent transport into a region of the system where available sunlight is limited (e.g., greater depth of a lake where light is attenuated or into the hyporeic zone or bed sediment of a stream).
Consistent with results in Figure 3-1, we observed 17α-TBOH to be most prone to regrowth, with almost 60% of the initial 17 α -TBOH mass being recovered over the 90 h dark period. Although we also observed photoproduct-to-parent reversion for 17β-TBOH and TBO, it occurred to a much lesser extent, yielding on the order of 10% of the initial mass over the same timescale. Nevertheless, in the absence of light, the rebound of TBA metabolite concentration is substantial enough to help sustain their environmental persistence.

The greater extent of regenerated metabolite formation in this series of experiments facilitated their analysis via NMR after a modest amount of sample concentration via solid phase extraction. Indeed, this NRM analysis verified that the species generated during the extended dark period were indeed the parent TBA

metabolites. For example, NMR analysis of the 6-day regeneration product mixture of 17β-TBOH (compare Figures 3-4 through 3-6) indicated the presence of 17β-TBOH and a 11,12-dialdehyde decomposition product, which forms via hydrolysis (see Appendix A), in a 5:1 ratio, as well as multiple trace components that could not be identified. Thus, it appears that during an extended period, the photoproduct mixture, presumably dominated 12-hydroxy-17β-TBOH, can either further hydrolyze to higher order hydroxylated products (e.g., 11,12-dihydroxy-17β-TBOH) that subsequently decomposes to the 11,12-dialdehyde decomposition product. In parallel, dehydration of the 12-hydroxy-17β-TBOH also occurs, which ultimately results the regeneration of 17β-TBOH (see Scheme 3-1b).

Consistent with its greater rate of dehydration relative to 17β-TBOH (see Figure 3-3), NMR analysis of the 17α-TBOH product mixture after 6 days of storage in the dark revealed nearly exclusively 17α-TBOH (compare Figures 3-7 and 3-8) although a trace amount of the analogous 11,-12-dialdehyde decomposition product was also observed. Thus, the relative rate of dehydration relative to hydrolysis of the 12-hydroxy photoproduct determines the amount of parent metabolite regrowth over extended dark periods. We note that NMR analysis of TBO photoproduct mixtures was inconclusive, revealing 12-hydroxy trendione as the major product at the end of the extended dark period. This is not entirely unexpected, however, given that TBO exhibited the smallest rate and extent of photoproduct-to-parent reversion relative to 17α-TBOH and 17β-TBOH.

A final line of evidence in support of photoproduct-to-parent metabolite reversion was provided by LC/MS/MS analysis of 17β-TBOH product mixtures as a function of time in the absence of lite. Most notably, MS/MS scans of the product mixture after an extended period of dark storage were equivalent to the MS/MS scans of 17β-TBOH (Figure 3-9). Also apparent in the LC/MS/MS analysis of this dark sample was the lack of signals consistent with the primary photoproducts (e.g., 12-hydroxy-17β-TBOH)

observed after several hours of sunlight irradiation. Thus, as initially suspected with LC-DAD analysis and subsequently confirmed with NMR, the primary photoproducts of 17β-TBOH are not stable. Unique to TBA metabolites, it appears the 12-hydroxyl photoproduct not only undergoes hydrolysis to higher order hydroxylated products, as might be expected, but also is unexpectedly prone to dehydration, in which the loss of –OH group from the C12 position in the steroid ring allows the π-bond network to rearrange within the ring structure to the configuration originally present in the parent metabolite.

<div align="center">Influence of pH on Photoproduct-to-Parent</div>

<div align="center">Metabolite Reversion</div>

Experimental evidence clearly illustrates that the photoproduct-to-parent reversion mechanism is acid-catalyzed, and for certain species, also based-catalyzed. The inset of Figure 3-3 shows the maximum recovery of the parent metabolite when the product mixture generated after extended photolysis (4-6 h) were immediately either dropped to pH 2 via the addition of 5 M HCl or raised to pH 11 with the addition of 5 M NaOH.   These pH adjustments often resulted in the near immediate regrowth of parent TBA metabolite from which the photoproduct mixtures were generated. For example, at pH 2 the recovery of 17α-TBOH was 88 ($\pm$3)%, whereas the recovery at pH 12 was significant but slightly lower ($66 \pm 5\%$). The product-to-parent reversion was also acid-catalyzed for 17β-TBOH (which was confirmed via NMR; Figure 3-10) and TBO, but the extent of reversion was not as great as observed for 17α-TBOH (65 ± 7 and 32 ± 4, respectively). Interestingly, we did not observe any significant regrowth of 17β-TBOH and TBO under base-catalyzed conditions at pH 12.
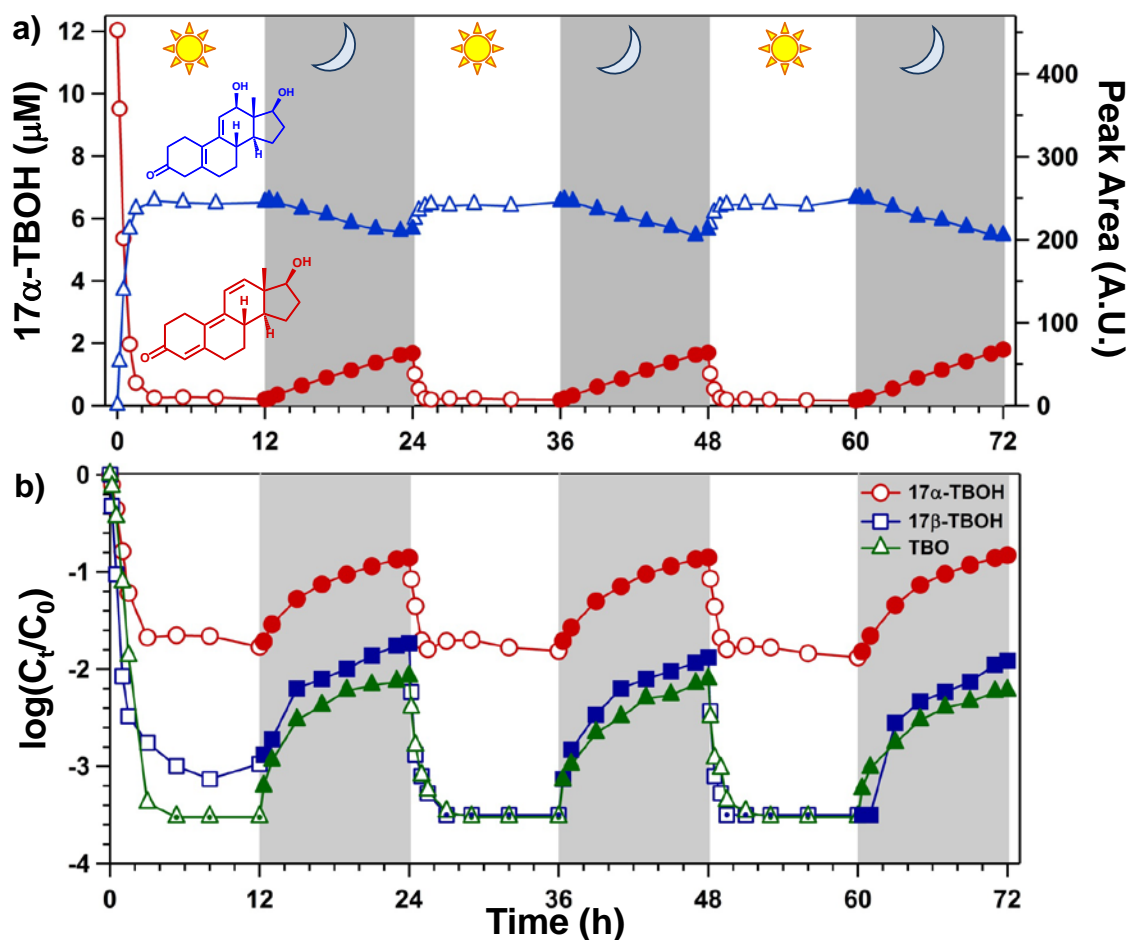
Figure 3-1. Day-night cycling of 17α-TBOH (red) and 12-hydroxy-17α-TBOH (blue). Data for 17α-TBOH are presented as aqueous concentration (left axis), whereas peak area measurements corresponding to spectrophotometric absorbance (at λ = 350 nm for 17α-TBOH and λ = 254 nm for 12-hydroxy-17α-TBOH) are also presented (right axis). Data collected during simulated solar irradiance are shown as open symbols, whereas data collected in the absence of light (shaded grey areas) are shown as solid symbols. Experiments were conducted at pH 7 using a 5 mM phosphate buffer.
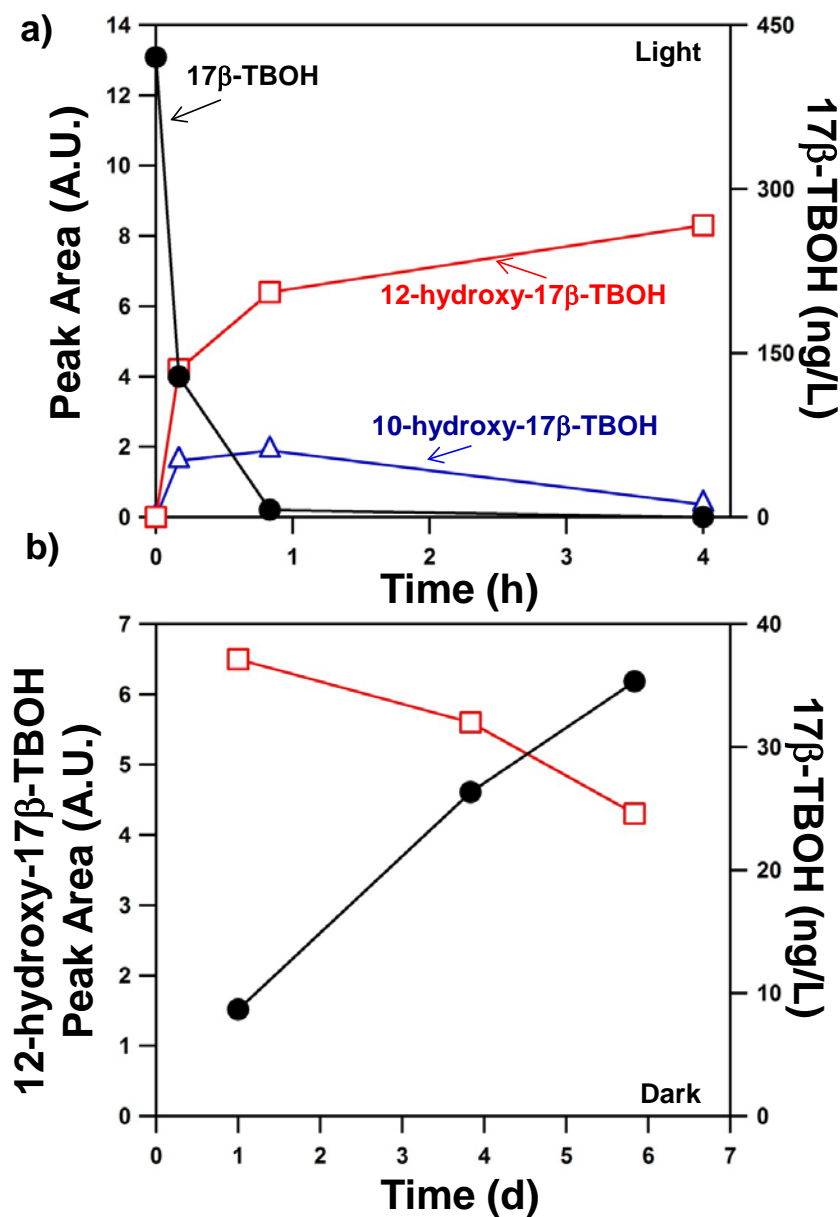
Figure 3-2. (a) Concentration profile for 17β-TBOH and its two major photoproducts, 12-hydroxy-17β-TBOH and the presumed 10-hydroxy-17β-TBOH as a function of time during irradiation. Experiments were conducted at an initial 17β-TBOH concentration of 420 ng/L (~1.5 nM) at pH 7. (b) Regrowth of 17β-TBOH (presented as concentration on the right y-axis) and decay of 12-hydroxy-17β-TBOH (presented as LC-DAD Peak Area) during the dark storage of the photoproduct mixture generated at after the 4 h of irradiation shown in panel (a).
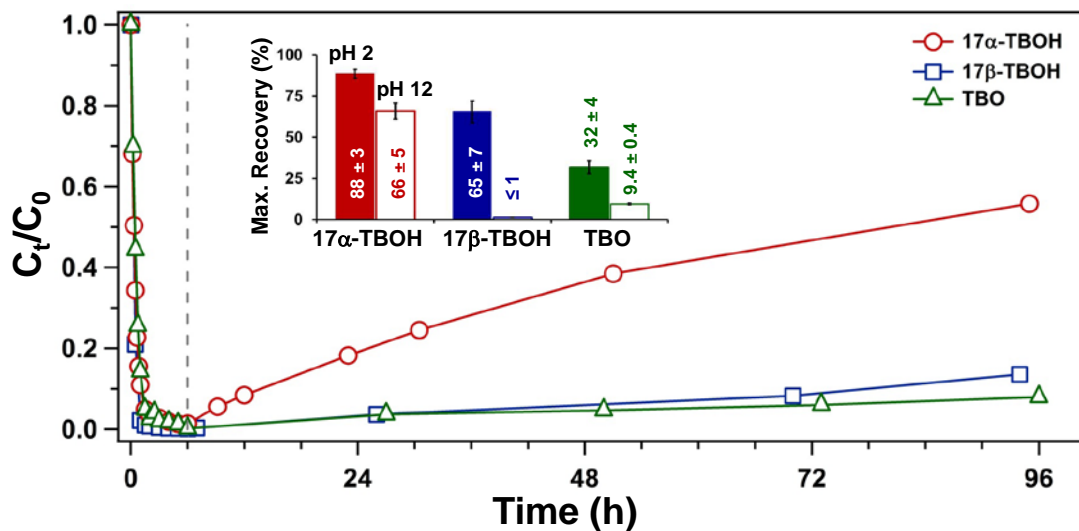
Figure 3-3. Regeneration of 17α-TBOH, 17β-TBOH, and TBO after 6 h of irradiation using simulated sunlight (dashed vertical line) followed by an extended period in which in the resulting photoproduct mixtures were maintained the absence of light at pH 7. All experiments were conducted with an initial steroid concentration of approximately 10 μM at pH 7 using a 5 mM phosphate buffer. The inset reports the percent recovery (mean and standard deviation of at least triplicate analysis) of each steroid when the photoproduct mixture generated after 6 h of irradiation was immediately acidified to pH 2 or increased to pH 12. Steroid regeneration via this pH adjustment was nearly instantaneous, and the steroids were subsequently stable at these extreme pH values. We note that to facilitate a rapid pH change in these systems, photolysis was performed in deionized water.
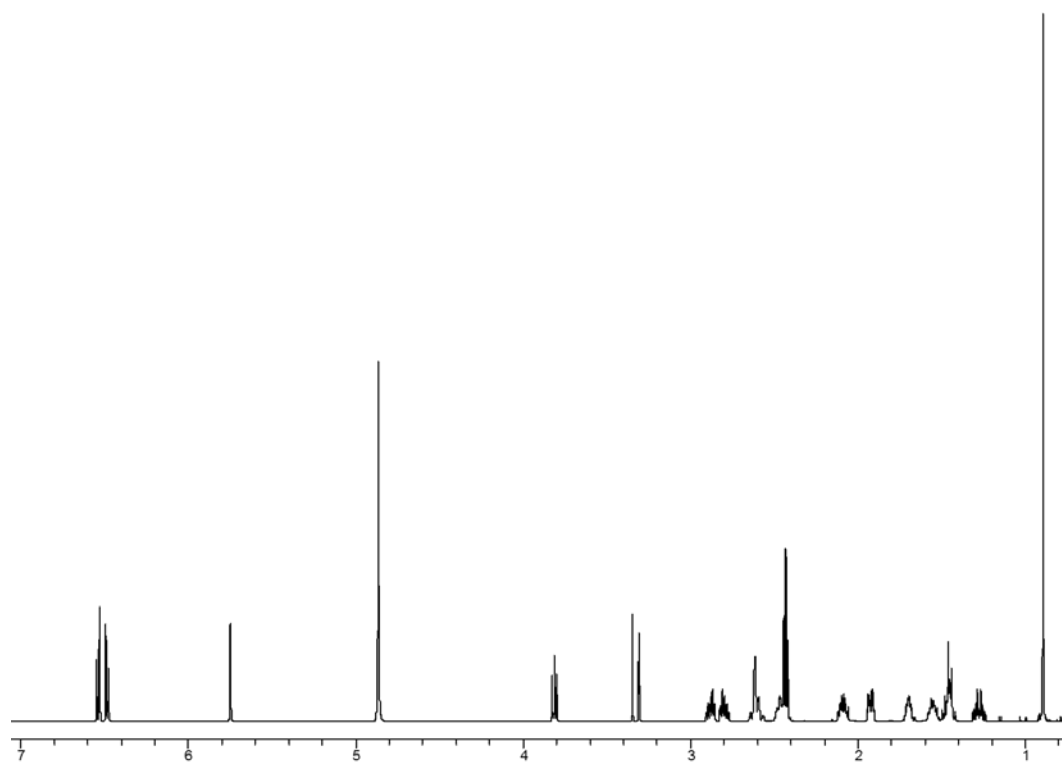
Figure 3-4. ^{1}H NMR spectrum (500MHz) of 17β-trenbolone in CD$_3$OD
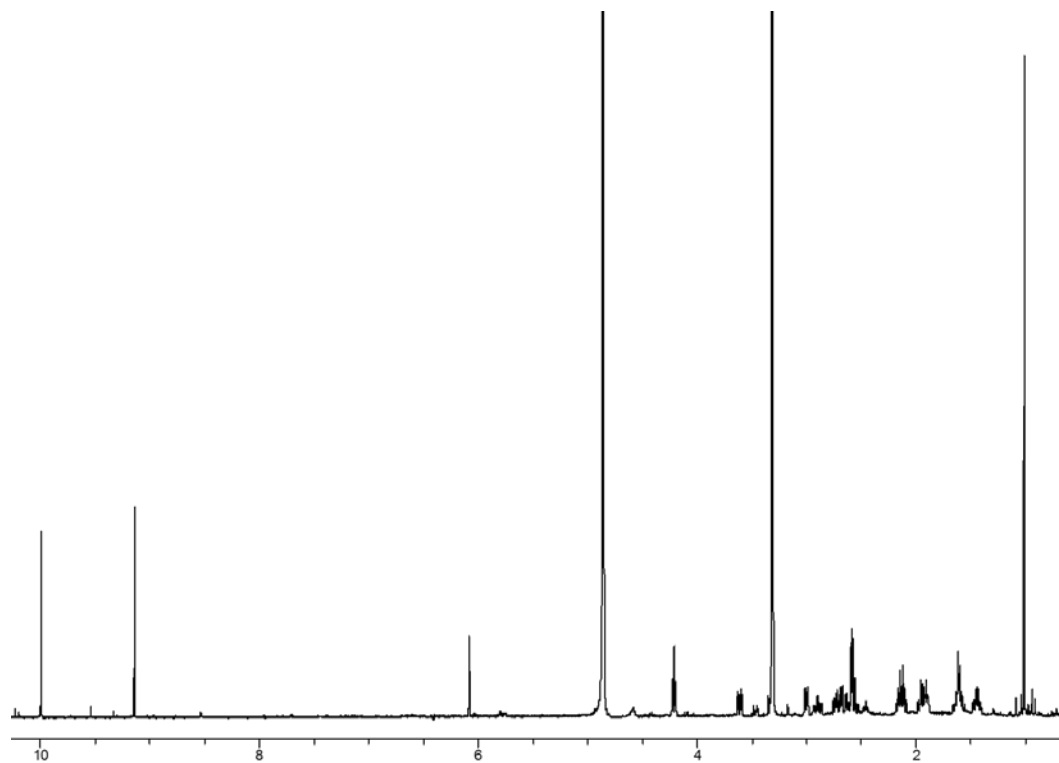
Figure 3-5. [^1]H NMR spectrum (500MHz) of dialdehyde decomposition product in CD$_3$OD
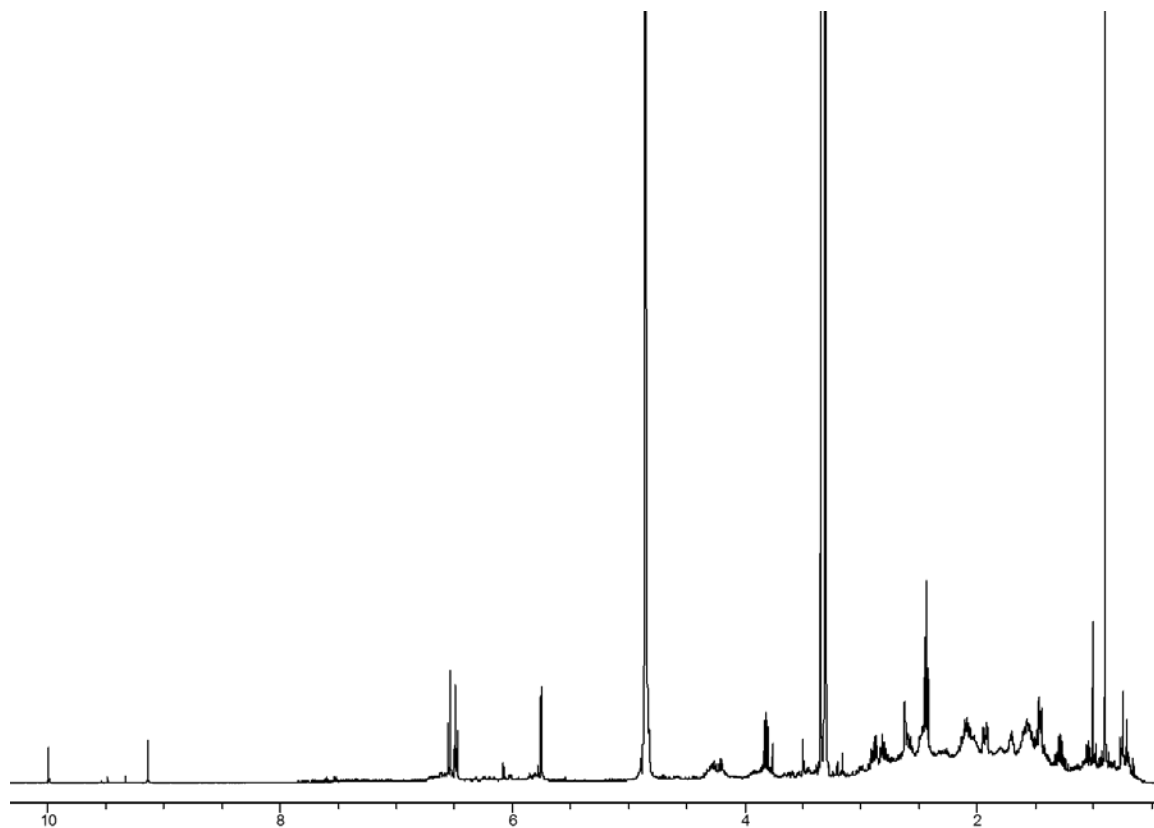
Figure 3-6. ^{1}H NMR spectrum of 17β-trenbolone day 6 regeneration photo products mixture. Diagnostic features of the dialdehyde decomposition product included the proton signals at δ_H 9.13 and δ_H 9.99.
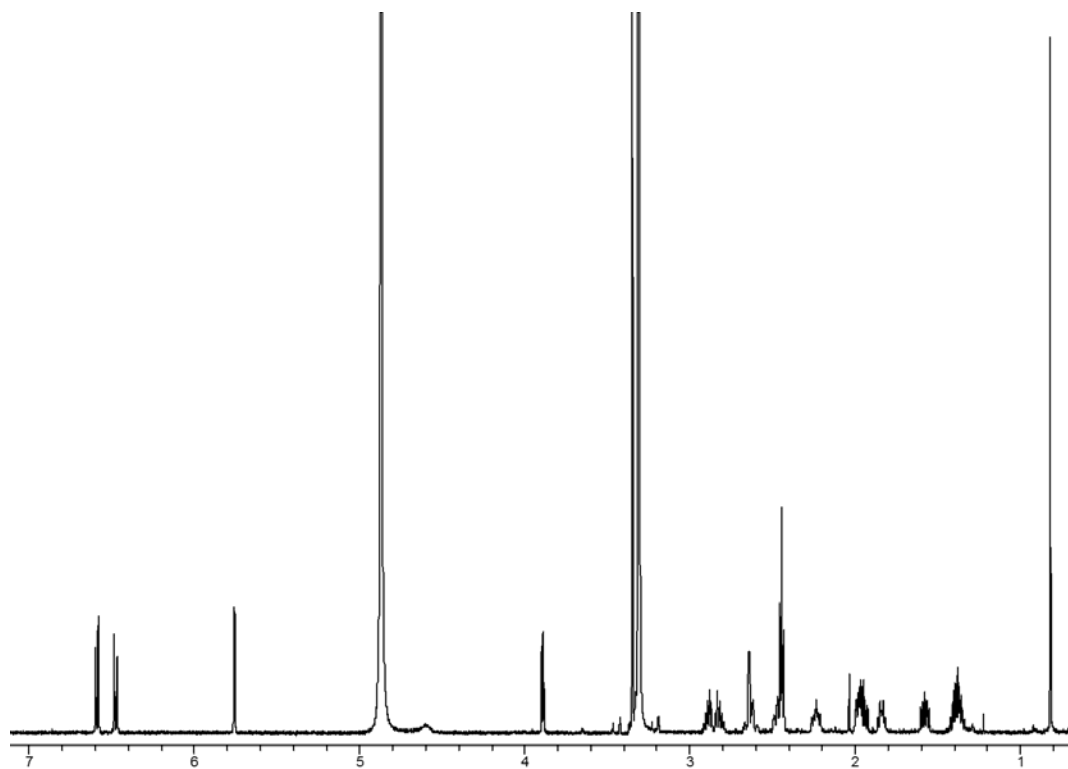
Figure 3-7. ^{1}H NMR spectrum (500MHz) of 17α-trenbolone in CD$_3$OD
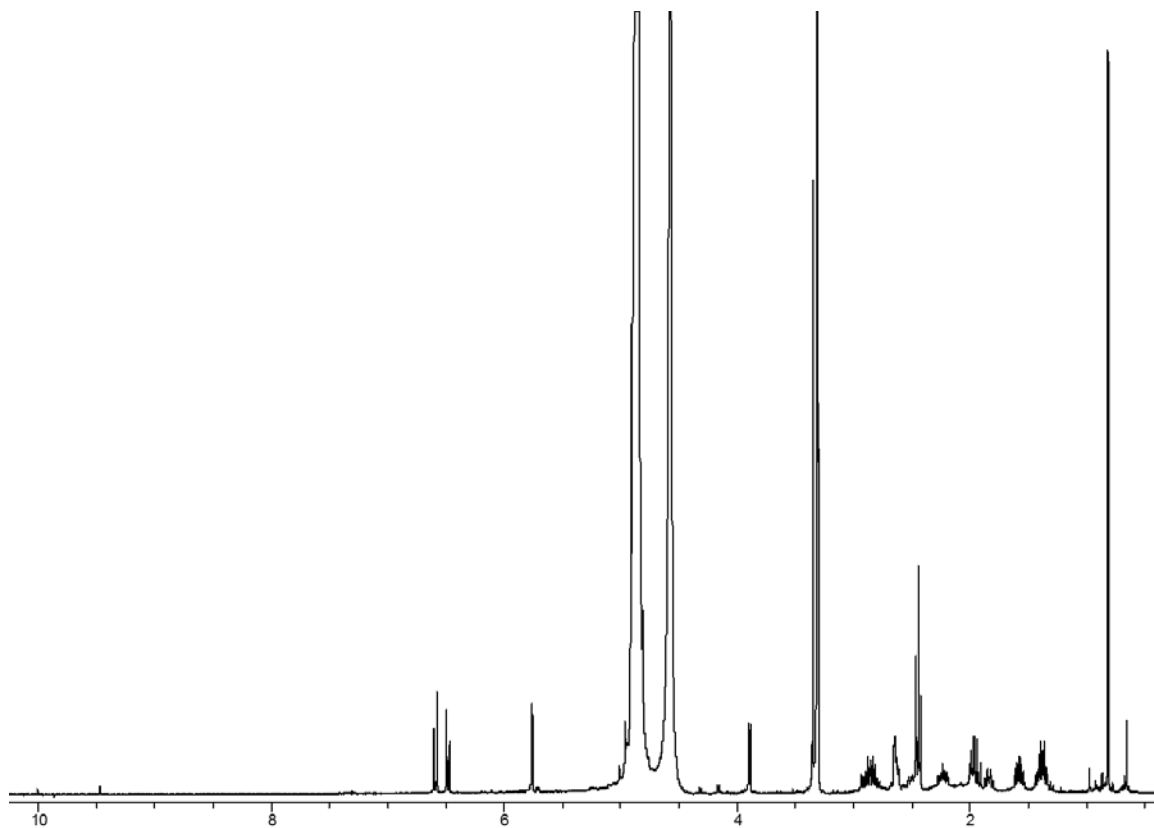
Figure 3-8. ^{1}H NMR spectrum of 17α-trenbolone day 6 regeneration photo products mixture. Diagnostic features of the trace dialdehyde product are observed at δ_H 9.47 and δ_H 10.01.

This observation of acid-catalyzed metabolite regrowth is consistent with our proposal that photoproduct-to-parent reversion results from the dehydration of 12-hydroxy photoproducts. Allylic alcohol groups on hydroxy steroids are often prone to dehydration under strongly acidic conditions, a reaction pathway often exploited in steroid synthesis. As shown in Scheme 3-1, one possible, and perhaps the most probable, end product of the acid-catalyzed dehydration of 12-hydroxy-17α-TBOH is 17α-TBOH. Several other end products that are isomers or similar structural analogues of 17α-TBOH can also be envisioned. We anticipate that analogous pathways are available to photoproducts of 17β-TBOH and TBO. Accordingly, we interpret the parent recoveries at pH 2 shown in Figure 3-3 represent that maximum amount of photoproduct mass available for reversion to the parent. As the rate of dehydration is nearly instantaneous at pH 2, differences in these recoveries among TBA metabolites most likely reflect differences in the amount of 12-hydroxy species generated via direct photolysis of each metabolite. Indeed, the recoveries at pH 2 are very close to the yield of 12-hydroxy product predicted from relative DAD response, as reported in Appendix A (83, 66, and 60% for 17α-TBOH, 17β-TBOH and TBO, respectively).

The base catalyzed reversion observed for 17α-TBOH is somewhat unexpected. Such high pH conditions would be expected to favor base-catalyzed hydrolysis reactions to yield higher order hydroxylated products. Indeed, we believe this likely explains why little to no base-catalyzed reversion was observed for 17β-TBOH and TBO. The observation of photoproduct-to-parent metabolite reversion at pH 12 for 17α-TBOH might suggest that such higher order hydroxylated products derived from 17α-TBOH are also prone to dehydration.

Thus far, experiments examining photoproduct-to-parent reversion have only observed this phenomenon in the absence of light. However, the dehydration of the12-hydroxy photoproduct should also be occurring in parallel to direct photolysis of TBA metabolites during irradiation. Accordingly, using 17α-TBOH as an example, the rate

law for its change in concentration over time during irradiation is as follows in equation 1:

$$d[17\alpha\text{-TBOH}]/dt = -k_{obs}(\text{photolysis})[17\alpha\text{-TBOH}] +$$

$$k_{obs}(\text{dehydration})[12\text{-hydroxy-}17\alpha\text{-TBOH}]$$

$$(1)$$

In equation 1, k_{obs}(photolysis) is the pseudo-first-order rate constant for direct photolysis, and k_{obs}(dehydration) is the pseudo-first-order rate coefficient for the dehydration of 12-hydroxy-17α-TBOH. We note that values of k_{obs}(photolysis) are reported in Chapter 2 for TBA metabolites, and can reasonably be approximated by the rate coefficient measured over short irradiation timescales (for which the concentration of 12-hydroxy photoproduct is relatively small and thus TBA metabolite production via dehydration can be ignored).

From equation 1, there may exist a point along the reaction coordinate at which the forward rate of metabolite loss via photolysis is equal to the rate of metabolite production via dehydration. This steady state with respect to TBA metabolite concentration could be achieved at sufficiently high concentrations of 12-hydroxy-17α-TBOH (which implies correspondingly low concentrations of 17α-TBOH). Also, such a condition could be attained under system conditions that favor dehydration such that the value of k_{obs}(dehydration) is large.

Based on Figure 3-3, solution pH will influence the value of k_{obs}(dehydration). Results of 17α-TBOH photolysis experiments conducted as a function of solution pH are shown in Figure 3-11a. Concentration data for 17α-TBOH are shown on a semi-log scale as a function of time, revealing generally that the highest rate and greatest extent of 17α-TBOH transformation were achieved at basic pH values (e.g., the half-life at pH 12 was about 14 minutes). In contrast, the slowest rate of decay was observed at pH 2, corresponding to a half-life ($t_{1/2}$ value) of 2.9 h for 17α-TBOH.
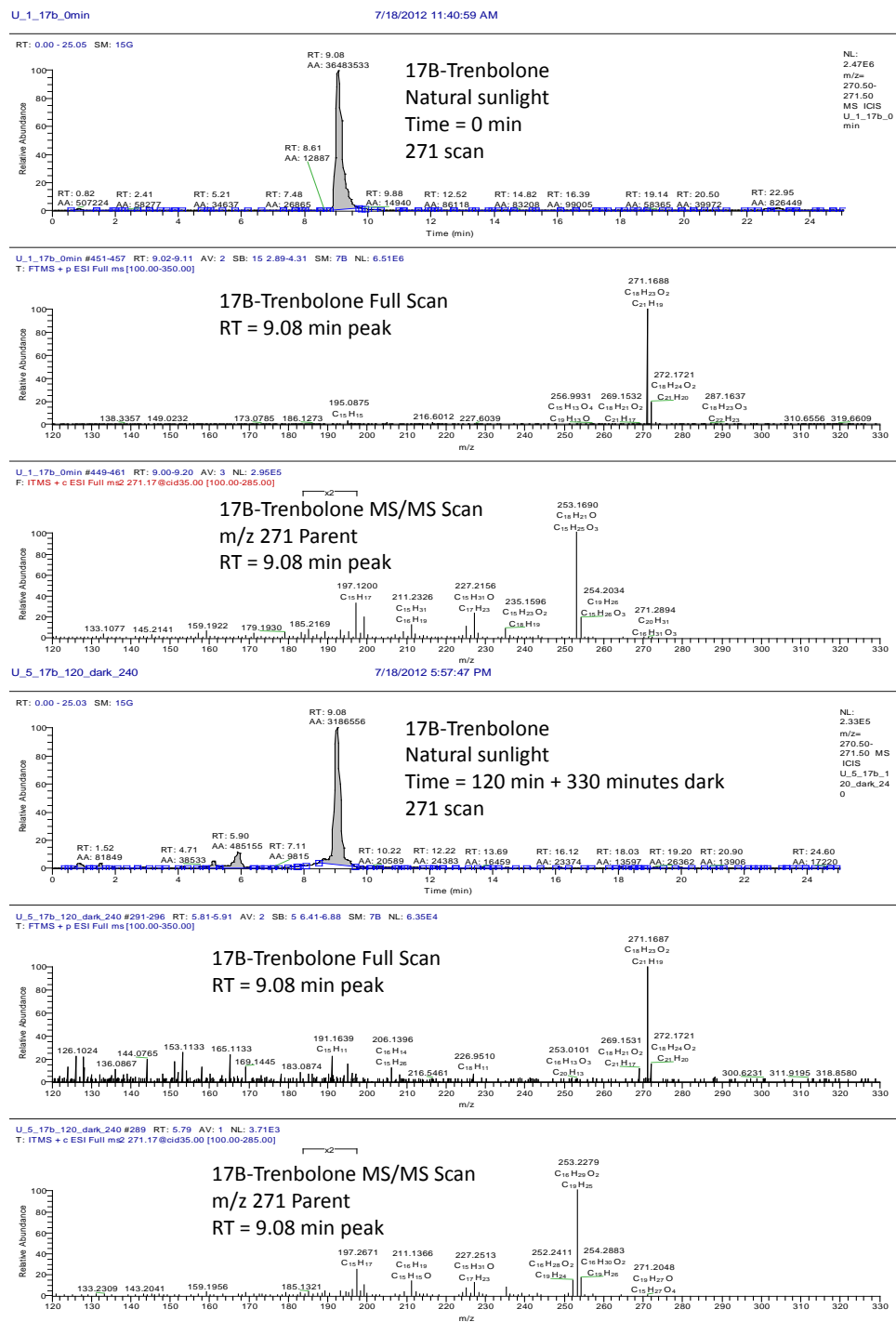
Figure 3-9. LC-MS/MS results for a 17β-TBOH solution analyzed prior to irradiation at pH 7 and after irradiation for 2 h followed by 5.5 hour of storage of the photoproduct mixture in the dark.
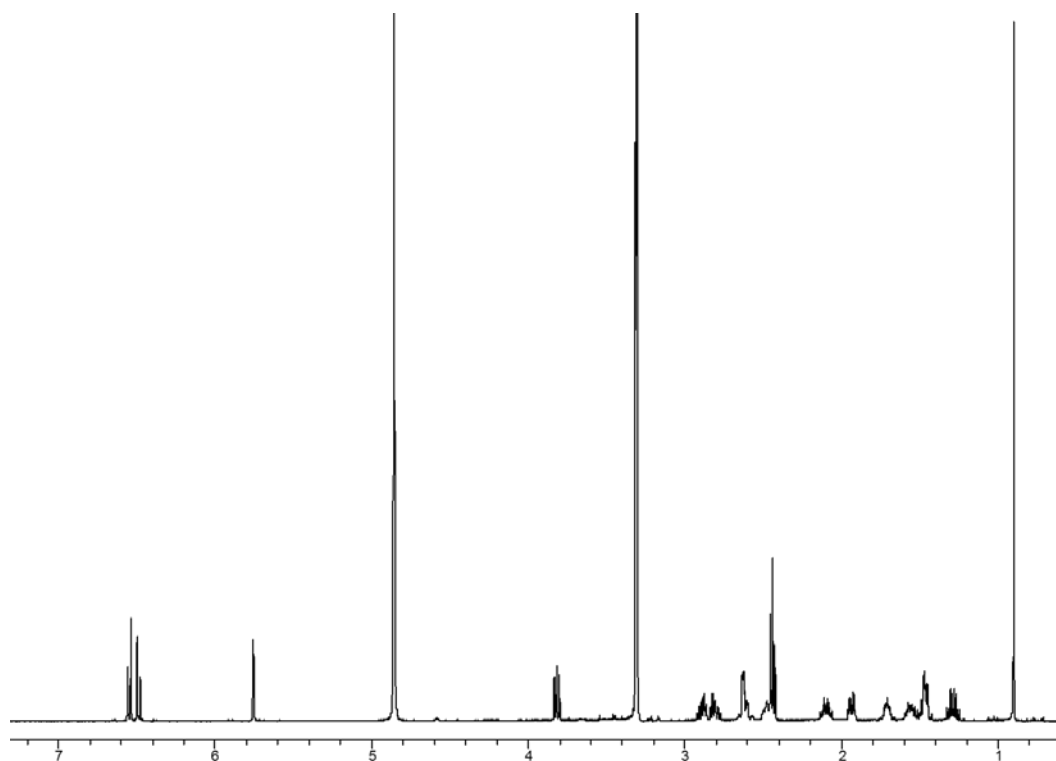
Figure 3-10. ^{1}H NMR spectrum of 17α-trenbolone day regeneration at pH 2

We attribute the dampened photoactivity at pH 2 to the high dehydration rate of 12-hydroxy-17α-TBOH under such conditions. From equation 1, a large value of k_{obs}(dehydration), which is expected at pH 2, would considerably enhance the rate of 17α-TBOH formation via dehydration, even at low concentrations of 12-hydroxy photoproduct. The net effect, therefore, would be for the rapid, acid-catalyzed rate of 12-hydroxy-17α-TBOH dehydration to counterbalance 17α-TBOH loss via photolysis. Indeed, formation of 12-hydroxy-17α-TBOH was not detectable via LC-DAD during photolysis experiments at pH 2, consistent with its rapid consumption via dehydration. It is also noteworthy that some loss of 17α-TBOH did indeed occur during irradiation, such that the rate of its product via dehydration is never equal to the rate of its decay photolysis. This likely reflects the fraction of 17α-TBOH being converted to species not susceptible to dehydration.

At pH 5, 7 and 9, two kinetic regimes for 17α-TBOH transformation were observed (see Figure 3-11a). An initially rapid loss of 17α-TBOH concentration was followed by a period of much slower degradation. At pH 5, the duration of this first regime was quite small (~15-30 minutes), but apparent in repeated experiments. Nevertheless, the rate of 17α-TBOH photolysis at pH 5 was essentially dominated by the slower, second kinetic regime, which yielded a photolysis rate constant (0.34 h^{-1}) on the order of that observed and described previously for pH 2.

At pH 7 and 9, the two kinetic regimes are clearly evident, and a first-order rate coefficient could be estimated for each regime assuming exponential decay. Interestingly, the initially fast decay rate yield coefficients at pH 7 and 9 (~ 2 h^{-1}) comparable to that observed at pH 12. In this fast kinetic regime, roughly 95% of the initial 17α-TBOH mass is consumed. In contrast, the slower kinetic regime produced rate coefficients (~0.2 h^{-1}) more in line with that measured at pH 2. Thus, at pH 7 and 9, the last 5% of 17α-TBOH mass will persist over considerably greater timescales the majority of system mass.

These two kinetic regimes observed at these circumneutral pH values are reminiscent of behavior observed for so-called photostationary reactions [97-99]. Such photolysis reactions are essentially reversible; they achieve steady-state when the forward rate of reactant photolysis is matched by the rate at which the primary photoproduct is photolyzed back into the reactant. Photostationary reactions typically show similar biphasic kinetics. However, it is worth emphasizing again that at pH 5, 7 and 9, we never truly achieve a steady-state in 17α-TBOH concentration, which is continuously decreasing over time, just at different rates. Another distinction is that our primary photoproduct, 12-hydroxy-17α-TBOH, is not photoactive.

In our systems, the two kinetic regimes clearly visible at pH 7 and 9 reflect the competing reaction processes taking place during irradiation of 17α-TBOH. As described in equation 1, 17α-TBOH loss results from its phototransformation to 12-hydroxy-17a-TBOH, while its production is occurring concurrently as a result of the dehydration of 12-hydroxy-17α-TBOH represents a path by which 17α-TBOH can be generated during irradiation. Initially, the high concentration of 17α-TBOH relative to the photoproduct causes the rate of the forward decay process to dominate, producing a net loss of 17α-TBOH over time. However, as the concentration of 17α-TBOH decreases, so too does its rate of the photolysis. Meanwhile, the rate of 12-hydroxy-17α-TBOH dehydration increases along the reaction coordinate due to its accumulation in the closed experimental system. Accordingly, the slower kinetic regime must reflect the point along the reaction coordinate where the rate of dehydration almost equals photolysis, which seems to occur after ~95% transformation of 17α-TBOH.

Also presented in Figure 3-11b the increase in 17α-TBOH concentration observed in the absence of light for the 6 h photoproduct mixtures generated at each pH value in Figure 3-11a. We note that at pH 2 and pH 12, 12-hydroxy-17α-TBOH was never detected at appreciable quantities and we can only presume it reacted too quickly at each pH (back to 17α-TBOH at pH 2 and onto higher order hydroxy products at pH 12) to

accumulate. As such, there was no rebound in the concentration of 17α-TBOH when the photoproduct mixtures at pH 2 and 12 were stored in the dark.

As is to be expected from the acid -catalyzed nature of the dehydration reaction involving 12-hydroxy-17α-TBOH, the rate of 17α-TBOH regrowth was greater initially at pH 5 than at pH 7. This is consistent with the much shorter period of rapid 17α-TBOH photolysis observed in Figure 3-11a, as the greater rate of dehydration is able to nearly equal the forward rate of 17α-TBOH photolysis earlier along the reaction coordinate. Surprisingly, however, the increase in 17α-TBOH concentration as a function of time was greatest at pH 9, far exceeding the regrowth rate at pH 7. This was unexpected, primarily because there minimal difference was observed in the decay kinetics of 17α-TBOH during photolysis between pH 7 and 9 (see Figure 3-11a). If the rate of 12-hydroxy-17α-TBOH dehydration was greatest at pH 9 relative to pH 5 and 7, then we would expect to see the onset of the slower kinetic regime much earlier along the reaction coordinate than is actually observed at pH 9. The rapid rate of 17α-TBOH regeneration observed at pH 9 only leads us to conclude that some of the higher order hydroxy products derived from 12-hydroxy-17α-TBOH via hydrolysis must also be prone to this reversion process.

<center>Influence of Temperature on Photoproduct-to-Parent</center>

<center>Metabolite Reversion</center>

In addition to pH, we also found temperature to have a large impact on the persistence of 17α-TBOH in surface waters. For product mixtures generated at pH 7 after 6 h of photolysis, the dark regrowth rate of 17α-TBOH increased markedly from 5 to 35 °C (Figure 3-12), a temperature range chosen to mimic seasonable variations likely to be encountered in surface waters. Indeed, assuming an initially linear increase in 17α-TBOH concentration over time, the rate of reversion increases by a factor of 30 over this temperature range. The greater rate of reversion at 35 °C ultimately allows a more

complete recovery of 17α-TBOH at pH 7 (nearly 80% of the initial mass present over 60 h in the dark). Also, this greater rate results in almost 30% of the 17α-TBOH being regenerated over a typical diurnal (12 h) dark cycle. Estimates for the initial rate of 17α-TBOH regrowth were used to construct an Arrhenius plot (Figure 3-12b), from which activation energy (E_a value) of 1.1 kJ/mole was obtained for the reversion reaction, value much smaller than that typically observed for the dehydration of alcohols [100, 101], suggesting the –OH group on 12-hydroxy-17α-TBOH is highly labile.

3.5   Environmental Implications

TBA and its metabolites already fit the profile of a constituent of emerging concern with respect to their environmental impact. TBA is broadly utilized in animal agriculture, so there is a clear and high volume route of entry for TBA metabolites into the natural environment. Negative impacts on ecosystem health, specifically their impact on the reproductive capabilities of aquatic organism, have also been documented. In light of these observations, an attribute touted by the chemical manufacturer [46] is its limited persistence in surface waters due to its rapid chemical transformation via direct photolysis, relying on the faulty paradigm that transformation implies removal.

Here, we show unequivocally that TBA metabolites, most notably the dominant metabolite 17α-TBOH, are far more persistent in surface waters due to the previously unrecognized reversible nature of its direct phototransformation. The regrowth of TBA metabolites in surface waters is attributable to two chemical factors: (1) the highly reactive nature of the allylic hyrdroxyl group present at the C12 position of the dominant phototransformation product for each TBA metabolite and (2) the presumed superior thermodynamic stability of the unique 4,9,11-triene structure shared by all metabolites relative to the meta-stable 12-hydroxy photoproduct. Together, therefore, coupled photolysis and dehydration reactions provide a viable route by which TBA metabolites can be produced to significant quantities and persistent to greater extent in surface waters.
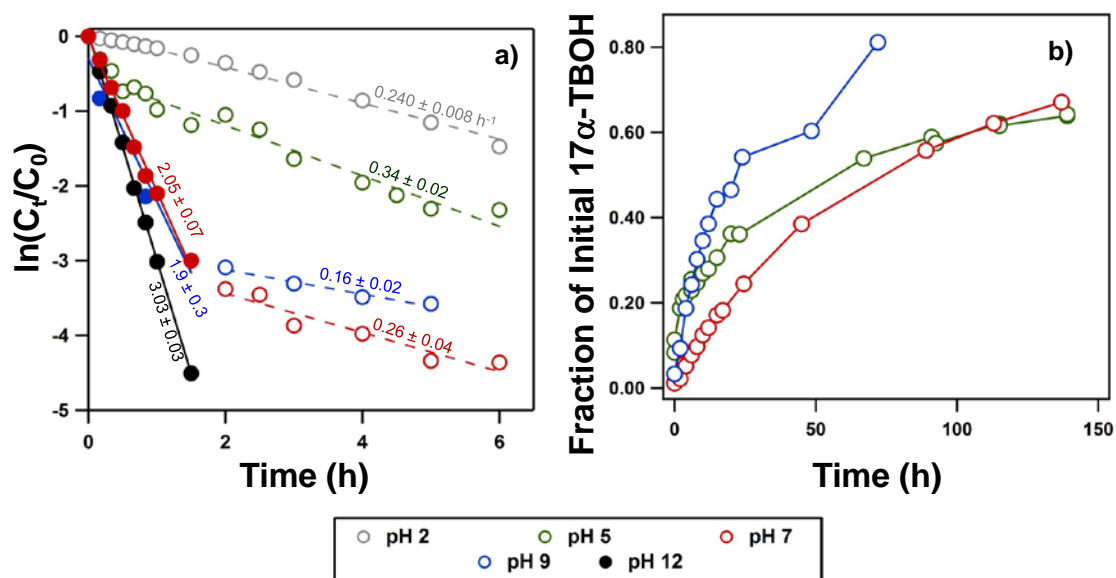
Figure 3-11. (a) Plots of the natural log of normalized 17α-TBOH concentration as a function of time at different pH values. Kinetics are biphasic at pH 5, 7 and 9, where decay is initially rapid (solid symbols) only to slow over time (open symbols). Both initially and over longer timescales, 17α-TBOH decay follows exponentially, allowing pseudo-first order rate coefficients to be determined for each regime (best-fit linear regressions and the resulting k_{obs} values from this analysis are provided). At extreme pH values, biphasic kinetics are not observed, with the rate constant for 17α-TBOH decay at pH 12 being more than an order of magnitude greater than measured at pH 2. (b) Regeneration of 17α-TBOH as a function of pH for the photoproduct mixtures generated in panel (a) after 6 hours of irradiation. 17α-TBOH regeneration is presented as a fraction of the total mass initially present in a system.
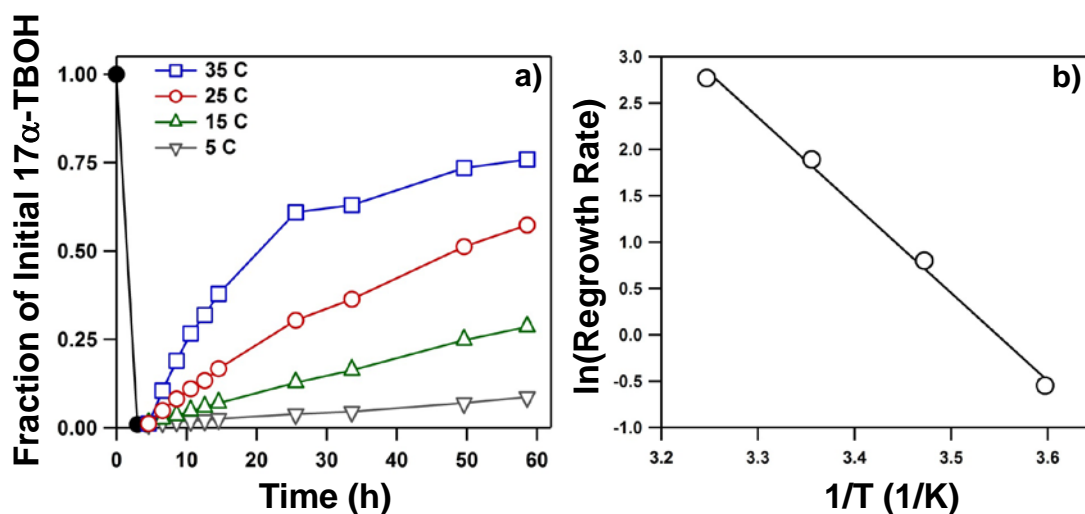
Figure 3-12. (a) Influence of temperature on the regeneration of 17α-TBOH. 17α-TBOH regeneration is presented as a fraction of the total mass initially present in a 10 mM solution that was irradiated for 4 h at 25 °C and then divided into four samples that were stored in the dark at the temperatures listed. (b) An Arrhenius plot of the natural log of the regrowth rate as a function of inverse temperature (in Kelvin). Regrowth rates were determined from data presented in (a) from the initially linear ($t < 15$ h) increase in 17α-TBOH concentration over time.

We should note that this photoproduct-to-parent reversion is highly unique. To the best of our knowledge, no other coupled photolytic-hydrolytic cycles exist in the literature. Further, when specifically focused on steroids, appreciable rates of dehydration for hydroxyl steroids are rarely, if ever, observed in neutral pH aqueous solutions.

The practical implications for this photoproduct-to-parent reversion mechanism in agriculturally impacted waters are steep. First, estimates of surface water half-life based entirely on empirically measured rates of direct photolysis will likely vastly underestimate the true persistence of TBA metabolites in surface waters. Second, the amount of TBA metabolites present in surface waters will be dependen on the amount of 12-hydroxy photoproduct present in the system. As a proof of concept, we have conducted respike experiments at pH 7 in which we see the concentration of 17α–TBOH achieved after extensive photolysis gradually increasing as more and more mass is added to the system (Figure 3-13). The accumulation of 12-hydroxy-17α-TBOH over time in the closed reactor gradually over time increases the rate of dehydration and the formation of17α-TBOH as a result of this process. Similar trends in concentration over time would be expected for a closed system, such as a retention pond, that receives agricultural runoff impacted with 17α-TBOH.

Further, we anticipate that the concentration profiles of TBA metabolites in surface waters will be highly sensitive to aquatic chemistry and system conditions. System pH will be a critical determinant. Also, the concentration profiles should be cyclic in nature, exhibiting both diurnal (light-dark) and seasonal (i.e., greater prevelance of reversion in the warm summer months) patterns. The worst case scenario would be a mildly acidic water supply during the summer months, for which the measurable quantities of TBA metabolites at night will greatly surpass values measured in samples collected during daylight hours.

Ultimately, this work provides a clear example for when transformation does not equate with removal. For TBA metabolites, it is no longer sufficient simply to measure

metabolite concentration. Rather, going forward, all occurrence studies must also assess with equal importance the concentration and persistence of its major phototransformation products.
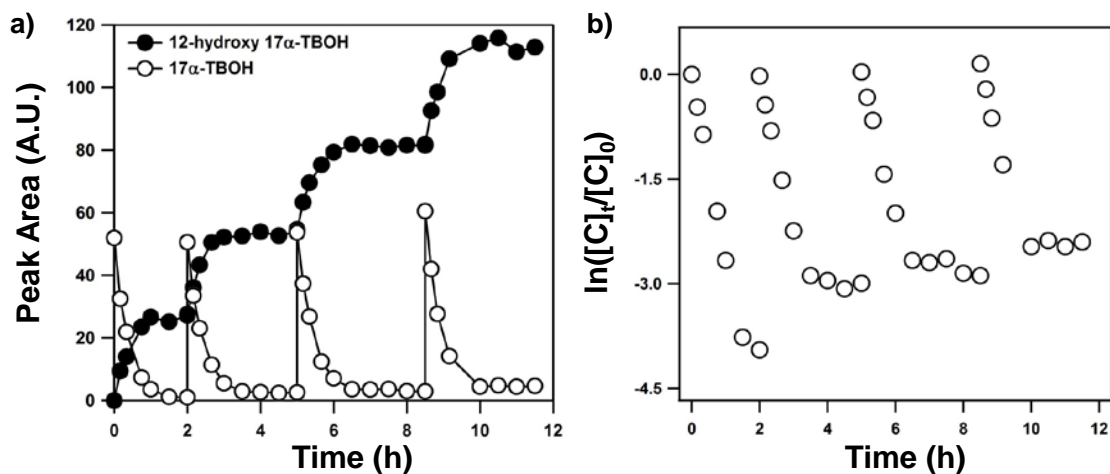
Figure 3-13. (a) Results of re-spike experiments at pH 7 and 25 °C monitoring the concentration of 17α-TBOH and its major photoproduct 12-hydroxy-17α-TBOH over time. The amount of each species is presented based on peak area response measured via LC-DAD. Sequentially, 1 μM 17α-TBOH was added to the reactor, allowing the photostable 12-hydroxy-17α-TBOH to accumulate over time. (b). Semi-log plot of 17α-TBOH concentration as a function of time for the respike experiments shown in panel (a). On a semi-log scale, the gradual increase in the concentration of 17α-TBOH near completion of each photoreaction is clearly observed.

CHAPTER IV. SORPTION AND MINERAL-PROMOTED

TRANSFORMATION PATHWAYS OF SYNTHETIC GROWTH

PROMOTERS IN SOIL SYSTEMS

4.1   Abstract

The widespread use of trenbolone acetate, melengestrol acetate and zeranol as synthetic hormone growth promoters in animal agriculture has resulted in their frequent detection in surface water and soil where they may threaten ecosystem health as possible endocrine disrupting compounds. This work examines the fate of these synthetic growth promoters and their major metabolites (SGPMs) in soil, focusing on their interactions with soil organic matter and their susceptibility to mineral-promoted oxidation and hydrolysis reactions. Sorption kinetics and isotherm experiments with organic rich Pahokee Peat reveal generally high affinity for SGPMs for organic matter. However, the extent of SGPM sorption, as well as sorption reversibility, did not always scale with simple metrics for hydrophobicity (e.g., octanol-water partitioning), suggesting that uptake of certain SGPMs (i.e., those with greater polarity) may be influenced by specific chemical interactions (e.g., hydrogen bonding). In systems with model soils exhibiting a range of soil organic carbon contents (1%-5.9%), SGPM behavior was consistent with coupled sorption on soil organic carbon and reaction with the underlying inorganic mineral phase. Unlike systems with Pahokee Peat, sorption equilibrium could not be achieved and SGPM mass balances could not be closed in most soil systems. In soil systems, the relative extent of sorption versus reaction is influenced by the amount of soil organic carbon and SGPM hydrophobicity. Although transformation products were not detectable, experiments with metal oxides representative of naturally occurring mineral phases (e.g., MnO_2, SiO_2, and iron oxides) indeed show loss of SGPM mass over time, consistent with their transformation, presumably via mineral-promoted hydrolysis and/or oxidation reactions. We provide the first results that SGPMs will be highly less stable in

soil than typically expected as a result of mineral-promoted transformation pathways that occur in parallel to sorption. Further, the timescales of these abiotic transformation processes are likely to make them relevant when compared to timescales associated with their microbially mediated transformation.

4.2   Introduction

The environmental fate of synthetic hormones used as growth promoters in animal agriculture has received increasing scrutiny due to their potential adverse impacts on ecosystem health. Trenbolone acetate (TBA), melengestrol acetate (MGA) and zeranol are three synthetic hormone growth promoters approved for use by the U.S. Food and Drug Administration in animal husbandry to improve meat production [29, 30, 102]. Widespread use has resulted in these synthetic growth promoters and their primary metabolites (SGPMs; Table 4-1) being frequently detected in water and soil near animal agriculture operations. In soil, specifically, levels on the order of 1-100 ng/kg have been frequently reported [16, 17, 36, 103]. Their presence is noteworthy because of their likely role as endocrine disrupting compounds. For example, a series of studies by Ankley et al. found that 17α-trenbolone and 17β-trenbolone, stereoisomeric metabolites of androgenic trenbolone acetate, decreased fecundity in the female fathead minnow at exposure levels of 10-30 ng/L [22, 39].

We have previously shown in Chapters 1 and 2 that photolysis represents the major transformation pathway for SGPMs, with half-lives of direct photolysis on the order of one hour or less in certain cases. In soil, on the other hand, biotransformation is believed to be the major sink for this emerging pollutant class. Khan et al. [87] reported half-lives of 17α-trenbolone, 17β-trenbolone and trendione in different soils represented aerobic microcosms between 4 and 100 h, with some variation resulting from a dependence of transformation rate on TBA metabolite concentration.

Table 4-1. Structures of SGPMs used in sorption studies. The numbers adjacent to each structure represent reported [7] logK_{ow} values (octanol-water partitioning coefficients). Values in red were measured by the method described below.

4.21

Trenbolone Acetate

3.08/3.09 17β-trenbolone

2.63 Trendione

2.72 17α-trenbolone

3.93 Melengestrol Acetate

3.39 Melengestrol

3.88 Zeranol

3.29 β –Zearalanol

4.10 Zearalanone
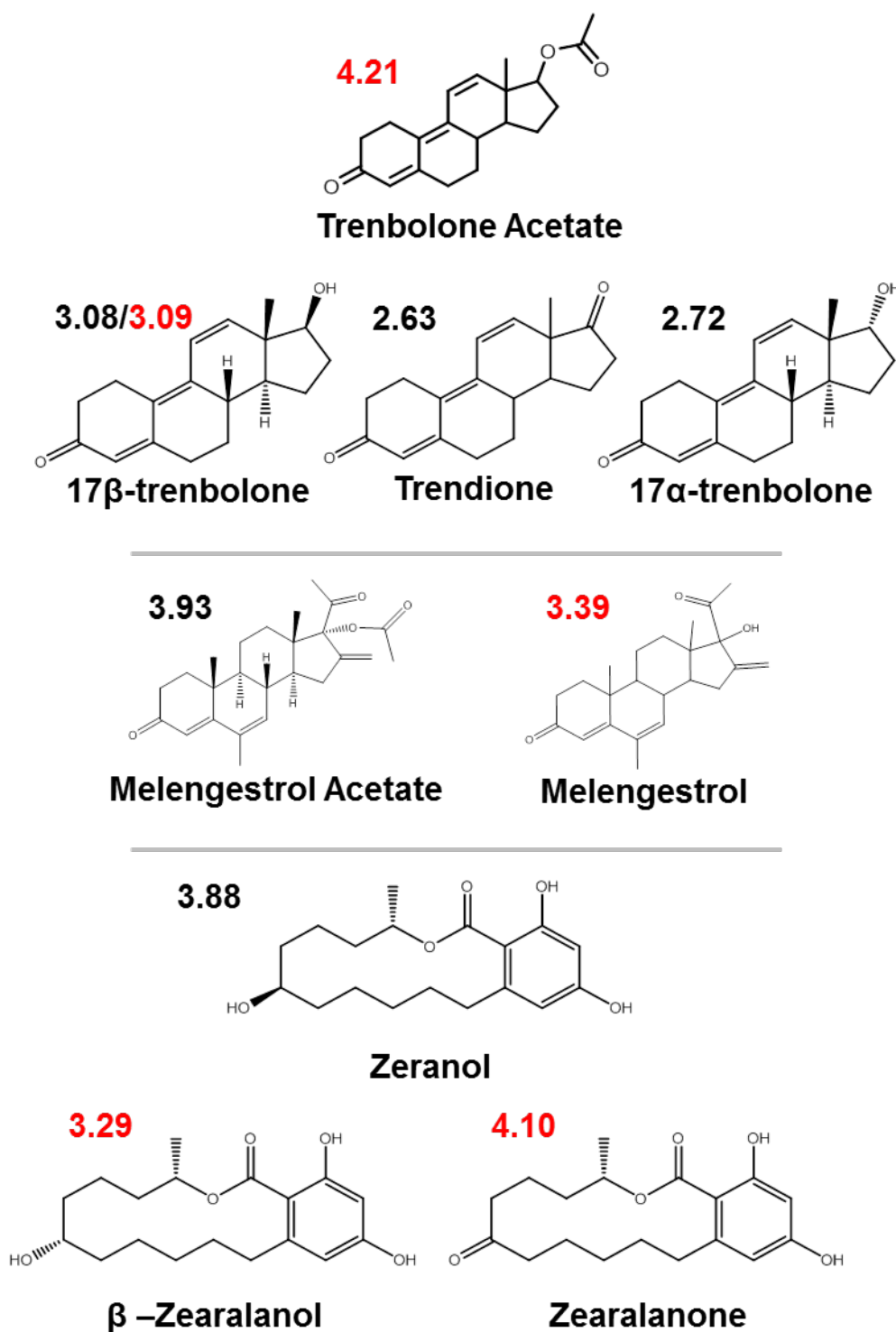
Sorption is another process that will impact SGPM fate in soil systems, where they occur after land application of manure or upon irrigation with water impacted by feedlot runoff. Sorption is a critical determinant not only for the rate of SGPM biotransformation (i.e., sorbed phases as generally less bioavailable), but also their mobility in the surface and in turn their potential to migrate into underlying groundwater aquifers or into an adjacent water body. Schiffer et al. [48] investigated the transport of 17β-trenbolone (17β-TBOH) and MGA through columns packed with relatively low organic carbon (0.3% and 1.6%) soil materials from a German luvisol. Although breakthrough of both compounds was observed within the first pore volume, column effluent concentrations did not achieve inflow concentration levels for either 17β-TBOH ($C_{effluent} \sim$ 24-34% $C_{influent}$) or MGA ($C_{effluent} < 0.05\%$ $C_{influent}$). They proposed that both compounds, with moderate to high $\log K_{ow}$ values (see Table 4-1), exhibited high affinity for soil organic carbon, concluding that movement of these compounds into the subsurface would be minimal [48]. However, a major drawback of the work by Schiffer et al. [48] was that 17β-TBOH and MGA loss was equated to sorption even though their column systems were not sterilized to limit biodegradation nor were attempts made to close the mass balance in their column systems by extracting sorbed species.

Subsequent laboratory studies with steroid hormones have supported a scenario in which hydrophobic interactions primarily dictate hormone sorption on soils [49, 50, 52, 53]. For example, Khan et al. [49] developed sorption isotherms for the trenbolone family of compounds [17β-TBOH, 17α-trenbolone (17α-TBOH) and trendione (TBO)] on five sterilized (via autoclaving) soils exhibiting a range in soil organic carbon content (0.48%-7.5%). To address the potential for biodegradation, isotherms were developed using mass extracted (with methanol) from equilibrated soil suspensions, which generally closed the mass balance in their system. They reported a good correlation between their sorption distribution coefficient (using the Freundlich adsorption coefficient, K_f in L/kg, from their non-linear isotherms) and soil organic carbon content (R^2 values >0.97) [49].

They concluded that the hydrophobic-type partitioning into soil organic matter was likely the dominant force driving sorption. However, they also proposed that additional, non-hydrophobic interactions such as hydrogen bonding involving the phenol or ketone groups likely also contributed to the uptake of TBA metabolites by soils [49].

In a subsequent study by the same group, Qiao et al. [51] measured the association of 17α-TBOH, 17β-TBOH and TBO with two commercial humic acids (Aldrich humic acid and Leonardite humic acid) to further evaluate isomer-specific interactions between steroids and soils. Most of their sorption isotherms exhibited non-linearity, indicating the contribution of some surface site-specific H-bonding and π-π interactions during TBA metabolite partitioning. Further, they observed that relative trends in sorption for 17β-TBOH and 17α-TBOH on their soils (more uptake for 17β-TBOH was observed relative to 17α-TBOH) was opposite of the trends in their retention times on a reverse phase LC column with a polar mobile phase (17β-TBOH eluted before 17α-TBOH). This provided another line of evidence that specific bonding interactions were likely important for the TBA family.

Most recently, Card et al. [50] developed sorption isotherms of several endocrine disrupting compounds including 17α-TBOH, 17β-TBOH, TBO, MGA and zeranol with three agriculture soils with different organic carbon content (1.1%-7.7%). They reported $\log K_{oc}$ and K_{ow} values measured experimentally, as well as sorption isotherms collected on each model soil. To account for possible biotransformation, these studies employed autoclaving for soil sterilization, and also constructed sorption isotherms based on the mass of SGPM recovered via extraction of equilibrated soils with organic solvents (e.g., methanol). Using this approach, they found that sorption isotherms were generally linear for most solute-soil combinations and that K_d values were well correlated with the soil organic carbon content (i.e., %OC), similar to the correlation that was also previously reported for 17α-TBOH, 17β-TBOH and TBO by Khan et al. [49]. They concluded,

therefore, that sorption of SGPMs in soil was primarily dominated by hydrophobic interactions with soil organic matter.

Nevertheless, questions still remain about some fundamental aspects of SGPM partitioning in soil systems. While the work of Card et al. [50] and Khan et al. [49] proposed that hydrophobic interactions were primarily responsible for uptake, other results from the same laboratory [51], which considered the uptake of 17α-TBOH,17β-TBOH and TBO onto humic acids, proposed a different driving force for adsorption. Specifically, Qiao et al. [51] suggested that specific interactions rather than hydrophobic partitioning (as would be expected for correlations with soil organic carbon content) dictated sorption. Thus, questions persist as to what characteristics of the SGPM and soil are truly most critical for sorption. Another factor yet to be addressed is that nearly all prior studies with SGPMs [48-50, 52, 53] have failed to consider whether sorption is reversible. This detail is necessary for predicting the extent to which sorption will affect SGPM mobility as they are transported through soil systems.

A final factor that has yet to merit any research focus is the possibility that inorganic phases present in soil may also influence the fate of SGPMs. While inorganic mineral phases could potentially function as sorbents, particularly when electrostatic interactions or surface complexation are important routes for uptake, they may also be able to promote various transformation reactions. For example, melengestrol acetate and the zeranol family of compounds have hydrolyzable ester functionalities. Also, resonance resulting from 4,9,11-triene structure in the trenbolone family of compounds yields several carbon centers that are electron deficient and may also be prone to attack by nucleophiles under certain conditions. Although hydrolysis is reported to be slow at near-neutral pH values for these compounds [34, 45, 46], metal oxides commonly found in soil are known to catalyze hydrolysis reactions via the formation of surface complexes that are more prone to attack by H_2O or OH^- than the freely dissolved molecule. In addition to hydrolysis, manganese and iron oxides minerals can also oxidize a wide range of organic

compounds including species such as estrone, 17β-estradiol and estradiol, which have similar structure moieties to SGPMs [54, 55]. Thus, it is likely that SGPMs, particularly metabolites of TBA and MGA which are more prone to photooxidation than estrogens, will also be highly reactive toward such metal oxide oxidants commonly encountered in soil. Currently, however, studies have yet to consider a role for metal catalyzed hydrolysis and oxidation for SGPMs, and thus such pathways merit consideration.

In this Chapter, we explore abiotic pathways influencing the fate of SGPMs in soil systems. The rate and extent of SGPM sorption was considered both in a model, organic rich soil (Pahokee Peat) as well as several commercially available model soils exhibiting a range of soil organic carbon (1.0-5.9%) more representative of soil systems. To limit SGPM loss in all experiments to only abiotic processes, all soils were first sterilized with sodium azide (NaN_3). Sorption kinetics and isotherm experiments were conducted at pH 7, and trends in sorption were evaluated both within (e.g., 17α-TBOH, 17β-TBOH, and TBO) and across families (e.g., comparing TBA metabolites, MGA and melengestrol and zeranol metabolites) of SGPMs to evaluate the types of interactions driving their sorption in soil. For isotherm experiments, the extent to which SGPM sorption was reversible was also explicitly addressed. In all cases, solvent extraction of equilibrated soils was used to recover the mass of sorbed SGPM, and loss of mass over time in our experimental systems was interpreted as evidence for nonconservative abiotic processes (e.g., reaction with inorganic mineral phases). To explore the potential for such abiotic transformation pathways, experiments were also conducted to monitor the stability of select SGPMS (17β-TBOH, MGA and zeranol) in the presence of metal oxides representative of those naturally occurring in soil. Results from this study will help to provide insight into environmental fate and mobility of SGPMs in subsurface environments, thus improving our ability to predict the potential immobilization pathways as well as exposure risks associated with this emerging pollutant class in the natural environment.

4.3   Experimental Methods

Reagents

All SGPMs were available commercially including 17β-TBOH (Sigma-Aldrich,> 95%), 17α-TBOH (Cerilliant, 99%), TBO (Steraloids), melengestrol acetate (Sigma-Aldrich, 96%), melengestrol (Steraloids Inc., 99%), zeranol (Sigma-Aldrich, 97%), β -zearalanol (Sigma-Aldrich, 97%) and zearalanone (Sigma-Aldrich, 97%). Methanol (Fisher, HPLC grade) was used to prepare stock solutions of SGPMs and as a mobile phase for HPLC analysis along with acetonitrile (Fisher, HPLC grade). A phosphate buffer from monobasic potassium phosphate (Fisher, 99%) was used in all sorption experiments. Sodium azide (Fisher, 99%) was used to sterilize soils. Sodium bicarbonate (Fisher, ACS grade) and ferric nitrate nonahydrate (Fisher, ACS grade) were used to synthesize the iron oxide ferrihydrite while sodium permanganate monohydrate (Sigma-Aldrich, ≥97%) and manganese (II) chloride (Sigma-Aldrich, ≥99%) were used in manganese oxide synthesis. Silica dioxide (99%) powder was used as received from Sigma-Aldrich. All solutions were prepared in deionized water (Millipore, Q-Grad2).

Model soils and mineral oxides

Eight model soils exhibiting a range in soil organic carbon content were used in sorption studies (Table 4-2). Pahokee Peat and Elliott soils were purchased from the International Humic Substances Society (IHSS), while several other soils were acquired through AGVISE Laboratories (Northwood, ND and Benson, MN). The soils from AGVISE Laboratories have different textures and a range of organic carbon content, the details of which are provided in Table 4-2. For the data provided in Table 4-2, the organic carbon content of Pahokee Peat and Elliott soil were determined via the Lloyd Kahn Method [104] with analysis conducted by the commercial laboratory Test America. The organic carbon content of all the other soils were supplied by the vendor (AGVISE Laboratories) and quantified from the loss-on-ignition methods [105].

A mineral phases representative of naturally occurring metal oxides, commercially available silica dioxide (SiO_2; Sigma-Aldrich, 99%) was used to represent the main component in natural soils. Ferrihydrite was synthesized using standard method [106] and manganese dioxide (MnO_2) was synthesized via the method of Murray [107].

Briefly, for ferrihydrite synthesis a peristaltic pump was set to a rate of 4.58 mL/min, and 1.0 L of 0.48 M $NaHCO_3$ was added dropwise to a continuously stirred 1.0 L solution of 0.4000 M $Fe(NO_3)_3 \cdot 9H_2O$. During the transfer, the solution changed from bright orange to dark brownish red with no visible precipitate. The suspension was separated into 250 mL Nalgene bottles and microwaved one at a time until boiling occurred, shaking every 40 s (most boiled after 120 s). Immediately after heating, each suspension was plunged into an ice bath until it reached ~20 °C. In order to remove the counter ions present from the synthesis, the cooled suspensions were placed into dialysis bags (MWCO=3500), which were placed in Milli-Q H_2O. The water was changed three times per day for three days. The resulting suspensions were placed in a number of weigh boats and placed in a fume hood to dry. A mortar and pestle were used to grind the dry, dark reddish brown particles into a fine powder with subsequent sieving with a 53uM sieve.

For manganese oxide, both 100 mL of 0.1 M $NaMnO_4$ and 100 mL of 0.15 M $MnCl_2$ were prepared. 4 mL of 5 M NaOH was added dropwise into the $NaMnO_4$ solution, and then the $MnCl_2$ solution was added dropwise (at 5 mL/min) into $NaMnO_4$ solution. The final suspension was washed 3 times by centrifuging aliquots of 40 mL and replacing aqueous phase with MilliQ DI water. The suspension was air dried to form MnO_2. Dry solids were ground and filtered through a 53µM copper sieve.

Table 4-2. Texture and organic carbon content (w/w%) for the model soils used in sorption experiments.

Soil Name	Vendor	Texture	Organic Carbon (%)
PVLPF	Agvise	Loam	5.9
PVPF	Agvise	Sandy Loam	5
DUL	Agvise	Clay Loam	3.3
Elliot	IHSS	Silt Loam	3.1
LBLS	Agvise	Sandy Loam	3
EL-7	Agvise	Loam	2.8
RMN	Agvise	Loamy Sand	1

Soil sterilization

Soils were sterilized by adding sodium azide (NaN_3) as described by Wolf et al. [108], with the exception that the dose was increased to 30.8 mmol NaN_3/kg soil [109]. Briefly, 36-180 mg of soil was added to 20 mL glass beakers to which Milli Q water was added to a final volume of 18 mL. This suspension was then incubated with appropriate volume of 1 M or 200 mM NaN_3 for 72 h at room temperature. Preliminary experiments also considered sterilizing soil samples via autoclaving at 121°C and 15 psi for 30 minutes [108]. Ultimately, we chose to use azide as our primary sterilization method because it gave the least amount of SGPM loss from solution when compared to non-sterilized (used as received) soils, in which some biotransformation likely occurred.

Octanol-Water (K_{ow}) Partition Coefficient

An adjusted method was used based on Karickhoff and Brown, 1979 [110]. In general, reagent grade of octanol was extracted once by 0.1 N NaOH, twice with Milli Q water. Sodium sulfate was dropped in the solution to collect water and then was filtered out through a 0.2μM filter paper. The SGPM was prepared in the octanol at or near saturation concentrations. A small volume of this octanol solution (1 ml) was equilibrated with appropriate volume of Milli Q water (6 ml). Equilibrium was achieved by shaking the samples on the shaker at 200 rpm for 24 hours. Subsequent to equilibration, the samples were centrifuged in glass centrifuge tubes at 3000 rpm for 20 minutes. And the phases were sampled out of the centrifuge tubes. A subsample of the octanol phase (10 μl) was withdrawn by glass syringe into an autosampler vial with appropriate amount of methanol (1 ml). The water phase was directly withdrawn with glass pipets into an autosampler vial. The samples in autosampler vials were then measured on the HPLC.

Sorption experiments

Batch sorption studies first explored the rate of SGPM sorption and the timescales necessary to achieve equilibrium. Experiments were conducted at pH 7.0 in a 5 mM phosphate buffer. Kinetic rate experiments used initial SGPM concentrations between 2-4 µM and a soil loading of 2-10 g/L. Sorption isotherms were collected over a range of initial concentrations (1-10 µM) at a constant sorbent loading of 2 g/L at room temperature. These initial concentrations are higher than environmentally relevant, but were necessary to facilitate SGPM analysis via HPCL with diode array detector. In all cases, the highest initial concentration used for each SGPM was below their reported aqueous solubilities (e.g., 1330, 2.6 and 15 µM for 17α-trenbolone, MGA and zeranol) [34, 45, 46]. Nevertheless, control experiments were conducted in the absence of soil but with otherwise identical solution phase conditions to ensure the aqueous phase stability of the SGPMs at these initial concentrations.

To initiate sorption kinetic and isotherm studies, a small volume (2-18 µl) of SGPM methanolic stock solution was added to a suspension of sterilized soil via syringe to achieve the desired initial concentration. In all cases, the use of the methanolic stock resulted in no more than 0.1% of methanol by volume. Sorption experiments were conducted in glass beakers whose contents were well-mixed via a glass-coated magnetic stir bar and electronic stir plate. Reactors were sealed with Parafilm to slow evaporation and covered in Al foil to prevent photoreactions.

Kinetic studies were typically conducted over the course of one week, during which samples were taken at pre-determined time intervals to monitor the change in SGPM solution concentration over time. For sorption isotherms, equilibrium was typically established after 3 days, at which time samples were collected to monitor the mass of SGPM remaining in solution. The extent to which sorption was reversible was also considered in these isotherm experiments. After collection of the aqueous sample at equilibrium, the entire remaining suspension was centrifuged and a fixed volume (typically 8 mL) of supernatant was replaced by fresh buffer to perturb the sorption

equilibrium that had been established. The altered suspension was then allowed to mix for the same amount of time as was necessary to establish equilibrium (typically 3 days), at which time aqueous samples were taken to measure the aqueous phase SGPM concentration.

Samples of suspension were separated via centrifugation at 3000 rpm for 5 minutes and the supernatant was analyzed subsequently on HPLC-DAD to quantify the dissolved phase concentration of SGPM. Centrifugation was chosen for solids removal rather than filtration because most commercially available filters (PTFE or Nylon) resulted in some loss of SGPMs during solid-liquid separation. Using this approach, the amount of SGPM sorbed to the soil was quantified via mass balance from the difference in the initial SGPM concentration in the reactor and the aqueous phase concentration of SGPM present in solution at equilibrium.

At the conclusion of all sorption experiments, the mass of SGPMs sorbed onto the soil sample was also quantified via after extraction using organic solvent. Specifically, the entire suspension was centrifuged, the supernatant was removed, and 3 mL of either methanol or dichloromethane (DCM) was added to the soil. The resulting suspension was sonicated for 5 minutes, which was found to be sufficient for recovery of the sorbed mass into either methanol or DCM. After sonication, the suspension was centrifuged once again to separate the organic solvent from the solid, and a sample of the solvent phase was collected for immediate HPLC analysis.

Exploring SGPM reactivity toward metal oxides

Reactions with metal oxides (SiO_2, MnO_2, and ferrihydrite) were conducted at pH 7.0 in 5 mM phosphate buffer at room temperature. Experiments were conducted over a range of oxide loading (1-10 g/L) and SGPM initial concentration (1-5 µM). The oxide suspensions were allowed to equilibrate with the buffer solution for 20 minutes, after which the pH of the system was adjusted (if necessary) back to 7 using 1 M HCl or

NaOH. Once the pH was stabilized, a small volume of methanolic stock solution was used to deliver the SGPM to the suspension. Reactors were covered by Al foil to avoid photodegradation and the suspension was well-mixed using a glass-coated magnetic stir bar and stir plate. Over time, a 1 mL aliquots of suspension were collected, centrifuged to separate the metal oxide from the aqueous phase, and the supernatant then was transferred to an amber autosampler vial for immediate HPLC analysis.

<u>Analytical Method</u>

Samples were analyzed on a 1200 Series Agilent HPLC-DAD equipped with an Eclipse XBD-C18 column (4.6 × 150 mm, 5 μm particle size). Analysis of trenbolone family members used a mobile phase of 50:50 acetonitrile (ACN):H_2O, a flow rate of 1 mL/min, an injection volume of 25 μl and a 350 nm detection wavelength [87]. Analysis of melengestrol family members used a mobile phase of 60:40 ACN:H_2O, a flow rate 1 mL/min, an injection volume of 25 μl and a 300 nm detection wavelength [48]. Analysis of α-zearalanol and β-zearalanol used a mobile phase of 60:40 methanol (MeOH):H_2O, a flow rate 1.5 mL/min, an injection volume of 20 μl and a 210 nm detection wavelength [72], whereas zearalanone analysis used a mobile phase of 8:46:46 MeOH:H_2O:ACN [73], a flow rate 1 mL/min, an injection volume of 25 μl and a 210 nm detection wavelength.

4.4   Results and Discussion

<u>SGPM Sorption on Pahokee Peat</u>

Initial kinetic experiments were used to gauge the timescales necessary to achieve presumed sorption equilibrium in systems with Pahokee Peat. These kinetic experiments revealed that most the solution concentration of SGPMs reached near steady-state (i.e., no further loss of solution phase concentration over time) Peat by 3 days in suspensions with 2 g/L and ~5 μM SGPM originally in the suspension (Figure 4-1). A notable

exception was β-zearalanol (data not shown) for which the aqueous concentration decreased steadily over time until it was no longer detectable in solution after one week. Although not entirely understood, we were unable to identify any conditions (e.g., lower solid loadings) under which the solution phase concentration of β-zearalanol reached a steady-state, and we also observed β-zearalanol to be the only species for which soil free controls also exhibited an appreciable concentration loss over time. Due to these challenges encountered in the β- zearalanol system, its sorption behavior was not extensively explored in subsequent experiments.

We also note that although the aqueous concentration of certain TBA metabolites was still declining slightly after 3 days of reaction, we found that equilibrium in these systems could be achieved over this timescale in reactors with slightly modified conditions (e.g., at higher concentrations Pahokee Peat at 10 g/L and 17β-TBOH at 70 μM in our systems).

In isotherm experiments, we assumed that sorption equilibrium was achieved within 3 days for all compounds. Sorption isotherms are shown in Figure 4-2, in which data are presented on a log-log scale. Also shown are fits in which SGPM sorption on Pahokee Peat is assumed to obey the Freundlich isotherm model (equations 4-1 and 4-2).

$$C_s = K_f C_w^{1/n} \qquad (4\text{-}1)$$

$$\log C_s = \log K_f + 1/n \log C_w \qquad (4\text{-}2)$$

In equations 4-1 and 4-2, C_s represents the concentration of SGPM sorbed to the Pahokee Peat, while C_w is the aqueous phase concentration after 3 days, at which sorption equilibrium was assumed to be achieved. The model parameters obtained from the linearized form of the Freundlich isotherm equation (equation 4-2) and regression analysis of experimental data are summarized in Table 4-3. These are the Freundlich adsorption capacity parameter, K_f, and the Freundlich adsorption intensity parameter, $1/n$, which indicates the degree of non-linearity in the sorption isotherm.
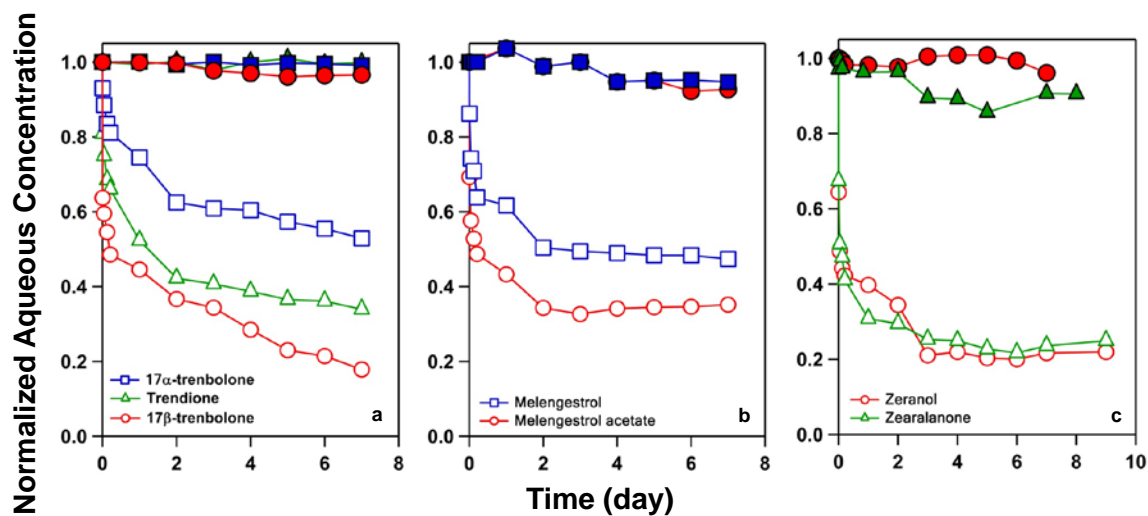
Figure 4-1. Results of kinetic experiments monitoring the extent of SGPM uptake on Pahokee Peat over time at pH 7.0. Data are also shown for control systems without any Pahokee Peat. Systems contained 2 g/L of Pahokee Peat and typically an initial concentration ~5 μM of SGPM. Additional experimental details are provided in the text.

The Freundlich isotherm parameters can be used to evaluate for trends in SGPM sorption that may lend insight into the fundamental processes driving their uptake on Pahokee Peat. For example, K_f values indicate the magnitude of sorption [111], and correlations between K_f values and metrics of sorbate hydrophobicity (e.g., K_{ow} values) as evidence for hydrophobic interactions driving sorption (e.g., [112]). For SGPMs, Khan et al. [49] previously interpreted a linear correlation between K_f values for 17β-TBOH, 17α-TBOH and TBO and soil organic carbon content as evidence of hydrophobic interactions contributing to, if not dominating, their sorption.

In our experiments, the largest K_f values for Pahokee Peat were measured for zeranol (1.33 ± 0.06) and it metabolite zearalanone (0.94 ± 0.04), as well as 17β-TBOH (0.98 ± 0.02) and MGA (0.83 ± 0.01). No clear trends in K_f values were observed within or across families of different growth promoters. For example, within the TBA family 17β-TBOH was far more prone to sorption than 17α-TBOH, which only differs because of the stereochemistry of the –OH group at the C17 position in the steroid ring structure. Similarly, when using octanol-water partitioning coefficients (K_{ow} values) as a potential predictor of SGPM sorption, no correlation with K_f values were discernible for Pahokee Peat (Figure 4-3). That values of K_{ow} are generally poor predictors of SGPM sorption on organic-rich Pahokee Peat suggests that specific interactions (e.g., hydrogen bonding) between sorbate and sorbent contribute to uptake, at least in some cases.

Table 4-3. Freundlich adsorption isotherm parameters obtained via linear regression (see equation 4-2) of experimental data. Values represent 95% confidence intervals associated with the regression analysis. The units for values of K_f are $\mu mol^{(1-\frac{1}{n})} L^{\frac{1}{n}} g^{-1}$.

SGPM	K_f	n
17β-TBOH	0.98 ± 0.02	1.58 ± 0.09
17α-TBOH	0.39 ± 0.02	1.47 ± 0.07
TBO	0.61 ± 0.02	1.18 ± 0.05
MGA	0.83 ± 0.01	1.11 ± 0.04
Melengestrol	0.44 ± 0.02	1.38 ± 0.07
Zeranol	1.33 ± 0.06	0.90 ± 0.02
Zearalanone	0.94 ± 0.04	1.07 ± 0.08
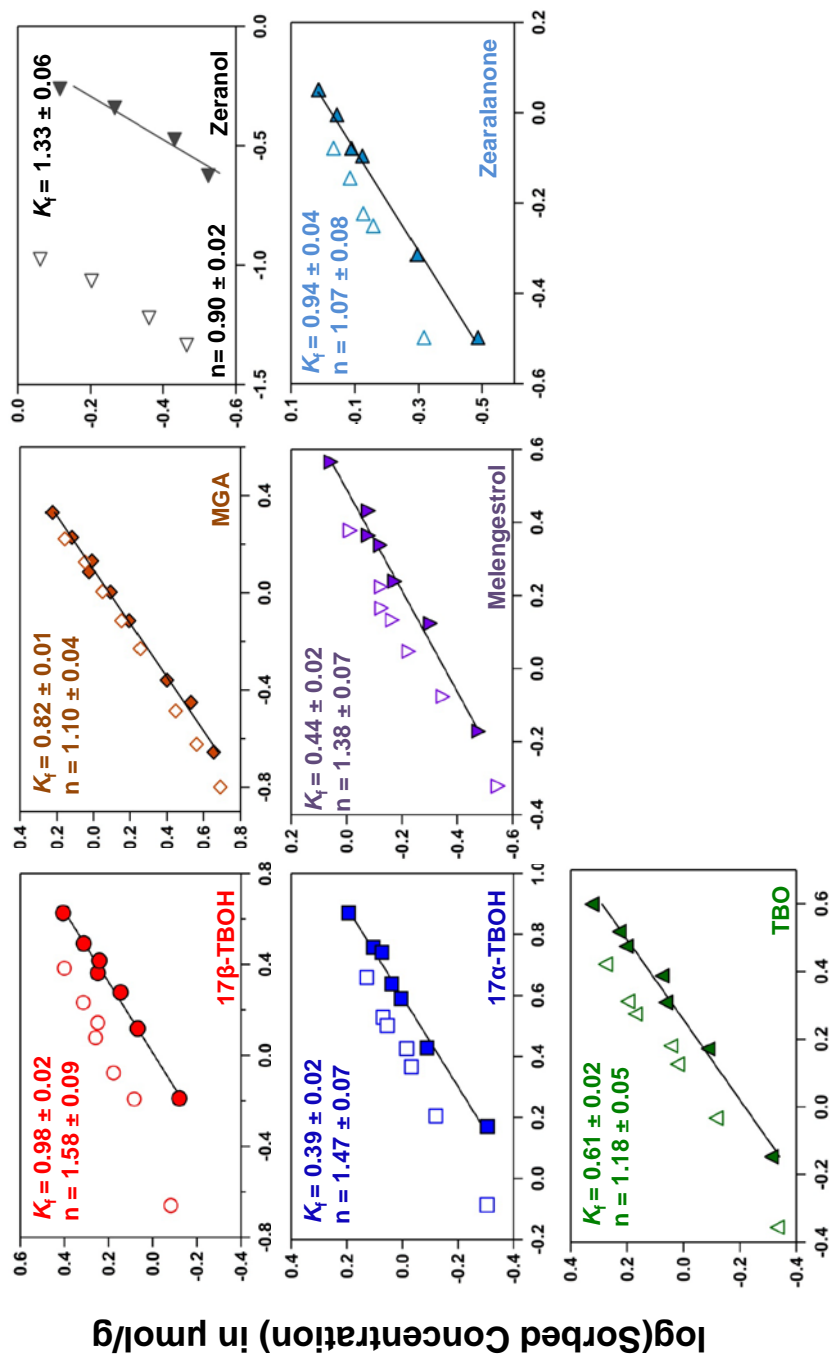
log(Dissolved Concentration) in μM

Figure 4-2. Linearized Freundlich isotherms for SGPMs on Pahokee Peat. Solid data indicate measured concentrations after 3 days, whereas open symbols correspond to data collected to test the reversibility of sorption according to the protocol described in the text. Linear regression and resulting best-fit parameters (values of K_f and $1/n$) are shown. All data were collected at pH 7 in a 5 mM phosphate buffer. Additional experimental details are provided in the text.

A notable difference across SGPMs in the Pahokee Peat system was that some resulted in non-linear isotherms, while others produced a linear equilibrium relationship. Values of *n* obtained from regression analysis of the linearized Freundlich isotherm equation are shown in Figure 4-4. The greatest degree of non-linearity was observed for 17β-TBOH, 17α-TBOH and melengestrol, whereas the isotherms for zeranol and zearalanone were essentially linear. Linear isotherms are most often observed for the uptake of hydrophobic sorbates onto organic matter, for which hydrophobic interactions are responsible for sorption and there is an excess of such sorption sites available on organic matter [42]. In contrast, non-linear isotherms are typically observed for sorption of more polar compounds on organic matter, for which specific interactions will also contribute to sorption [42].

Consistent with these scenarios, trends in Figure 4-4 generally show that isotherms become more linear as SGPMs become more hydrophobic (based on K_{ow} values). We therefore interpret the non-linear sorption isotherms of 17β-TBOH, 17α-TBOH and melengestrol as evidence of a limited number of specific sites on Pahokee Peat that are responsible for their sorption. This outcome is consistent with the prior works of Khan et al. [49] and Quiao et al. [51], both of which implicated specific interactions as playing a prominent role in the sorption of TBA metabolites in soil and humic acid systems. For zeranol and zearalanone, on the other hand, the linearity of their isotherms is consistent with an excess of hydrophobic sites on Pahokee Peat suitable for partitioning. This control of their sorption behavior may be linked to the aromatic nature of zeranol and it metabolites.
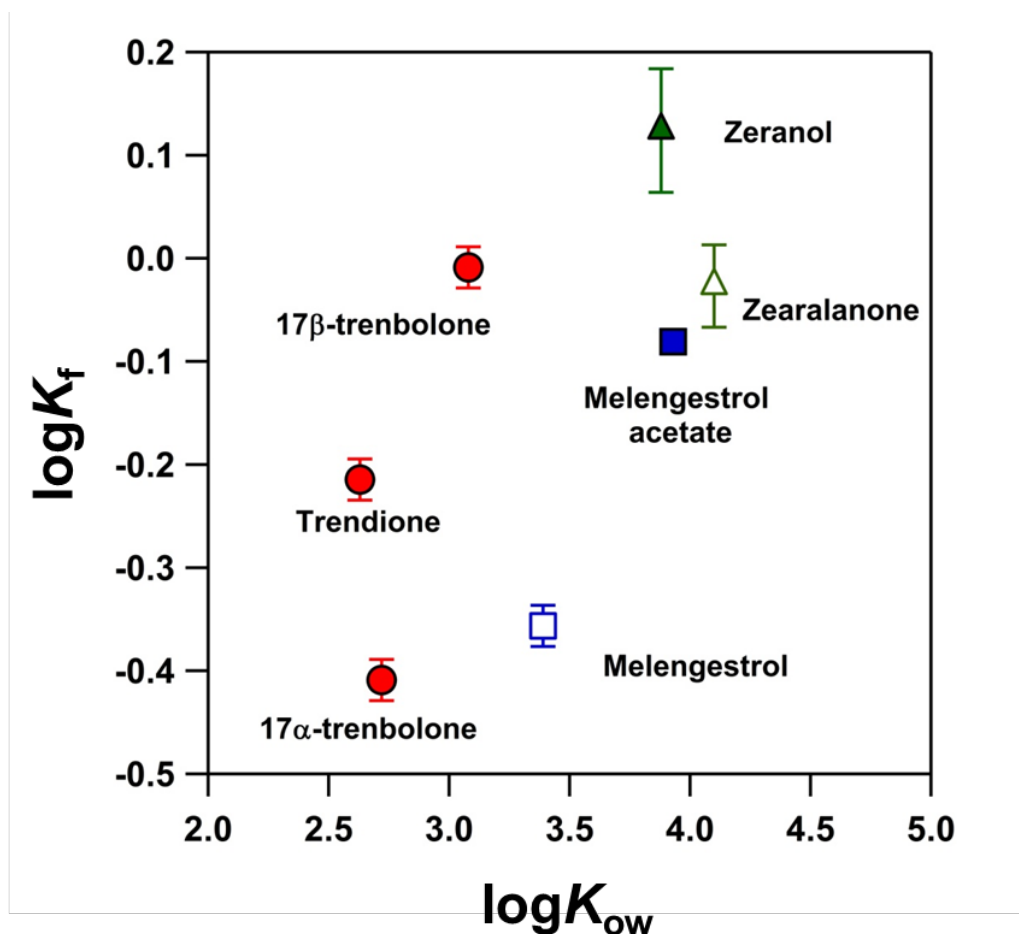
Figure 4-3. Log-log plot of the Freundlich coefficient (K_f) measured via sorption isotherms with each SGPM on Pahokee Peat versus the reported octanol-water coefficients (K_{ow} values) for SGPMs. The logK_{ow} values shown as solid symbols were obtained from the literature [7], whereas open symbols represent values measured using the method described above. Uncertainties represent 95% confidence intervals associated with the linear regression analysis used to determine the experimental K_f values.
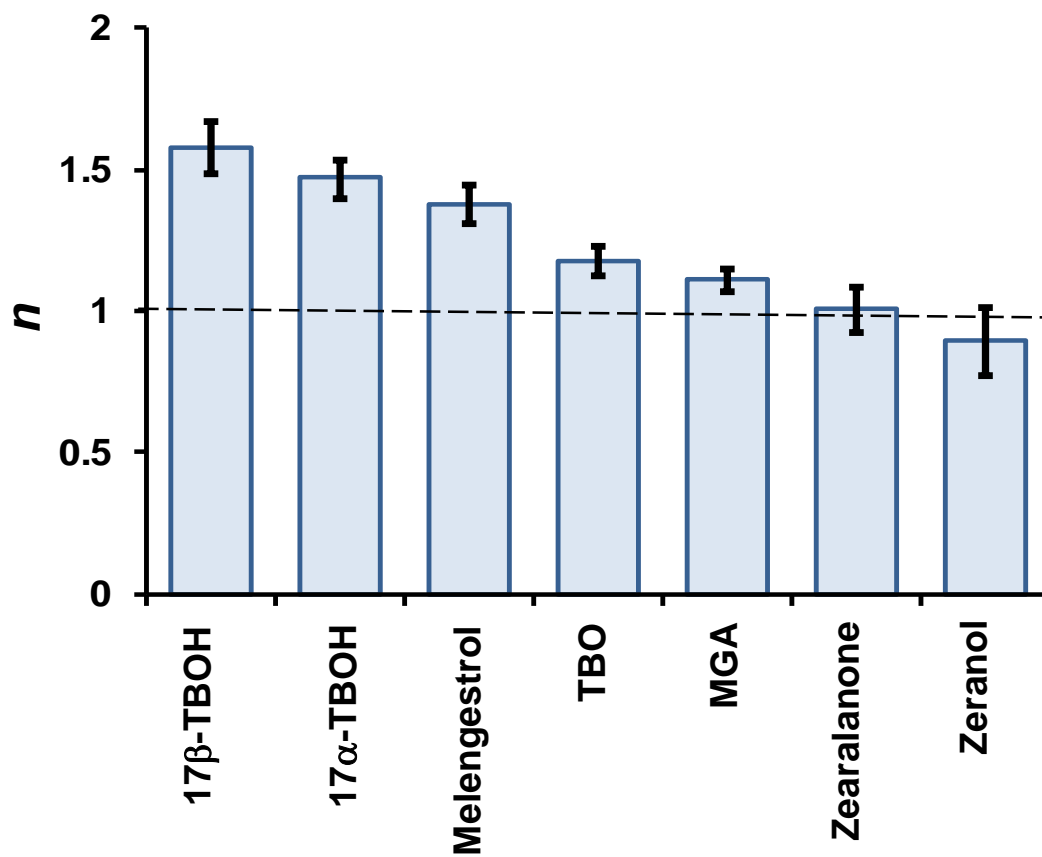
Figure 4-4. Plot of n values of each SGPM obtained from fitting sorption isotherms with Pahokee Peat using a Freundlich model. The n value indicates the degree of isotherm non-linearity, with an n value of 1 (indicated by the dashed line) equivalent to a linear sorption isotherm. Uncertainties represent 95% confidence intervals associated with the linear regression analysis used to determine the experimental n values.

Comparing trends in *n* values within a family of compounds also can provide some insights as to the functional groups that may promote sorption via specific interactions. Specifically, isotherms for 17β-TBOH and 17α-TBOH exhibited greater nonlinearity (i.e., a statistically greater value of n) relative to TBO, while the isotherm for melengestrol exhibited greater nonlinearity relative to MGA. In each of these cases, the presence of an –OH group at the C17 position results in sorption behavior via specific interactions versus non-specific, hydrophobic interactions for structural analogues without this hydroxyl group (i.e., TBO has a carbonyl group (-C=O) at the C17 position, while MGA has an acetate moiety). We propose, therefore, that the –OH group at the C17 position of steroidal SGPMs has a critical role in sorption, likely via its ability to participate in hydrogen bonding with this functionality.

A final consideration with regard to SGPM sorption is the extent to which the process is reversible.   Data pertaining to the reversibility of each SGPM is also presented in Figure 4-3, where open symbols indicate data collected after sorption equilibrium (achieved after 3 days) was disrupted as described previously and the Pahokee Peat system was allowed to once again achieve steady-state over 3 days. In Figure 4-3, overlap between open and solid symbols indicates a sorption process that is truly reversible.

Interestingly, MGA was the only SGPM to sorb onto Pahokee Peat reversibly. Data suggest that sorption of 17α-TBOH, TBO, melengestrol and zearalanone was partially reversible, whereas zeranol and 17β-TBOH were essentially irreversible. In Figure 4-2, irreversibility for zeranol and 17β-TBOH is evidenced by the identical concentration of sorbed species being achieved at lower aqueous phase concentrations 3 day after system equilibrium was perturbed. It is important to note that for compounds that were not reversibly adsorbed, we were able to recover all of the sorbed mass via extraction of equilibrated soils with methanol. Specifically, fractional recoveries via methanol extraction were 1.10 ± 0.08, 0.99 ± 0.07, 1.17, 1.65 ± 0.10, 1.25 ± 0.12, $1.05 \pm$

0.09 and 1.24 ± 0.11 for 17β-TBOH, 17α-TBOH, trendione, MGA, melengestrol, zeranol and zearalanone, respectively. Thus, we are confident that all loss in these Pahokee Peat systems is attributable to sorption and not a non-conservative processes such as chemical transformation reactions or biodegradation.

The trends in reversibility are noteworthy. MGA, which produces a linear adsorption isotherm and attaches to the Pahokee Peat primarily through hydrophobic interactions, appears the most weakly bound. In contrast, zeranol, which also appears to sorb primarily via hydrophobic interactions, is essentially irreversibly bound. Thus, it is clear that hydrophobic interactions with Pahokee Peat exhibit a range of strength, which are not easily predictable based upon the characteristics of the SGPM; the experimentally measured value of K_{ow} for MGA is greater, albeit slightly, than that measured for zeranol [50]. Likewise, it is equally notable that 17β-TBOH, for which specific interactions likely contribute to bonding, was the other species which adsorbed to Pahokee Peat irreversibly. 17β-TBOH is among the more polar of SGPMs considered herein, and specific interactions such as hydrogen bonding are usually considered relatively weak. Nevertheless, it appears to be the most strongly bound to the Pahokee Peat. Thus, when predicting mobility in soils and the potential for retardation via partitioning into soil organic matter, it will be difficult to make generalizations about SGPM behavior based simply upon K_{ow} values. Not only does this traditional metric of hydrophobicity fail to predict the extent of uptake onto soil organic matter within and across SGPM families, but it also appears to have little correlation with the extent to which sorption is reversible.

SGPM Sorption on Model Soils

Another approach to assessing the importance of hydrophobic interactions on SGPM sorption is to examine trends in uptake across a range of soils exhibiting systematically varied organic carbon contents. Using the commercially available soils in Table 4-2, sorption rates and the timescale needed to achieve sorption equilibrium were

evaluated for 17β-TBOH, MGA and zeranol (Figure 4-5). For MGA, there was an initially sharp aqueous phase concentration drop over the first several hours, after which concentration was essentially stable over the remainder of the 6 day period for all soils. While this concentration profile is reminiscent of that observed for MGA in Pahokee Peat systems, it is notable that the amount of MGA lost from solution did not scale with soil organic carbon content. Rather, we observed an approximate inverse relationship, in which soils with the highest organic carbon content (PVPF with 5.0% and PVLPF with 5.9%) actually resulted in the smallest amount of MGA loss from solution.

Unlike with Pahokee Peat, the solution phase concentrations of 17β-TBOH and zeranol failed to reach a steady-state, even after 6 days of mixing with soils (while soil free controls were stable over the same timescale). For 17β-TBOH, there was no apparent relationship between the rate of disappearance and the soil organic carbon content. On the other hand, zeranol exhibited behavior expected if hydrophobic interactions were the driving force for sorption on organic-containing soils. However, the inability to achieve sorption equilibrium in these model soil systems, while it was readily achieved with much higher organic carbon content Pahokee Peat systems, suggests that other processes may be occurring that influence the loss of SGPMs from solution.

Based on additional experiments with select model soils, we believe sorption occurs simultaneously with abiotic chemical transformation reactions in these soil systems. Figure 4-6 shows plots of plots of concentration versus time for 17β-TBOH, MGA and zeranol for a low (RMN; 1% OC) and high (PVLPF; 5.9% OC) organic carbon content soil, which are identical to the data previously shown in Figure 4-5 for these soils. However, also shown are data corresponding to the total mass recovery in the system over time, measured using the same extraction technique with methanol that successfully recovered all sorbed mass from Pahokee Peat during our isotherm experiments.

In all systems shown, we observed at least some loss in the recoverable SGPM mass, and the extent of this loss generally increased over time. For 17β-TBOH and zeranol, there was little, if any, difference in the measured aqueous concentration and the total recoverable mass, including any sorbed species recovered by extraction of the soil with methanol. Equivalent behavior was also observed for both soil systems considered. The agreement in the profiles of aqueous concentration and total mass over time is consistent with all loss in these systems being attributable to non-conservative processes, presumably a reaction promoted by the soil, rather than sorption. We believe that the loss is due to mineral-promoted reactions such as hydrolysis or oxidation occurring at the surface of the underlying inorganic phases in these soils. We note, however, that no products were detected using our LC-DAD methods, suggesting any such products are either too polar to be separated on our C-18 column or are no longer chromophoric.

Results with MGA shed some light on the factors controlling the rate at which SGPMs are consumed in soil systems via such non-conservative processes (i.e., transformation reactions). For both soils in Figure 4-6, the aqueous phase concentration of MGA showed near identical profiles. Initially the amount of MGA in solution decreased rapidly, with about 60-70% of the solution concentration disappearing within the first day. After this initial phase, the amount of MGA in solution remained relatively constant over the remaining 5 days of the experiment.

Despite the agreement in the aqueous phase concentration profiles, the profiles for the total mass of MGA were distinct for each soil systems. For the high organic carbon containing PVLPF, the mass of MGA in suspension was relatively constant over time, with 90% remaining after 5 days. Thus, in the high organic carbon soil, most if not all of the MGA loss from solution was due to sorption. In contrast, MGA mass decreased steadily over time in the low organic carbon soil RMN, with only 50% remaining after 6 days. In the low organic carbon soil, the rapid, initial MGA loss from solution appears to result entirely from sorption, as the total mass recovery for the system is near 100%
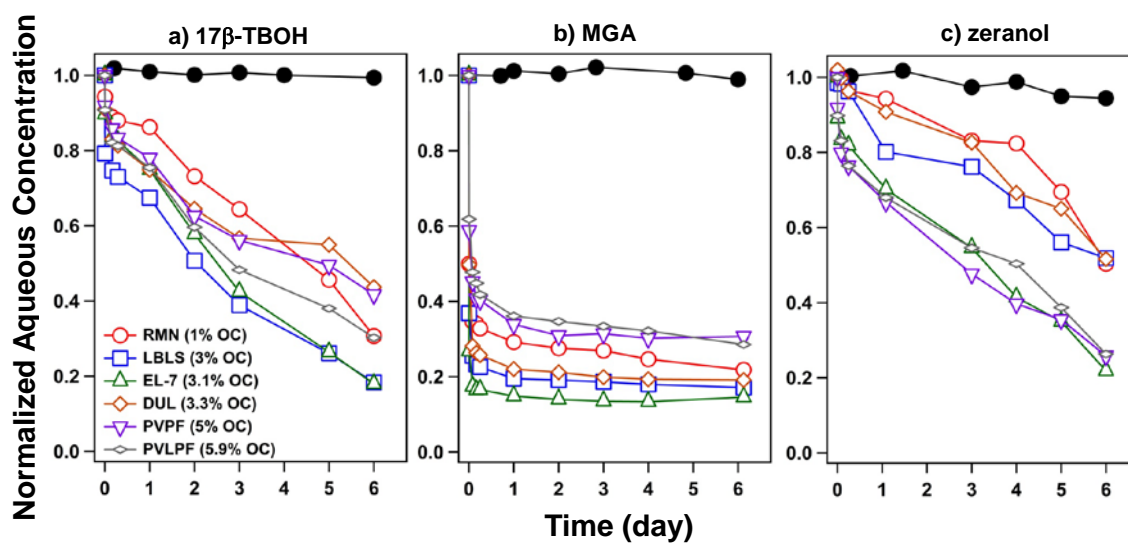
Figure 4-5. Change in aqueous phase concentration over time for (a) 17β-TBOH, (b) MGA, and (c) zeranol 4 g/L suspensions of each model soil. All experiments were conducted in 5 mM phosphate buffer at pH 7. The initial concentration of each SGPM was 4 µM, 2µM and 2 µM for 17β-trenbolone, MGA and zeranol, respectively.
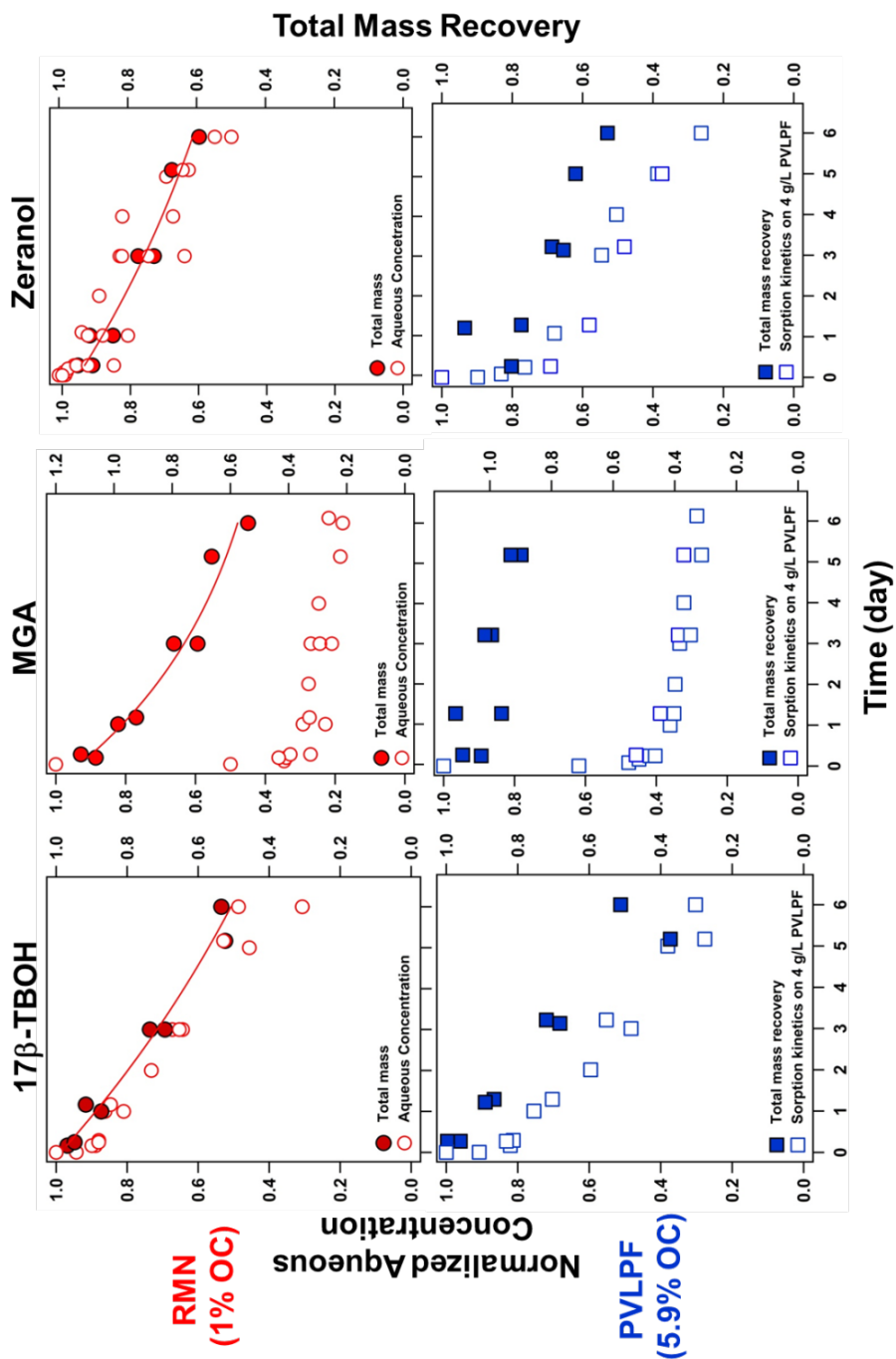
Figure 4-6. Plots of aqueous phase concentration change over time of 17β-TBOH, MGA and zeranol on two model soils, RMN (red) and PVLPF (blue) which represent the soils with lowest (1%) and highest (5.9%) organic carbon content. Also presented (solid symbols) is data pertaining to the total mass of each species in the systems over time, including the mass that was recoverable from extraction of solids with methanol. The loading of RMN and PVLPF was 4 g/L, the initial concentration of each SGPM was ~ 2 μM, and the experiments were operated in 5 mM phosphate buffer at pH 7.

over the timescales associated with this initial loss. However, while there is relatively little change in the solution phase concentration of MGA between days 2 and 6, the total mass of MGA in the systems decreases by roughly 50% over this same time period. These results suggest, therefore, that the initially sorbed MGA must be labile and susceptible to reaction over time.

The results with MGA suggest a two-step process for our proposed mineral-promoted transformation pathway. The SGPM must first sorb to the organic matter layer that coats the particle, through which the SGPM must then diffuse to react at the surface of the underlying inorganic phase. Because MGA has the highest reported K_{ow} value and its sorption onto organic matter appears controlled primarily via hydrophobic interactions, it is not surprising that the extent of its reaction is dependent upon the carbon content of the soil. Specifically, for soil with high organic carbon content, MGA appears to stay tightly associated with the organic phase and resistant to transformation at the underlying mineral interface. In contrast, its association with the low organic carbon content soil must be weaker, allowing MGA to diffuse through the organic layer to react extensively at the surface of the inorganic phase. This is a notable difference because the driving force for MGA adsorption is nearly identical in both soil systems based on the aqueous phase concentration profiles in Figure 4-5 and 4-6.

The different behavior observed for 17β-TBOH and zeranol, which reacted extensively in both soil systems, is somewhat unexpected. From experiments with Pahokee Peat, these species, along with MGA, were most prone to sorption, exhibiting the greatest extent of uptake during our isotherm experiments. Further, 17β-TBOH and zeranol were irreversibly bound to Pahokee Peat while MGA sorption was essentially reversible. We can only conclude that MGA must be less prone to transformation via the inorganic mineral phases present in the soil relative to 17β-TBOH and zeranol, such that the rate and extent of MGA partitioning into and out of the soil organic matter can in turn influence its rate of transformation.

Reactivity of SGPMs toward inorganic mineral phases

To assess the potential for inorganic mineral phases in soil to catalyze rates of SGPM transformation via pathways including hydrolysis and oxidation, additional experiments examined their stability in suspensions of several metal oxides representative of those naturally occurring in soil. Figure 4-7 shows the reactivity manganese oxide, a capable oxidant for a range of contaminants of emerging concern including hormones [54], toward 17β-TBOH, MGA and zeranol at pH 6. Zeranol was most reactive, undergoing near complete transformation over the course of 0.5 h at a relative low loading (1 g/L) of MnO_2. 17β-TBOH also was not stable in the presence of MnO_2. Although not as reactive as zeranol, the rate of 17β-TBOH increased with MnO_2 solid loading (from 1-10 g/L), behavior that is consistent with a reaction involving the MnO_2 surface. Also for 17β-TBOH, LC-DAD provided evidence of product formation. The product was considerably more polar than 17β-TBOH, eluting very early (~1.1 min) on our reverse-phase C18 column. Finally, MGA was essentially stable in suspensions at the highest loading of MnO_2 considered at pH 6 (10 g/L). Assuming 17β-TBOH and zeranol are oxidized by MnO_2, a scenario that requires confirmation, it appears that MGA is considerably less reactive than these other SGPMs. We note that MGA transformation did occur to a limited extent at more extreme suspension conditions (20 g/L at pH 4).

Iron oxides such as ferrihydrite are weaker oxidants than MnO_2 and may also potentially catalyze hydrolysis reactions through surface interactions (so-called "mineral-promoted hydrolysis) [113]. In suspensions of ferrihydrite (5 g/L at pH 7), a modest amount of loss of both 17β-TBOH and MGA was observed, consistent with its ability to promote such transformation processes (Figure 4-8). Assuming a pseudo-first-order loss process, data correspond to half-lives of 12 and 17 days for MGA and 17β-TBOH, respectively. The relative trend in reactivity is notable; despite relatively slow rates of
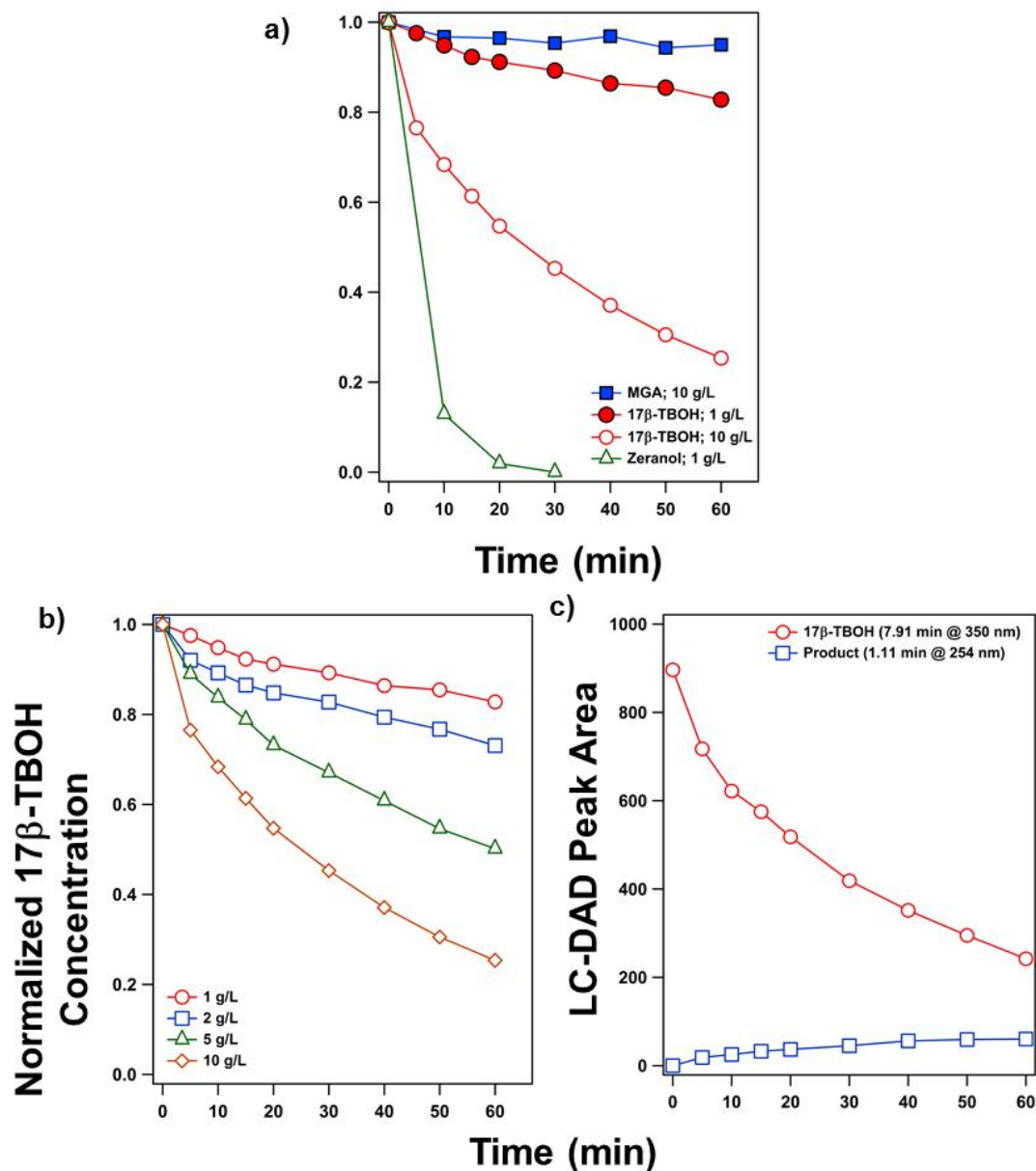
Figure 4-7. Aqueous phase concentration change over time of (a) MGA, 17β-TBOH and zeranol in suspensions of MnO_2. (b) 17β-TBOH in suspension of MnO_2 with different solid loadings. Also shown in panel (c) is the growth (based upon LC-DAD peak area) of a transformation product generated over time during 17β-TBOH reaction with MnO_2. All experiments were conducted in 5 mM $NaClO_4$ at pH 6. The initial concentration of 17β-TBOH, MGA and zeranol in panel (a) and (b) are 10 µM, 2 µM and 2 µM, respectively. The data in panel (c) correspond to 10 g/L MnO_2 with a 10 µM initial 17β-TBOH concentration.
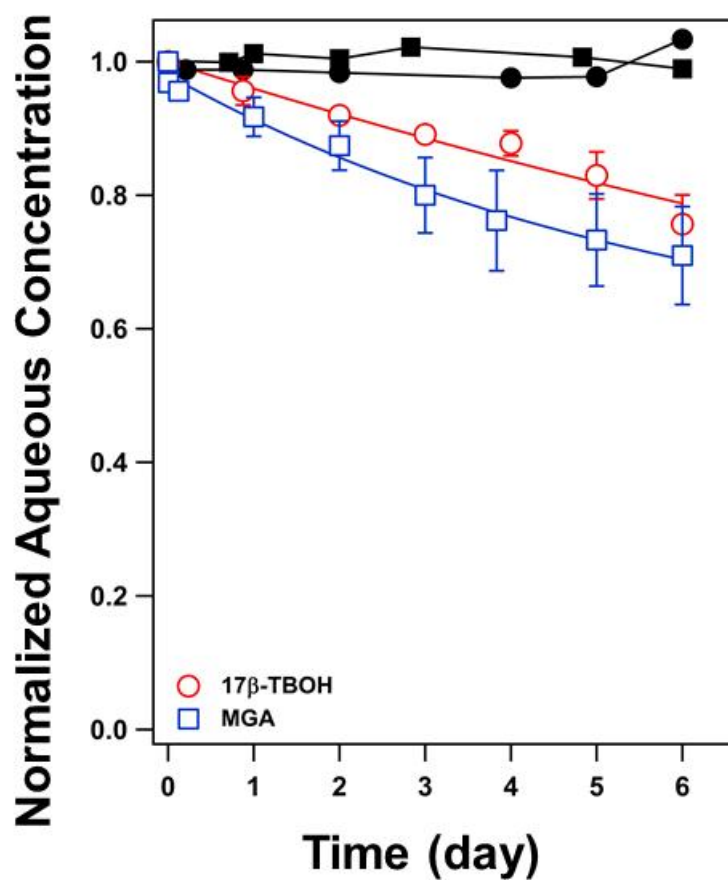
Figure 4-8. Aqueous phase concentration change of 17β-TBOH and MGA in ferrihydrite suspensions (5 g/L). Reactions were conducted in 5 mM phosphate buffer at pH 7. Lines are exponential decay model fits from which half-lives were calculated. Data are also presented from control systems conducted in the absence of solid (solid black symbols).
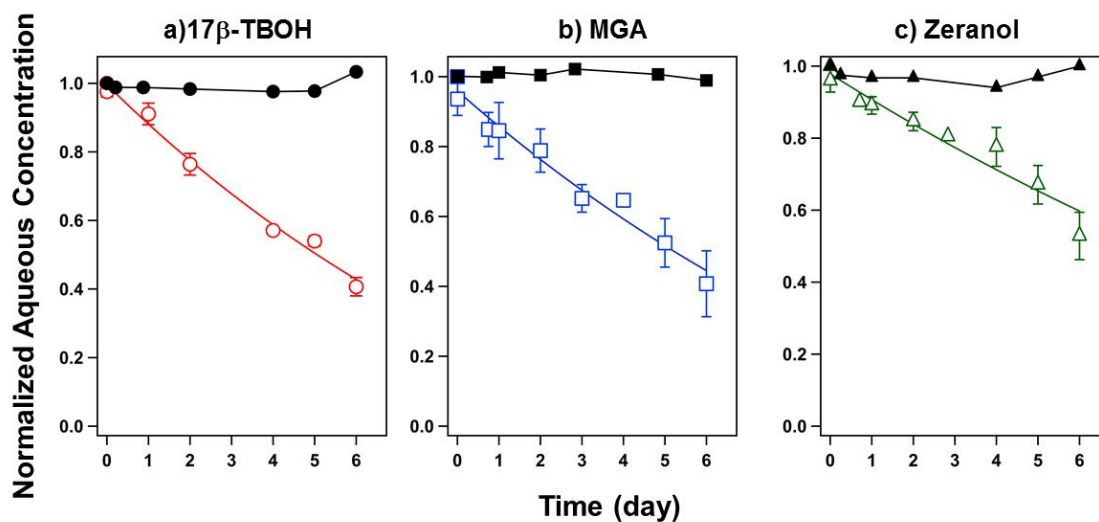
Figure 4-9. Reaction of 17β-TBOH, MGA and zeranol with 10 g/L SiO$_2$ at pH 7. Lines represent exponential decay model fits from which half-lives were calculated. Experiments were conducted in 5 mM phosphate buffer at pH 7 and used initial concentrations of 4 µM, 2 µM and 2 µM for 17β-TBOH, MGA and zeranol, respectively.

transformation, MGA was consistently more reactive than 17β-TBOH. This is the opposite trend observed for MnO_2, which is reasonably assumed to be an oxidant for SGPMs. We propose, therefore, that the ferrihydrite surface promotes the hydrolysis of MGA and 17β-TBOH rather than functioning as an oxidant (for which we would expect little to know reactivity toward MGA). Unfortunately, however, products for this transformation reaction were not detectable. This is particularly noteworthy for MGA, as melengestrol, one likely hydrolysis product which is easily detectable via our analytical methods, was not observed. We maintain that the loss of MGA and 17β-TBOH in these systems does indeed result from transformation reactions. Attempts to recover the any mass of MGA and 17β-TBOH sorbed to the surface via solvent (methanol) extraction were unsuccessful, consistent with non-conservative processes being responsible for loss in ferrihydrite suspensions.

As a final evaluation of mineral-promoted transformation pathways, we examined the stability of 17β-TBOH, MGA and zeranol in suspensions of SiO_2 (10 g/L) at pH 7 (Figure 4-9). SiO_2 is not a viable oxidant, so the only transformation pathway it would be expected to promote is hydrolysis. Solution phase concentration of 17β-TBOH, MGA and zeranol decreased over time in these SiO_2 suspensions, and we were unable to recover any of this lost mass via solvent extraction of the SiO_2 at the conclusion of the experiment. We conclude, therefore, that SiO_2 surfaces can indeed promote the hydrolysis of SGPMs in soil, although reaction products were once again not detected. This result is noteworthy because of the predominance of aluminosilicate minerals in most soil systems. Given its abundance in soil, it is reasonable to expect that abiotic SGPM transformation promoted by SiO_2 could influence their persistence and fate in soil systems.

Similar to observations with ferrihydrite, 17β-TBOH and MGA exhibited comparable rates of decay in SiO_2 ($t_{1/2}$ values of 4.9 and 5.3 days, respectively). Because 17β-TBOH and MGA share an identical A ring in the steroid structure, these similar

timescales may be an indication that hydrolytic attack (i.e., –OH addition) occurs somewhere within the A ring. Zeranol, which has a clearly identifiable hydrolysable center at its carbonyl group, decays at a slightly slower rate compared to the other SGPMs ($t_{1/2}$ of ~ 8 days).

From experiments with mineral suspensions, it reasonable to conclude that the SGPM loss previously observed in experiments with model soils is indeed attributable to surface promoted reactions at the underlying mineral surface. Oxidation by MnO_2 appears to be a viable pathway for the trenbolone acetate family as well as zeranol and its metabolites. All families of SGPM also appear prone to hydrolysis. We note that the timescales of transformation in metal oxides systems is actually slow relative to the rates of mass loss detected in model soil systems, in which such metal oxides are typically minor components making up only a few percent of soil by mass. Based on the loss rates measured in model soil systems, one would expect much greater rates of transformation in pure metal oxide systems. We propose that the higher than expected rates of transformation in the model soil systems indicates a necessary role of soil organic matter to concentrate SGPM at the particle surface. Given the polar nature of metal oxide surfaces it is reasonable to expect that rates of mineral-promoted pathways would be influenced by the minimal degree of interaction anticipated with most SGPMs, which are moderately hydrophobic in most cases.

4.5   Environmental Implications

Results presented herein indicate that the fate of SGPMs in soil is likely far more complex than currently realized. While sorption and biodegradation were previously thought to be the dominant soil processes controlling SGPM fate, we provide evidence herein that abiotic transformation reactions catalyzed by mineral surfaces can occur over timescales comparable to those previously reported for biotransformation [87]. It is likely, therefore, that these previously unrecognized transformation pathways may

influence the persistence of SGPMs in soil, as well as represent a route for the introduction of novel hormone transformation products that may also pose a risk to ecosystem health.

Generally, we conclude that SGPM sorption will only dominate in soil systems with very high organic carbon content. The Pahokee Peat systems used herein may indeed be a reasonable approximate of organic-rich agricultural topsoil or land applied manure, both of which would then be expected to retain SGPMs via sorption. However, the degree of such sportive interactions will not be simple to predict. Specifically, the extent of SGPM uptake and the reversibility of the sorption process cannot be predicted with simple metrics of compound hydrophobicity such as K_{ow} values, which are typically used as a starting point in predicting pollutant fate in soil. In particular, more polar species (i.e., those with functionalities capable of hydrogen bonding) will be most difficult to model fate in soils, as their extent of interaction with organic-rich soil will be influenced heavily whether the soil possesses sites suitable for more specific binding interactions.

A clear need arising from this work is the identification of mineral-catalyzed transformation products. Given the unique behavior of transformation products previously presented in Chapter 3, the fate of hydrolysis and oxidation products must not be overlooked. For hydrolysis and oxidation, it is highly probable that transformation products will exhibit some level of hydroxylation. As in Chapter 3, such hydroxylated products may be of limited stability in the environment, particularly those generated from TBA metabolites, and allow for the formation of novel steroid byproducts with potentially adverse implications for ecosystem health.

CHPATER V. CONCLUSIONS

5.1   Rates and Mechanisms of

Growth Promoter Photolysis

In Chapter 2, the direct photolysis rates of the trenbolone acetate (TBA) and melengestrol acetate (MGA) families of compounds are reported, as are the rates and mechanistic details for the indirect photolysis of zeranol and its metabolites. The photolysis of these compound classes had not previously been investigated under conditions representative of sunlit surface waters. Thus, these fundamental details provided in Chapter 2, as well as more practical considerations such as the influence of common aquatic variables (e.g., temperature, pH, and co-solutes) on these processes, fill a sizeable void in our understanding of growth promoter environmental fate. The key results from Chapter 2 are summarized in the following.

Direct Photolysis of TBA and MGA Family Compounds

All experimental evidence collected herein points to the TBA and MGA families being highly reactive and readily photolyzed in sunlit surface waters. For example, direct photolysis half-lives for these compounds typically ranged between ~0.25-1 h upon both natural and simulated sunlight irradiation. The photoactivity of the TBA and MGA families can largely be tied to their chemical structures. Both possess conjugated π-bond systems that result in absorbance patterns that overlap to some degree with the solar spectrum, which is requisite for direct photolysis. Also, as is reported in Chapter 2, both families of compounds exhibit photoefficiencies on par with those previously reported for structurally similar compound classes.

Rates of direct photolysis were largely invariant across a broad spectrum of water chemistries. For example, there was no pH dependence observed for direct photolysis, which would be expected because the TBA and MGA families are neutrally charged over

environmentally relevant pH values. Another notable finding was that dissolved organic matter had only a minimal influence on the direct photolysis of these compounds, resulting in a small to modest amount of light screening. These observations have value when attempting to extend the observations from Chapter 2 more generally to agriculturally impacted surface waters. Specifically, the near-constant rates of direct photolysis measured over the range of aquatic conditions should allow fate models to better account for the contribution of photolysis to these species' environmental persistence.

From the results gathered and presented in Chapter 2, therefore, it is clear that direct photolysis represents an important, if not the dominant, loss process for the TBA and MGA families in sunlit natural waters. Based solely on the decay of the parent compounds measured in Chapter 2, it is tempting to conclude that compounds from the TBA and MGA families are unlikely to persist for more than a few hours due to their propensity for direct photolysis. This may very well be the case for the MGA family. However, as is discussed in greater detail in Chapter 3, the fate of TBA and its metabolites are far more complex in sunlit surface waters as a result of the instability observed for the major product generated by direct photolysis.

Indirect Photolysis of Zeranol Family Compounds

Unlike compounds in the TBA and MGA families, the aromatic chromophoric moiety on zeranol and its metabolites does not allow for significant absorbance within the solar spectrum. While they are stable with respect to direct photolysis, these compounds are readily degraded in irradiated solutions of model humic and fulvic acids. Experiments detailed in Chapter 2 provide fundamental insights as to the photooxidants generated from dissolved organic matter (DOM) irradiation that are responsible for zeranol decay. Notable among these reactive photooxidants was triplet excited state

DOM, a species known to play an important role in the indirect photolysis of structurally analogous substituted phenols[43, 114].

From a more practical perspective, results presented in Chapter 2 clearly outline the aquatic chemical variables critical to controlling the timescales of zeranol indirect photolysis, and thus persistence in surface waters. The variables of primary importance are the nature and quantity of dissolved organic matter, which will determine the concentration and types of photooxidants generated upon irradiation. The presence of other species capable of generating photooxidants must also be considered. For example, preliminary results in Chapter 2 show that nitrate, which generates hydroxyl radical upon photolysis, can also mediate the transformation of zeranol in sunlit waters. Finally, the last critical variable is pH. Zeranol and its metabolites exhibit pKa values that are reasonably close to the pH values encountered in surface waters. As such, a small but highly reactive fraction of the mono- and di-anionic forms of zeranol and its metabolites will be present, and evidence suggests these deprotonated forms exhibit the greatest activity toward photogenerated oxidants.

Collectively, these considerations make the fate of zeranol relatively difficult to predict in surface waters. Given the range of solution variables that influence the rate of zeranol indirect photolysis, an accurate model or prediction of zeranol persistence will require a well-characterized surface water. This can be particularly challenging, especially when one must also consider the range of potential competitive species that may reactive preferentially with photogenerated oxidants, and thereby promote zeranol persistence.

5.2   Photoproduct-to-Parent Reversion for

Trenbolone Acetate Metabolites

The results in Chapter 3 illustrate the reversion mechanism by which the primary photoproduct of the trenbolone family, a monohydroxylated species, transforms back into

the hormonally active TBA metabolite from which it was generated. This unique set of sequential photolysis and dehydration reactions essentially allows for the photolysis of TBA metabolites to be reversible in surface waters. Fundamentally, we attribute this unique reactivity the highly reactive nature of the allylic hydroxyl group generated during photolysis and the presumed stability of the 4,9,11-triene structure present in TBA metabolites. The presence of such allylic hydroxyl groups should be recognized as a potentially highly reactive moiety in other steroids and steroid transformation products. In the case of hydroxylated transformation products (as may be encountered through biotransformation or mineral catalyzed pathways), such an allylic hydroxyl group is likely to be prone to acid and/or base catalyzed dehydration reactions that provide a route back to the non-hydroxylated starting material.

Practically speaking, these results complicate our understanding of the fate of trenbolone acetate metabolites in sunlit surface waters. Indeed, as illustrated in Chapter 2 and 3, direct photolysis rates of trenbolone family members were typically fast, with half-lives on the order of 0.5-1 hour. However, a closer inspection shows that this photolysis reaction does not proceed to completion; at long irradiation timescales, the concentration of trenbolone compounds in the presence of light reaches a near-steady state at a low concentration (typically at ~2% of the initial concentration). At this stage, the forward rate of photolysis is equally countered by the dehydration reaction, in essence causing the decay of trenbolone acetate metabolites to appear photostationary. From this result, we suspect that in all surface waters in which TBA metabolites degrade exclusively by direct photolysis, a non-zero, near-constant concentration should exist after this equilibrium has been achieved during daylight hours. Further, the magnitude of this concentration will increase as more of the primary photoproduct (i.e., 12-hydroxy trenbolone) is present in solution, as this would increase the rate of the photoproduct-to-parent reversion reaction. Finally, other non-conservative processes (e.g., sorption, biotransformation or abiotic

reaction) would be required to disrupt this equilibrium and completely remove the TBA metabolites from the water column.

In the dark, when the forward photolysis reaction is no longer occurring, dehydration of the primary photoproduct should result in a rebound in the concentration of TBA metabolite over time. In some instances, this rebound will be significant. Results in Chapter 3 found the dehydration process to be pH and temperature dependent. For instance, slightly acidic (pH 5) or basic (pH 9) conditions, as well as warm temperatures (35 °C), resulted in roughly 30-40% of the initial 17α-TBOH mass being regenerated in a single 12 h dark period. Much greater recoveries are observed over longer dark periods, as might be encountered when the primary photoproduct is transported out of the photic zone of a surface body.

Collectively, this day-night behavior should produce a cyclic pattern for TBA metabolites in surface waters. This photoproduct-to-parent reversion phenomenon is greatest for 17α-TBOH, and occurs to a lesser extent for 17β-TBOH and trendione. The differences between these compounds is still not well understood, but likely relates to the relative amount of the 12-hydroxy photoproduct generated for each species, as well as the relative rate of dehydration versus hydrolysis to higher order hydroxylated products (e.g., di- and trihydroxy trenbolone varieties). Nevertheless, the consequences of this cyclic process are great. Although TBA metabolites appear to undergo rapid direct photolysis, a characteristic touted by the chemical manufacturer as evidence of their limited environmental persistence, their lifetime in surface waters is likely to be much longer than estimated solely from initial rates of photodecay. Rather the fate and impact of these compounds in the environment can only be assessed accurately if the behavior of their photoproducts is explicitly considered.

As a result of this discovery, we believe there are currently no reliable occurrence data pertaining to the TBA metabolites in surface waters. Concentrations measured in occurrence studies will be highly dependent on the time of day in which samples were

collected, the quality of the surface water, and the season in which the data were collected. For example, samples collected in daylight could potentially ignore or grossly underestimate a large body of TBA metabolites that exist as a metastable hydroxyl trenbolone species, which would be quick to revert back into parent metabolite in the absence of sunlight. Further, it is quite possible, if not nearly certain, that traditional approaches to sample storage such as acidification, refrigeration, and liquid-liquid extraction will substantially bias results of any occurrence study. We contend, therefore, that studies failing to quantify the amount of trenbolone photoproducts in their samples are likely to underestimate the amount of TBA metabolites truly present in surface waters. Such behavior could explain numerous reports of low detection frequency of TBA metabolites, despite their extensive use and release into the environment. It may also help to explain instances where evidence of endocrine disruption in aquatic organisms is reported even though complementary solution phase analysis fails to identify any known endocrine disrupting compounds.

5.3   Sorption and Mineral –promoted Reactions

Chapter 4 describes the abiotic interactions of SGPMs with various soil components that are likely to influence their mobility upon release into the environment. Generally, we observed that SGPMs exhibit a relatively high affinity for organic rich soil such as peat. For example, all SGPMs rapidly sorbed onto Pahokee Peat, with solid-water equilibrium being achieved in 3 days or less, generally resulting in 40%-80% of the initial SGPM mass (typically 1-2 mg/L) being associated with the organic material (typically present at 844 mg/L). Melengestrol acetate was the only compound to sorb via a completely reversible pathway, whereas sorption of most other SGPMs was partially reversible. Exceptions were 17β-trenbolone and zeranol, whose sorption was entirely irreversible on Pahokee Peat. Notably, however, within and across families of SGPMs, trends in the extent and reversibility of sorption on an organic-rich matrix were not

predictable simply based upon measures of compound hydrophobicity (e.g., reported or estimated $\log K_{ow}$ values). It appears, therefore, that factors other than hydrophobicity influence SGPM uptake. This behavior will complicate attempts to accurately model the extent to which SGPM transport is retarded in soil and the subsurface due to partitioning into soil organic matter.

Perhaps the most important result obtained in Chapter 4 is the observation of inorganic mineral-promoted transformation reactions for each class of SGPM. Experiments using model soils (with organic carbon contents between 1-5.9%) were characterized generally by rapid SGPM loss and equilibrium, expected for a sorption, was not typically observed. Most notably, the amount of SGPM mass lost over time typically could not be recovered using solvent extraction techniques that proved successful in closing the mass balance in sorption studies previously described with Pahokee Peat.

Collectively, we interpret these findings from sterilized soil systems as evidence for non-conservative chemical transformation reactions occurring in parallel to SGPM sorption on soil organic matter. We propose a scenario in which sorbed SGPMs diffuse through the soil organic matter layer to react, presumably via hydrolysis or oxidation, at the interface with the underlying inorganic mineral phase. Consistent with such a scenario, results are also presented in Chapter 4 showing the instability of 17β-TBOH, MGA and zeranol in suspensions with metal oxides representative of those naturally occurring in soil (ferrihydrite, SiO_2 and MnO_2). Notably, however, while appreciable solution phase concentration loss was observed, products for these transformation pathways were only detected in a few limited cases (e.g., oxidation of 17β-TBOH by MnO_2).

Differences in the concentration versus time profiles for zeranol, 17β-TBOH, and MGA suggest that the relative importance of sorption versus reaction in inorganic-containing soil system depends in part on the amount of organic carbon present in the soil, the hydrophobicity of the SGPM, and the presence of available reactive (e.g.,

hydrolysable or oxidizable) centers on the SGPM. Specifically, hydrophobic SGPMs (i.e., species with large $\log K_{ow}$ values) in combination with relatively high soil organic carbon content are conditions that tend to favor sorption without reaction. We assume such conditions result in the SGPM being bound tightly in the soil organic matter, and less likely to diffuse to the inorganic substrate surface for reaction.

Results in Chapter 4 greatly advance our understanding of SGPMs in soil systems. They paint a picture in which the fate of SGPMs in soil will be far more dynamic, and as such complicated, than currently envisioned. Sorption, which will not necessarily scale with soil organic matter content and SGPM hydrophobicity, will occur in parallel to transformation pathways such as hydrolysis and oxidation. The rates of these processes are fast enough that they should occur over timescales comparable to that reported for biotransformation [12, 17]. Thus, the contribution of these abiotic processes must not be ignored when attempting to assess the fate of SGPMs in soil. This will also require a better understanding of the factors promoting their mineral-promoted transformation, and the nature of the products generated from these reactions.

5.4   Future Research

This work significantly improves our understanding of the persistence and fate of SGPMs in the natural environment. For instances, the timescales and/or extent of most key abiotic processes involving SGPMs are presented herein. These include quantitative details on the rates and half-lives of photolysis (direct and indirect), the timescales and yields for photoproduct-to-parent reversion cycling occurs for TBA family compounds, the extent of SGPM sorption and corresponding partitioning coefficients in organic-rich matter, and the relative contribution of sorption and abiotic chemical transformation in soil systems best characterized by inorganic phases coated in a small layer of organic matter. However, some details regarding the environmental fate of SGPMs require further experimentation, while outcomes of this work also opened up several new lines

for future investigation. A few topics related to the current work that merit follow-up are discussed subsequently.

Biotransformation of SGPMs

All results presented herein pertain to abiotic systems. Thus, the rate (e.g., half-lives) and controls (e.g., influence of system variables) of SGPM biotransformation merit further investigation. Such biotransformation data are necessary to have a complete dataset pertaining to the fate of SGPMs in the natural environment. This dataset would then be ideal for developing a numerical model to predict the fate and persistence of this emerging pollutant class in a range of settings.

In previous study, it is suggested that half-lives of TBA and MGA metabolites were typically ranging from several hours to a few days, but half-lives exceeding 250 days were observed in anaerobic environments such as liquid manure [12, 17]. Similar studies for estrogens suggest that redox state plays an important role in biodegradation. Most observations of highly persistent steroids (half-lives > 30d) occur in anoxic or anaerobic environments and studies demonstrate that alternations in redox condition can significantly affect the environmental fate of steroids across a range of environments [12, 115-117]. So it is worthy to determine the rate constants and half-lives for SGPMs by evaluating aerobic and anaerobic degradation pathways in a range of environmental systems.

Validation of photoproduct-to-parent reversion

for trenbolone acetate metabolites

Perhaps the most significant finding from this study comes from Chapter 3, where we discovered that dehydration of their primary photoproducts is a viable route by which the metabolites of trenbolone acetate (i.e., 17a-TBOH, 17b-TBOH and TBO) can be regenerated in surface waters. This outcome must be validated in a field setting. From

the results presented in Chapter 3, we anticipate that the concentrations of these trenbolone metabolites in surface waters should exhibit several characteristic trends in response to this reversion process. First, their concentration should reveal a diurnal cycle, being largest at night when the rate of dehydration is no longer counterbalanced by the rate of metabolite photolysis. Second, the temperature dependence of the dehydration process, and thus parent metabolite regeneration, should result in a seasonal dependence in their surface water concentrations. Finally, the pH-dependent nature of the dehydration process (i.e., typically being greatest at lower pH values) should result in higher concentrations in more acidic waters.

Such field studies will require new methodologies for the sampling and handling of surface waters intended for analysis. Most sample preservation methods (e.g., acidification, storage a cold temperature) will influence the extent to which the 12-hydroxy photoproduct reverts back into the parent metabolite from which it was generated. Thus, these field-scale validation studies should not draw upon previous methods used to analyze for trenbolone acetate metabolites in surface water. Rather, new methods that explicitly assess the extent of photoproduct-to-parent reversion, and account for this mechanism when quantifying metabolite concentrations, will be necessary.

<div align="center">Confirmation of zeranol species involved</div>

<div align="center">in indirect photolysis reactions</div>

In Chapter 2, we reported that the rates and mechanisms of indirect photolysis of the zeranol family of compounds was pH dependent. Unlike the TBA and MGA families, zeranol and its metabolites possess ionizable –OH groups on their phenolic ring that can be deprotonated at pH values that are environmentally relevant. In Chapter 2, the pH-dependent reactivity observed in irradiated DOM suspensions was attributed to photooxidants reacting primarily with the monodeprotonated form of zeranol. This is a scenario that requires further validation that would be relatively straightforward to

conduct experimentally. We envision a study examining the DOM-mediated indirect photolysis of zeranol and its metabolites over a broader range of pH than that considered in Chapter 2 (e.g., from pH 4 to pH 10). These studies with model DOM systems would be completed by speciation modeling using reported pKa values for the zeranol family of compounds. Finally, experiments in model reactive oxygen species (ROS) systems (e.g., Rose Bengal for singlet oxygen production) would also be conducted as a function of pH.

The goal of such a work would not only be to validate the hypothesis put forth in Chapter 2 about the monodeprotonated species governing reactivity toward photooxidants but also to use speciation modeling in complement with model ROS systems to report second order rate constants for reaction of each zeranol species (i.e., fully protonated, monodeprotonated and dideprotonated) with singlet oxygen and hydroxyl radical. These rate constants would be valuable in predicting the importance of such processes in DOM-containing surface waters impacted by zeranol.

<div align="center">

Identification and fate studies with

SGPM transformation products

</div>

In Chapter 2 and 3, phototransformation products were only identified for the trenbolone acetate family. Future work must also identify the direct photolysis transformation products for melegestrol acetate and melengestrol, as well as those generated via the indirect photolysis of zeranol. Notably, zeranol's phototransformation products will likely prove the most challenging to identify because of the more complex aquatic matrices necessary for their production. Given the unique chemistry exhibited by the primary product generated via photolysis of trenbolone acetate metabolites, future work must not simply identify the structures of these transformation products. Rather, stability and fate studies should be examined to determine if such unique chemical pathways may be available to other SGPM photoproducts.

Finally, we have confirmed in Chapter 4 that SGPMs are reactive toward various metal oxides, although several key details of these transformation pathways remain unknown. It is necessary to further investigate the mechanism and transformation products generated from these heterogeneous reactions. Further, a more detailed consideration of the system variables (e.g., pH, SGPM concentration) that influence the rate and products of such reactions is also warranted.

APPENDIX A. IDENTIFICATION AND ENVIRONMENTAL
IMPLICATIONS OF PHOTO-TRANSFORMATION PRODUCTS OF
TRENBOLONE ACETATE METABOLITES

A.1   Abstract

Androgenic, anabolic steroids such as trenbolone acetate (TBA) are widely used
in animal agriculture. However, evidence for the widespread occurrence of TBA
metabolites such as 17β-trenbolone (17β-TBOH), 17α-trenbolone (17α-TBOH), and
trendione (TBO) is relatively scarce, potentially due to rapid transformation via
mechanisms like photolysis. To assess TBA metabolite fate and ecological implications
of TBA metabolite photoproducts, we investigated direct photolysis transformation
pathways and assessed photoproduct ecotoxicology. High resolution, accurate mass
liquid chromatography-tandem mass spectrometry identified a range of mono-, di- and
tri- hydroxylated products that were no longer photoactive, with primary photoproducts
consisting of monohydroxy species and presumptive diastereomers. Also observed were
successive higher order hydroxy end products probably formed via subsequent reaction
of primary photoproducts. Concurrent NMR analysis confirmed the formation of 12-
hydroxy-17β-trenbolone (2.2 mg), 10,12-dihydroxy-17β-trenbolone (0.7 mg), and 11,12-
dialdehyde (1.0 mg) products after irradiation of 10-12 mg 17β-trenbolone. Though
unconfirmed by NMR, our data suggests that the formation of stereoisomeric products
also may occur, likely due to the reactivity of the unique 4,9,11 conjugated triene bond
structure of trenbolone. *In vivo* exposure studies employing Japanese medaka (*Oryzias
latipes*) indicate that low concentrations of 17α-TBOH photoproduct mixtures can alter
ovarian follicular development, and TBA metabolite photoproducts alter whole body
17β-estradiol levels. Therefore, direct photolysis yields transformation products with
strong structural similarity to their parent compounds, and these products still retain

enough biological activity to elicit observable changes to endocrine function in aquatic organisms.

A.2   Introduction

In the United States and several other countries, the anabolic, androgenic steroid hormone trenbolone acetate (TBA) is widely used as a growth promoter in beef cattle production [17, 22, 87] . For example, TBA is 15 -50 times more androgenically and anabolically potent than testosterone, which are primary reasons it is such an effective steroid [58]. We estimate that annual TBA production and use likely exceed 4800 kg/year in the U.S., and some studies report that 60-90% of U.S. beef cattle receive TBA implants [50, 87, 118, 119]. This data suggest that TBA is one of the highest production synthetic steroids in use, while the widespread use of TBA and the large scale typical of animal agriculture operations also imply that this steroid or its metabolites likely are widespread in environments affected by animal agriculture. As many studies demonstrate endocrine disruption and impaired reproduction in aquatic organisms resulting from exposure to potent endogenous and synthetic steroids [21-23, 25, 120], assessing the fate of TBA and related metabolites in aquatic environments is a priority.

After implant release, TBA is converted to the active androgen 17β-trenbolone (17β-TBOH), which is further metabolized to 17α-trenbolone (17α-TBOH) and trendione (TBO) [17]. Together, these metabolites, especially 17α-TBOH which composes 95% of the known TBA metabolite mass excreted, account for approximately 8% of the total TBA implant mass, with the remainder comprised of uncharacterized metabolites [17]. Mass balance calculations suggest that 80 μg/day of 17α-TBOH is excreted from implanted cattle, resulting in 17α-TBOH concentrations potentially as high as several thousand ng/L in runoff from animal agriculture sites such as confined animal feeding operations (CAFOs) [17, 121]. 17β-TBOH and TBO also have been detected in runoff and soils near animal agriculture operations, although at lower concentrations that 17α-TBOH [16, 91, 121-123].

Low concentrations of TBA metabolites can affect morphology and reproductive output in exposed aquatic organisms. For example, Ankley *et al*. and Jensen *et al*. report fecundity

reduction in fathead minnows at 11-27 ng/L for 17α-TBOH and 17β-TBOH, respectively [22, 39]. No-effects concentrations for these compounds are likely even lower, and are probably similar to the ~1 ng/L no-effects concentrations frequently reported for estrogenic steroids [124, 125]. In addition, skewed sex ratios, physiological masculinization, and inhibited embryonic development are observed in fish exposed to 17α-TBOH and 17β-TBOH [91, 120, 121]. 17β-TBOH may also act as a genotoxicant in fish [126]. To date, no ecotoxicology studies have been reported for TBO, likely due to the only recent commercial availability of TBO standards.

The large mass of TBA used in animal agriculture suggests that TBA metabolites should be relatively widespread in the aquatic environment. Yet these compounds are detected rather infrequently compared to endogenous steroids like estrogens with similar chemical properties, and often at lower concentrations than would be expected from TBA mass usage alone [16, 121, 127]. For example, in our own experience, analysis of runoff and soils from beef cattle CAFOs with extensive trenbolone usage has sometimes resulted in no-detects for known TBA metabolites even when we expected detection [123]. However, a number of ecotoxicology studies have reported instances of endocrine disruption in aquatic organisms in close proximity to animal agriculture operations, although related chemical analyses, including known TBA metabolites, was unable to identify causative agents [25, 91, 120, 128, 129]. These observations suggest the potential importance of transformation mechanisms (*e.g.*, biotransformation, photolysis, mineral promoted hydrolysis) and related product formation on TBA metabolite fate in aquatic environments. Also, the 4,9,11 triene structure characteristic of trenbolone is quite unique and is very rare among synthetic steroids, suggesting that novel transformations and products may be especially characteristic of this steroid class.

A companion manuscript previously reported that direct photolysis represents the dominant phototransformation mechanism for 17α-TBOH, 17β-TBOH, and TBO, and that the timescales of this process are quite short (half-lives <1 h) [130]. Thus, due to the rapid rate of direct phototransformation and the likely dominance of this degradation pathway in surface waters [130], the objective of this study was to investigate photo-transformation pathways of

known TBA metabolites (17α-TBOH, 17β-TBOH and TBO) and related photoproduct formation by utilizing high resolution (HR), accurate mass liquid chromatography-tandem mass spectrometry (LC-MS/MS) analysis. Nuclear magnetic resonance (NMR) analysis was used on a subset of 17β-TBOH samples that had been photolyzed, then fractionated, to verify major product structures. Finally, the endocrine disrupting capability of photoproduct mixtures was assessed using *in vivo* and *in vitro* bioassays for estrogenic and androgenic endpoints.

A.3   Experimental Methods

Chemicals and HR-LC/MS/MS Studies

17α-TBOH (17α-hydroxyestra-4,9,11-trien-3-one) was obtained through BDG Synthesis (Lower Hut, NZ). 17β-TBOH (17β-hydroxyestra-4,9,11-trien-3-one) and trendione (4,9,11-estratriene-3,17-dione) were obtained from Sigma Aldrich (St. Louis, MO) and Steraloids (Newport, RI), respectively. HPLC-grade solvents were obtained from Fisher (Pittsburg, PA). If necessary, samples were extracted on 6 mL C-18 solid phase extraction cartridges (Restek, Bellefonte, PA). Stock solutions (2-10 mg/L) for each of the steroid analytes were prepared in silanized volumetric glassware, then serially diluted to create working standards. Deionized water was obtained from a Milli-Q system (Millipore, Billerica, MA, USA).

Photolysis Studies

Most photolysis experiments were conducted in natural sunlight in mid-day conditions without cloud cover, in Reno NV (LAT 39.54, LON -119.81). Ambient temperatures averaged 15-23°C during these experiments. Cylindrical (12 mm diameter) borosilicate glass flasks were filled (no headspace) with 50 mL deionized water spiked with ~100 µL of concentrated steroid stock solution to a final 2-3 µM concentration. Dark controls consisted of identical flasks wrapped in foil, although analysis of these samples demonstrated no decay under these experimental conditions. At predetermined

time points (0, 45, 120 minutes), 2 mL samples were collected and HPLC-grade methanol added (90% water, 10% methanol v/v) for immediate HR-LC-MS/MS analysis.

A subset of photolysis experiments were conducted using simulated sunlight using a light source and conditions described elsewhere [130]. As larger solution volumes were necessary for this study, a different solar simulator (Suntest) was used, with otherwise identical conditions, to irradiate 100 mL borosilicate glass beakers containing 2-3 µM TBA metabolites. As for the natural sunlight studies and using the same sampling intervals, 30 mL aqueous samples were SPE extracted on preconditioned C-18 SPE cartridges, chilled, and overnight shipped from the University of Iowa to UNR for analysis. Upon arrival, SPE samples were extracted with 5 mL aliquots of methanol, blown down to reduce methanol volume to 200 µL, and diluted with deionized water (90% water, 10% methanol v/v) for HR-LC-MS/MS analysis. In most cases, initial photo-product identification, estimation of parent metabolite transformation and photoproduct stability were performed using standard high pressure liquid chromatography-diode array detector (HPLC-DAD) or low resolution LC-MS/MS analysis [130].

<center>HR-LC-MS/MS Analysis</center>

High resolution LC-MS/MS analysis was used to identify photoproducts. Though several chromatography gradients were used for separation (*e.g*., Figures 1, 2) [130], the following separation was used for most analysis of the TBA metabolites and the comparative data presented in the results and discussion section. Separations utilized a Paradigm Multi-Dimensional Liquid Chromatography (MDLC) instrument (Michrom Bioresources) using a Genesis Lightning C-18 4 µm particle, 200Å pore size (2.1 x 100 mm) column (Grace Davison). Solvent A was 0.1% acetic acid in water and solvent B contained 0.1% acetic acid in ACN. Eluent flow rate was 200 µL/min and the solvent gradient ranged from 25% B to 72% B over 18 min, followed by 100% B for 1 min, for a

25 minute total run time. Eluted compounds were analyzed using an LTQ-Orbitrap XL (ThermoElectron) detector equipped with an Ion Max source using Xcalibur v 2.0.7 software for data processing. The MS was operated in data-dependent mode switching between Orbitrap-MS for high resolution full scan data and LTQ-MS/MS for low resolution tandem mass spectrometry fragmentation data. Full scan spectra (m/z 100–350) were acquired in the positive ion mode with resolution of 100,000 in profile mode. The three most intense data-dependent peaks at each analysis interval were subjected to MS/MS using collision-induced dissociation with a minimum signal of 5000, isolation width of 3.0 amu, and normalized collision energy of 35.0%. Ions already selected were dynamically excluded for 30 seconds after a repeat count of 2 with a repeat duration of 10 seconds. Also, during each sampling scan, all ions of m/z 271.17 and 269.15, representing 17α- or 17β-TBOH parents and TBO respectively, were subjected to MS/MS analysis using collision-induced dissociation with a normalized collision energy of 35.0% and an isolation width of 3.0 amu.

NMR Analysis

Structural elucidation of the most stable 17β-TBOH photoproducts was accomplished by NMR. Due to the high cost of 17α-TBOH and TBO standards, structural elucidation of photoproducts for these compounds by NMR was not performed, although results from 17β-TBOH NMR analysis can likely provide valuable insight into the corresponding photoproducts generated from direct photolysis of 17α-TBOH and TBO.

For NMR analysis, mixtures of 17β-TBOH photoproducts were generated using the solar simulator (120 minutes of irradiation was sufficient for 98+% transformation of 17β-TBOH parent). These photoproduct mixtures were then fractionated using a Beckman System Gold HPLC with a model 166 UV detector (detection at 254 nm). The sample was separated into 8 fractions each corresponding to 1 minute of retention time. This fractionation procedure utilized a reversed–phase HPLC equipped with Grace

Apollo 5–µm C_{18} column (10 x 250 mm) and a method calling for 25–72% MeCN–H_2O over 13 minutes, 72–100% over 2 minutes, and isocratic 100% MeCN for 5 minutes at a flow rate of 2 mL/min). Degradation product structures present in each fraction were then assigned independently by analysis of 1D and 2D nuclear magnetic resonance (NMR) data, including ^{1}H NMR, COSY (Correlation Spectroscopy), HSQC (*Heteronuclear Single Quantum Coherence)*, and HMBC (*Heteronuclear Multiple Bond Correlation)* experiments. Two–dimensional experiments were performed on a 600–MHz Bruker AVANCE–III equipped with a 1.7–mm triple–resonance (^{1}H, ^{13}C, ^{15}N) inverse probe. Proton NMR experiments were carried out on a Bruker AVANCE 500.

Theoretical Methods

To assist in their identification, the UV/vis spectra for proposed product structures were calculated using computational chemical calculations. All calculations were performed using Gaussian 09 version B02 [131].

All calculations were performed using Gaussian 09 version B02 [131]. Proposed product structures were optimized using M06-2X [132] functional in combination with 6-31+G(d,p) basis set. Geometries were optimized without any constraints followed by the vibrational frequency analysis. The absence of negative frequencies confirmed that structures were on the potential energy surface minima. UV/vis spectra were calculated using time dependent density functional theory (TDDFT) calculated electronic transitions obtained using a large 6-311+G(2df,2p) basis set and the same functional. Calculated excitation energy values were broadened by 20 nm Lorentzian broadening to better represent experimental data. Solvation effects were simulated using the SMD model [46].

Photoproduct Ecotoxicology

To evaluate the potential biological effects of TBA metabolite photoproducts, both *in vivo* and *in vitro* bioassays were used to assess product mixtures generated from 17β-TBOH, 17α-TBOH, and TBO phototransformation. *In vivo* studies employed female

Japanese medaka (*Oryzias latipes*) as test organisms, and both histological and whole body steroid level analyses were performed after exposure to photoproduct mixtures. *In vitro* studies employed assays based upon rainbow trout (*Oncorhynchus mykiss*) liver hepatocytes to quantify vitellogenin induction upon exposure to photoproducts [133].

Medaka and in vivo exposure: Adult female Japanese medaka (*Oryzias latipes*) > 90 days old posthatch (20.35 ± 1.09 mm, 0.107 ± 0.059 g) were used from an ongoing culture at the University of California, Riverside. Fish were held in 1 L containers with carbon filtered freshwater (25 °C) with a 16:8 hour light:dark cycle. During experimentation, water quality parameters were monitored. Medaka were fed live brine shrimp (*Artemia* spp.) nauplii *ad libitum* twice daily.

Fish were exposed to the solvent carrier methanol (0.01% v/v) and nominal concentrations of 17α-TBOH, 17β-TBOH, and TBO photoproduct mixtures (predicted 1, 10, and 100 ng/L mixture concentrations in the tank) with n = 3 independent replicates with 10 fish per replicate for each compound. Water changes (100%) and re-dosing of TBA metabolite photoproducts occurred every 48 hours. After 14 days, the fish were euthanized using buffered MS-222 (250 mg/L; Sigma-Aldrich, St. Louis, MO). Fork length (cm) and weight (g) were recorded. Fish were reared and handled under an approved protocol that followed the policies and guidelines of the University of California, Riverside Institutional Animal Care and Use Committee.

Preparation of Photolysis Product Mixtures: Solutions of each trenbolone metabolite were prepared in DI water to an initial concentration typically between 15-100 μM. These solutions were irradiated under a 1000 W Xeon arc lamp for 4 hours, which was sufficient for more than 95% transformation of the TBA metabolite. About 50 mL of the resulting photoproduct mixture was then passed through a C18 cartridge and subsequently eluted with 5-10 ml methanol. The phototransformation products mixture in methanol was stored in an amber vial at 4°C to avoid light and biodegradation until use in the ectoxicological studies.

Histological analysis: After the exposure period, five whole fish were placed in Bouin's fixative (Ricca Chemical Company, Arlington, TX) for 48-hours and then transferred to 70% ethanol. Fish were processed via a series of graded ethanol followed by xylene and infiltrated and embedded with paraffin wax. Fish were sectioned using a manual rotary microtome to a thickness of 5 µm and stained with hematoxylin and eosin (Richard Allen Scientific, Kalamazoo, MI). The ovaries were examined using a light microscope and images were captured using a digital camera attached to the microscope. Ovarian follicles were staged based on morphological characteristics previously established for teleost fishes [134]. The percentage of primary, secondary, and vitellogenic stage follicles was quantified as: # staged follicles / # total follicles * 100.

Sex steroid analysis: Due to the small size of medaka, an insufficient amount of blood plasma could be obtained for direct measurement of sex steroids. Therefore, whole body extractions were performed [86]. Briefly, whole fish were homogenized in a buffer (100 mM phosphate buffer, 100 mM KCl, 1 mM EDTA, pH 7.4), then diethyl ether was added to the homogenate and vortexed followed by centrifugation at 3000g for 5 minutes. The ether supernatant was then collected, and this step was repeated twice to insure quantitative extraction. The supernatant was dried down with nitrogen in a 37 °C water bath and reconstituted with steroid assay buffer. 17β-Estradiol (E2), testosterone (T), and 11-ketotestosterone (11-KT) were measured using commercially available EIA kits following the manufacturer's protocol (Cayman Chemical, Ann Arbor, MI).

In vitro vitellogenin assay: Given the small size of medaka liver, obtaining a sufficient number of hepatocytes for primary cell culture also was not feasible. Therefore, to determine the estrogenic effects of TBA metabolite parents [135] and TBA metabolite photoproducts, rainbow trout (*Oncorhynchus mykiss*) hepatocytes were utilized. Hepatocytes were isolated from the livers of 12 fish using the protocol of Lavado *et al*. [131]. Briefly, hepatocytes were obtained using enzymatic digestion with trypsin followed by mechanical disaggregation and centrifugation using Percoll

(Amersham Biosciences, Uppsala, Sweden). Hepatocytes were seeded in a 48-well culture plate with a density of 1×10^6 cells/well with 17β-estradiol (100 ng/L) as a positive control and each of the TBA metabolite parents and photoproducts (1000 ng/L, with 5 replicate wells/treatment) were incubated with hepatocytes for 24 hours at 18 °C. After incubation, the cells were resuspended in PBS, centrifuged at 5200g for 5 minutes and the pellet was washed twice with PBS. The RNA was immediately isolated from the cells using a commercially available kit (SV Total RNA Isolation System, Promega, Madison, WI) following the manufacturer protocol. Vitellogenin mRNA was quantified via qPCR using iScript One-Step RT-PCR kit with SYBR Green (Bio-Rad, Hercules, CA) using the following rainbow trout primer set: tVit-364 5'-CCCACTGCTGTCTCTGAAACAG-3' (sense primer) and tVit-565 5'-GACAGTTATTGAGATCCTTGCTCTTG-3' (antisense primer). β-actin was used as a housekeeping gene using the following primer set: 5'-GTCCTTCATGATTCTCTGCTGA-3' (sense primer) and 5'-ACTCGGGGTTCATTTGCATAAACA-3' (antisense primer). A total of 250 nM of each primer (vitellogenin or β-actin) was added to the 25 mL PCR reaction vial (containing SYBR Green RT-PCR Reaction Mix, 100 ng mRNA hepatocyte sample, and iScript Reverse Transcriptase for One-Step RT-PCR). Real-time reactions were performed using an iCycler-MyIQ Single Color Real-Time PCR Detection System (Bio-Rad, Hercules, CA) with the following reaction parameters: 10 min at 50 °C, 5 min at 95 °C, 40 cycles of 10 s at 95 °C, and 30 s at 56 °C with data collected at the end of each cycle. Following the amplification reaction, a melt curve analysis was determined between 60 - 95 °C with data collection at 0.1 °C intervals. The Ct was selected within the linear phase of amplification. Data analysis was performed using IQ5 (Bio-Rad, Hercules, CA). To determine the estrogenicity of the TBA metabolites and subsequent photolysis products, the estradiol equivalency (EEQ; ng/L exposure treatment response) was determined using an E2 dose-response curve calculated at various concentrations of E2 (*e.g.*, 4×10^{-12} M, 4×10^{-11} M, 4×10^{-10} M, 4×10^{-9} M, 4×10^{-8} M, 4×10^{-7} M, 4×10^{-6} M, and 4×10^{-5} M).

Statistical analysis: Statistical analyses were performed using a two-way analysis of variation (ANOVA) and a one-way ANOVA followed by a Tukey's multiple means comparison (GraphPad Prism version 5.0a for Windows, GraphPad Software, LaJolla, CA). The level of significance was determined at $p < 0.05$ for all statistical analyses.

A.4 Results and Discussion

<u>Photoproduct Analysis</u>

As described in detail in our prior work [130], all TBA metabolites rapidly decay to residual levels upon irradiation, with corresponding increases in the concentrations of primary photoproducts (Figure A-1). Under conditions of direct photolysis in natural sunlight, half-lives for 17α-TBOH, 17β-TBOH, and TBO were 31, 25, and 23 min, respectively [130]. We observe all major TBA metabolite photoproducts (*i.e.*, those in Figure A-1) to be photostable, consistent with their absorption maxima decreasing from 350 nm for the parent TBA metabolites, a value characteristic of the 4,9,11 triene system, to 240-260 nm for the major products detectable by HPLC-DAD (Figure A-1, A-2) [130]. This suggests that disruption of the conjugated 4,9,11 π-bond system of the parents has occurred, shifting product absorption essentially out of the solar spectrum. This effect reduces the potential for further direct phototransformation and increases product persistence [130]. We note that the minor decay observed for products of 17β-TBOH and TBO appears attributable to a non-photochemical process (*e.g.*, hydrolysis), as the same rate of decay is observed in dark samples. Such non-photolytic transformation pathways of these major products are the focus of a subsequent investigation. Another observation from initial HPLC-DAD analysis is the striking similarity in the absorbance spectra of all major photoproducts.

We interpret this as evidence that the major photoproducts of 17α-TBOH, 17β-TBOH, and TBO are likely all similar in structure, implying conservation of phototransformation mechanisms among the TBA metabolite family (Figure A-2).

However, there are some apparent differences in the nature of the products. For instance, each metabolite has a unique ratio of major to minor product (based on HPLC-DAD peak areas 17α-TBOH, 17β-TBOH and TBO are 5:1, 2:1, and approximately 1.5:1, respectively). We also note that the primary photoproducts of 17β-TBOH are substantially more polar than primary photoproducts of 17α-TBOH and TBO based on their relative elution times.

To build upon this initial HPLC-DAD data, high resolution LC-MS/MS analysis was the primary tool used to investigate the transformation pathways and products initiated by direct photolysis of 17β-TBOH, 17α-TBOH, and TBO. Because pure standards for potential photoproducts are not available for direct comparison, characterization of prospective photoproducts in irradiated samples was accomplished using the following screening criteria: 1) time dependent growth of chromatographic product peaks which were not present in the standard or control solutions; 2) comparison of observed product accurate masses with predicted accurate mass; and 3) similarity of product MS/MS fragments with observed parent fragments.

Observed accurate masses and MS/MS spectra for 17α-TBOH, 17β-TBOH, and TBO parents are found in Table A-1. Using the Orbitrap detector, concurrent full scan (all) and MS/MS spectra (most) were collected for the most intense peaks in the 20 minute run over a 120-350 amu range (*e.g*., Figure A-3). Peak identification consisted of examining all peaks with a minimum integrated area unit of 10,000 or greater in single mass chromatograms over the 250-350 amu range, which is where we expected most potential product masses to occur. Peaks were eliminated as prospective photoproducts if their observed mass was not within 0.03 amu of the predicted product structure exact mass. Then, for observed peaks with accurate masses close enough to the predicted exact mass to imply a structural relationship, MS/MS fragment comparisons were performed, with photoproducts typically exhibiting at least 3-4, and occasionally as many as 8, of the same MS/MS fragments as parents. In particular, fragments at m/z 159 and 133 were

particularly diagnostic of trenbolone, as these fragments are conserved across all parents and present in nearly all of the identified photoproducts (Table A-1). However, this fragment comparison approach was most effective when photoproduct masses were closest to parent masses. At the larger masses (*e.g*., trihydroxy species), fragment conservation began to diminish as these structures fragmented by increasingly unique mechanisms.

Two substantial analytical challenges were encountered with this approach. First, photoproducts exhibited decreased ionization efficiency in positive ESI mode compared to the parent TBA metabolites that contain an intact 3-keto, 4-ene structure that can ionize efficiently in positive ion electrospray [136]. Alteration of the 3-keto, 4-ene structure in the steroid A ring typically significantly reduces ionization efficiency in positive ion electrospray, implying reduced ionization for products exhibiting loss of the resonance stability of the 4,9,11 triene system [136]. For example, the structural analog 9,11-delta-estradiol has been proposed as a potential biotransformation product of 17β-TBOH [36]. Using positive ionization mode, the observed peak area for a 3 µM standard of 9,11-delta-estradiol (*i.e*., the only potential structural analog with an available standard) was far less than 1% of the observed peak areas for TBA metabolites at 3 µM. Additionally, summing the peak areas of parents and observed photoproducts was not conservative through the transformations, implying substantial variation in ionization and peak area responses between parents and products. This variable product ionization in positive ionization mode precludes estimation of product yields using the HR-LC-MS/MS analysis, and is characteristic of many steroids, such as estrogens, which often are analyzed utilizing alternative ionizations. Given the potential difficulty in resolving minor from major products due to ionization differences, we included all products related to TBA metabolites in this analysis.

Table A-1. Observed MS/MS fragments for 17α-TBOH, 17β-TBOH and trendione standards used for identification of photo-products. Although high resolution FT-MS detection was used for full scan spectra, low resolution IT-MS detection was employed for all MS/MS spectra, reducing the mass precision observed for these fragments.

	17α-TBOH m/z	**17β-TBOH m/z**	**Trendione m/z**
Predicted [M+H]$^+$ Exact Mass	271.1698	271.1698	269.1541
Observed [M+H]$^+$ Mass (FT-MS)	271.1681	271.1681	269.1523
MS/MS Fragments (IT-MS)	253.2	253.3	251.2
	243.3	235.2	233.2
	225.3	227.2	225.2
	211.1	211.2	207.2
	197.2	197.2	195.2
	183.2	185.3	
		179.2	169.2
	159.2	*159.2*	*159.2*
	147.2	145.3	143.2
	133.2	*133.2*	*133.2*
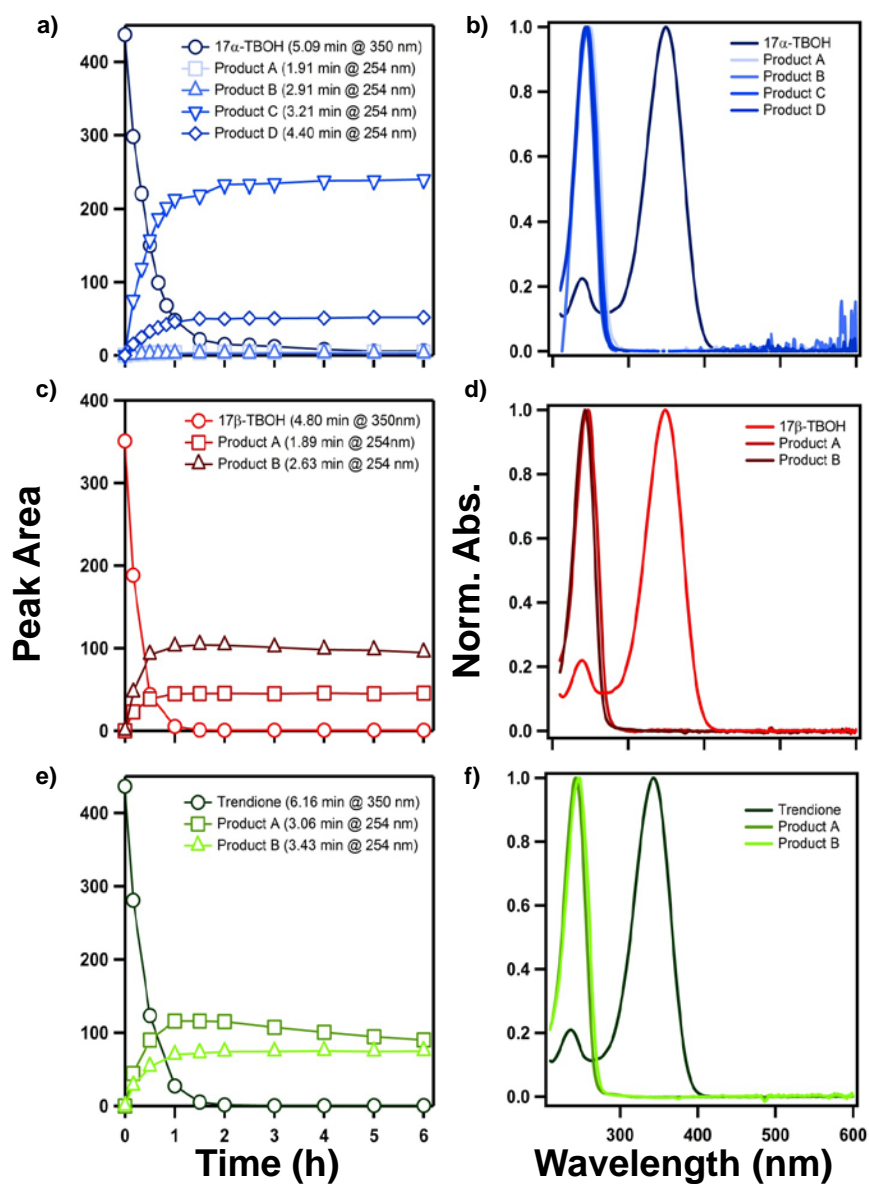
Figure A-1. Representative time courses and corresponding UV/vis absorbance scans for each species detected during direct photolysis experiments with (a,b) 17α-TBOH, (c,d) 17β-TBOH and (e,f) TBO. All experiments at pH 7 with ~10 μM initial concentration.
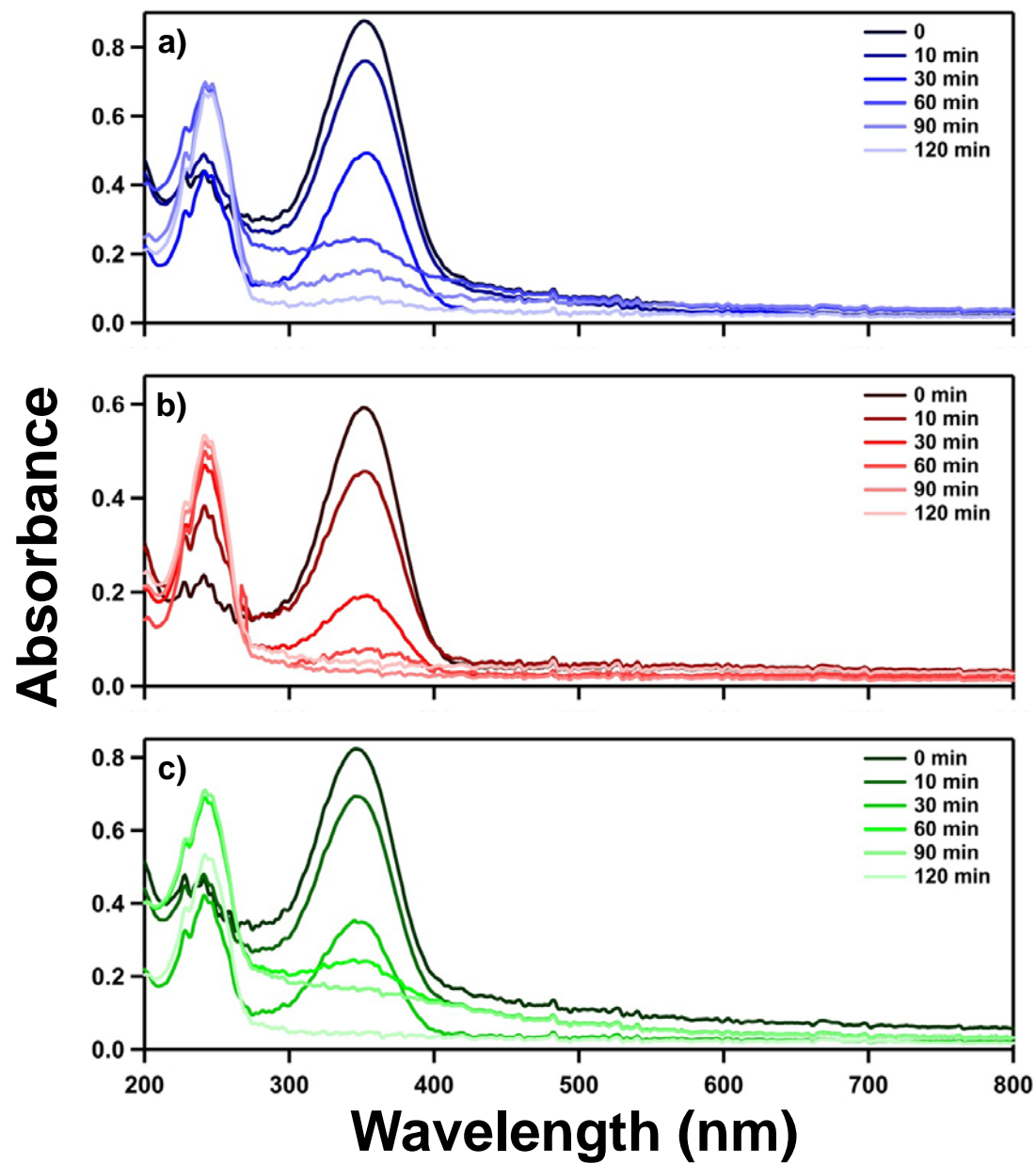
Figure A-2. UV/vis absorbance scans for 10 µM solutions of (a) 17α-TBOH, (b) 17β-TBOH and (c) TBO as a function of irradiation time.
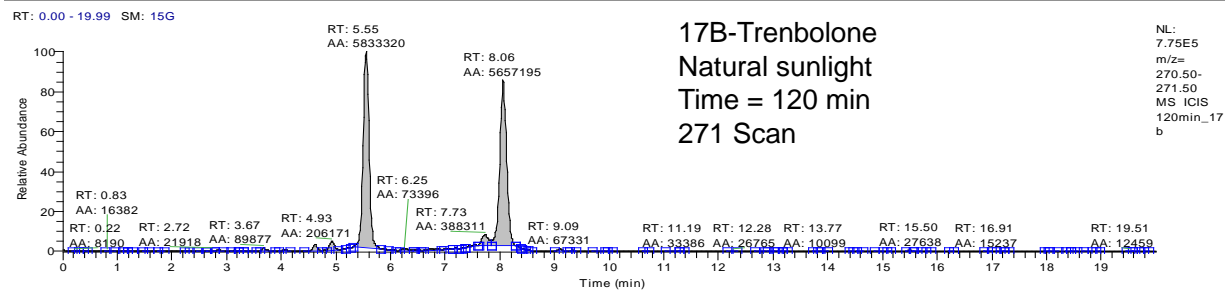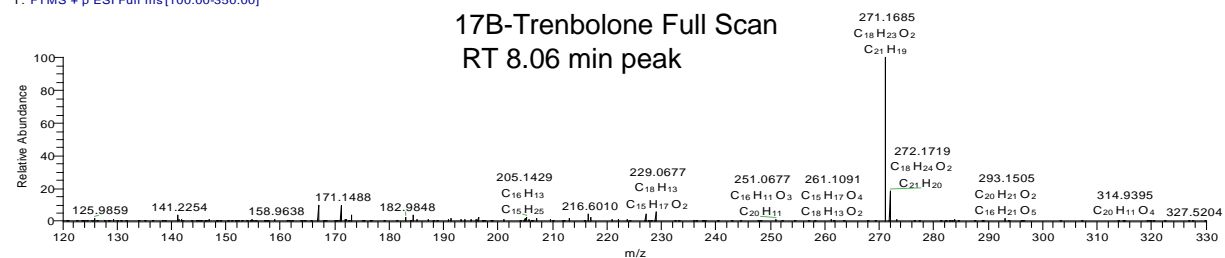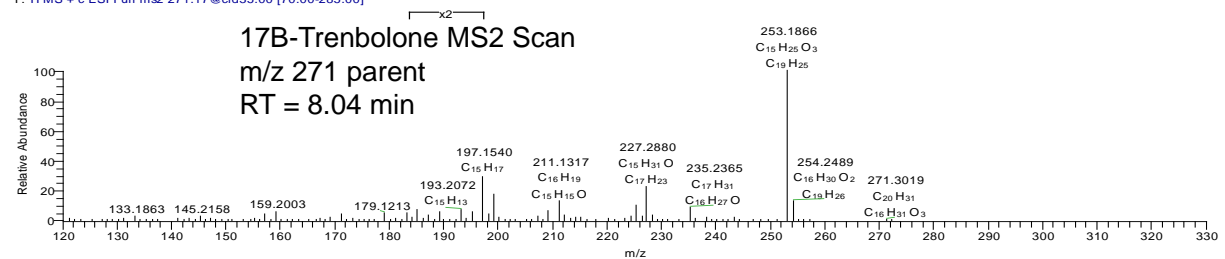
Figure A-3. Representative LC chromatogram, high resolution full scan spectra, and MS/MS spectra for 17β-TBOH at 8.06 minutes after 120 minutes in natural sunlight. The peak at 5.55 minutes is the dominant 12-hydroxy-trenbolone photoproduct, and we propose that the small peak at 4.93 minutes represents the proposed 10-hydroxy product. Chromatograms and spectra for additional products of 17β-TBOH, as well as photoproducts of 17α-TBOH and TBO are available in Figures A5-A21.

Second, under the ionization conditions used in the Orbitrap detector, we finally

determined that no $[M+H]^+$ molecular ions (expected m/z 289.1805) were observed for

monohydroxy-trenbolone species which were subsequently confirmed by NMR

(discussed in detail later). Instead, $[M+H-H_2O]^+$ fragment ions (observed m/z 271.1685)

were observed for the monohydroxy species, initially leading to much confusion

regarding the correct mass/structure assignments for these products. However, ancillary

LC-MS/MS analysis with a different instrument yielded the expected m/z 289 mass for

two monohydroxy product $[M+H]^+$ molecular ions forming from 17α-TBOH, although at

low abundance ($< 5\%$) relative to the $[M+H-H_2O]^+$ fragment ion (Figure A-2). For these

m/z 271 photoproducts, the characteristic decrease in LC retention time (*e.g.*, Figures A-

6, A-11, or A-18) due to their increased polarity is considered to be the best diagnostic of

their presence in HR-LC-MS/MS data. This approach is complicated by the fact that

these $[M+H-H_2O]^+$ ion species cannot be differentiated from potential structural analogs

and stereoisomers of the parent TBA metabolites with m/z 271.1685 $[M+H]^+$ ions,

although we expect that structural analogs and stereoisomeric products should exhibit

relatively longer chromatographic retention times that are much closer to observed parent

retention times.

Under these chromatographic conditions, 17α-TBOH, 17β-TBOH, and TBO

standards eluted at 8.06, 8.31, and 9.55 min, respectively (Figures A-3, A-5, A-10, and

S15). This analysis indicated that TBA metabolite transformation products were

primarily monohydroxy, dihydroxy, and trihydroxy species, often detected as groups of

closely eluting peaks (presumably diastereomers) in product chromatograms (Table A-2).

Hydroxylated products are often characteristic of photochemical transformations, as

hydroxyl addition is a common photo-oxidation pathway and subsequent photolysis or

hydrolysis reactions form secondary and tertiary products [137, 138]. For example,

HPLC-DAD analysis observed 2-4 primary products observed upon direct photolysis of

17α-TBOH and 17β-TBOH (Figure A-1). In the case of 17β-TBOH, 2 product peaks

were observed by HPLC-DAD (Figure A-1c, A-1d) and confirmed by HR-LC-MS/MS (Figures A-3, A-6, retention times of 4.93 min for the minor product and 5.55 min for the dominant product) as hydroxy-trenbolone products with $[M+H-H_2O]^+$ ions at m/z 271.1685.

Subsequent NMR analysis of products from 17β-TBOH confirmed one of its two primary products as 12-hydroxy-trenbolone, and also observed 10,12-dihydroxy-trenbolone and an 11,12-dialdehyde species, although NMR analysis was limited to those products with high yields and sufficient stability. As further confirmation, calculated UV/vis spectra for these product structures identified by NMR are consistent with those observed via LC-DAD (compare Figures A-1, A-2 and A-22). Based on the HR-LC-MS/MS and NMR data, and the observed 0.61 minute separation between the two peaks, we propose that the minor product peak (4.93 min) likely represents 10-hydroxy-trenbolone, which further hydrolyzes along with the 12-hydroxy species (5.55 min) to form the 10,12-dihydroxy-trenbolone and 11,12-dialdehyde species observed by NMR. However, it is also possible that these two peaks represent very well resolved diastereomers of 12-hydroxy-trenbolone, although we were unable to confirm these identities with our analyses. Thus, the data would seem to suggest an initial photolytic transformation to the monohydroxy species, with subsequent higher order hydroxylated products forming via hydrolysis, as the absorption maxima of the monohydroxy products no longer fall within the solar spectrum (Figures A-1, A-2 and A-22). A third, minor m/z 271.1685 peak also was observed at 7.73 minutes (Figure A-3), although we cannot determine whether this is a third monohydroxy species or a closely eluting stereoisomeric or structural analog photoproduct. Because four m/z 271.1685 photoproducts were observed for 17α-TBOH, we consider this 7.73 minute product to likely correspond to the analogous 17α-TBOH products, though at minor yield for 17β-TBOH. Based on these observations, a proposed coupled photolysis and hydrolysis transformation pathway for

17β-TBOH is presented (Figure A-23). As will be discussed subsequently, we believe analogous transformation pathways occur for 17α-TBOH and TBO.

In addition to the monohydroxy products, rapidly eluting 17β-TBOH products observed by HR-LC-MS/MS included m/z 303, 305, and 321 species, which likely arise from subsequent hydrolysis of the primary photoproducts to secondary and tertiary dihydroxy, trihydroxy or dialdehyde products. Though these polar fractions were analyzed by NMR, the fractions did not always contain sufficient signal, consistent with minor products. Several poorly resolved m/z 303.1583 products eluted between 3 and 4 minutes (Figure A-7), and may include the 11,12-dialdehyde species observed by NMR, but also may represent a family of dihydroxy species or diketone products of unknown structure. Additionally, one m/z 305.1739 product was observed at 2.90 minutes (Figure A-8), and likely represents the 10,12-dihydroxy-trenbolone product observed by NMR. Although the 11,12-dialdehyde tertiary product observed by NMR strongly suggests the presence of a corresponding 11,12-dihydroxy-trenbolone secondary product, other m/z 305 dihydroxy species were not observed. Also, unlike the m/z 305 dihydroxy product, the m/z 303 products presumably include a third π-bond elsewhere in the molecule, although additional studies are needed to elucidate these structural differences. Finally, two trihydroxy peaks at m/z 321.1688, one dominant peak at 3.57 minutes and a much smaller peak at 4.01 minutes, were observed (Figure A-9). Based upon the structures of the other products observed by NMR, hydroxy addition at the C10, C11, and C12 positions to form the trihydroxy species seems to be the most likely pathway, but tertiary C5 and C9 positions also are possibilities with similar electronic structures.

As expected from similar UV/vis absorbances, HR-LC-MS/MS analysis of 17α-TBOH and TBO photoproducts suggested many similarities to transformation mechanisms observed for 17β-TBOH, with a couple of notable exceptions. For example, instead of the three, more polar, m/z 271.1685 products observed for 17β-TBOH, which represent the 10- and 12-hydroxy-trenbolone $[M+H-H_2O]^+$ ions and a third hydroxy

species or structural analog, four m/z 271.1685 products were observed for 17α-TBOH, including one product which eluted at 10.25 minutes, a full 1.94 minutes later than the 17α-TBOH parent (Figures A-11 to A-14). The three early (*i.e.*, more polar) m/z 271 product peaks of 17α-TBOH elute at 4.91, 6.20, and 7.42 minutes. Due to the close similarity in relative retention times, we propose that the first two of these peaks (observed as $[M+H-H_2O]^+$ ions) correspond to the analogous 10-hydroxy and 12-hydroxy-trenbolone products observed for 17β-TBOH. For the third 17α-TBOH product (7.42 min), no m/z 289 parent peak was apparent in the ancillary LC-MS/MS data (Figure A-4), although this product might correspond to the 7.73 minute peak only weakly observed for 17β-TBOH.

However, the close proximity to the 8.31 minute retention time of the parent 17α-TBOH also might suggest that this peak is a $[M+H]^+$ ion of a photolytically generated stereoisomer or structural analog of 17α-TBOH. Similarly, the 10.25 minute product peak almost certainly suggests formation of a much less polar stereoisomer or structural analog of 17α-TBOH, as oxidized products cannot account for the increased retention time. Possible structural attributes that could account for this increased retention time might include stereochemical inversion or rearrangement of the C13 methyl group, as was observed for photochemically-induced rearrangement of C13 methyl for lumi-estrone [139, 140]. Further product isolation and NMR characterization would be required to resolve this data, although the high cost of 17α-TBOH standard currently limits our ability to perform this analysis.

Similar to 17β-TBOH photoproducts, several poorly resolved m/z 303.1581 peaks at 3-4 minutes are observed for 17α-TBOH which again likely represent dialdehyde or dihydroxy products of unknown structure (Figure A-15). Two m/z 321.1687 peaks also are observed (Figure A-16), a dominant peak at 4.75 minutes and a much smaller peak at 3.71 minutes, that represent trihydroxy products. Unlike products observed for 17β-TBOH, no m/z 305 dihydroxy products are observed for 17α-TBOH, which probably

indicates that these products are less stable (*i.e.*, rapidly react to form tertiary products) compared to the 10,12-dihydroxy-17β-TBOH product. For TBO, an analogous set of products are observed, although apparently more limited in range. Two $[M+H-H_2O]^+$ ions at m/z 269.1528 are observed upon TBO irradiation (presumably analogous 10-hydroxy and 12-hydroxy products), along with a single m/z 303 dihydroxy product and a single trihydroxy-trendione species at m/z 319.1532 (Figures A-18 to A-21). Unlike the primary hydroxy products observed for 17α- and 17β-TBOH, peak areas for the observed primary TBO hydroxy species are substantially larger, which might indicate increased yields, decreased reactivity to secondary products, or more effective positive ionization of the trendione photoproducts due to the C17 ketone. No other TBO products were observed with this analysis.

<div align="center">Photoproduct Ecotoxicology</div>

This is the first study to investigate the biological effects of TBA metabolite photoproducts on the reproductive development of a vertebrate species. *In vivo* ecotoxicology studies with medaka suggest that photoproduct mixtures retain biological activity and also indicate potential mechanisms of action. Additional details from these studies can be found as follows. Observed effects were most pronounced for 17α-TBOH photoproducts. For example, female medaka exposed to 17α-TBOH products (10 and 100 ng/L nominal concentrations) for 14 days resulted in alteration of the ovarian follicle composition at different developmental stages (Figure A-24). Exposure to concentrations as low as 10 ng/L 17α-TBOH photoproducts significantly increased the percentage of vitellogenic follicles from 6.3 ± 5.2 % (controls) to 30.4 ± 2.9% (Figure A-24b). Although the percentage of primary stage ovarian follicles did not significantly change at this exposure, there is a trend for a decrease in primary stage follicles compared to control fish. At higher exposures (100 ng/L 17α-TBOH photoproducts), the percentage of primary stage ovarian follicles was significantly reduced from 77.4 ± 10.6% (controls) to

$40.3 \pm 4.6\%$, while vitellogenic follicles increased from 6.3% (controls) to $31.6 \pm 12.9\%$. No similar effects were observed for analogous 17α-TBOH exposures at equivalent concentrations (p = 0.1724). Interestingly, 17α-TBOH photoproduct mixtures had the highest estrogenicity (4.25 ± 0.06 ng E2/L), but whole body 17β-estradiol (pg/mg) levels were reduced and androgen levels did not change after exposure to 17α-TBOH photoproducts (Figures A-25, A-26). These results suggest that 17α-TBOH photoproducts either directly act upon the ovary advancing the ovarian follicles into vitellogenic growth or indirectly by acting upon the liver to induce vitellogenin production to be incorporated into ovarian follicles.

In contrast, 17β-TBOH photoproducts did not alter the composition of medaka ovaries after exposure, but did elevate whole body E2 levels and also were estrogenic (3.00 ± 0.01 ng/L, Figures A-24, A-25, A-26). For comparison, liver hepatocyte bioassays suggest that 17α-TBOH photoproduct mixtures were significantly more estrogenic (p<0.001) than 17α-TBOH, and 17β-TBOH photoproduct mixtures were significantly more estrogenic than 17β-TBOH (p=0.0474). Similar to 17β-TBOH products, exposure to TBO photoproducts did not alter the composition of medaka ovaries even though whole body E2 (pg/mg) levels significantly increased at the 100 ng/L exposure. TBO photoproducts increased vitellogenin mRNA levels in hepatocytes indicating that these products also are estrogenic (3.43 ± 0.04 ng/L, Figure A-26), although no significant difference in estrogenicity (p = 0.0634) was observed between TBO and TBO photoproducts. Most surprisingly, the observed biological effects of 17β-TBOH and TBO photoproduct mixture exposures generally exhibited inverse trends when compared to 17α-TBOH photoproduct exposures (Figure A-26). These results indicate that although 17β-TBOH and TBO photolysis products are estrogenic and elevate whole body E2 levels, they apparently do not act upon the ovary by stimulating ovarian follicle development.

Histological analysis: For the *in vivo* medaka treatment with 17α-TBOH photoproducts at the lowest concentration (1 ng/L) for a 14 day exposure, no significant ($p > 0.05$) difference in the composition and percentage of ovarian follicles in medaka was observed (Figure A-24). However, there was a significant difference ($p = 0.008$, $p = 0.0018$ respectively) in ovarian composition in medaka exposed to 10 ng/L and 100 ng/L 17α-TBOH photoproducts for 14 days. Similarly, medaka exposed to 10 ng/L 17α-TBOH photoproducts had ovaries with significantly ($p = 0.0031$) more vitellogenic stage follicles compared to other TBA metabolite photoproduct treatments (primary stage $p = 0.3217$, secondary stage $p = 0.8411$; Figure A-24B). The percentage of primary ovarian follicles also were significantly ($p = 0.038$) reduced in the ovaries of medaka exposed to 100 ng/L 17α-TBOH photoproducts and had a significant ($p = 0.0351$) increase in vitellogenic ovarian follicles (Figure A-24C).

Sex steroid levels: Medaka treated with 17α-TBOH photoproducts for 14 days had significant ($p < 0.0001$) reductions in whole body E2 levels (pg/mg; Figure A-21) at all mixture doses. 17β-estradiol significantly ($p = 0.0053$) decreased in fish with increasing concentrations of 17α-TBOH. Most interestingly, though a trend upward is observed, no difference ($p = 0.1691$) in E2 levels was observed after exposure to 17β-TBOH; while a trend upward also is observed, a significant ($p = 0.0473$) increase in E2 levels was observed after exposure to TBO photoproducts (Figure A-21A). The TBA photolysis product mixtures did not significantly alter androgen levels in medaka (T: $p = 0.4920$ and 11-KT: $p = 0.1755$; Figure A-21).

In vitro vitellogenin assay: An *in vitro* analysis to quantify the production of vitellogenin mRNA incubated with 1000 ng/L TBA metabolite photoproducts in rainbow trout hepatocytes was used to determine the overall E2 equivalency (ng/L) as a measure of the estrogenicity of the photoproduct mixtures. All TBA metabolite photolysis product mixtures showed some estrogenic properties (Figure A-22). 17α-TBOH photolysis products exhibited the greatest relative *in vitro* estrogenic activity (4.25 ± 0.06

ng/L) followed by TBO photolysis products (3.43 ± 0.04 ng/L) and 17β-TBOH photolysis products (3.00 ± 0.01 ng/L; Figure A-22).

A.5 Implications

Understanding the fate of TBA metabolites and related products in environmental systems is important because both 17α-TBOH and 17β-TBOH are potent steroid structures that can alter endocrine function and reduce reproductive output in aquatic organisms [22, 25, 39].   However, despite the large mass production and widespread use of TBA in animal agriculture, 17α-TBOH, 17β-TBOH, and TBO are infrequently detected in receiving waters or runoff impacted by animal agriculture. Observations of 0 – 350 ng/L are typically reported, often at detection frequencies of only a few percent of samples and with low median concentrations [16, 91, 121-123, 141]. This data may suggest that a considerable mass of uncharacterized TBA-related transformation products exists in environments affected by animal agriculture utilizing trenbolone. More interestingly, observations of effects consistent with endocrine disruption in receiving waters affected by animal agriculture are commonly reported [25, 120, 142, 143], along with variations in the biological effects of 17β-TBOH on aquatic organisms that cannot be explained by concurrent chemical analysis [91, 142]. Therefore, characterization of novel products arising from environmental steroid transformations may improve the assessment of the potential ecological risks of TBA metabolites. This process is particularly important when transformation products are closely related in structure to parent molecules, as the potential for steroid receptor binding and related biological effects is strongly dependent on structural similarity (*e.g*., conservation of steroidal A-ring, importance of C3 and C17 positions) to parent molecules [139, 144, 145].

Although we certainly cannot address these possibilities in full with this study, we observe several characteristics of TBA metabolites that may suggest potential explanations for some of these data. Most of these characteristics arise from the 4,9,11 triene structure of TBA, unique among steroids, and it is reasonable to expect similarly

unique reactivity and fate of TBA metabolites in the aquatic environment. First, TBA metabolite photoproducts, at least initially, strongly resemble parent compounds and retain many key structural attributes related to steroid function. Conservation of the basic steroid ring structure likely is the most important element with respect to conserving or altering receptor binding and related biological activity, and the initial photo-oxidations are certainly not altering the steroid ring structure. Photoproducts also exhibit shifts in absorption maxima to wavelengths out of the solar spectrum which imply increased environmental persistence of conserved steroidal structures in these products relative to parent molecules. Increasing polarity of photoproducts (as evidenced by decreased chromatographic retention times) also implies reduced partitioning to environmental surfaces and increased transport potential in affected waters.

Second, although we have not been able to confirm any structures with NMR, there are indications that photo-transformation processes may potentially lead to the formation of structural analogs or stereoisomers of the TBA metabolites. For example, although they are very likely minor products, the 7.73 and 7.42 minute photo-products of 17β-TBOH and 17α-TBOH, respectively, are eluting after the observed hydroxy-trenbolone species (*e.g*., ~5 minute retention time) and only ~0.6 min before the parent compounds. The proximity in retention time to parent TBA metabolites may suggest that closely related structural analogs or stereoisomeric products formed. Similarly, the observed product at 10.25 minutes after 17α-TBOH photolysis may be direct evidence for such a transformation to a structural analog with unknown chemical and biological activity. We speculate that structural analogs or stereoisomers potentially have similar chemical and biological characteristics to the parent molecules, with important implications for both environmental fate and ecotoxicology if these uncharacterized products form and are stable in environmental systems. For example, we might expect that structural analogs with retention times substantially different from parent TBA metabolites would yield a "no detect" for samples under typical analytical conditions

although a very closely related compound is actually present (*e.g.*, 10.25 minute 17α-TBOH product). Conversely, structural analogs could elute at nearly identical times to parents, yielding a case of mistaken identity and potential false positive at that retention time for a structure with different chemical behavior and biological activity. For example, our HR-LC-MS/MS analysis of 9,11-delta estradiol, the only commercially available structural analog we could identify, demonstrated that despite its inefficient ionization, 9,11-delta estradiol essentially co-eluted with 17α- and 17β-TBOH while yielding many MS/MS fragments conserved with TBA metabolites, including the diagnostic m/z 133 and 159 fragments. For any analysis employing more efficient ionization techniques, the co-occurrence of these compounds in a sample may have been difficult to resolve under conditions typical for environmental analyses.

Third, the ecotoxicology data, although not extensive, certainly suggests that photoproduct mixtures retain biological activity even after near complete photo-transformation of parents. TBA metabolites are detected in surface waters and CAFO runoff at low-moderate ng/L concentrations and are of concern to aquatic organisms in receiving waters impacted by agricultural runoff [17, 121, 122, 143]. Photo-transformation is likely a major degradation pathway for these compounds in some receiving waters. TBA metabolites themselves (17α-TBOH, 17β-TBOH, and TBO) can alter circulating steroid levels and ovarian composition with reduced primary ovarian follicles and increases in vitellogenic follicles in several species of fish [22, 135, 141]. Key differences in this study are the photoproducts exposures and the use of static exposures (this study) as compared to flow-through systems, which may increase the importance of transformation processes to toxicology assessment. In the current study, only female medaka exposed to 17α-TBOH photoproducts experienced reproductive dysfunction with altered ovarian follicle composition (decreased percentage of primary ovarian follicles and an increase in vitellogenic follicles) and reduced 17β-estradiol levels. We believe these effects likely are due to estrogenic properties of the 17α-TBOH

photoproduct mixture. Interestingly, using the same measure of estrogenicity, 17α-TBOH had the lowest relative estrogenic activity, with 17β-TBOH having greater activity and TBO the greatest activity of the three. These observations indicate that TBA metabolites themselves have very different effects on the adult teleost ovary compared to photoproducts mixtures generated from these parent compounds, though both are bioactive at similar concentrations.

Our results suggest altered ovarian development in fish exposed to 17α-TBOH photolysis products, and while 17β-TBOH and TBO photolysis products do have estrogenic properties and also alter E2 levels, they may not impact reproduction in the same manner. A key characteristic of estrogenic activity in steroids is the presence of an aromatic "A" ring [140, 143]. We speculate that the conjugated 4,9,11 triene system of trenbolone may be effectively structurally poised to develop an aromatic A-ring upon simple shifts in the conjugated π-bond system during transformations, potentially providing a mechanism for conversion of the androgenic TBA parents to estrogenic products. This process might be promoted by abiotic processes such as photo-enolization, which would be expected to yield at least two π-bonds in the TBA metabolite product A-ring. Also, hydroxylation is a common transformation pathway for steroids [142, 144-146] and we speculate that subsequent dehydration reactions also may provide a potential initiating mechanism for A-ring aromatization. Steroids are often prone to acid-catalyzed transformations that give rise to unsaturated derivatives [94]. This behavior is well documented for steroids with an allylic hydroxyl group at the C3 position, for which acid-catalyzed elimination followed by rearrangement can yield 3,5-diene structures [94, 147]. Most relevant to our photoproducts, reports of allylic 10-hydroxy steroids have also been shown to undergo acid-catalyzed dehydration, where rearrangement produces an aromatic A-ring structure [95].

During our experiments, we have on occasion observed unexpectedly high concentrations of parent 17β-TBOH and 17α-TBOH in samples collected after periods of

irradiation that, based on our prior reports of rates for direct photolysis, should have eliminated nearly all (>99%) of the parent mass. We propose that some phototransformation pathways are reversible for TBA metabolites, particularly if photogenerated hydroxy steroids are prone to dehydration reactions. Indeed, we have found that decreasing the pH of our photoproduct mixtures to pH 2 results in the near-immediate formation of a secondary product that co-elutes with the parent TBA metabolites and absorbs at the characteristic 350 nm wavelength for the 4,9,11triene system. This result is consistent, therefore, with acid-catalyzed dehydration of hydroxyl photoproducts regenerating the TBA metabolite from which they were produced or possible stereoisomers of the TBA metabolite. While detailed follow up studies supporting this observation will be presented elsewhere, it is clear to us that abiotic regeneration of parent TBA metabolites or similar structures from primary photoproducts does occur under certain conditions. Further studies to evaluate the mechanisms and implications of potential product to parent reversion, particularly at circumneutral pH, are ongoing.

In any case, the observations of closely related photoproducts, including potential structural analogs or stereoisomers, and estrogenic attributes of products suggest the presence of novel transformations and unique reactivities of the TBA metabolite family. Although our existing data is limited, and often well beyond the original scope of our environmental fate studies, effectively understanding the environmental fate and ecological implications of this class of anabolic steroids, widely used in animal agriculture, should consider some of these transformation mechanisms. A key element of all of these studies is a focus upon the stability of the parent TBA metabolites and any structurally similar products because their potential ecological significance will be strongly dependent on their environmental persistence.

Table A-2. Observed photoproducts of 17α-TBOH, 17β-TBOH, and TBO.

Proposed Product	Retention Time[min]	Product Ion	Mass	Comment
17α-TBOH parent	*8.31*	*[M+H]⁺*	*271.1685*	
10-hydroxy-17α-trenbolone	4.91	[M+H-H₂O]⁺	271.1684	proposed structure by analogy to confirmed 17β-TBOH products
12-hydroxy-17α-trenbolone	6.20	[M+H-H₂O]⁺	271.1685	proposed structure by analogy to confirmed 17β-TBOH products
unknown	7.42	likely [M+H]⁺	271.1684	potential stereoisomer or structural analog of 17α-TBOH
unknown	10.25	likely [M+H]⁺	271.1685	likely stereoisomer or structural analog of 17α-TBOH
unknown	3.34, 3.74, 3.98	[M+H]⁺	303.1581	poorly resolved group of potential dialdehyde or dihydroxy products of unresolved structure
trihydroxy-17α-trenbolone	3.71	[M+H]⁺	321.1687	potential 10,11,12 trihydroxy product, but other hydroxylation sites also possible
trihydroxy-17α-trenbolone	4.75	[M+H]⁺	321.1687	dominant trihydroxy product
17β-TBOH parent	*8.07*	*[M+H]⁺*	*271.1685*	
10-hydroxy-17β-trenbolone	4.93	[M+H-H₂O]⁺	271.1685	proposed structure. Less stable, decays to secondary products quickly
12-hydroxy-17β-trenbolone	5.55	[M+H-H₂O]⁺	271.1685	NMR confirmed. Dominant product.
hydroxy-17β-trenbolone?	7.73	[M+H-H₂O]⁺	271.1685	Potential hydroxy-trenbolone product or 17β-TBOH structural analog.
Presumed dialdehyde or dihydroxy products	3.03, 3.36, 3.70, and others	[M+H]⁺	303.1583	poorly resolved group of potential dialdehyde or dihydroxy products of unresolved structure. NMR confirmed 11,12 dialdehyde present.
10,12-dihydroxy-17β-trenbolone	2.90	[M+H]⁺	305.1739	NMR confirmed 10,12 dihydroxy structure.
trihydroxy-17β-trenbolone	3.57	[M+H]⁺	321.1688	dominant trihydroxy product
trihydroxy-17β-trenbolone	4.01	[M+H]⁺	321.1688	trihydroxy product of unresolved structure

Table A-3. Continued

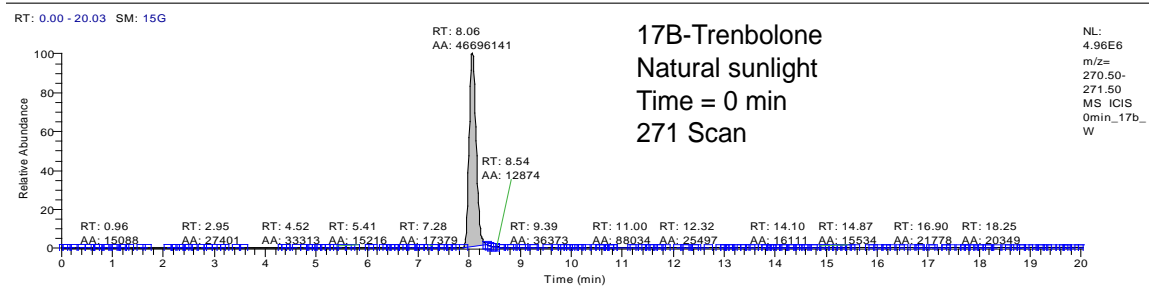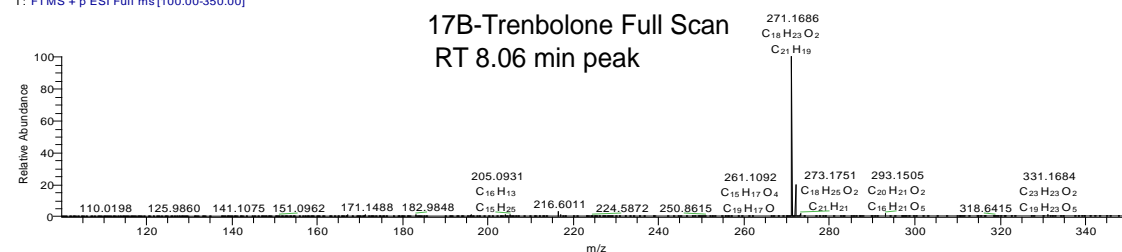| *TBO parent*	*9.54*	*[M+H]$^+$*	*269.1528*	
10-hydroxy-trendione	6.10	[M+H-H$_2$O]$^+$	269.1528	proposed structure by analogy to confirmed 17β-TBOH products
12-hydroxy-17β-trenbolone	6.47	[M+H-H$_2$O]$^+$	269.1528	dominant product. Proposed structure by analogy to confirmed 17β-TBOH products
dialdehyde or dihydroxy	3.29	[M+H]$^+$	303.1582	observed product
trihydroxy-trendione	3.34	[M+H]$^+$	319.1531	potential 10,11,12 trihydroxy product, but other hydroxylation sites also possible
trihydroxy-trendione	4.04	[M+H]$^+$	319.1532	potential 10,11,12 trihydroxy product, but other hydroxylation sites also possible. Dominant trihydroxy product.
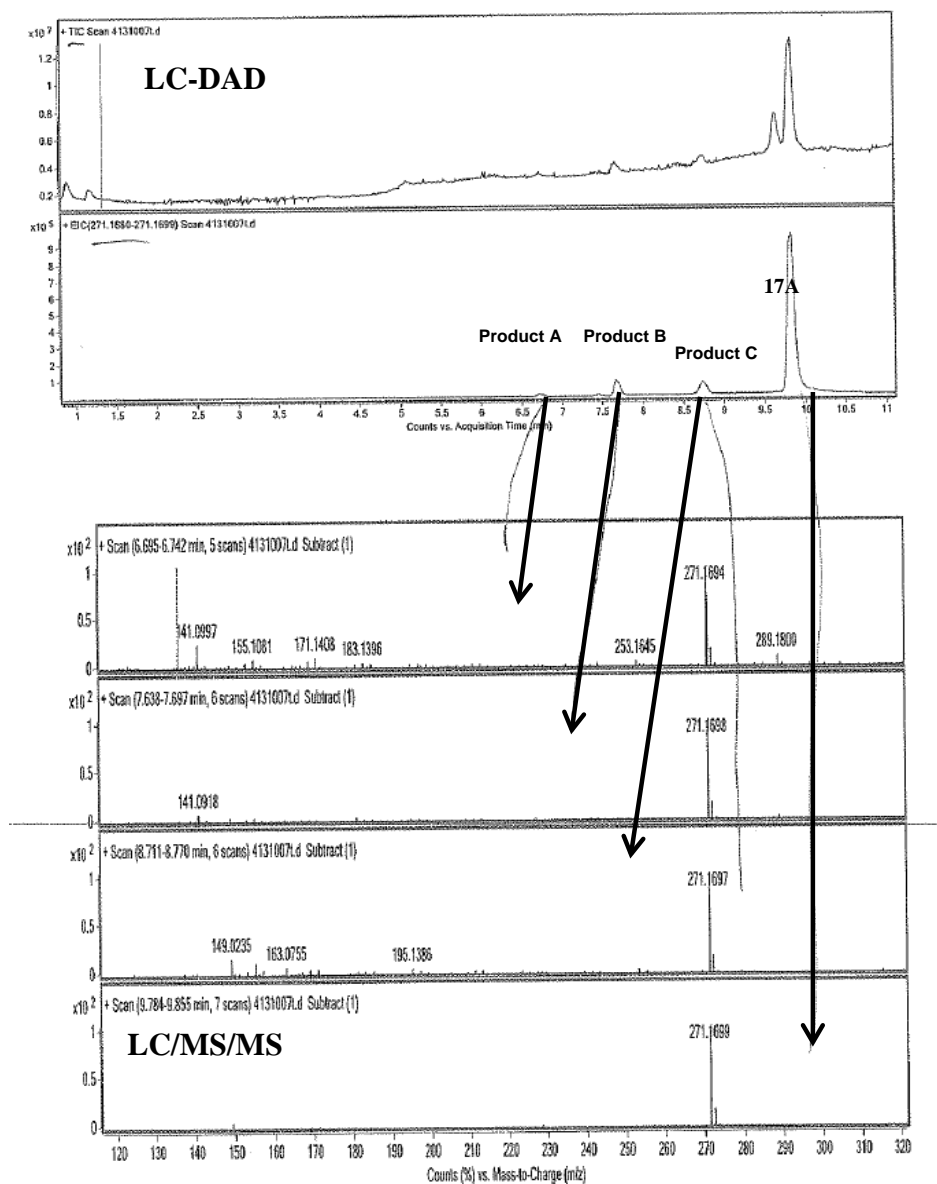
Figure A-4. LC-DAD and LC/MS/MS (not the high resolution Orbitrap instrument) analysis of 17α-trenbolone and photoproducts after irradiation. Note the slight m/z 289 peaks observed for the first two products. These m/z 289 peaks were not observed in the Orbitrap HR-LC/MS/MS analysis, leading us to conclude that we observed $[M+H-H_2O]^+$ ions with the Orbitrap.

Figure A-5. Initial 17β-TBOH parent chromatogram, full scan spectra, and MS/MS spectra prior to initiating the photolysis experiment.

Figure A-6. Observed 17β-TBOH product chromatogram, full scan spectra, and MS/MS spectra after 120 minutes of irradiation. Monohydroxy product peaks ($[M+H-H_2O]^+$ ions) are observed at 4.93, 5.54, and 7.69 minutes, with the dominant 12-hydroxy product at 5.54 minutes. Note the similar full scan and MS/MS scans observed for these products as compared to 17β-TBOH in Figure A-5 and Figure A-1.

Figure A-7. Observed 17β-TBOH product chromatogram, full scan spectra, and MS/MS spectra after 120 minutes of irradiation. The poorly resolved m/z 303 peaks observed at 3-4 minute retention times likely represent secondary and tertiary dialdehyde or dihydroxy products.

Figure A-8. Observed 17β-TBOH product chromatogram, full scan spectra, and MS/MS spectra after 120 minutes of irradiation. Based on the results of the NMR analysis, we propose that the m/z 305 peak at 2.90 minutes represents 10,12-dihydroxy-trenbolone.

RT: 0.00 - 20.01 SM: 15G

RT: 3.57
AA: 3801626

**17B-Trenbolone
Natural sunlight
Time = 120 min
321 Scan**

NL:
5.71E5
m/z=
320.50-
321.50
MS ICIS
120min_17
b_W

RT: 0.17
AA: 10467

RT: 1.23   RT: 3.06   RT: 4.01   RT: 5.51   RT: 7.24   RT: 8.32   RT: 10.05 RT: 11.35 RT: 12.72   RT: 14.64   RT: 16.60 RT: 17.49   RT: 19.52
AA: 10351   AA: 58285 AA: 298638   AA: 48594 AA: 25439 AA: 6854 AA: 17495 AA: 13358 AA: 33858   AA: 30055   AA: 29398 AA: 9105   AA: 21272

Time (min)

120min_17b_W #394 RT: 3.56 AV: 1 SB: 15 4.45-5.10 SM: 7B NL: 1.83E6
T: FTMS + p ESI Full ms[100.00-350.00]

**17B-Trenbolone Full Scan
RT 3.57 min peak**

321.1688
$C_{18} H_{25} O_5$
$C_{22} H_{25} O_2$

315.0857
$C_{24} H_{11} O$
$C_{21} H_{15} O_3$

129.4741 141.3003   154.9898 167.0673   184.5559 191.5696   212.0826 $C_{16} H_{13} O$ 221.0879   241.6011   249.5873   275.0887 285.1478   303.1584
$C_{15} H_{16} O$ $C_{15} H_{25} O$ $C_{15} H_{15} O_5$ $C_{18} H_{21} O_3$ $C_{18} H_{23} O_4$
$C_{19} H_{15} O_2$ $C_{21} H_{17} O$ $C_{22} H_{23} O$

m/z

120min_17b_W #397 RT: 3.57 AV: 1 NL: 1.22E5
T: ITMS + c ESI d Full ms2 321.17@cid35.00 [75.00-335.00]

x2

**17B-Trenbolone MS2 Scan
m/z 321 parent
RT = 3.57 min peak**

304.2597
$C_{19} H_{28} O_3$
$C_{22} H_{24} O$

131.2334   147.2204 159.2309   175.1830   197.2276   211.2344   239.1802   248.3180 267.1774 275.1700 286.2744   305.3419
$C_{15} H_{15} O$ $C_{15} H_{27} O_2$ $C_{17} H_{19} O$ $C_{17} H_{28} O$ $C_{16} H_{27} O_3$ $C_{20} H_{19} O$ $C_{15} H_{26} O_5$ $C_{19} H_{29} O_3$
$C_{17} H_{23} O_3$ $C_{19} H_{26} O_2$

m/z

Figure A-9. Observed 17β-TBOH product chromatogram, full scan spectra, and MS/MS spectra after 120 minutes of irradiation. The m/z 321 peaks at 3.57 and 4.01 minutes are trihydroxy-trenbolone species of unresolved structure.

Figure A-10. Initial 17α-TBOH parent chromatogram, full scan spectra, and MS/MS spectra prior to initiating the photolysis experiment.
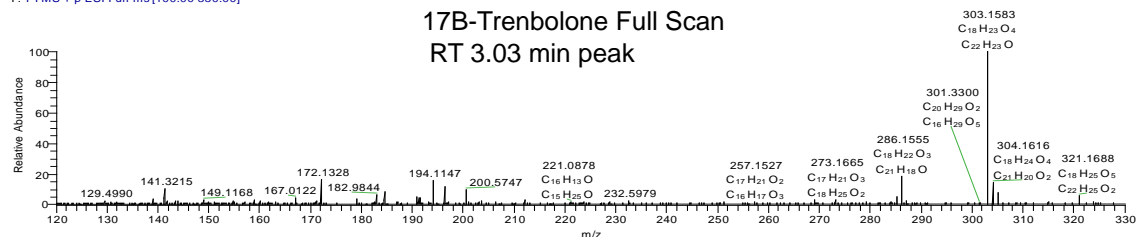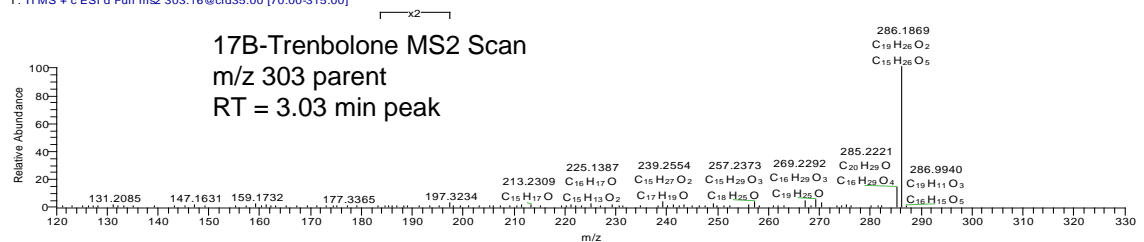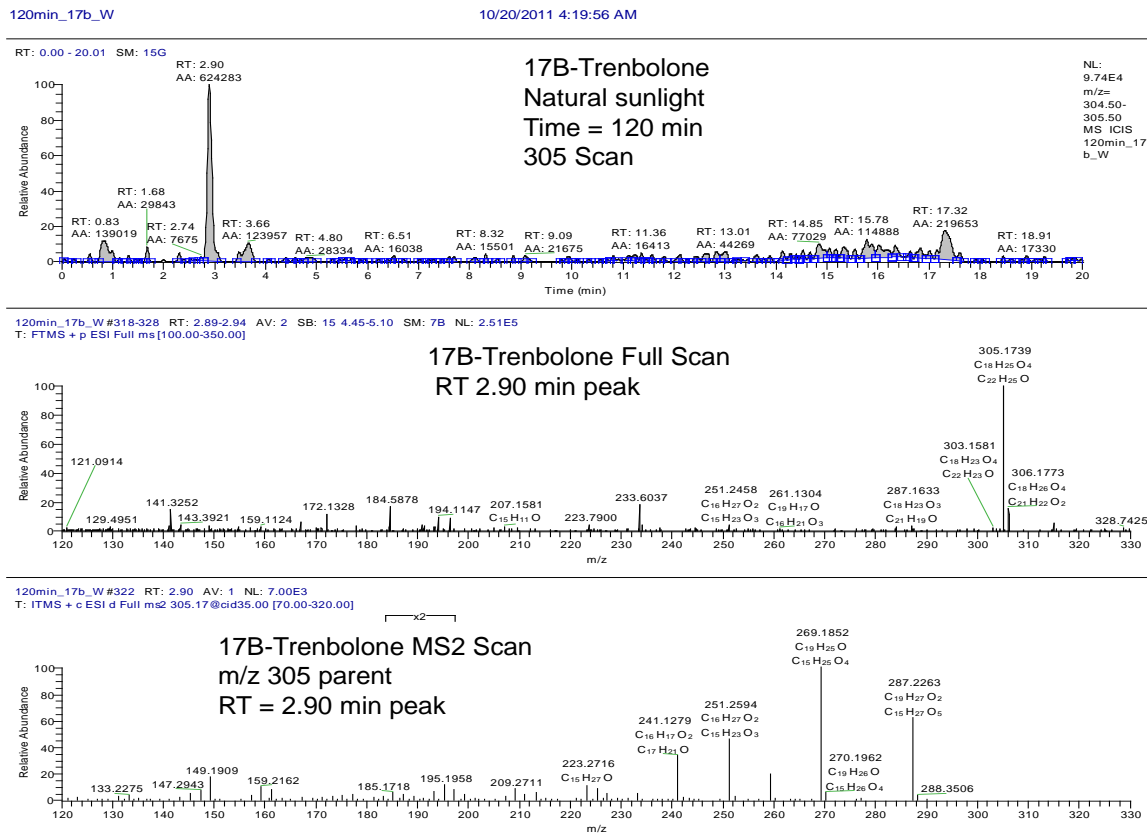
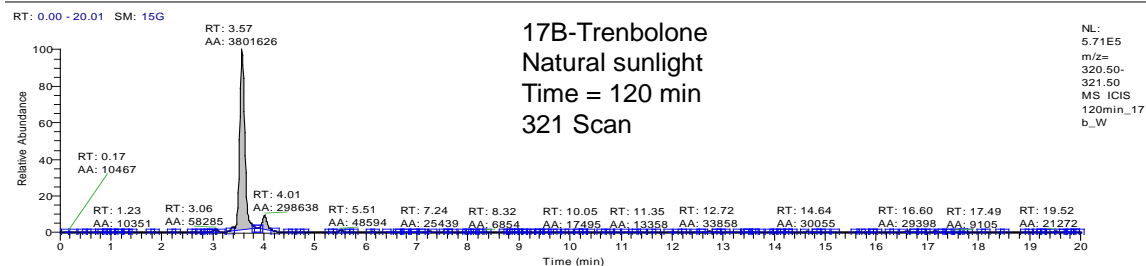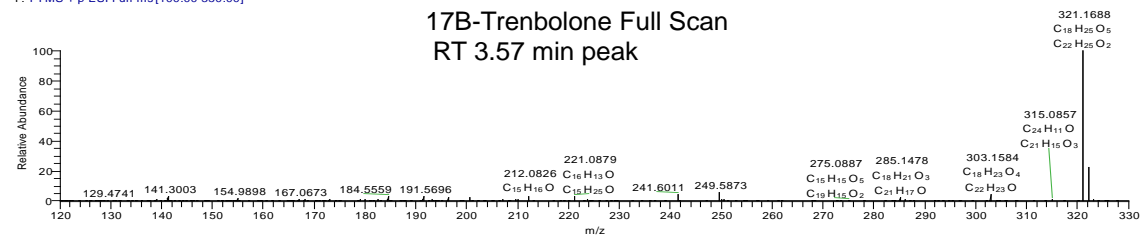**Figure A-11.** Observed 17α-TBOH product chromatogram, full scan spectra, and MS/MS spectra after 120 minutes of irradiation for the m/z 271 peak at 4.91 minutes. Monohydroxy product peaks ([M+H-H2O]+ ions) are observed at 4.91, 6.20, and possibly 7.42 minutes. By analogy with 17β-TBOH products, we propose that the 6.20 minute peak is the dominant 12-hydroxy product, with the 10-hydroxy product at 4.91 minutes.

Figure A-12. Observed 17α-TBOH product chromatogram, full scan spectra, and MS/MS spectra after 120 minutes of irradiation for the dominant m/z 271 peak at 6.20 minutes.
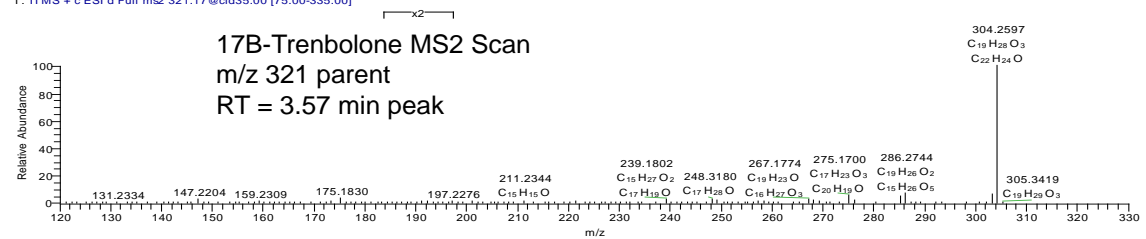
Figure A-13. Observed 17α-TBOH product chromatogram, full scan spectra, and MS/MS spectra after 120 minutes of irradiation for the m/z 271 peak at 7.42 minutes. Due to its proximity to the 17α-TBOH parent at 8.31 minutes, this may represent a [M+H]$^+$ ion of a 17α-TBOH stereoisomer or structural analog, although it could also be a [M+H-H$_2$O]$^+$ ion of another uncharacterized hydroxy-trenbolone product.
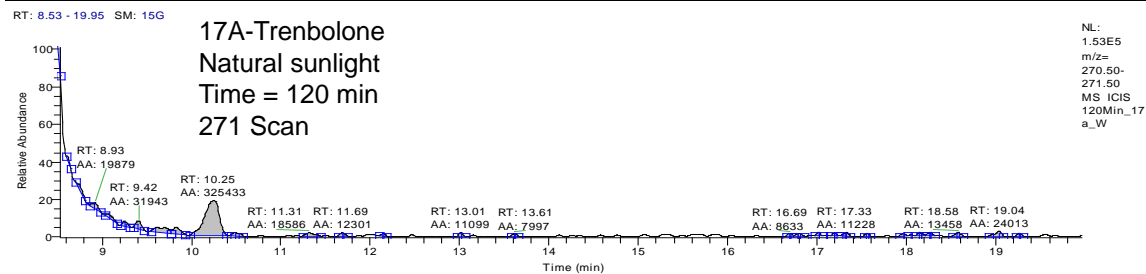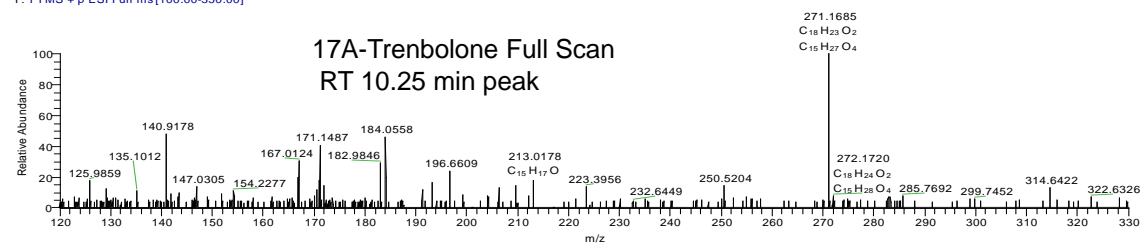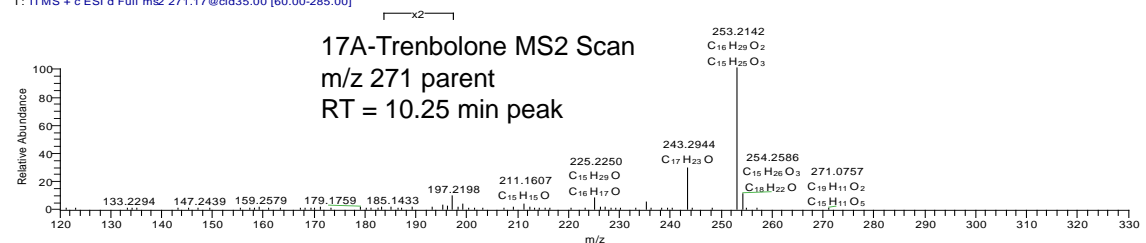
Figure A-14. Observed 17α-TBOH product chromatogram, full scan spectra, and MS/MS spectra after 120 minutes of irradiation for the m/z 271 peak at 10.25 minutes. Due to its much later retention time, suggesting decreased polarity relative to the parent 17α-TBOH at 8.31 minutes retention time, we suggest that this product is likely a structural analog or stereoisomer of 17α-TBOH. However, the structure of this product has not been isolated and further characterized.
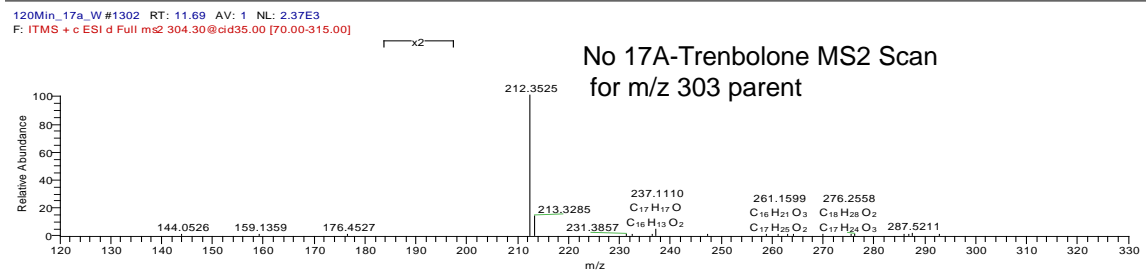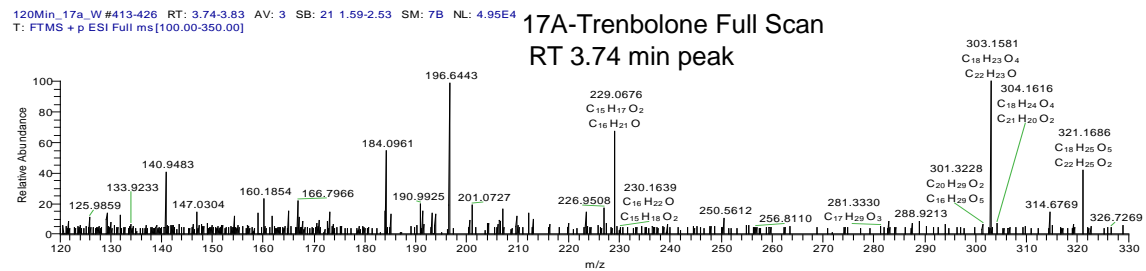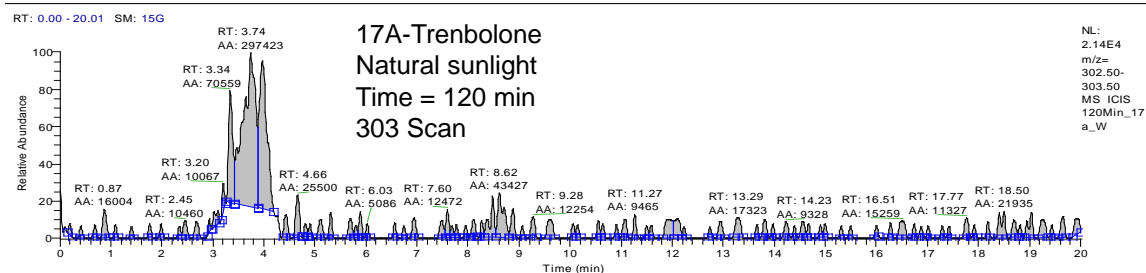
Figure A-15. Observed 17α-TBOH product chromatogram and full scan spectra after 120 minutes of irradiation for the poorly resolved m/z 303 peaks observed at 3-4 minute retention times. As for 17β-TBOH, these peaks likely represent secondary and tertiary dialdehyde or dihydroxy products. No MS/MS spectra were collected for these particular products.
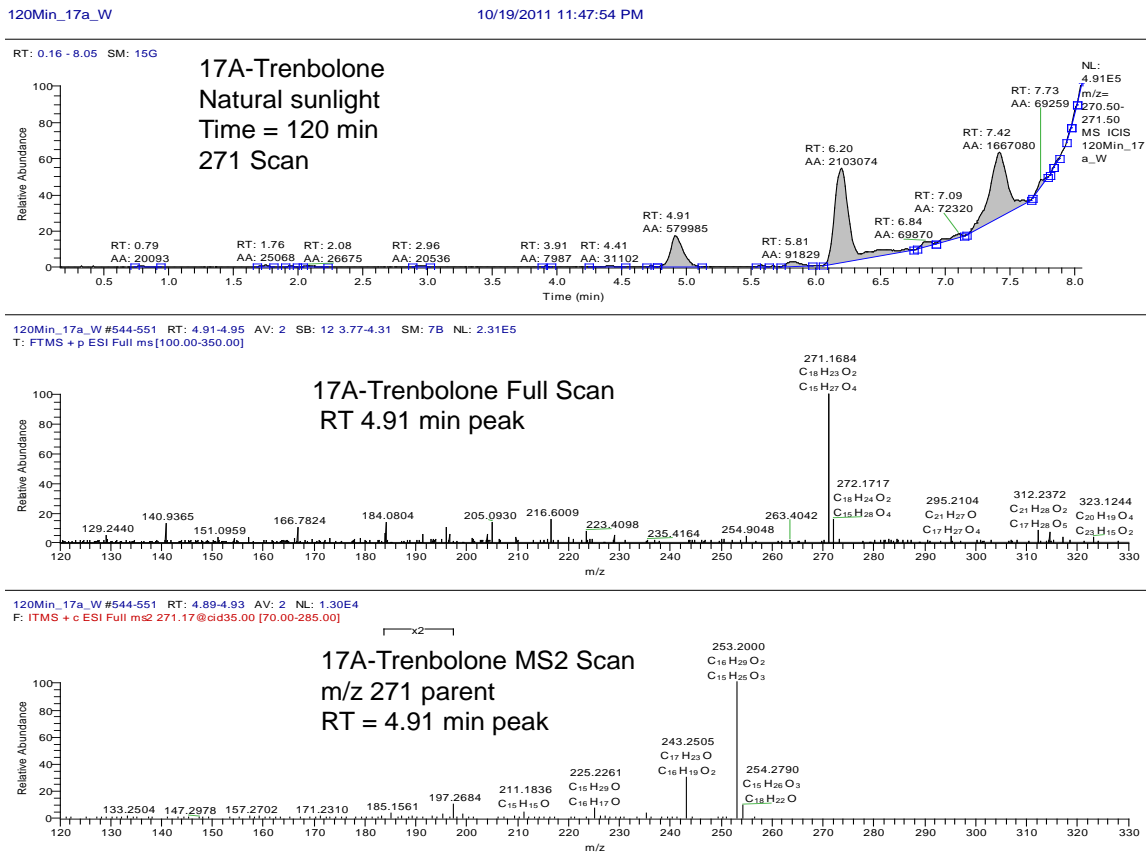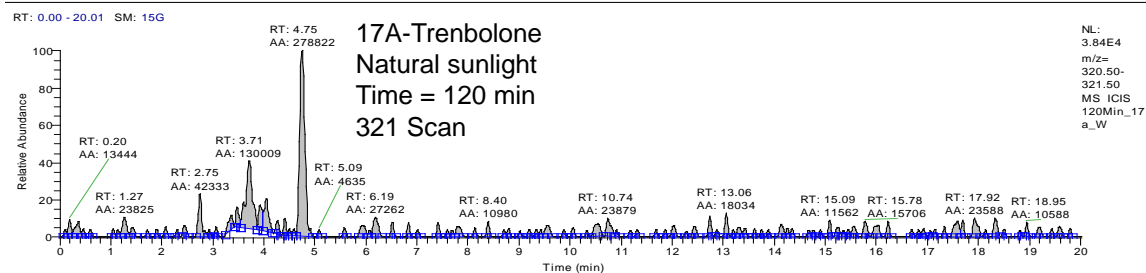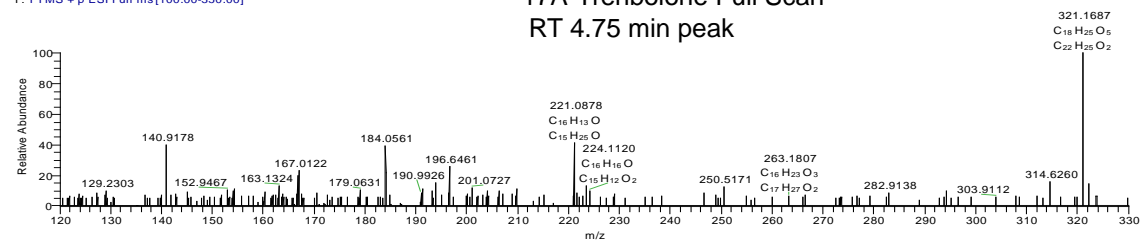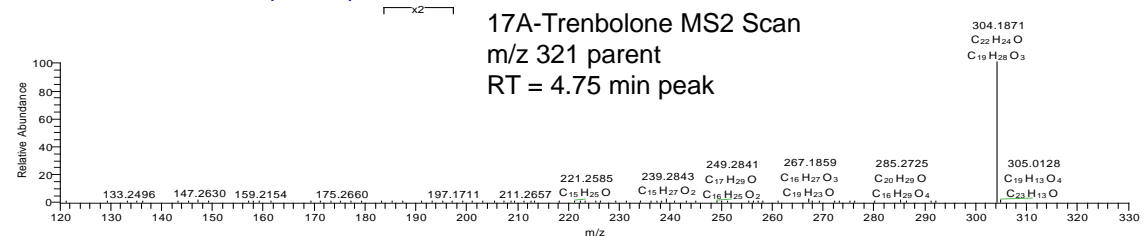
Figure A-16. Observed 17α-TBOH product chromatogram, full scan spectra, and MS/MS spectra after 120 minutes of irradiation. The m/z 321 peaks at 3.71 and 4.75 minutes are trihydroxy-trenbolone products of unresolved structure.

Figure A-17. Initial TBO parent chromatogram, full scan spectra, and MS/MS spectra prior to initiating the photolysis experiment.
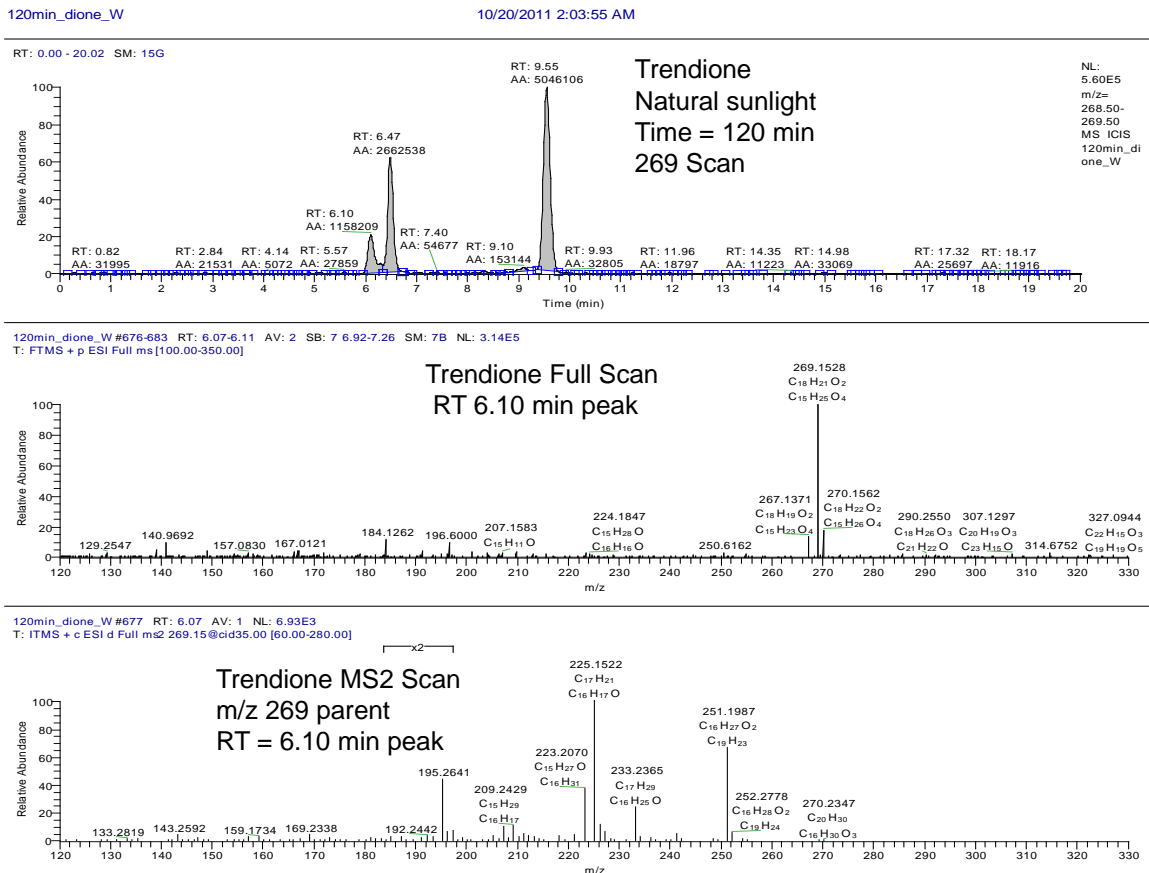
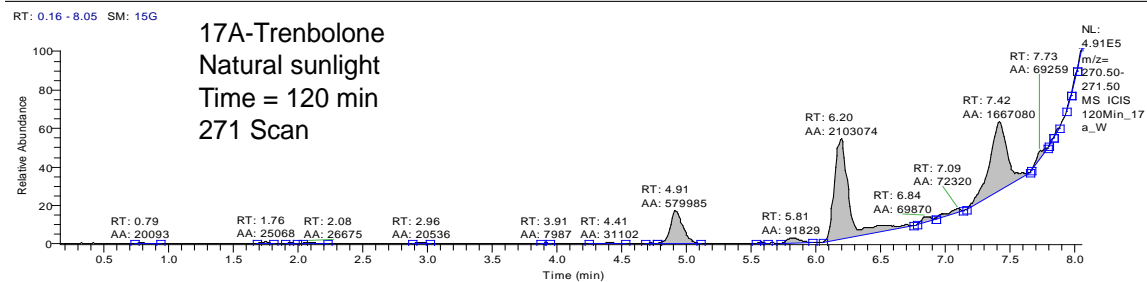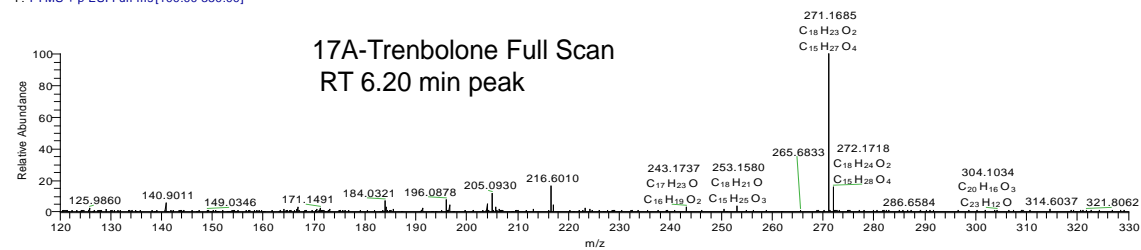**Figure A-18.** Observed TBO product chromatogram, full scan spectra, and MS/MS spectra after 120 minutes of irradiation for the m/z 269 peak at 6.10 minutes. Monohydroxy product peaks ($[M+H-H_2O]^+$ ions) are observed at 6.10 and 6.47 minutes. By analogy with 17β-TBOH products, we propose that the 6.47 minute peak is the dominant 12-hydroxy product for TBO, with the 10-hydroxy product at 6.10 minutes.
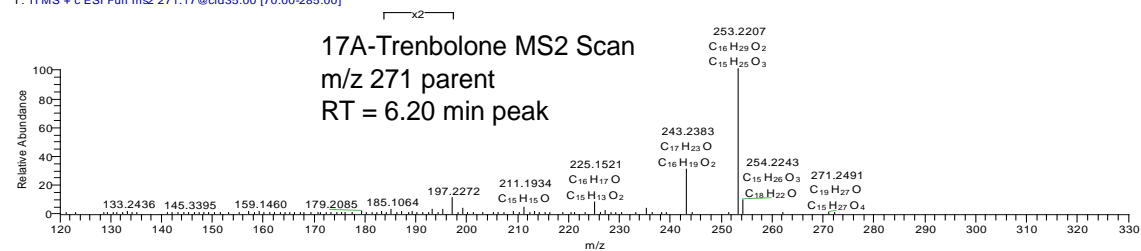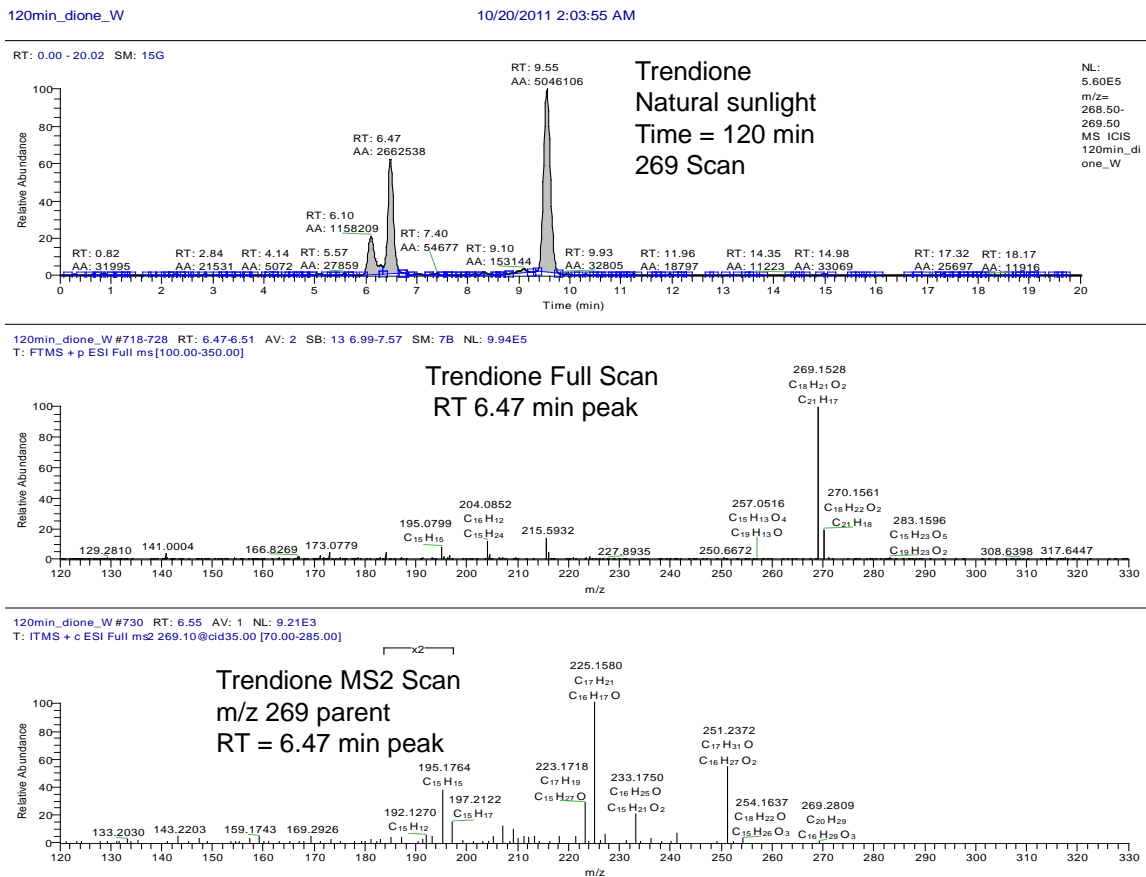
Figure A-19. Observed TBO product chromatogram, full scan spectra, and MS/MS spectra after 120 minutes of irradiation for the dominant m/z 269 peak at 6.47 minutes. This is the dominant TBO photoproduct.
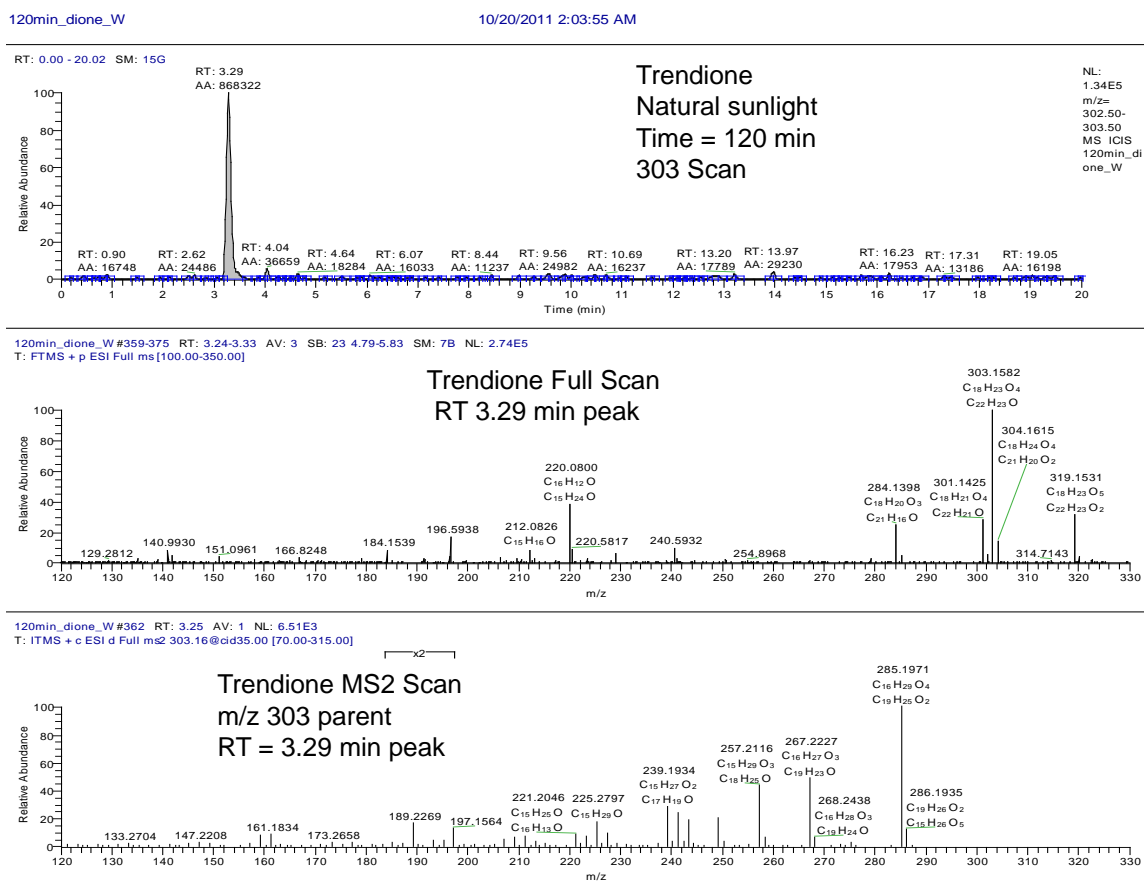
Figure A-20. Observed TBO product chromatogram and full scan spectra after 120 minutes of irradiation for the m/z 303 peak observed at 3.29 minutes. As for 17β-TBOH and 17α-TBOH, this peak likely represents secondary or tertiary dialdehyde or dihydroxy products.
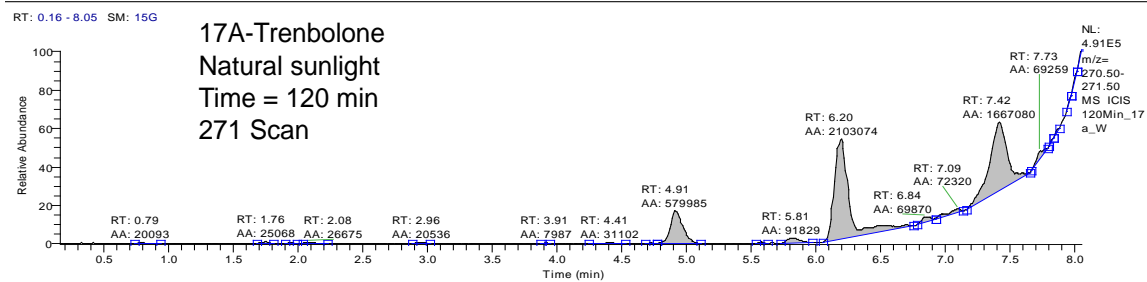
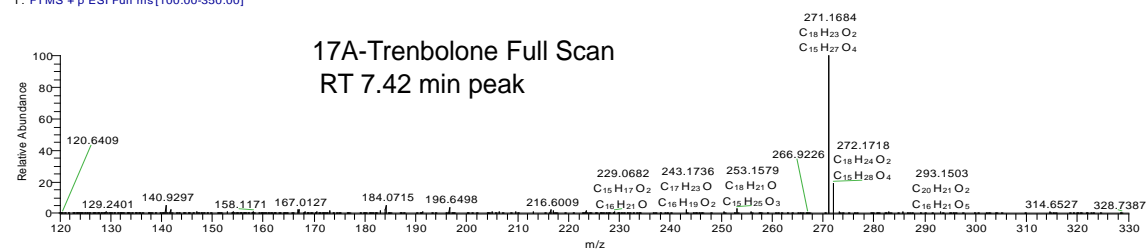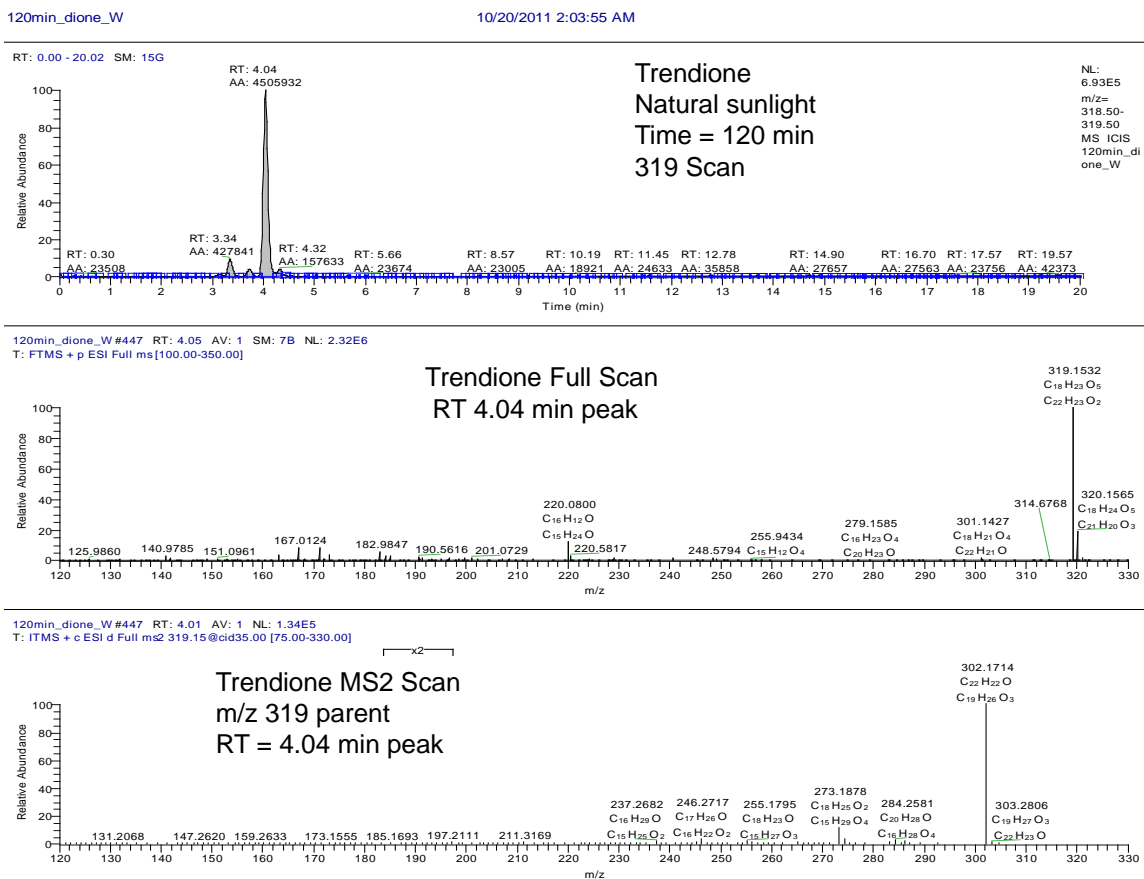**Figure A-21.** Observed TBO product chromatogram, full scan spectra, and MS/MS spectra after 120 minutes of irradiation. The m/z 319 peaks at 3.24 and 4.04 minutes are trihydroxy-trendione products of unresolved structure.
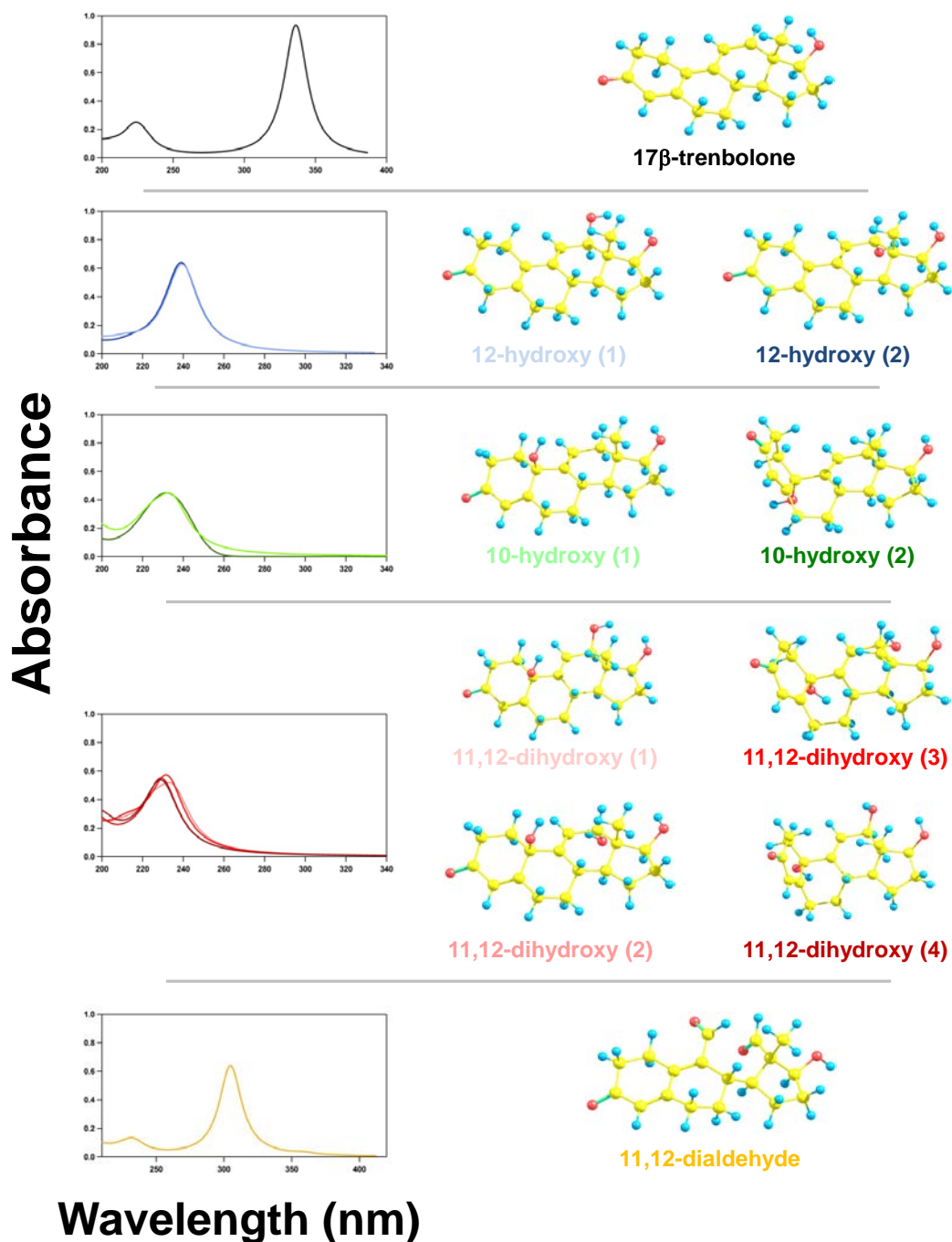
Figure A-22. Calculated UV/vis absorbance scans for photoproducts of 17β-trenbolone. Spectra are shown for all possible stereoisomers, and the optimized structures from computational chemistry calculations are provided. Aside from the 11,12-dialdehyde product, all photoproducts possessed similar absorbance spectra. This prevented us from definitively distinguishing whether the two major products detected with LC-DAD were diastereomers of 12-hydroxy or a mixture of 12- and 10-hydroxy species.

17B-Trenbolone*
Chemical Formula: $C_{18}H_{22}O_2$
Exact Mass: 270.16198
Molecular Weight: 270.36608

10-hydroxy-TBOH
Chemical Formula: $C_{18}H_{24}O_3$
Exact Mass: 288.17254
Molecular Weight: 288.38136

12-hydroxy-TBOH*
Chemical Formula: $C_{18}H_{24}O_3$
Exact Mass: 288.17254
Molecular Weight: 288.38136

10,12-dihydroxy-TBOH*
Chemical Formula: $C_{18}H_{24}O_4$
Exact Mass: 304.16746
Molecular Weight: 304.38076

11,12-dihydroxy-TBOH
Chemical Formula: $C_{18}H_{24}O_4$
Exact Mass: 304.16746
Molecular Weight: 304.38076

10,11,12-trihydroxy-TBOH
Chemical Formula: $C_{18}H_{24}O_5$
Exact Mass: 320.16237
Molecular Weight: 320.38016

11,12-dialdehyde-TBOH*
Chemical Formula: $C_{18}H_{22}O_4$
Exact Mass: 302.15181
Molecular Weight: 302.36488

Figure A-23. Proposed 17β-TBOH phototransformation pathway. Though product stereoisomers are not shown, most products have several diastereomeric or epimeric forms possible. Products marked with an asterisk were structurally confirmed by NMR, although without stereochemical resolution. We propose analogous transformation pathways for 17α-TBOH and TBO phototransformation.
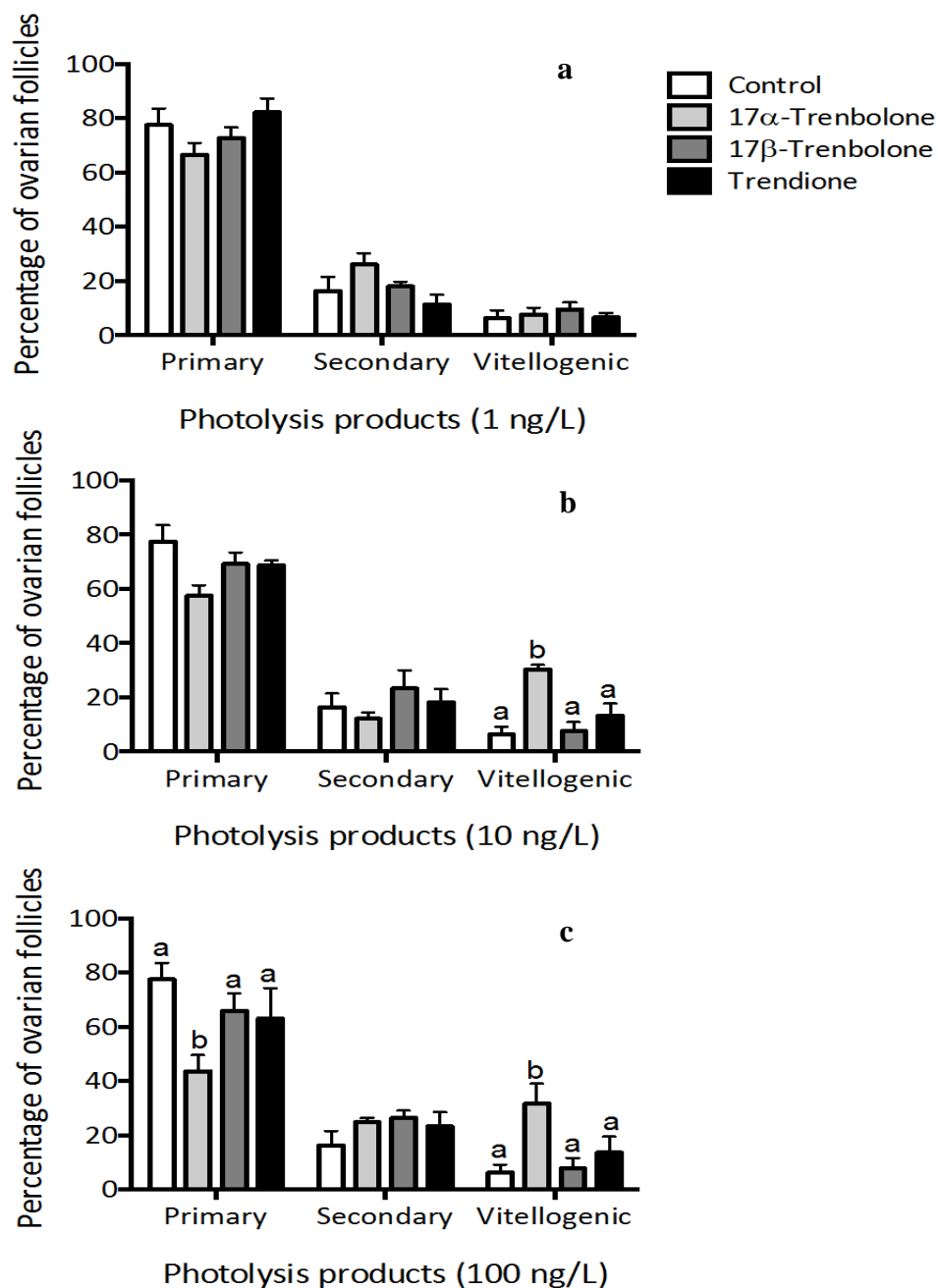
Figure A-24. Percentage of ovarian follicle stages (primary, secondary, and vitellogenic stage follicles) of Japanese medaka after 14-day exposure to TBA metabolite photoproducts at different concentrations: A. 1 ng/L ($p > 0.05$); B. 10 ng/L ($p = 0.008$); and C. 100 ng/L ($p = 0.0018$). Data are shown as mean ± S.E.M.; different letters indicate significant differences.
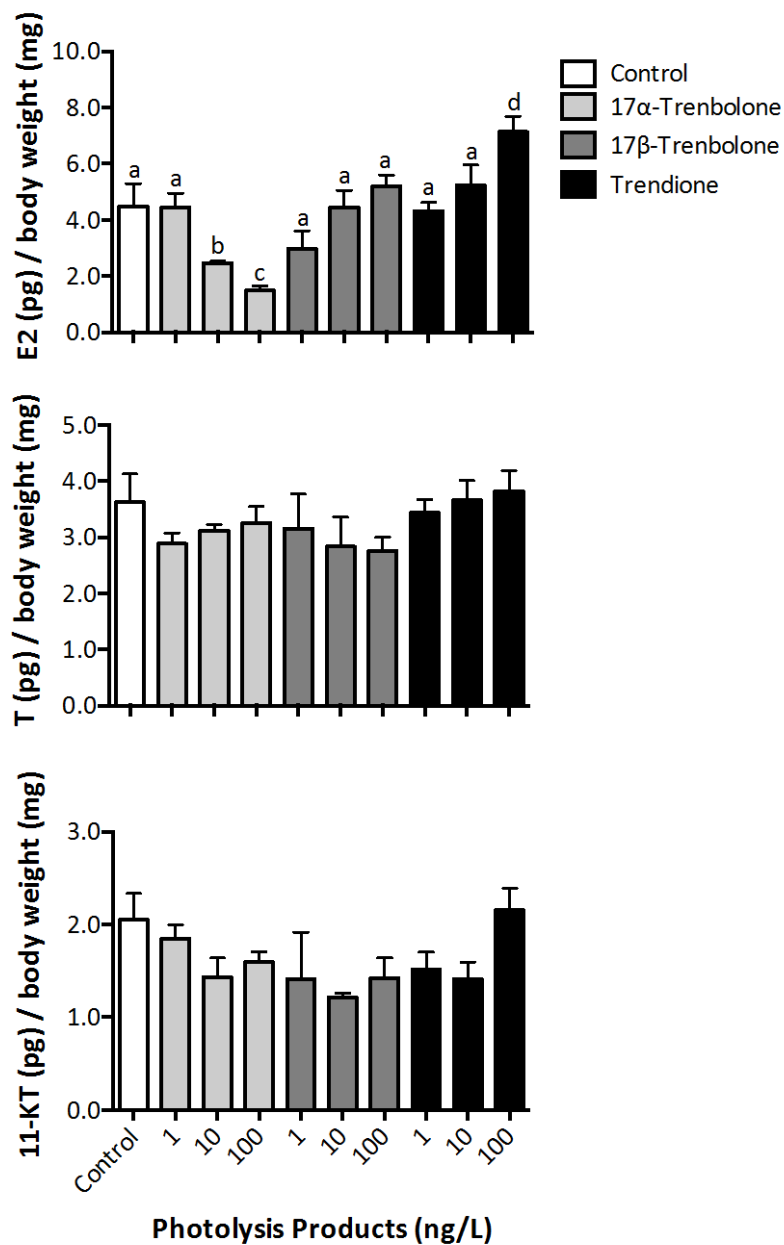
Figure A-25. Sex steroid levels of Japanese medaka exposed to TBA metabolite photoproduct mixtures for 14 days. A. 17β-Estradiol (E2; $p < 0.0001$), B. Testosterone (T; $p = 0.4920$), and C. 11-ketotestosterone (11-KT; $p = 0.1755$). Data are shown as mean ± S.E.M.; different letters indicate significant differences.
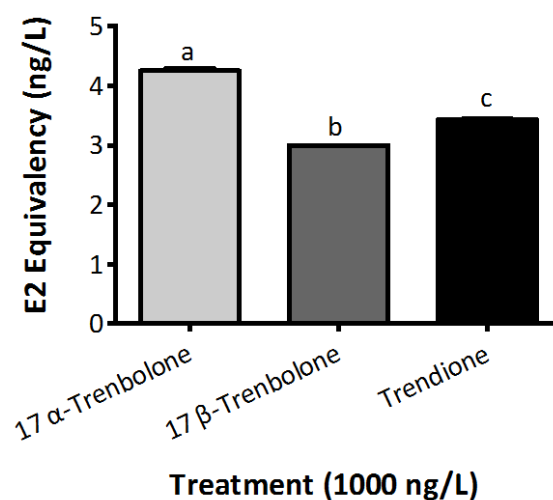
Figure A-26. *In vitro* vitellogenin mRNA in rainbow trout hepatocytes after exposure to TBA metabolite photoproducts as a measure of mixture estrogenicity (ng/L; $p < 0.0001$). Data are shown as mean ± S.E.M.; different letters indicate significant differences. Also, the estrogenicity of 17α-TBOH and 17β-TBOH photoproduct mixtures were also significantly different from 17α-TBOH and 17β-TBOH parents. *In vitro* vitellogenin mRNA in rainbow trout hepatocytes after exposure to TBA metabolite photoproducts as a measure of mixture estrogenicity (ng/L; $p < 0.0001$). Data are shown as mean ± S.E.M.; different letters indicate significant differences. Also, the estrogenicity of 17α-TBOH and 17β-TBOH photoproduct mixtures were also significantly different from 17α-TBOH and 17β-TBOH parents.

APPENDIX B. INFLUENCE OF ORGANIC SURFACE COATINGS
ON THE SORPTION OF THE ANTICONVULSANTS PHENYTOIN
AND CARBAMAZEPINE ON MINERAL SURFACES

B.1   Abstract

Here, we explore the role that sorption to mineral surfaces plays in the fate of two commonly encountered effluent-derived pharmaceuticals, the anticonvulsants phenytoin and carbamazepine. Adsorption isotherms and pH-edge experiments are consistent with electrostatics governing anticonvulsant uptake on metal oxides typically found in soil and aquifer material (e.g., Si, Al, Fe, Mn, and Ti). Appreciable, albeit limited, adsorption was observed only for phenytoin, which is anionic above pH 8.4, on the iron oxides hematite and ferriydrite. Adsorption increased substantially in the presence of cationic and anionic surfactants, species also commonly encountered in wastewater effluent. For carbamazepine, the enhanced uptake results entirely from organic interactions with the hydrophobic tails of surfactant surface coatings. For phenytoin, adsorption also arises from the ability of surfactants to alter the net charge of the mineral surface and thereby further enhance favorable electrostatic interactions with its anionic form. Collectively, our results demonstrate that although pristine mineral surfaces are likely not major sinks for most pharmaceuticals and personal care products (PPCPs) in the environment, their alteration with organic matter, particularly surfactants, can considerably increase their ability to retain PPCPs in subsurface systems.

B.2   Introduction

Sorption (herein encompassing both adsorption and absorption) on soil, sediments and suspended colloids in surface waters represents a potential natural sink for some pharmaceuticals and personal care products (PPCPs) [148-150]. While the sorption of moderate to strongly hydrophobic PPCPs on organic matter and biosolids has been

extensively investigated [151-154], inorganic phases (e.g., aluminosilicate clays and iron (oxyhydr)oxides) may be of equal or greater importance for certain PPCP classes in natural systems. These inorganic phases tend to be more polar, exhibiting surface charge from the acid-base character of their surface hydroxyl groups [155, 156]. Accordingly, they will interact with moderately polar PPCPs exhibiting low octanol-water partitioning coefficients $(K_{ow}$ values) [151], PPCPs possessing hydrogen-bonding functionalities, and PPCPs with ionizable moieties that allow for pH-dependent electrostatic interactions. For example, common veterinary antimicrobials (e.g., ciprofloxacin and tetracycline) sorb on clays (e.g., Kaolin and Ca-montmorillonite) at environmentally relevant pH [148, 157-159], driven largely by pathways independent of hydrophobicity including cation exchange, surface complexation and hydrogen bonding [159].

Although the role of clay minerals as sorbents for ionizable PPCPs is relatively well established, the sorption capacity exhibited by other naturally occurring inorganic phases has received less focus. For example, iron and aluminum oxides are typically present as high surface area coatings on grains in soil and sediment [160, 161], and exhibit both positive and negative charges at environmentally relevant pH values due to their high zero-point of charge relative to other metal oxides. Moreover, the influence of accumulated organic matter on the sorption capacity of such mineral surfaces must also not be overlooked [162], especially as PPCPs often enter the environment via wastewater effluent with relatively high organic loads. In effluent-impacted systems, both natural [111, 163] and anthropogenic (e.g., surfactants) forms of organic matter [164] will sorb to mineral surfaces. Such surface coatings, particularly surfactants, can alter not only the extent but also the mechanism of PPCP uptake by altering the chemical character of the mineral-water interface.

In a noteworthy study by Hari et al. [165], sorption of the uncharged PPCPs acetaminophen and carbamazepine on Canadian River alluvium only occurred in the presence of cationic (CPC) and nonionic surfactants (NP9), behavior attributed to

increased hydrophobic interactions between PPCPs and adsorbed surfactant layers. Notably, however, more complex sorption behavior was observed in their study with nalidixic acid, an anionic, quinolone antibiotic. A four-fold enhancement in nalidixic acid, sorption was only observed in the presence of the cationic surfactant and at high pH. The authors attributed this behavior to the formation of ion pairs between the cationic surfactant and the deprotonated form of nalidixic acid that in turn reduced the solubility of nalidixic acid and promoted adsorption. In a subsequent study, Kibbey et al [166] also suggested that the enhanced sorption of cationic propranolol on the same Canadian River alluvium and a model feldspar in the presence of an anionic surfactant (SBDS) resulted from ion-pair formation.

In this work, we investigate the ability of various metal oxide mineral surfaces to function as sorbents for PPCPs, and the influence that natural and anthropogenic forms of organic matter exert on their activity as sorbents. Batch kinetic and equilibrium sorption experiments were conducted over a range of pH values with six metal oxides including the iron (oxyhydr)oxides hematite (α-Fe_2O_3), goethite (α-FeOOH) and the amorphous phase ferrihydrite, an aluminum oxide (γ-Al_2O_3), titanium dioxide (TiO_2) and silica dioxide (SiO_2), all of which represent naturally occurring phases present in soil, sediments and suspended colloids. The sorption capacity of these metal oxides was investigated both in the absence and presence of model forms of organic matter including a humic acid (Fluka humic acid), a cationic surfactant (CPC) and an anionic surfactant (SBDS). Our use of pure oxide phases rather that more complex soil mixtures will allow us to establish the relative contribution of each phase to PPCP sorption in natural systems.

The PPCPs investigated are the prescription anticonvulsants phenytoin and carbamazepine, which are among the most recalcitrant to traditional wastewater treatment and thus are likely to be discharged in effluent [167, 168]. In addition to their practical significance as persistent PPCPs, phenytoin and carabamzepine provide a unique juxtaposition of physicochemical properties ideal for probing the mechanisms of uptake

in metal oxide systems. Whereas carbamazepine is neutrally charged over environmentally relevant pH values, phenytoin possesses an ionizable functionality (pKa 8.3; [169]) to facilitate electrostatic interactions with surfaces in slightly basic waters. When neutrally charged, however, the reported K_{ow} values for phenytoin is comparable to carbamazepine (2.47 and 2.48, respectively; [170, 171]). Under such conditions, therefeore, we expect that both should display comparable uptake in organic matter-containing mineral systems if hydrophobic interactions drive their uptake. In each of the aforementioned metal oxide systems, the extent and reversibility of phenytoin and carbamazepine sorption were investigated as a function of pH, PPCP initial concentration, and organic matter concentration.

B.3   Experimental Methods

Reagent List

Phenytoin (5,5-Diphenyhydantation; 99%; Sigma Aldrich) and carbamazepine (99%; Sigma Aldrich) were used as received, and stock solutions of each compound were prepared in methanol (HPLC grade; Fisher). Organic buffers used in sorption experiments included MOPS (>99.5%; Sigma-Aldrich), Trizma hydrochloride (reagent grade, Sigma-Aldrich), MES (≥99%; Sigma-Aldrich) and HEPES (>99.5%; Sigma-Aldrich). Iron oxides were synthesized from solutions of ferric nitrate nonahydrate (Fisher; certified ACS) and sodium bicarbonate (Fisher, ACS grade). Organic matter used in sorption experiments included the cationic surfactant cetylpyridinium chloride (CPC; Sigma-Aldrich, 99+%), the anionic surfactant sodium dodecylbenzene sulfonate (SDBS; 99+%; ACS reagent grade), and Fluka humic acid (FHA). All aqueous solutions were prepared in deionized water (Milipore, Q-Grad 2). Solvents used for HPLC analysis of phenytoin and carbamzepine included methanol (HPLC grade; Fisher), acetone (HPLC grade; Fisher), acetonitrile (HPLC grade; Fisher) and a phosphate buffer prepared from potassium phosphate monobasic (ACS certified grade; Fisher).

Sorbent Materials and Characterization

Six different metal oxides were used in sorption experiments. These included three

nanoscale iron oxides hematite (α-Fe$_2$O$_3$),goethite (α-FeOOH), and ferrihydrite, all of

which were synthesized using standard methods[160, 172]. The identity of all synthetic

iron oxides was verified via comparison of X-ray diffraction (XRD) patterns to accepted

standards [160]. The sorption capacity of commercially available forms of micron-sized

silica dioxide particles (SiO$_2$; Sigma-Aldrich), an alumina nanopowder (α-Al$_2$O$_3$; Sigma-

Aldrich), and a titanium oxide nanopowder (TiO$_2$; Sigma-Aldrich) were also investigated.

The specific surface area of all sorbents was quantified with N$_2$-BET adsorption

isotherm measurements on a Micromeritics Accelerated Surface Area and Porosimetry

System 2010. The nanoscale iron oxides of hematite (100 m^2/g), goethite (110 m^2/g) and

ferrihydrite (250 m^2/g) exhibited the greatest specific surface areas relative to the

commercially available alumina (25 m^2/g) and titanium dioxide (anatase; vendor reported

50 m^2/g) nanopowders and the silica dioxide particles (7 m^2/g).   As electrostatic

interactions were expected to influence anticonvulsant sorption, the zeta potential, which

is the average potential in an imaginary surface (surface of shear) that is considered to lie

close to the solid surface, and within which the fluid is stationary during an electrokinetic

process [173], of each sorbent suspension was measured as a function of pH (from pH 6.8

to 8.2). Suspensions of each metal oxide (0.5-5 g/L) were prepared and allowed to

equilibrate overnight prior to analysis. Approximately 1.5 mL of well-mixed suspension

was transferred to 3 mL microcuvette for analysis using a ZetaPals zeta potential analyzer

(Brookhaven Instruments).

Sorption Experiments

Sorption experiments were conducted in suspensions of each metal oxide, as well

as in suspensions containing each metal oxide in the presence of different forms of

organic matter (i.e., CPC, SDBS and FHA). The entire suspension was centrifuged after 2

h sorption experiment and certain amount of the supernatant (1-2.5 ml) was analyzed for aqueous phase concentration and replaced by fresh buffer. The entire suspension was allowed to react for additional 2 h at which the aqueous phase concentration was analyzed. In both types of systems, anitconvulsant sorption was examined as a function of the initial anticonvulsant concentration (i.e., sorption isotherms) and as a function of the suspension pH (i.e., pH-edge experiments). Select kinetic experiments examined the rate of sorption so as to establish the timescale necessary to achieve equilibrium in our experimental systems.

For sorption experiments conducted in the absence of organic matter, sorption isotherms and pH-edge experiments used a metal oxide loading of either 5 or 10 g/L. Sorption isotherms were collected at a several pH values between 6 and 8.5 while varying the initial anticonvulsant concentration between 1-18 mg/L (~10-60 µM). For pH-edge experiments, a fixed anticonvulsant concentration (typically 15 mg/L) was employed while varying the suspension pH from 5 to 8.5 with an appropriate 25 mM organic buffer (MES for pH 5 and 6, HEPES for pH 7 and 7.5, and Tris for pH 8 and 8.5) in 25 mM NaCl to poise system ionic strength. Prior to addition of phenytoin or carbamazepine, each solid phase was equilibrated with the appropriate buffer solution for approximately 0.5 h, and if pH drift was observed a strong acid (1 M HCl) or base (1 M NaOH) was used to return the pH to the desired value.

Sorption isotherms and pH-edge experiments were also conducted as a function of CPC and SDBS concentration (5-200 µM or ~1.5-70 mg/L), as well as FHA concentration (1-50 mg/L). Relatively high organic matter concentrations, which for CPC and SDBS approached reported critical micelle concentrations (CMCs), were intentionally explored so as to better mimic systems impacted by extensive exposure to effluent organic matter. Otherwise, experimental conditions and protocols in systems containing organic matter were identical to those described above for pure metal oxide suspensions. Notably, preliminary experiments revealed that the rate an extent of

anticonvulsant sorption were not influenced by the order of organic matter and anticonvulsant addition to the to the metal oxide suspension. Thus, for the majority of the experiments, the organic matter was added to the pre-equilibrated buffer suspension prior to anticonvulsant addition.

To initiate all sorption experiments, a small volume (~ 6-60 µL) of methanolic stock solution was delivered via syringe into 6 mL of pH-equilibrated suspension to produce the desired initial concentration of anticonvulsant. Experiments were conducted in 10 mL vials that were crimp-sealed with butyl rubber plug septa. Once assembled, these vials were covered by aluminum foil to avoid light and placed on an apparatus that mixed the reactors end-over-end at 60 RPM. After 2 hours, which kinetic experiments revealed was sufficient to achieve equilibrium, the vials were removed from the rotator and 1 mL of suspension was withdrawn for analysis. To remove the solid phase, aqueous samples were transferred to plastic microcentrifuge tubes and centrifuged for 5 minutes at 10,000 RPM on a Eppendorf Microcentrifuge. Centrifugation was necessary as significant loss of phenytoin and carbamazpine was observed when 0.2 µM syringe-driven filters (either nylon or Teflon) were used to remove the sorbent, presumably due to sorption on the filter media.

After centrifugation, a volume of aqueous supernatant was transferred to a 2.5 mL amber autosampler vial for HPLC analysis (described below) to quantify the phenytoin and carbamazepine remaining in solution after sorption. The amount of anticonvulsant sorbed to the metal oxide was then determined from the difference between the aqueous concentration of pharmaceutical at equilibrium and the initial concentration present in the system, which was determined from a series of control reactors prepared simultaneously without sorbent. The control reactors without sorbent also allowed us to monitor the stability of phenytoin and carbamazepine in our experimental systems over time; in all controls, these compounds were stable without any measurable loss.

The reversibility of anticonvulsant sorption was explored via additional sorption isotherm experiments with phenytoin. After sorption equilibrium was achieved (after 2 h), the solid phase and associated phenytoin were separated from solution via centrifugation, at which time a portion of the supernatant was replaced with fresh buffer to disrupt disequilibrium. After the resuspended sorbent particles were mixed for an additional 2 h, additional aqueous samples were collected and analyzed to construct the desorption isotherm.

Finally, experiments also were conducted to measure sorption of organic matter on each metal oxide in the absence of pharmaceuticals. Procedures for these experiments were identical to that described above for anticonvulsant sorption. After sample collection and centrifugation, the extent of surfactant uptake was quantified through analysis of supernatants using a Shimadzu 5050 total organic carbon (TOC) analyzer. Humic acid sorption was quantified via analysis of supernatants with both TOC and UV_{254} analysis.

<center>Analytical Methods</center>

Analysis of phenytoin and carabamezpine was performed on an Agilent 1200 series HPLC equipped with photodiode array detector and an Agilent Eclipse XDB-C18 5 µm column (4.6 cm $\times$ 150 mm). Samples were analyzed at a flow rate of 1 mL/min with a mobile phase of 10 mM phosphate buffer/methanol/acetonitrile/acetone in a ratio of 55/22/12/11 by volume that was adjusted manually to pH 7 [174]. The HPLC method utilized an injection volume was 10 µl and detection wavelength of 210 nm. Aqueous surfactant concentrations were determined using a Shimadzu 5050 TOC analyzer. To avoid contributions to TOC analysis from buffers, data presented were collected in suspensions without buffers whose pH was maintained at a constant value manually via acid or base addition. Aqueous FHA concentrations were analyzed via UV254 analysis on a Genesys UV-Vis equipment from Thermo Fisher. FHA standard solutions were prepared by diluting certain amount of stock solution in buffers to achieve various

concentrations (5-50 mg/L) and the corresponding absorbance was subsequently measured on UV-Vis at 254 nm to obtain a calibration curve.

B.4   Results and Discussion

Anticonvulsant Sorption on Pristine Metal Oxide Surfaces

Ferrihydrite and hematite were the only active sorbents toward phenytoin, both exhibiting maximum uptake near pH 7.5-8 (Figure B-1). On these iron oxide surfaces, uptake was rapid, with kinetic studies suggesting equilibrium was achieved by the first sampling point (~10 min).   Even at the maximum in pH-edge experiments, sorption was modest at best; maximum adsorbed concentrations of phenytoin on ferrihydrite and hematite represent only ~10-15% of the total phenytoin mass in the systems.

Observed trends in pH-dependent adsorption suggest that electrostatic interactions play an important role in promoting phenytoin adsorption on hematite and ferrihydrite surfaces. Based on its reported pKa value, phenytoin exhibits appreciable anionic character at and above pH 8.3, which will in turn interact favorably with positive and neutrally charged surfaces sites on ferrihydrite and hematite (pH$_{zpc}$ of 6.8 and 8.2, respectively; [160]). Zeta potential measurements (Figure B-2) support such a scenario, as the net surface change on ferrihydrite and hematite is positive to near-neutral up to approximately pH 7.5-8, corresponding with the pH range where maximum phenytoin uptake was measured. Notably, adsorption of carbamazepine, which lacks ionizable functional groups, was not measurable on any sorbent across the pH range.

While favorable electrostatics likely contribute to phenytoin adsorption, they may not be the only controlling factor. Notably, zeta potential measurements indicate similar positive to near-neutral surface charges on goethite and aluminum oxide up to roughly pH 8, even though no phenytoin adsorption was observed in these metal oxide systems. The result with aluminum oxide may in part be rationalized by the difference in its specific surface area (26 m^2/g) relative to hematite (100 m^2/g) and ferrihydrite (250 m^2/g).

However, this explanation fails to account for the lack of uptake on goethite, which has a specific surface area (110 m^2/g) comparable to that of hematite. Therefore, specific interactions such as hydrogen bonding, rather than simple charge considerations, may also play a role in phenytoin uptake on pristine metal oxides.
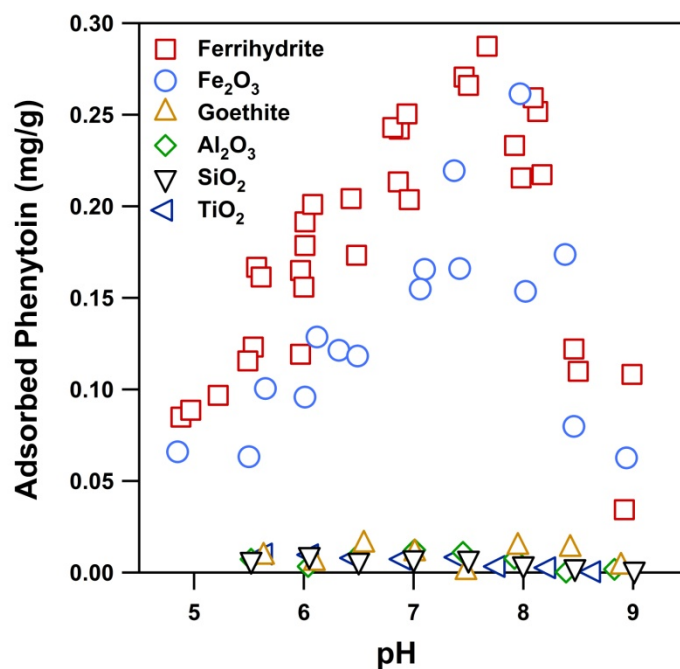
Figure B-1. Adsorption of phenytoin as a function of pH in metal oxide suspensions. Experiments were conducted with a solid loading of either 5 or 10 g/L and an initial phenytoin concentration of 15 mg/L. Solutions contained 25 mM of an appropriate pH buffer and 25 mM NaCl. Data for ferrihydrite and hematite represent results of replicate experiments, which were conducted at least in duplicate. No adsorption of carbamazepine was observed in similar pH-edge experiments with pristine metal oxides.
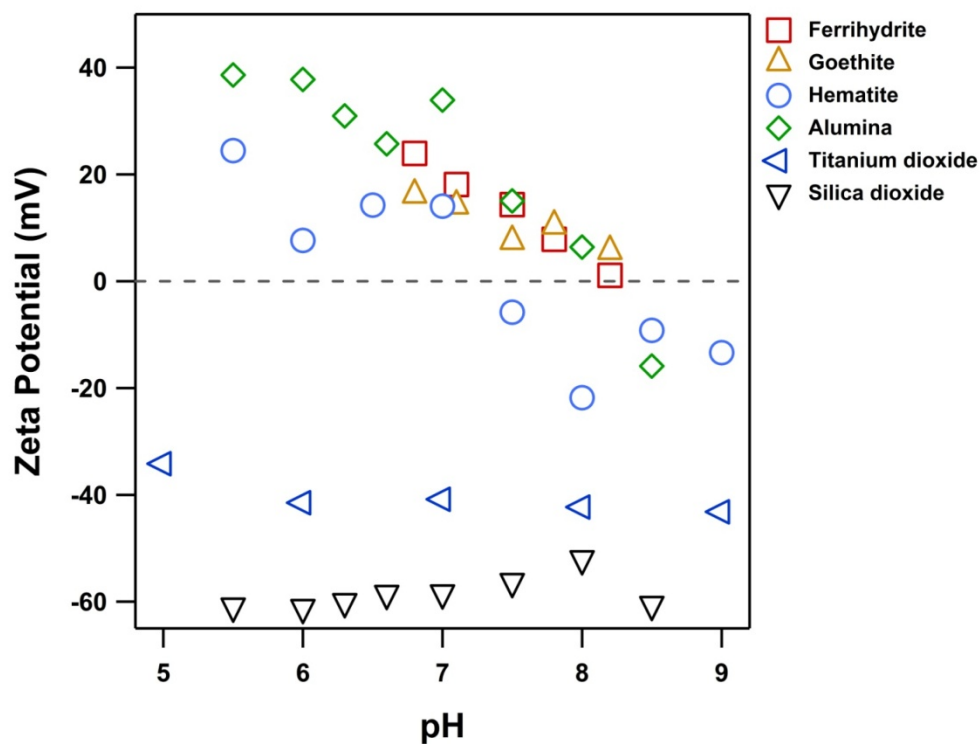
Figure B-2. Zeta potential values as a function of pH for metal oxide suspensions considered herein. MES was used to maintain pH at 5-6.5, HEPEs was used to maintain pH at 7-7.5 and Trizma was used to maintain pH at 8-9. To achieve the absorbance of 0.3-0.35 at 546 nm for the requirement of zeta potential measurement, the solid loading used for ferrihydrite, goethite, hematite, alumina, titanium dioxide and silica dioxide were 0.5 g/L, 0.3 g/L, 0.5 g/L, 0.2 g/L, 0.2 g/L and 0.15 g/L, respectively.

Additional experiments with ferrihydrite and hematite revealed approximately linear isotherms for phenytoin sorption in both suspensions. Using the Freundlich model to describe adsorption ($C_{sorb} = K_f C_{aq}^{1/n}$; Figure B-3a), model fits from non-linear regression analysis were statistically indistinguishable from unity at the 95% confidence interval. Notably, phenytoin adsorption on ferrihydrite and hematite was completely reversible (Figure B-3b), suggesting relatively weak binding interactions. The reversible behavior is also consistent with either long-range electrostatic interactions or relatively weak specific interactions (e.g., hydrogen bonding) being primarily responsible for phenytoin uptake in these systems.

<div align="center">Influence of Natural Organic Matter on</div>

<div align="center">Anticonvulsant Sorption on Metal Oxides</div>

Sorption isotherms with ferrihydrite and hematite were subsequently conducted in the presence of Fluka Humic Acid (FHA). Over a wide range of FHA concentrations (up to 50 mg/L), no influence on phenytoin sorption was observed (Figure B-4). Studies in the absence of phenytoin indicated that essentially all of the FHA was adsorbed on ferrihydrite and hematite under the experimental conditions employed (pH 7.5-8.0, 5 g/L iron oxide), resulting in surface concentrations up to 10 mg FHA/g iron oxide. Thus, coatings of FHA on ferrihydrite and hematite play neither an inhibitory (e.g., steric blocking) nor a promoting (e.g. hydrophobic partitioning into the FHA coating) role in phenytoin sorption. As with pristine metal oxide, sorption of carbamazepine was not measurable in FHA-coated ferrihydrite and hematite systems.
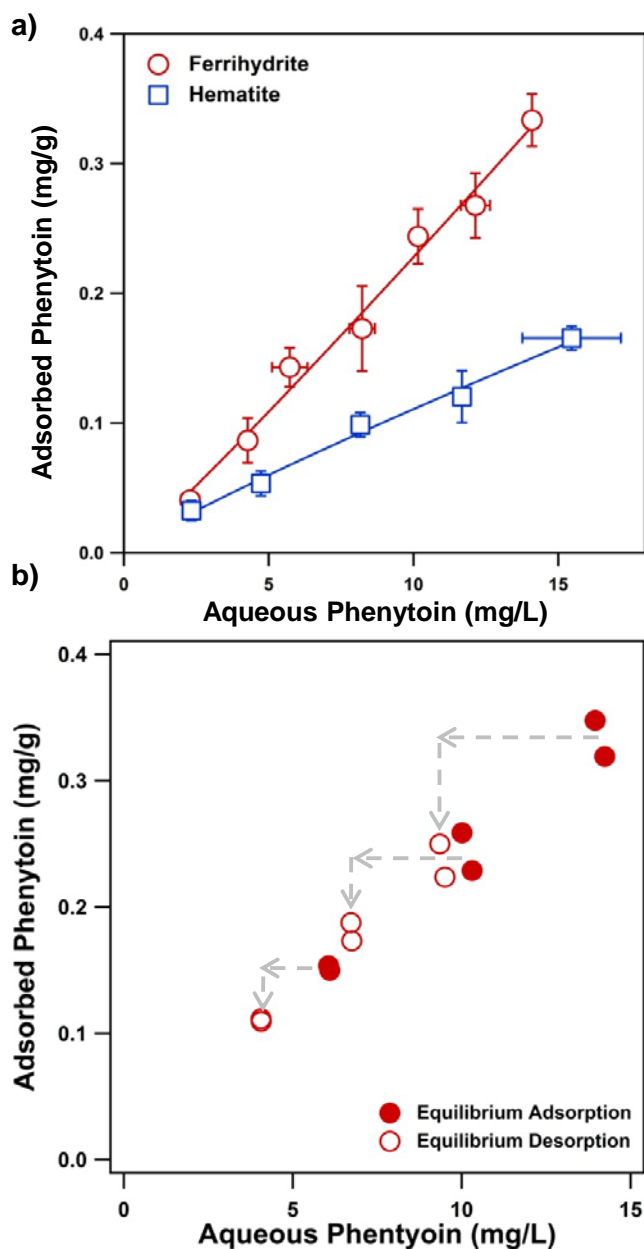
Figure B-3. (a) Adsorption isotherms for phenytoin in ferrihydrite and hematite suspensions. Lines represent Freundlich model fits for sorption isotherms (equations from non-linear regression analysis are shown). Uncertainty represents standard deviation of at least triplicate measurements. (b) Equilibrium adsorption and desorption isotherms for phenytoin in ferrihydrite suspensions. After 2 h of adsorption equilibrium, ferrihydrite solids and associated phenytoin were recovered and resuspended while replacing 2 mL of the supernatant with fresh buffer to introduce disequilibrium. After 2 h, additional aqueous samples were collected and analyzed to construct the desorption isotherm. Results of duplicate experiments are shown. All isotherm experiments were conducted with a solid loading of 10 g/L and initial phenytoin concentrations ranging between 2.5-18 mg/L. Solutions contained 25 mM of HEPES buffer and 25 mM NaCl at pH 7.5.
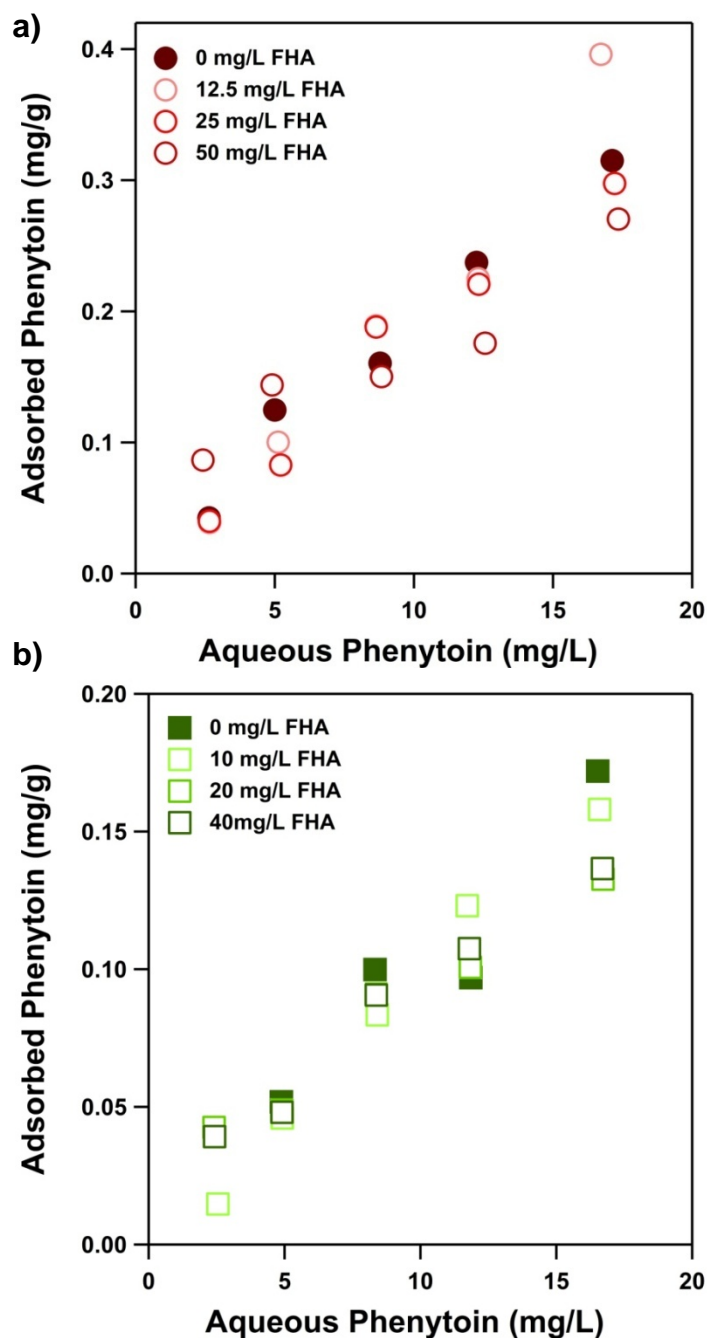
Figure B-4. Adsorption isotherms for phenytoin in (a) ferrihydrite and (b) hematite suspensions in the presence and absence of Fluka humic acid (FHA) as a model natural organic matter. Data are shown for a range of FHA concentrations. Experiments were conducted with a solid loading of 5 g/L and initial phenytoin concentrations ranging between 2.5-18 mg/L. Solutions contained 25 mM of HEPES buffer and 25 mM NaCl at pH 7.5 for ferrihydrite and pH 8 for hematite suspensions.

Influence of Cationic and Anionic Surfactants on

Anticonvulsant Sorption: Ferrihydrite and Hematite

In contrast to FHA, cationic (CPC) and anionic (SDBS) surfactants considerably enhanced phenytoin sorption on ferrihydrite and hematite. Sorption isotherms for phenytoin in CPC- and SDBS-containing ferrihydrite suspensions are shown in Figure B-5. Data were collected at pH 6 for experiments with anionic SDBS (Figure B-2a) and pH 8.5 for cationic CPC (Figure B-2b). These conditions provide favorable electrostatic interactions between the surfactants and the ferrihydrite surface, which is positively charged at pH 6 and negatively charged at pH 8.5.

In all instances, phenytoin sorption in surfactant-containing systems was non-linear, and best described by the Freundlich isotherm (model fits are shown). Additionally, increasing the mass of available surfactant generally increased the amount of phenytoin associated with the mineral surface. However, some notable differences were observed between the behavior of phenytoin in anionic and cationic surfactant-containing systems. The extent of phenytoin sorption on ferrihydrite increased monotonically with increasing concentration (Figure B-2a), with the greatest uptake in systems with 70 mg/L of total SBDS (~200 μM). In contrast, while the amount of sorbed phenytoin generally increased with CPC concentration, essentially no difference in uptake was observed between the highest two CPC concentrations investigated (35 and 70 mg/L). Comparable trends in phenytoin uptake as a function of CPC and SDBS concentration were also observed for hematite (Figure B-6).

These trends in phenytoin sorption isotherms are best explained by measured differences in the extent of SDBS and CPC sorption on iron oxides. Isotherms of SDBS sorption on ferrihydrite revealed that essentially all available surfactant was bound to the ferrihydrite surface at pH 6.0 over the concentrations explored (up to 70 mg/L). Thus, sorbed SDBS concentrations increased in a one-to-one manner with the total SDBS available in

suspension. In contrast, CPC exhibited clear non-linear sorption on ferrihydrite at pH 8.5 with the highest concentrations of total CPC producing near identical amounts of sorbed CPC (Figure B-7). These trends in surfactant sorption generally scale with phenytoin uptake, suggesting that the extent of phenytoin sorption is controlled by the amount of surfactant available on the ferrihydrite surface (Figure B-8).

Insights into the mechanism by which each surfactant promotes phenytoin uptake are provided by the pH-dependent sorption observed in surfactant-containing ferrihydrite suspensions. Results of pH-edge experiments examining sorption of CPC and SDBS on ferrihydrite, as well as phenytoin uptake on surfactant-coated ferrihydrite, are shown in Figure B-9. Data in Figure B-3 were collected over the range from pH 6.0-8.5, and with a total surfactant concentration of 70 mg/L (~200 μM), although identical pH dependent trends were also obtained at lower surfactant concentrations [35 mg/L (~100 μM)]. At all pH, SDBS exhibited roughly 5-10-fold greater sorption on ferrihydrite than CPC (Figure B-3a). CPC sorption on ferrihydrite was largely independent of pH, with approximately 1.5 mg of CPC sorbed per gram of ferrihydrite at all pH. In contrast, trends in SDBS sorption follow the expected pH-edge behavior for anions on iron oxides, in which sorption was greatest at lower pH and decreased with increasing pH. Notably, the pH independence of sorbed CPC suggests that some mechanism other than simply electrostatics may be responsible for its uptake, perhaps specific interactions between the π-bonds in its pyridine moiety and the sites on the ferrihydrite surface.
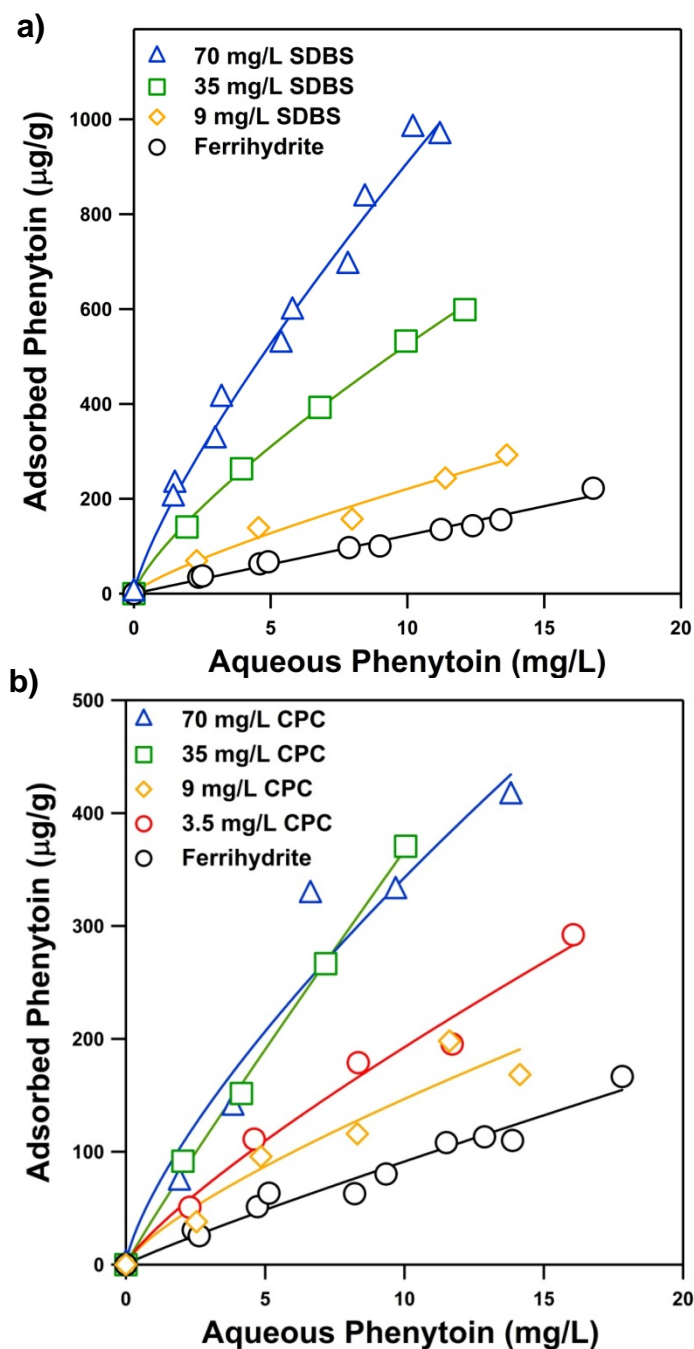
Figure B-5. Adsorption isotherms for phenytoin in suspensions of ferrihydrite with varying concentrations of (a) anionic surfactant SDBS and (b) cationic surfactant CPC. Experiments were conducted with a solid loading of either 5 or 10 g/L and an initial phenytoin concentration between 2.5-18 mg/L. For SDBS, experiments were conducted at pH 6.0 (with 25 mM MES), whereas experiments with CPC were conducted at pH 8.5 (with 25 mM Tris). Solutions also contained 25 mM NaCl. Data are also shown for sorption on to ferrihydrite in surfactant-free suspensions at these same pH values. Lines represent Freundlich model fits for sorption isotherms (equations from non-linear regression analysis are shown).
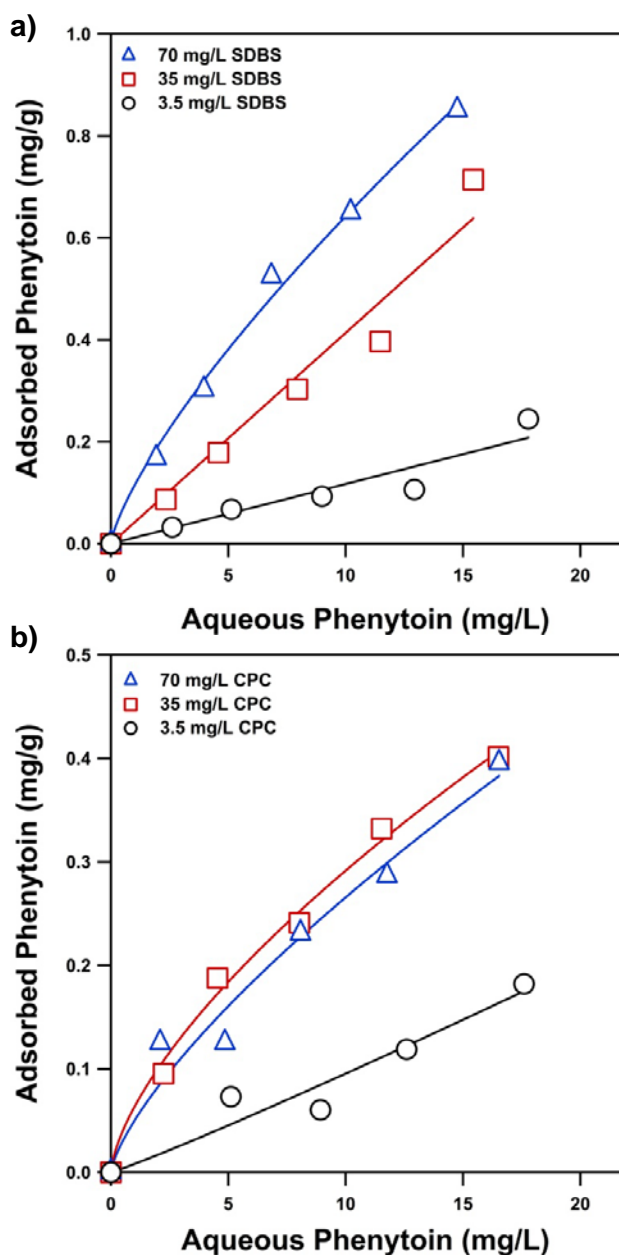
Figure B-6. Adsorption isotherm for phenytoin in suspensions of hematite with varying concentrations of (a) the anionic surfactant SDBS and (b) the cationic surfactant CPC. Experiments were conducted with a solid loading of either 5 or 10 g/L and an initial phenytoin concentration between 2.5-18 mg/L. For SDBS, experiments were conducted at pH 6.0 (with 25 mM MES), whereas experiments with CPC were conducted at pH 8.5 (with 25 mM Tris). Solutions also contained 25 mM NaCl. Data are also shown for sorption on to pristine ferrihydrite surfaces at these same pH values. Note that isotherms for adsorption on pristine hematite surfaces are not shown because of the level of uptake was insufficient at lower initial phenytoin concentrations (< 15 mg/L) to accurately measure via our analytical methods. Lines represent Freundlich model fits for sorption isotherms obtained from non-linear regression analysis (equations from non-linear regression analysis are shown).
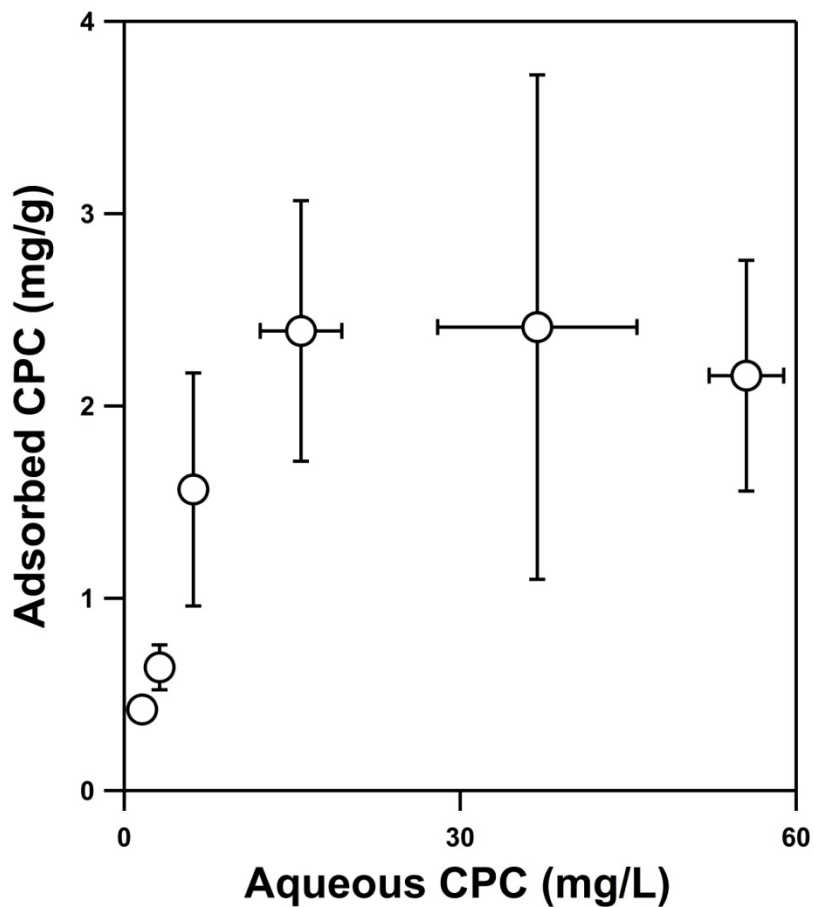
Figure B-7. Adsorption isotherm for cationic surfactant CPC on ferrihydrite at pH 8.5. Experiments were conducted with a ferrihydrite loading of either 5 or 10 g/L and an initial CPC concentration between 3-60 mg/L. Solutions contained 25 mM NaCl and were conducted in the absence of pH buffer to avoid interference during TOC analysis for CPC quantification. Uncertainties represent one standard deviation for at least duplicate analyses.
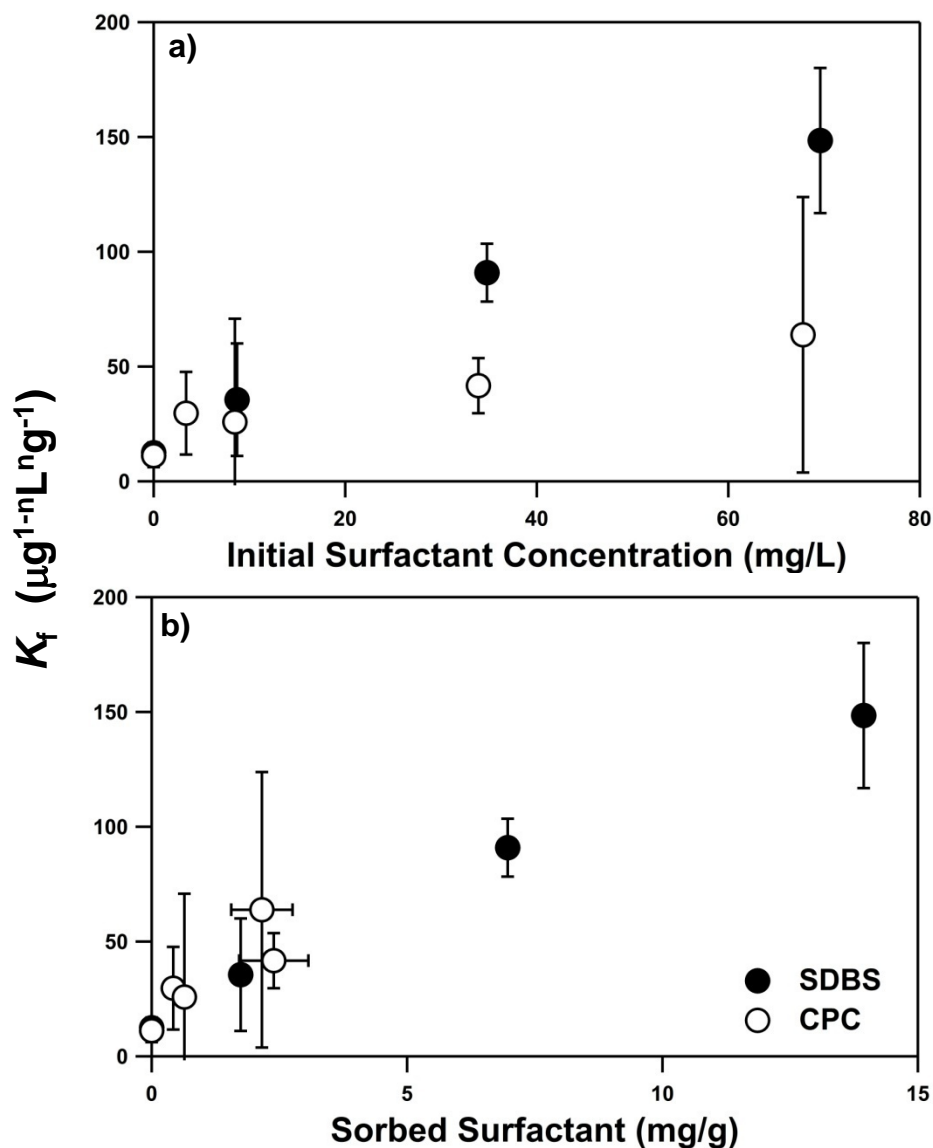
Figure B-8. Freundlich coefficients (K_f values) obtained from the sorption isotherms for phenytoin in ferrihydrite suspensions containing SDBS and CPC. Data are shown as a function of (a) initial surfactant concentration and (b) sorbed surfactant concentrations determined from isotherm experiments with each surfactant in the absence of phenytoin. Uncertainties represent 95% confidence intervals associated with non-linear regression modeling of phenytoin isotherms, shown in Figure B-2, according to the Freundlich equation. Experimental details of the isotherm experiments, conducted at pH 6.0 with SDBS and pH 8.5 with CPC, are included in the text as well as the caption for Figure B-2 in the main text.

Phenytoin sorption exhibited different pH-dependent trends in SDBS- and CPC-containing ferrihydrite suspensions (Figure B-9b). Phenytoin sorption on SDBS-coated ferrihydrite was enhanced at all pH values relative to pristine ferrihydrite surfaces, and, as was observed for the isotherms in Figure B-2, the extent of phenytoin sorption scaled with the sorbed SDBS concentration. Specifically, pH-dependent trends for phenytoin sorption in SDBS-containing suspensions mirrored those for SDBS adsorption (compare Figures B-9a and B-9b). As phentyoin is only neutrally charged or anionic over the pH range investigated, its enhanced sorption in the presence of SDBS cannot be explained by ion- paring, as has previously been suggested for surfactant promoted sorption of other PPCPs [175]. Instead, this behavior is most consistent with partitioning into the hydrophobic SDBS-layer on the ferrihydrite surface via interactions between neutral phenytoin and the alkyl chain of SDBS. The decrease in phenytoin sorption at higher pH likely arises from repulsive electrostatic forces between the negatively charged, SDBS-coated surface and the deprotonated fraction of phenytoin, which increases near its pKa value. Notably, these repulsive forces are not enough to prevent phenytoin uptake; sorption at pH 8.5 is still enhanced relative to pristine ferrihydrite suspensions even though roughly half of the available phenytoin exhibits anionic character at this pH value.

In contrast, pH-dependent sorption of phenytoin in CPC-coated ferrihydrite suspensions, while enhanced, roughly mirrored the pH-edge behavior on pristine ferrihydrite surfaces with maximum uptake between pH 7 and 7.5 (compare Figure B-9b to Figure B-1). As the amount of CPC sorbed on ferrihydrite is essentially constant over this pH range (see Figure B-9a), the pH-dependence of phentyoin sorption suggests factors in addition to sorbed CPC concentration contribute to the extent of uptake.

These additional factors likely relate to the influence of CPC on the electrostatics of the mineral-water interface. For example, the nearly constant amount of sorbed CPC should also increase in the net charge on the ferrihydrite surface at each pH value, which in turn would be expected to promote electrostatic interactions as phenytoin approaches
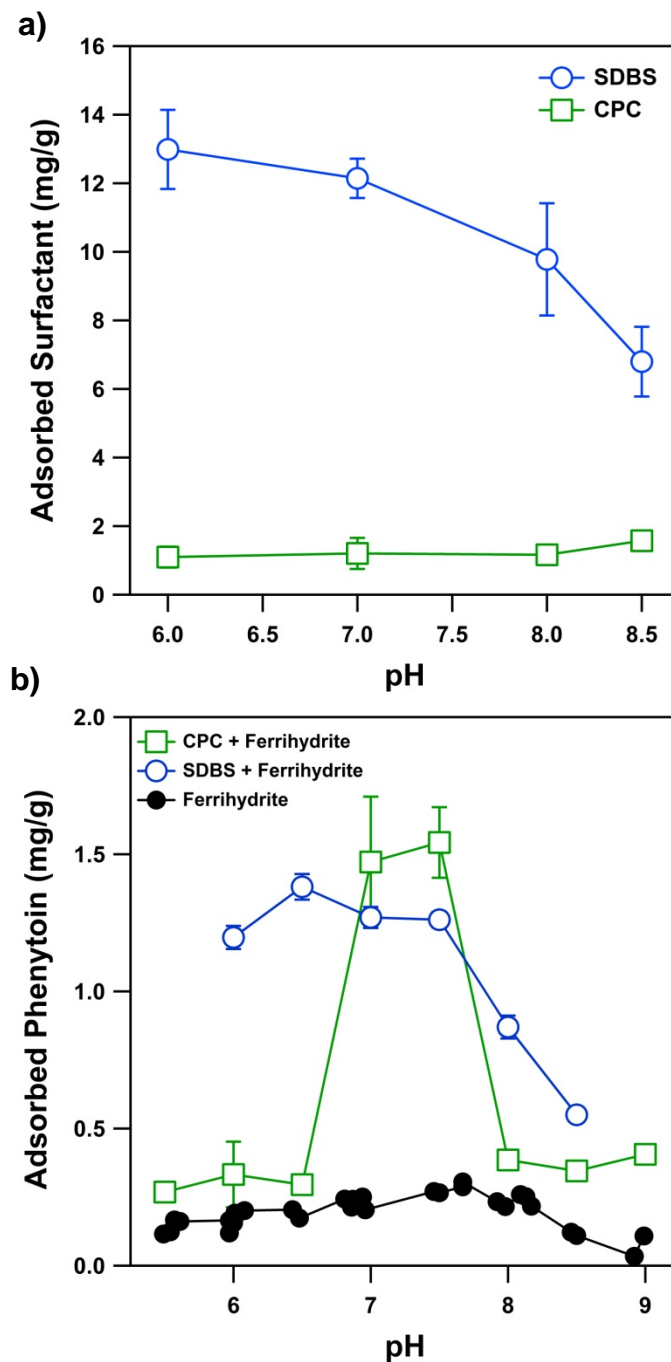
Figure B-9. pH dependent (a) sorption behavior of CPC and SDBS on ferrihydrite and (b) phenytoin sorption on CPC- and SDBS-coated ferrihydrite particles. A total surfactant concentration of 200 μM (70 mg/L) was used to collect all data, but similar pH-dependent trends were also observed with a surfactant concentration of 100 μm (35 mg/L), which is below CMC for CPC. Uncertainty represents one standard deviation of at least duplicate measurements. For phenytoin sorption, data collected in ferrihydrite suspensions without surfactant are presented for comparison.

its pKa value. Such a scenario agrees with measured pH-dependent trends in zeta potential in the presence of CPC, which consistently resulted in a more positive surface charge in suspension. It is also possible that ion-pair formation between cationic CPC and anionic phenytoin contributes to the enhanced uptake, as has previously been invoked for surfactant-promoted sorption of PPCPs in soil suspensions. However, the greatest degree of ion pairing is anticipated at and above the pKa value of phenytoin, the amount of sorbed phenytoin is relatively low at these aquatic conditions.

Notably, the increase in sorption afforded by CPC is not uniform (Figure B-10), nor does it change in a monotonic fashion as a function of pH. Thus, in addition to promoting favorable electrostatic interactions, there are likely additional mechanisms acting in parallel that contribute to the enhanced phenytoin uptake.

A final line of evidence as to the mechanisms by which SDBS and CPC promote phenytoin sorption is found in their impact on carbamazepine sorption in ferrihydrite suspensions. Carbamazepine is neutrally charged over all pH values, thus any enhanced sorption will primarily result from partitioning into hydrophobic surfactant layers. Indeed, in SDBS-containing ferrihydrite suspensions (Figure B-11), carbamazepine uptake increased with total SDBS concentration, consistent with the ability of SDBS surface layers to increase sorption via hydrophobic interactions. In contrast, carbamazepine sorption remained unmeasurable in CPC-containing ferrihydrite suspensions (up to 70 mg/L of total CPC). Thus, without the possibility of producing more favorable electrostatic interactions or ion-pair formation, CPC exhibited no influence on the sorption. Presumably, the lower degree of CPC uptake on ferrihydrite relative to SDBS (see Figure B-3a) provides a much smaller reservoir of surface-bound CPC for hydrophobic partitioning of carbamazepine relative to the surface layer of SDBS.
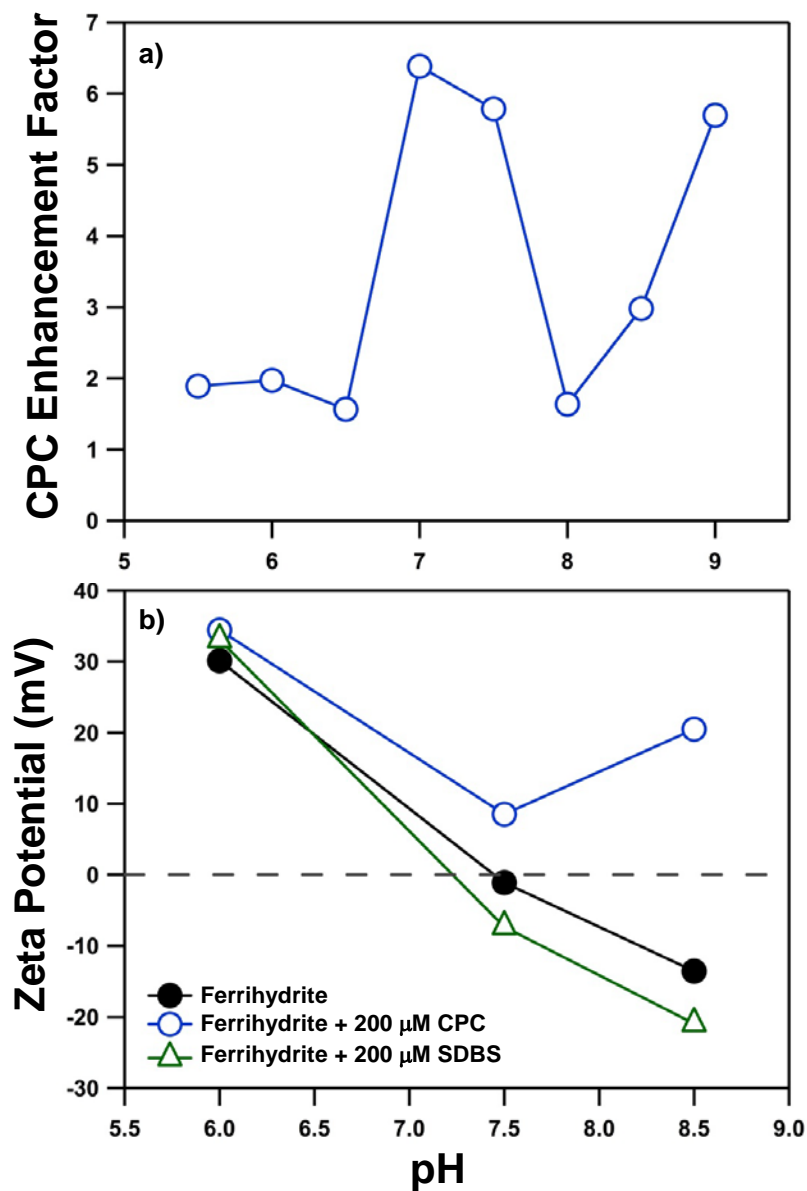
Figure B-10. (a) Increase in phenytoin sorption due to presence of CPC in ferrihydrite suspensions as a function of pH. Calculated by normalizing measured uptake in CPC-containing suspensions to uptake in absence of CPC. Enhancement is not constant, nor does it change monotonically with pH.(b) Influence of CPC sorption on zeta potential of ferrihydrite suspensions.
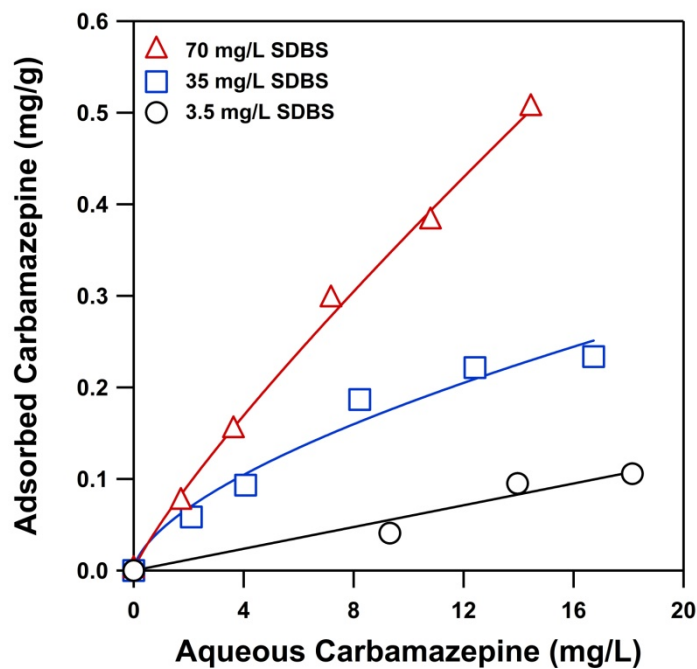
Figure B-11. Sorption isotherms for carbamazepine as a function SDBS concentrationin ferrihydrite suspensions. Experiments were conducted with a solid loading of 5 g/L, an initial carbmazepine concentration between 2.5-18 mg/L and at pH 6.0 (with 25 mM MES). Solutions also contained 25 mM NaCl. No sorption of carbamazepine was observed on pristine ferrihydrite surfaces, thus data in the absence of surfactant is not presented. Lines represent Freundlich model fits for sorption isotherms obtained from non-linear regression analysis (equations from non-linear regression analysis are shown).

Finally, the potential role for solution phase micelles in influencing anticonvulsant sorption in surfactant-coated ferrihydrite systems merits consideration. For SDBS-containing systems, all concentrations used herein are well below its reported critical micelle concentration (CMC) in water of 2.8 mM. While this value will vary with aqueous conditions (e.g., ionic strength), the near complete sorption of SDBS on ferrihydrite leaves very little free SDBS in solution, further decreasing the likelihood that any SDBS micelles are present in suspension. On the ferrihydrite surface, however, formation of hemi-micelles and SDBS bilayers most likely occurrs, which would contribute to the enhanced sorption of phenytoin and carbamazepine observed in SDBS-containing ferrihydrite suspensions.

For CPC, the reported CMC of approximately 130 μM (~ 40 mg/L) in 20 mM NaCl (ref) allows for the potential of micelle formation at some of the higher concentrations employed in our experiments.   From the sorption isotherm of CPC on ferrihydrite, aqueous concentrations exceeding the reported CMC will be produced above 150 μM (~ 50 mg/L) of total CPC mass. However, we do not believe our data support a significant influence of solution phase micelles because our trends in phenytoin sorption were observed at all CPC concentrations investigated, particularly those below the CMC (Figure B-12).

<center>Influence of Cationic and Anionic Surfactants on</center>

<center>Anticonvulsant Sorption: Non-sorbent Metal Oxides</center>

Coatings of SDBS and CPC were also able to make previously inactive metal oxides effective sorbents for phenytoin. Figure B-13 compares the uptake of phenytoin in various mineral suspensions (5 g/L) with a total concentration of 200 μM of either SDBS (pH 6.0) or CPC (pH 8.5). In the presence of SDBS (Figure B-13a), all metal oxides except TiO_2 and SiO_2 (data not shown) were effective sorbents for phenytoin. As expected, ferrihydrite and hematite were the most active sorbents on a per mass basis in

the presence of SDBS, resulting in sorbed phenytoin concentrations roughly three-fold greater than observed on goethite and alumina oxide. The lack of reactivity for TiO_2 and SiO_2 is not surprising, as these are the only two metal oxides with a net negative surface charge at pH 6 (see Figure B-2), and thus the degree of SDBS uptake was anticipated to be small. Indeed, relative trends in phenytoin uptake on SDBS-coated mineral surfaces generally reflect the amount of SDBS present on the metal oxide surface (Figure B-13b), consistent with enhanced phenytoin uptake via partitioning into the hydrophobic SDBS layer on the oxides' surfaces.

All metal oxides investigated also were active sorbents toward phenytoin in the presence of CPC (Figure B-14a). While the majority of the metal oxides exhibited roughly comparable sorption behavior toward phenytoin, silica dioxide (i.e., quartz) revealed markedly greater uptake than the other metals, exhibiting nearly two-fold greater sorption of phenytoin than the other oxides. As with SDBS, a loose correlation between trends in phenytoin and CPC sorption on metal oxide surfaces is observed (Figure B-14b). For example, SiO_2 and Al_2O_3 sorb the most and least amounts of CPC, respectively, which correlates with their respective affinity for phenytoin,. However, while SiO2 and TiO2 adsorbed nearly equivalent amounts of CPC, the extent of phenytoin sorption was far greater for SiO2, suggesting that additional factors contribute to the enhanced phenytoin sorption in the presence of CPC. For example, the SiO_2 used herein has a much smaller specific surface area relative to TiO_2. Such differences will likely cause the structure of the adsorbed surfactant layer to vary considerably between these systems even though the total mass of surfactant adsorbed is equivalent.

The ability of CPC to enhance the sorption activity of SiO_2 is notable because of its ubiquity in soils and sediments. Whereas the majority of the metal oxides considered herein possess negative surface charge only at relatively high pH values, the SiO_2 surface will be negatively charged over the entire range of environmentally relevant pH values.

Thus, its role as a sorbent in the presence of cationic surfactants is likely to be significant in subsurface systems over a broad range of pH values.
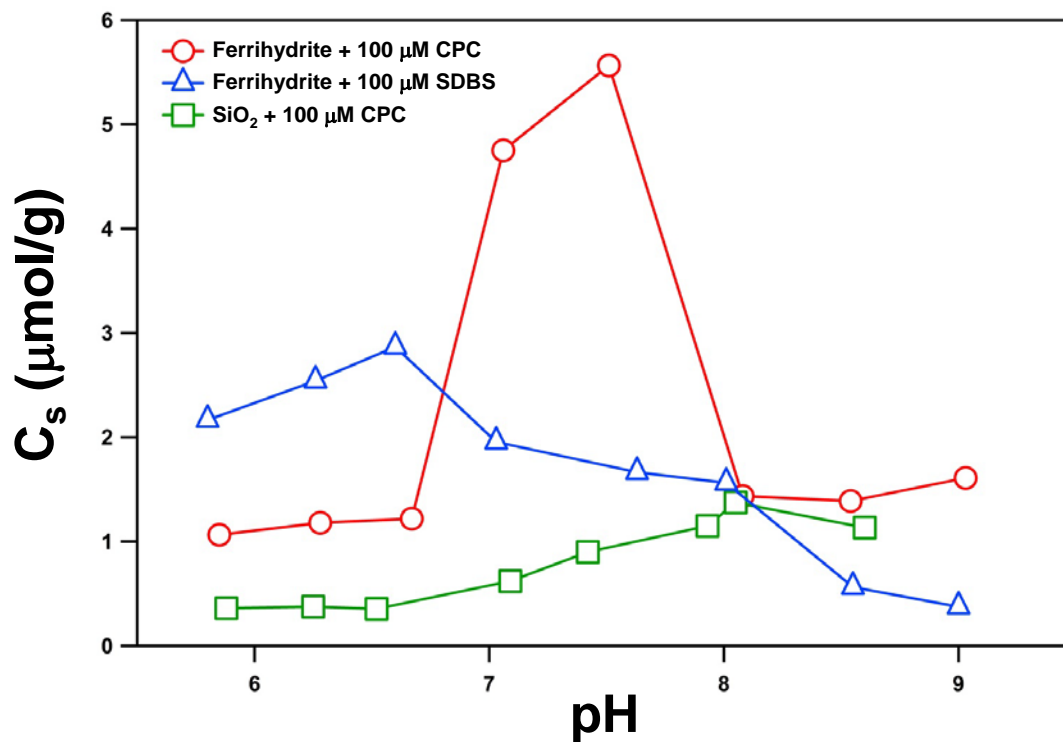
Figure B-12. pH edge adsorption data for phenytoin on SiO_2 and ferrihydrite in the presence of SBDS and CPC. Notably, all data were collected at an initial surfactant concentration of 100 μM, below the CMC for both surfactants.
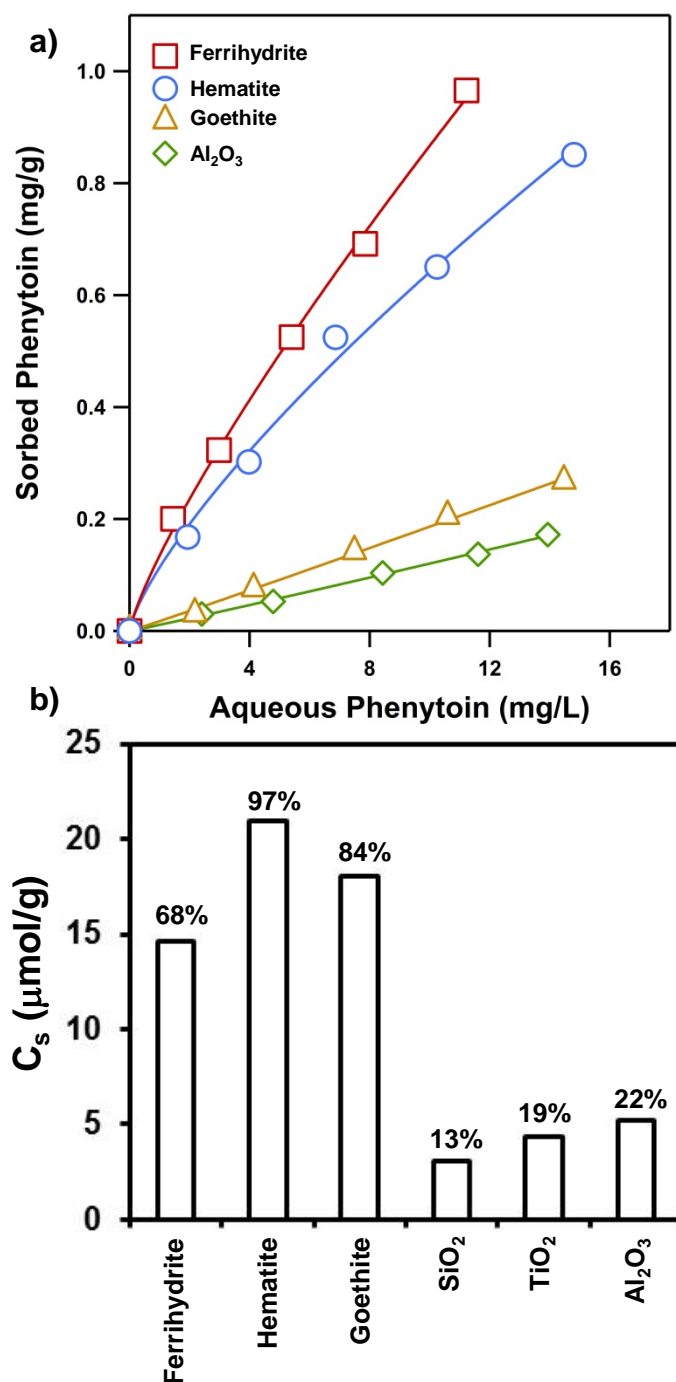
Figure B-13. (a) Influence of SDBS on phenytoin sorption in different metal oxide systems. All experiments conducted at 200 μM initial surfactant concentration and a solid loading of 5 g/L at pH 6.0. (b) Relative trends in surfactant uptake in each metal oxide systems are shown under these experimental conditions. Numbers correspond to percent of initial surfactant mass adsorbed at equilibrium.
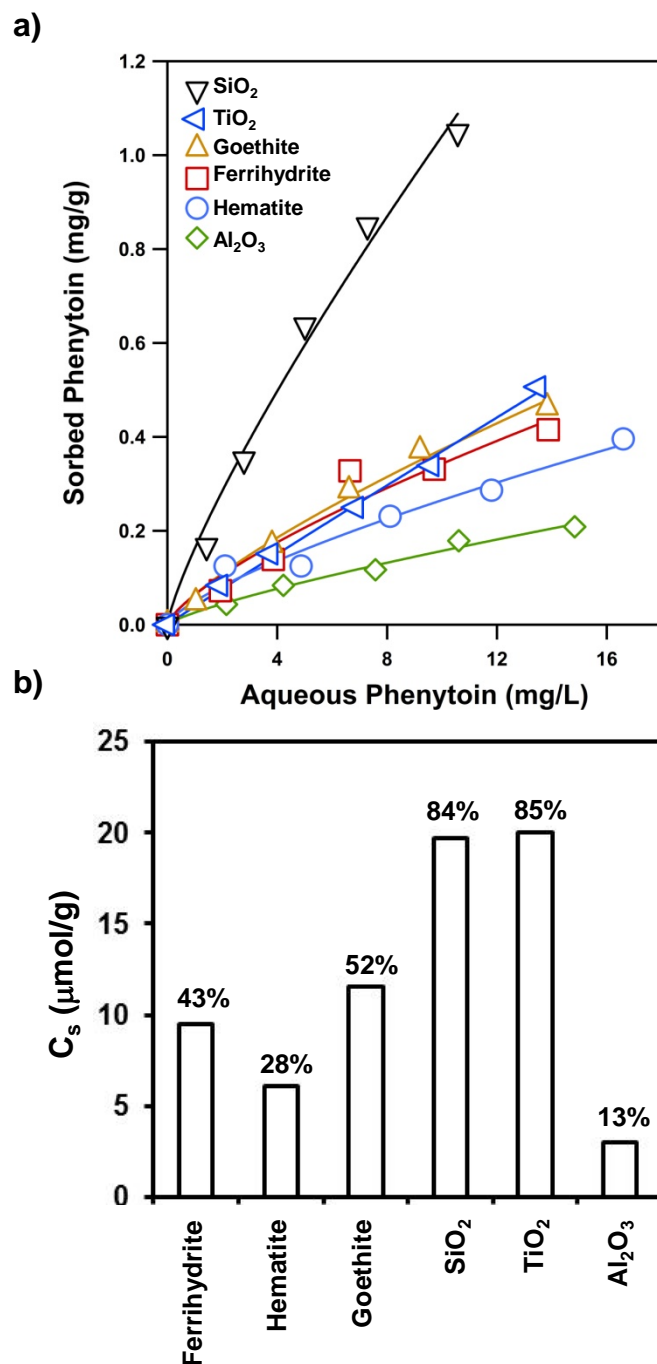
Figure B-14. (a) Influence CPC on phenytoin sorption in different metal oxide systems. All experiments conducted at 200 μM initial surfactant concentration and a solid loading of 5 g/L at pH 8. (b) Relative trends in surfactant uptake in each metal oxide systems are shown under these experimental conditions. Numbers correspond to percent of initial surfactant mass adsorbed at equilibrium.

Results of experiments examining the pH-dependent behavior of CPC sorption on SiO_2, as well as the pH-dependent uptake of phenytoin in CPC-containing SiO_2 systems are shown in Figure B-15. Once again, results in Figure B-4 were obtained in systems with a total CPC concentration of 200 μM (~70 mg/L), although isotherm experiments (Figure B-16) reveal that the greater uptake of CPC on SiO_2 results in aqueous phase concentrations (~25 mg/L) well below the reported CMC value. Over the range of pH values investigated (pH 6.0-8.5), the amount of sorbed CPC was essentially constant at approximately 8-9 mg of CPC/g SiO_2 (Figure B-15a). Unlike results with ferrihydrite (Figure B-9a), the constancy in sorbed CPC concentrations is consistent with electrostatic interactions driving CPC uptake on SiO_2 because the negative charge on SiO_2 is also roughly constant over this pH interval (Figure B-15b). In contrast, the amount of phenytoin sorbed in CPC-containing SiO_2 suspensions increased steadily as solution pH approached the pKa of phenytoin.

Trends in pH-dependent sorption on CPC-coated SiO_2 surfaces once again support favorable electrostatics as contributing to, if not entirely governing, phenytoin uptake. Zeta potential analyses (Figure B-15b) illustrate that as the amount of CPC sorbed on the SiO_2 surface increases, the net surface charge of the particles in suspension also becomes more positive. In fact, at very high initial CPC concentrations of 175 mg/L (~500 μM; beyond what was explored in phenytoin sorption studies) intended to achieve surface site saturation on SiO_2 the particles in suspensions are neutral to slightly positively charged. In turn, electrostatic interactions with the anionic form of phenytoin become more favorable, promoting uptake.

Finally, we note that select metal oxides functioned as sorbents for carbamazepine in the presence of surfactants, as was observed with surfactant-coated ferrihydrite. This behavior was most pronounced for goethite (α-FeOOH), which was unreactive toward both phenytoin and carbamazepine in the absence of surfactants. Notably, trends in

carbamazepine uptake as a function of surfactant loading (Figure B-17a) support the mechanisms proposed for enhanced phenytoin uptake in SDBS- and CPC- systems. Specifically, sorption of carbamazepine and phenytoin were enhanced by nearly equivalent amounts, as evidenced by the comparable trends in Freundlich coefficients from isotherm experiments in in SDBS-containing goethite suspensions at pH 6.0 (Figure B-17b). From its lack of ionizable groups, the promoted uptake of carbamazepine must be primarily from increased hydrophobic interactions with the SDBS layer on the goethite surface, which also are responsible for phenytoin uptake because it is neutrally charged at pH 6.0.

Unlike SDBS-containing suspensions, carbamazepine exhibited vastly different sorption tendencies relative to phenytoin in CPC-coated goethite systems at pH 8.5 (Figure B-17c). Whereas K_f values for carbamazepine were essentially invariant with CPC concentration, they increased steadily for phenytoin. This contrasting behavior further supports a scenario through which CPC enhances phenytoin uptake primarily as a result of its influence on the charge of the mineral water interface. In contrast, the small amount of carbamazepine uptake measurable in CPC-coated goethite suspensions suggests that a small fraction of phenytoin uptake may also result from its hydrophobic partitioning into the surface organic layer produced by the sorbed CPC. However, the dominant role of CPC in metal oxide suspensions appears to be creating more favorable electrostatic conditions through which anionic organics can sorb on the surfactant coated mineral surface.
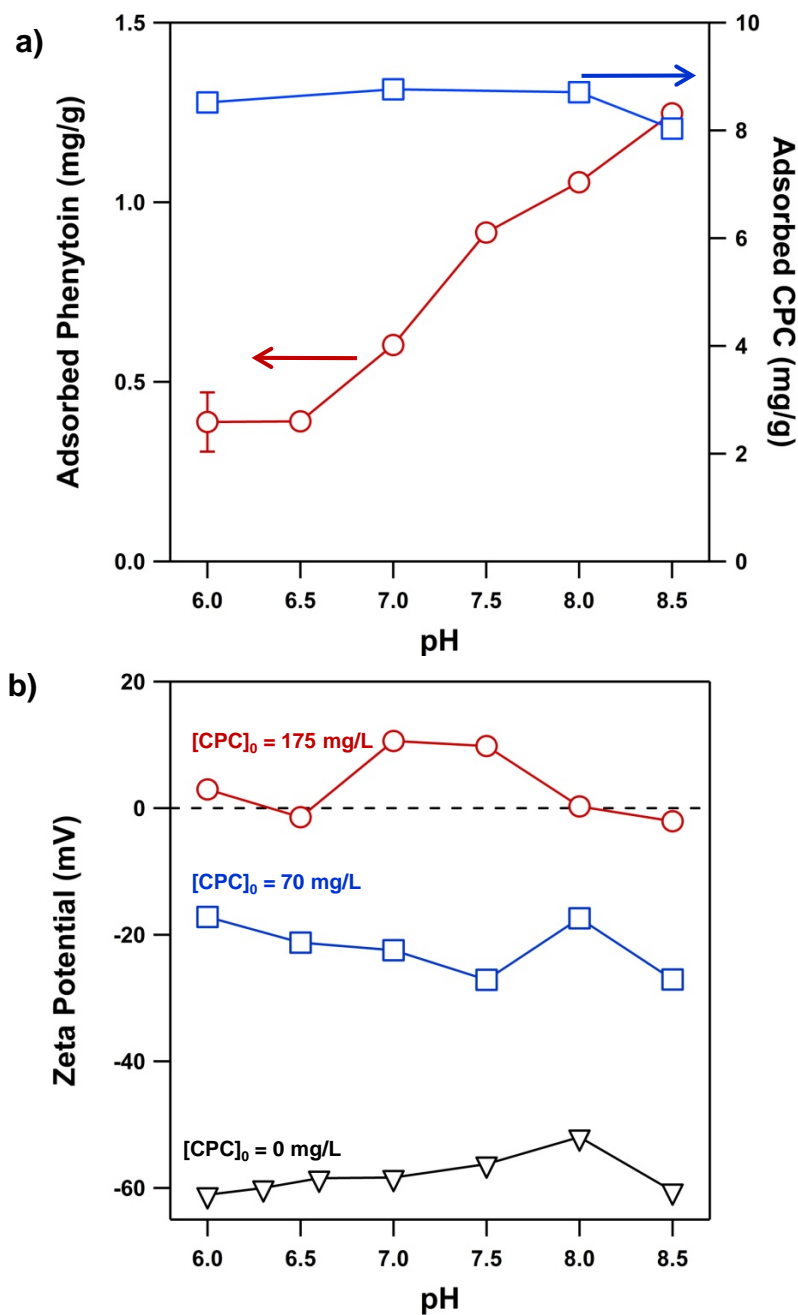
Figure B-15. (a) Adsorption of CPC on SiO_2 and the sorption of phenytoin in SiO_2 suspensions (5 g/L) containing 70 mg/L (~200 μM) of CPC. Results are shown as a function of solution pH. pH-edge experiments with phenytoin used an initial concentration of 13.9 mg/L (55 μM). (b) Influence of different initial CPC concentrations on zeta potential of SiO_2 suspensions shown as a function of pH. Suspensions (5 g/L) were prepared with the initial CPC concentration and pH indicated, allowed to equilibrate overnight, and then diluted for zeta potential analysis. In the diluted suspension, the final concentration of SiO_2 was 0.14 g/L and the total CPC concentrations were 0, 5.7 and 14.3 μM.
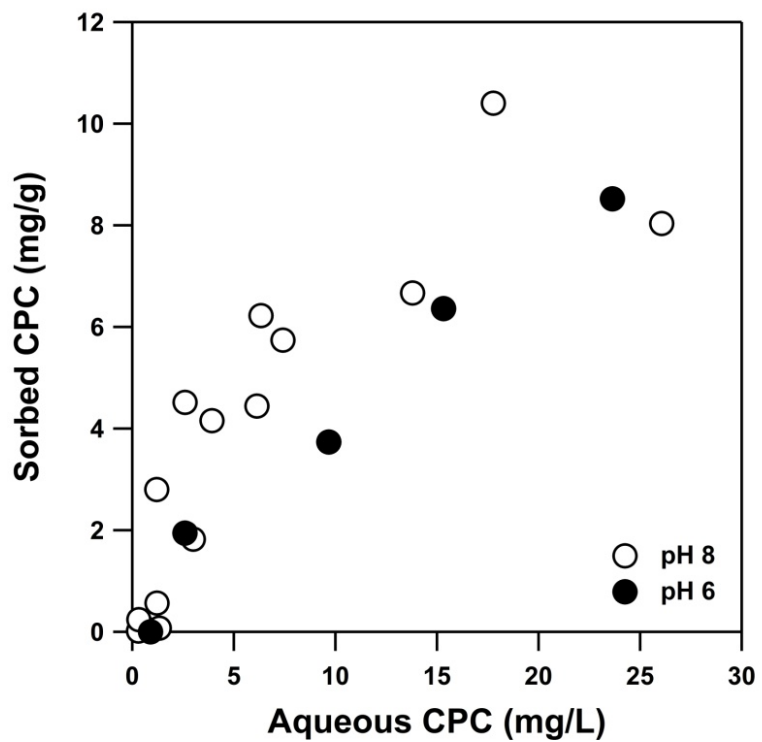
Figure B-16. Sorption isotherms for CPC at pH 6 and 8. Consistent with pH edge results, the amount of CPC sorbed was essentially constant over this pH range.
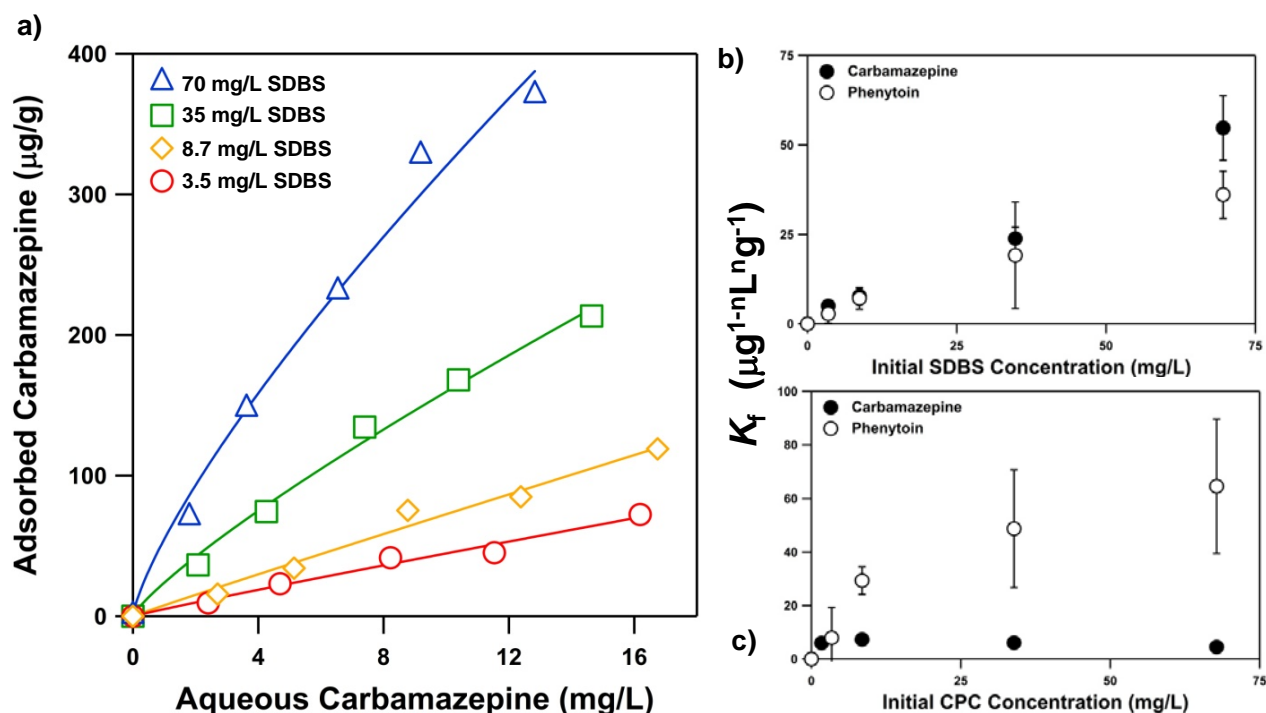
Figure B-17. (a) Sorption isotherms for carbamazepine in goethite suspensions containing SDBS, and a comparison of Fruendlich isotherm model fit parameters for phenytoin and carbamazepine in (b) SDBS and (c) CPC-containing goethite suspensions. Experiments were conducted with a solid loading of either 5 or 10 g/L and an initial carbamazepine concentration between 2.5-18 mg/L. For SDBS, experiments were conducted at pH 6.0 (with 25 mM MES), whereas experiments with CPC were conducted at pH 8.5 (with 25 mM Tris). Solutions also contained 25 mM NaCl. Lines in panel (a) represent Freundlich model fits for sorption isotherms (equations from non-linear regression analysis are shown). In panels (b) and (c), uncertainties represent 95% confidence intervals for K_f, which was model best-fit parameter obtained via non-linear regression analysis.

Reversibility of Anticonvulsant Sorption in

Surfactant-Containing Suspensions

A final set of isotherm experiments examined whether sorption of phenytoin in SDBS-containing ferrihydrite suspensions was irreversible. Experiments conducted with 5 g/L ferrihydrite in the presence of 70 mg/L SDBS revealed that phenytoin sorption was completely reversible (Figure B-18). Thus, although the presence of as SDBS can increase substantially the amount of phenytoin retained on metal oxide surfaces, the hydrophobic interactions primarily responsible for this enhancement are relatively weak and reversible. As with ferrihydrite suspensions in the absence of organic matter, true thermodynamic equilibrium appears to be achieved in these systems and perturbations introducing disequilibrium will result in release of phenytoin from the metal oxide surface.

B.5   Conclusion

Although ubiquitous in soil, colloids, and sediment systems, metal oxides are typically assumed to play a minimal role as sorbents of PPCPs relative to organic matter also present in these systems.   Indeed, the work herein demonstrates that only a select few naturally occurring oxide phases are relevant sorbents for PPCPs, and those with activity are rather limited in such capacity. Toward phenytoin and carbamazepine, activity of pristine metal oxide as sorbents appears largely predictable from simple considerations of electrostatics; iron oxides, as a result of their relatively high pH_{zpc} values, represent active sorbents for anionic phenytoin. Generally, therefore, sorption on metal oxides can be expected to influence, albeit to a limited extent, the fate and transport of ionizable PPCPs in natural systems.

More important in the fate of PPCPs, however, is the ability of metal oxides to accumulate surface layers of organic matter that in turn will impact the fate and transport of PPCPs in soil and sediments. Natural forms of organic matter (i.e., humic acids) are

less important in this capacity than anthropogenic organic matter in the form of cationic and anionic surfactants. The presence of cationic and anionic surfactants has the ability to enhance the sorption capacity of most metal oxides, at times considerably, toward both charged and uncharged PPCPs. Most notably, surface coatings of surfactants can create more favorable adsorption conditions via multiple mechanisms, ultimately transforming unreactive metal oxides into relatively high-capacity sorbents for PPCPs in soil and sediment systems. This behavior was most notable for SiO_2 suspensions, in which the positively charged surface induced by CPC sorption yielded the greatest uptake of phenytoin relative to the other metal oxides investigated at pH 8.5.

Ultimately, predicting the fate and transport of PPCPs in soil and sediment systems impacted by high levels of organic matter will be challenging, as several variables will dictate not only the extent but also the fundamental mechanisms responsible for their sorption. Results herein show that the most notable attribute for the sorbate (i.e., the PPCP) will be the presence of ionizable groups that result in a net charge on the compound at the ambient pH. With respect to the organic coatings, in addition to the type of organic matter (e.g., humic acid versus surfactants), the extent of sorption in all surfactant systems increased with the amount of surfactant accumulated on the metal oxide surface. However, while anticonvulsant sorption always scaled with amount of surface-bound surfactant, there are multiple pathways by which sorption can be enhanced. The first is the well-recognized role of adsorbed surfactant layers generating a new surface organic phase to facilitate hydrophobic partitioning of the PPCP, which was the dominant mechanism for carbamazepine and neutral phenytoin in SDBS-containing suspensions. We show here that surfactants can also promote sorption by altering the electrostatics of the mineral-water interface to produce more attractive forces that promote interaction between the oppositely charged sorbate and sorbent surface. This mechanism was dominant in CPC-containing systems in which phenytoin exhibited appreciable anionic character. One must also not discount the potential contribution of

ion pairing between charged PPCPs and counter-ion surfactants, which may have also contributed to the enhanced phenytoin uptake in CPC-containing suspensions. Finally, the nature of the metal oxide surface will also impact these sorption mechanisms, as the extent of surfactant-metal oxide interaction dictates the size of the organic surface layer available for hydrophobic partitioning and the magnitude of charging at the solid-water interface that alters the nature of electrostatic interactions.

The findings presented herein are most relevant to helping to assess the rate of PPCP transport in soil and subsurface environments such as those encountered during aquifer recharge with treated wastewater effluent or in soil aquifer treatment (SAT) systems. These are systems of growing importance with respect to water sustainability and wastewater management in which PPCPs and various other forms of effluent organic matter are likely to coexist. The sorption exhibited to a limited extent on pristine metal oxides and to a much greater extent on surfactant-coated metal oxides translates into slower rates of transport (i.e., higher retardation factors) during transport in porous media. During SAT, for example, reports of subsurface lifetime frequently reported for PPCPs may be longer given the additional retention to inorganics coated with anthropogenic organic matter that likely also persists in effluent. Notably, because uptake on both pristine and surfactant-coated metal oxides is entirely reversible, at least in some cases, it should not be assumed that such surfaces will serve as a long term sink of these compounds.

Future efforts must attempt to identify generalities in the mechanisms of organic-promoted PPCP sorption in mineral systems. The validity of the mechanisms proposed herein for phenytoin and carbamazepine sorption in the presence of CPC and SDBS need to be generalized across the spectrum of polarities demonstrated by various PPCPs and for the range of commercially available anionic and cationic surfactants. In particular, those surfactants most effective at influence sorption must be identified. In near-neutral pH ferrihydrite suspensions (see Figure B-3), for example, high levels of sorbed SDBS

(~10 mg/g) were required to achieve phenytoin uptake comparable to that measured with far lower levels of sorbed CPC (~ 1-2 mg/g), albeit in different pH regimes. The contributions of non-ionic surfactants to PPCP uptake also merit further consideration. Finally, focus must be paid to establish the behavior of other forms of organic matter likely to be present in the natural environment, extending beyond the model humic considered herein to more complex organics that may more closely mimic the behavior of anthropogenic surfactants (e.g,. biosurfactants).
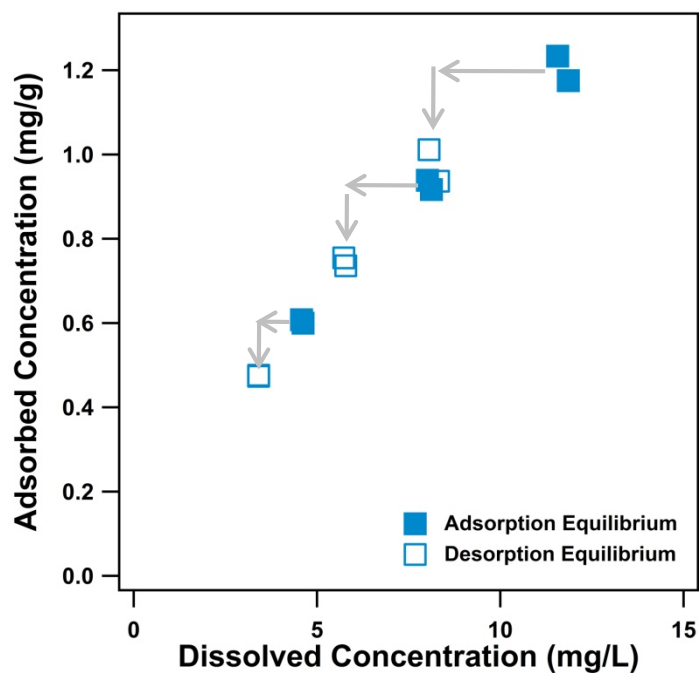
Figure B-18. Reversibility in surfactant coated ferrihydrite suspensions. Results from duplicate experiments are shown.

REFERENCES

1. Belfroid, A. C.; Van der Horst, A.; Vethaak, A. D.; Schäfer, A. J.; Rijs, G. B. J.; Wegener, J.; Cofino, W. P., Analysis and occurrence of estrogenic hormones and their glucuronides in surface water and waste water in The Netherlands. *Sci. Total Environ.* **1999,** *225*, 101-108.

2. Kasprzyk-Hordern, B.; Dinsdale, R. M.; Guwy, A. J., The occurrence of pharmaceuticals, personal care products, endocrine disruptors and illicit drugs in surface water in South Wales, UK. *Water Res.* **2008,** *42*, 3498-3518.

3. Kim, S. D.; Cho, J.; Kim, I. S.; Vanderford, B. J.; Snyder, S. A., Occurrence and removal of pharmaceuticals and endocrine disruptors in South Korean surface, drinking, and waste waters. *Water Res.* **2007,** *41*, 1013-1021.

4. Kolpin, D. W.; Furlong, E. T.; Meyer, M. T.; Thurman, E. M.; Zaugg, S. D.; Barber, L. B.; Buxton, H. T., Pharmaceuticals, Hormones, and Other Organic Wastewater Contaminants in U.S. Streams, 1999−2000: A National Reconnaissance. *Environ. Sci. Technol.* **2002,** *36*, 1202-1211.

5. LeBaron, R., *Hormones; a delicate balance*. First ed.; Regents of the University of Colorado: New York, 1972.

6. Campbell, N. A., *Biology*. 4th ed.; Addison Wesley Longman Menlo Park, 1996.

7. Khan, S. J.; Roser, D. J.; Davies, C. M.; Peters, G. M.; Stuetz, R. M.; Tucker, R.; Ashbolt, N. J., Chemical contaminants in feedlot wastes: Concentrations, effects and attenuation. *Environ. Int.* **2008,** *34*, 839-859.

8. Ying, G.; Kookana, R. S.; Ru, Y., Occurrence and fate of hormone steroids in the environment. *Environ. Int.* **2002,** *28*, 545-551.

9. Baronti, C.; Curini, R.; D'Ascenzo, G.; Di Corcia, A.; Gentili, A.; Samperi, R., Monitoring Natural and Synthetic Estrogens at Activated Sludge Sewage Treatment Plants and in a Receiving River Water. *Environ. Sci. Technol.* **2000,** *34*, 5059-5066.

10. Bodzek, M.; Dudziak, M., Elimination of steroidal sex hormones by conventional water treatment and membrane processes. *Desalination* **2006,** *198*, 24-32.

11. Desbrow, C.; Routledge, E. J.; Brighty, G. C.; Sumpter, J. P.; Waldock, M., Identification of Estrogenic Chemicals in STW Effluent. 1. Chemical Fractionation and in Vitro Biological Screening. *Environ. Sci. Technol.* **1998,** *32*, 1549-1558.

12. Lee, L. S.; Carmosini, N.; Sassman, S. A.; Dion, H. M.; Sepúlveda, M. S., Agricultural Contributions of Antimicrobials and Hormones on Soil and Water Quality. *Adv. Agron.* 2007, 93, 1-68.

13. Oulton, R. L.; Kohn, T.; Cwiertny, D. M., Pharmaceuticals and personal care products in effluent matrices: A survey of transformation and removal during wastewater treatment and implications for wastewater management. *J. Environ. Monitor.* **2010,** *12*, 1956-1978.

14.   Sedlak, D. L.; Gray, L. J.; Pinkston, K. E., Understanding Microcontaminants in Recycled Water. *Environ. Sci. Technol.* **2000,** *34*, 508-515.

15.   Ternes, T. A.; Stumpf, M.; Mueller, J.; Haberer, K.; Wilken, R. D.; Servos, M., Behavior and occurrence of estrogens in municipal sewage treatment plants — I. Investigations in Germany, Canada and Brazil. *Sci. Total Environ.* **1999,** *225*, 81-90.

16.   Gall, H. E.; Sassman, S. A.; Lee, L. S.; Jafvert, C. T., Hormone Discharges from a Midwest Tile-Drained Agroecosystem Receiving Animal Wastes. *Environ. Sci. Technol.* **2011,** *45*, 8755-8764.

17.   Schiffer, B.; Daxenberger, A.; Meyer, K.; Meyer, H. H., The fate of trenbolone acetate and melengestrol acetate after application as growth promoters in cattle: environmental studies. *Environ. Health Persp.* **2001,** *109*, 1145-51.

18.   Lange, I. G.; Daxenberger, A.; Schiffer, B.; Witters, H.; Ibarreta, D.; Meyer, H. H. D., Sex hormones originating from different livestock production systems: fate and potential disrupting activity in the environment. *Anal. Chim. Acta* **2002,** *473*, 27-37.

19.   Harries, J. E.; Sheahan, D. A.; Jobling, S.; Matthiessen, P.; Neall, P.; Routledge, E. J.; Rycroft, R.; Sumpter, J. P.; Tylor, T., A survey of estrogenic activity in United Kingdom in land waters. *Environmental Toxicology and Chemistry* **1996,** *15*, 1993-2002.

20.   Harries, J. E.; Sheahan, D. A.; Jobling, S.; Matthiessen, P.; Neall, P.; Sumpter, J. P.; Tylor, T.; Zaman, N., Estrognic activity in five united kingdom rivers detected by measurement of vitellogenesis in caged male trout. *Environ. Toxicol. Chem.* **1997,** *16*, 534-542.

21.   Jobling, S.; Nolan, M.; Tyler, C. R.; Brighty, G.; Sumpter, J. P., Widespread Sexual Disruption in Wild Fish. *Environ. Sci. Technol.* **1998,** *32*, 2498-2506.

22.   Ankley, G. T.; Jensen, K. M.; Makynen, E. A.; Kahl, M. D.; Korte, J. J.; Hornung, M. W.; Henry, T. R.; Denny, J. S.; Leino, R. L.; Wilson, V. S.; Cardon, M. C.; Hartig, P. C.; Gray, L. E., Effects of the androgenic growth promoter 17-beta-trenbolone on fecundity and reproductive endocrinology of the fathead minnow. *Environ. Toxicol. Chem.* **2003,** *22*, 1350-60.

23.   Kidd, K. A.; Blanchfield, P. J.; Mills, K. H.; Palace, V. P.; Evans, R. E.; Lazorchak, J. M.; Flick, R. W., Collapse of a fish population after exposure to a synthetic estrogen. *P. Natl. Acad. Sci. USA* **2007,** *104*, 8897-8901.

24.   Kolok, A. S.; Snow, D. D.; Kohno, S.; Sellin, M. K.; Guillette Jr, L. J., Occurrence and biological effect of exogenous steroids in the Elkhorn River, Nebraska, USA. *Sci. Total Environ.* **2007,** *388*, 104-115.

25.   Orlando, E. F.; Kolok, A. S.; Binzcik, G. A.; Gates, J. L.; Horton, M. K.; Lambright, C. S.; Gray, L. E.; Soto, A. M.; Guillette, L. J., Endocrine-disrupting effects of cattle feedlot effluent on an aquatic sentinel species, the fathead minnow. *Environ. Health Persp.* **2004,** *112*, 353-358.

26. Renner, R., Do cattle growth hormones pose an environmental risk? *Environ. Sci. Technol.* **2002,** *36*, 194A-197A.

27. Seki, M.; Fujishima, S.; Nozaka, T.; Maeda, M.; Kobayashi, K., Comparison of response to 17β-trenbolone among three small fish species. *Environ. Toxicol. Chem.* **2006,** *25*, 2742.

28. Kolok, A. S.; Sellin, M. K., The environmental impact of growth-promoting compounds employed by the United States beef cattle industry: history, current knowledge, and future directions. *Rev. Environ. Contam. Toxicol.* **2008,** *195*, 1-30.

29. Balter, M., *Scientific cross-claims fly in continuing beef war*. Science **1999**, 284, 1453-1455.

30. California Environmental Contaminant Biomonitoring Program (CECBP) Scientific Guidance Panel (SGP). *Synthetic Hormones in Animal Husbandry*, 2008. Available at: http://oehha.ca.gov/multimedia/biomon/pdf/120408 synhormonesdoc.pdf.

31. Sinnett-Smith, P. A.; Dumelow, N. W.; Buttery, P. J., Effects of trenbolone acetate and zeranol on protein metabolism in male castrate and female lambs. *Brit. J. Nutr.* **1983,** *50*, 225-34.

32. Pottier, J.; Cousty, C.; Heitzman, R. J.; Reynolds, I. P., Differences in the biotransformation of a 17β-hydroxylated steroid, trenbolone acetate, in rat and cow. *Xenobiotica* **1981,** *11*, 489-500.

33. Krzeminski, L. F.; Cox, B. L.; Gosline, R. E., Fate of radioactive melengestrol acetate in the bovine. *J. Agr. Food Chem.* **1981,** *29*, 387-391.

34. Upjohn Company. *Environmental Assessment: Melengestrol Acetate (MGA) for Suppression of Estrus for Heifers Intended for Breeding*; 1996. Available at: http://www.fda.gov/ucm/groups/fdagov-public/@fdagov-av- gen/documents /document /ucm071903.pdf

35. Kleinova, M.; Zöllner, P.; Kahlbacher, H.; Hochsteiner, W.; Lindner, W., Metabolic Profiles of the Mycotoxin Zearalenone and of the Growth Promoter Zeranol in Urine, Liver, and Muscle of Heifers. *J. Agr. Food Chem.* **2002,** *50*, 4769-4776.

36. Bartelt-Hunt, S. L.; Snow, D. D.; Kranz, W. L.; Mader, T. L.; Shapiro, C. A.; Donk, S. J. v.; Shelton, D. P.; Tarkalson, D. D.; Zhang, T. C., Effect of Growth Promotants on the Occurrence of Endogenous and Synthetic Steroid Hormones on Feedlot Soils and in Runoff from Beef Cattle Feeding Operations. *Environ. Sci. Technol.* **2012,** *46*, 1352-1360.

37. Durhan, E. J.; Lambright, C. S.; Makynen, E. A.; Lazorchak, J.; Hartig, P. C.; Wilson, V. S.; Gray, L. E.; Ankley, G. T., Identification of metabolites of trenbolone acetate in androgenic runoff from a beef feedlot. *Environ. Health Persp.* **2006,** *1*, 65-8.

38. Laganà, A.; Bacaloni, A.; De Leva, I.; Faberi, A.; Fago, G.; Marino, A., Analytical methodologies for determining the occurrence of endocrine disrupting

chemicals in sewage treatment plants and natural waters. *Anal. Chim. Acta* **2004,** *501*, 79-88.

39.   Jensen, K. M.; Makynen, E. A.; Kahl, M. D.; Ankley, G. T., Effects of the feedlot contaminant 17alpha-trenbolone on reproductive endocrinology of the fathead minnow. *Environ. Sci. Technol.* **2006,** *40*, 3112-7.

40.   Bauer, E. R.; Daxenberger, A.; Petri, T.; Sauerwein, H.; Meyer, H. H., Characterisation of the affinity of different anabolics and synthetic hormones to the human androgen receptor, human sex hormone binding globulin and to the bovine progestin receptor. *Apmis* **2000,** *108*, 838-46.

41.   Lauderdale, J. W.; Goyings, L. S.; Krzeminski, L. F.; Zimbelman, R. G., Studies of a progestogen (MGA) as related to residues and human consumption. *J. Toxicol. Env. Health* **1977,** *3*, 5-33.

42.   Schwarzenbach, R. P.; Gschwend, P. M.; Imboden, D. M., *Environmental Organic Chemistry*. John Wiley and Sons: New York: 2003.

43.   Canonica, S.; Jans, U.; Stemmler, K.; Hoigne, J., Transformation Kinetics of Phenols in Water: Photosensitization by Dissolved Natural Organic Material and Aromatic Ketones. *Environ. Sci. Technol.* **1995,** *29*, 1822-1831.

44.   van der Merwe, P. J.; Pieterse, J. W., Stability of zeranol, nandrolone and trenbolone in bovine urine. *Analyst* **1994,** *119*, 2651-3.

45.   Mallinckrodt Veterinary, Inc. Environmental Assessment for Zeranol. **1994**. Available at: http://www.fda.gov/ucm/groups/fdagov-public/@fdagov-av-gen/ documents /document/ucm071898.pdf

46.   Syntex Animal Health. *Synovex Plus (trenbolone acetate and estradiol benzoate) Implant Environmental Assessment*; 1995. Available at: http://www.fda.gov/ucm /groups/ fdagov-public/@fdagov-av-gen/documents/document/ucm072272.pdf

47.   Gryglik, D.; Olak, M.; Miller, J. S., Photodegradation kinetics of androgenic steroids boldenone and trenbolone in aqueous solutions. *J. Photoch. photobio. A* **2010,** *212*, 14-19.

48.   Schiffer, B.; Totsche, K. U.; Jann, S.; Kögel-Knabner, I.; Meyer, K.; Meyer, H. H. D., Mobility of the growth promoters trenbolone and melengestrol acetate in agricultural soil: column studies. *Sci. Total Environ.* **2004,** *326*, 225-237.

49.   Khan, B.; Qiao, X.; Lee, L. S., Stereoselective Sorption by Agricultural Soils and Liquid−Liquid Partitioning of Trenbolone (17α and 17β) and Trendione. *Environ. Sci. Technol.* **2009,** *43*, 8827-8833.

50.   Card, M. L.; Chin, Y.-P.; Lee, L. S.; Khan, B., Prediction and Experimental Evaluation of Soil Sorption by Natural Hormones and Hormone Mimics. *J. Agr. Food Chem.* **2011,** *60*, 1480-1487.

51.   Qiao, X.; Carmosini, N.; Li, F.; Lee, L. S., Probing the Primary Mechanisms Affecting the Environmental Distribution of Estrogen and Androgen Isomers. *Environ. Sci. Technol.* **2011,** *45*, 3989-3995.

52. Das, B. S.; Lee, L. S.; Rao, P. S. C.; Hultgren, R. P., Sorption and Degradation of Steroid Hormones in Soils during Transport: Column Studies and Model Evaluation. *Environ. Sci. Technol.* **2004,** *38*, 1460-1470.

53. Lee, L. S.; Strock, T. J.; Sarmah, A. K.; Rao, P. S. C., Sorption and Dissipation of Testosterone, Estrogens, and Their Primary Transformation Products in Soils and Sediment. *Environ. Sci. Technol.* **2003,** *37*, 4098-4105.

54. Xu, L.; Xu, C.; Zhao, M.; Qiu, Y.; Sheng, G. D., Oxidative removal of aqueous steroid estrogens by manganese oxides. *Water Res.* **2008,** *42*, 5038-5044.

55. Zhang, H.; Huang, C., Adsorption and oxidation of fluoroquinolone antibacterial agents and structurally related amines with goethite. *Chemosphere* **2007,** *66*, 1502-1512

56. Bloss, R. E.; Northam, J. I.; Smith, L. W.; Zimbelman, R. G., Effects of Oral Melengestrol Acetate on the Performance of Feedlot Cattle. *J. of Anim. Sci.* **1966,** *25*, 1048-1053.

57. Lefebvre, B.; Malouin, F.; Roy, G.; Gigu; K.; Diarra, M. S., Growth Performance and Shedding of Some Pathogenic Bacteria in Feedlot Cattle Treated with Different Growth-Promoting Agents. *J. Food Protect.* **2006,** *69*, 1256-1264.

58. Neumann, F., Pharmacological and Endocrinological Studies on Anabolic Agents. In *Anabolic Agents in Animal Production*, Lu, F. C.; Rendel, J., Eds. Thieme Publishers: Stuttgart, 1976; pp 253-264.

59. Lauderdale, J. W., Use of Melengestrol Acetate in Animal Production. In *Proceedings of the Symposium on Anabolics in Animal Production: Public Health Aspects, Analytical Methods, and Regulation*, Meissonnier, E.; Mitchell-Vigneron, J., Eds. Office International des Epizooties: Paris, France, 1983; pp 193-212.

60. Kuhn, H. J.; Braslavsky, S. E.; R., S. *Chemical actinometry (IUPAC technical report)*; Pure Appl. Chem. **2004,** pp 2105-2146.

61. Leifer, A., The kinetics of environmental aquatic photochemistry : theory and practice. American Chemical Society: Washington, DC 1988.

62. Dulin, D.; Mill, T., Development and evaluation of sunlight actinometers. *Environ. Sci. Technol.* **1982,** *16*, 815-820.

63. Goldstein, S.; Rabani, J., The ferrioxalate and iodide-iodate actinometers in the UV region. *J. Photoch. Photobio. A* **2008,** *193*, 50-55.

64. Stucki, J. W.; Anderson, W. L., The quantitative assay of minerals for Fe^{2+} and Fe^{3+} using 1,10-phenanthroline. 1. Sources of variability. *Soil Science Society of America Journal* **1981,** *45*, 633-637.

65. Kochany, J.; Bolton, J. R., Mechanism of photodegradation of aqueous organic pollutants. 1. EPR spin-trapping technique for the determination of hydroxyl radical rate constants in the photooxidation of chlorophenols following the photolysis of hydrogen peroxide. *J. Phys. Chem-US* **2002,** *95*, (13), 5116.

66. Haag, W. R.; Hoigne, J., Singlet oxygen in surface waters. 3. Photochemical formation and steady-state concentrations in various types of waters. *Environ. Sci. Technol.* **1986,** *20*, 341-348.

67. Park, J.-S.; Choi, H.; Cho, J., Kinetic decomposition of ozone and para-chlorobenzoic acid (pCBA) during catalytic ozonation. *Water Res.* **2004,** *38*, 2285-2292.

68. Dorfman, L. M.; Taub, I. A.; Harter, D. A., Rate Constants for the Reaction of the Hydroxyl Radical with Aromatic Molecules. *J. Chem. Phys.* **1964,** *41*, 2954-2955.

69. Bader, H.; Sturzenegger, V.; Hoigné, J., Photometric method for the determination of low concentrations of hydrogen peroxide by the peroxidase catalyzed oxidation of N,N-diethyl-p-phenylenediamine (DPD). *Water Res.* **1988,** *22*, 1109-1115.

70. DeRosa, M. C.; Crutchley, R. J., Photosensitized singlet oxygen and its applications. *Coordin. Chem. Rev.* **2002,** *233–234*, 351-371.

71. Buxton, G. V.; Greenstock, C. L.; Helman, W. P.; Ross, A. B. J., Critcial review of rate constants for reactions with hydrated electrons, hydrogen atoms, and hydroxyl radicals (OH/O) in aqueous solutions. *Phys. Chem. Ref. Data* **1988,** *17*, 513-886.

72. Kim, H. L.; Ray, A. C.; Stipanovic, R. D., Rapid separation and identification of urinary metabolites of zeranol by HPLC-UV spectrophotometry. *J. Agr. Food Chem.* **1986,** *34*, 312-315.

73. Visconti, A.; Pascale, M., Determination of zearalenone in corn by means of immunoaffinity clean-up and high-performance liquid chromatography with fluorescence detection. *J. Chromatogr. A* **1998,** *815*, 133-140.

74. Vulliet, E.; Falletta, M.; Marote, P.; Lomberget, T.; Païssé, J.-O.; Grenier-Loustalot, M.-F., Light induced degradation of testosterone in waters. *Sci. Total Environ.* **2010,** *408*, 3554-3559.

75. Lin, A. Y.-C.; Reinhard, M., Photodegradation of common environmental pharmaceuticals and estrogens in river water. *Environ. Toxicol. Chem.* **2005,** *24*, (6), 1303-1309.

76. Lambert, C.; Sarna, T.; Truscott, T. G., Rose bengal radicals and their reactivity. *J. Chem. Soc. Faraday T.* **1990,** *86*, 3879-3882.

77. Werner, J. J.; McNeill, K.; Arnold, W. A., Environmental photodegradation of mefenamic acid. *Chemosphere* **2005,** *58*, 1339-1346.

78. Zhang, T.; Hsu-Kim, H., Photolytic degradation of methylmercury enhanced by binding to natural organic ligands. *Nat. Geosci.* **2010,** *3*, 473-476.

79. Parker, J. G.; Stanbro, W. D., Optical determination of the rates of formation and decay of $O_2(^1\Delta_g)$ in H_2O, D_2O and other solvents. *J. Photochem.* **1984**, (25), 545-547.

80.   Kohn, T.; Nelson, K. L., Sunlighted-mediated inactivation of MS2 coliphage via exogenous singlet oxygen producted by sensitizers in natural waters. *Environ. Sci. Technol.* **2007,** *41*, 192-197.

81.   Kochany, J.; Bolton, J. R., Mechanism of photodegradation of aqueous organic pollutants. 2. Measurements of the primary rate constants for reaction of hydroxyl radicals with benzene and some halobenzenes using an EPR spin-trapping method following the photolysis of hydrogen peroxide. *Environ. Sci. Technol.* **1992,** *26*, 262-265.

82.   Zepp, R. G.; Schlotzhauer, P. F.; Sink, R. M., Photosensitized transformations involving electronic energy transfer in natural waters: role of humic substances. *Environ. Sci. Technol.* **1985,** *19*, 74-81.

83.   Boreen, A. L.; Arnold, W. A.; McNeill, K., Triplet-Sensitized Photodegradation of Sulfa Drugs Containing Six-Membered Heterocyclic Groups: Identification of an SO2 Extrusion Photoproduct. *Environ. Sci. Technol.* **2005,** *39*, 3630-3638.

84.   Canonica, S.; Jans, U.; Stemmler, K.; Hoigné, J., Transformation kinetics of phenols in water: photosensitization by dissolved natural organic material and aromatic ketones. *Environ. Sci. Technol.* **1995,** *29*, 1822-1831.

85.   Canonica, S.; Hellrung, B.; Wirz, J., Oxidation of phenols by triplet aromatic ketones in aqueous solution. *J. Phys. Chem. A* **2000,** *104*, 1226-1232.

86.   Trudeau, V. L.; Heyne, B.; Blais, J. M.; Temussi, F.; Atkinson, S. K.; Pakdel, F.; Popesku, J. T.; Marlatt, V. L.; Scaiano, J. C.; Previtera, L.; Lean, D. R. S., Lumiestrone is photochemically derived from estrone and may be released to the environment without detection. *Front. Endocrinol.* **2011,** *2*, 1-13.

87.   Khan, B.; Lee, L. S.; Sassman, S. A., Degradation of synthetic androgens 17a- and 17b-trenbolone and trendione in agricultural soils. *Environ. Sci. Technol.* **2008,** *42*, 3570-3574.

88.   Zepp, R. G.; Hoigne, J.; Bader, H., Nitrate-induced photooxidation of trace organic chemicals in water. *Environ. Sci. Technol.* **1987,** *21*, 443-450.

89.   Johnson, B. J.; Hathaway, M. R.; Anderson, P. T.; Meiske, J. C.; Dayton, W. R., Stimulation of circulating insulin-like growth factor I (IGF-I) and insulin-like growth factor binding proteins (IGFBP) due to administration of a combined trenbolone acetate and estradiol implant in feedlot cattle. *J. Anim. Sci.* **1996,** *74*, 372-9.

90.   Webster, J. P.; Kover, S. C.; Bryson, R. J.; Harter, T.; Mansell, D. S.; Sedlak, D. L.; Kolodziej, E. P., Occurence of trenbolone acetate metabolites in simulated confined animal feeding operation (CAFO) runoff. *Environ. Sci. Technol.* **2012,** *46*, 3808-3810.

91.   Soto, A. M.; Calabro, J. M.; Prechtl, N. V.; Yau, A. Y.; Orlando, E. F.; Daxenberger, A.; Kolok, A. S.; Guillette, L. J.; Le Bizec, B.; Lange, I. G.; Sonnenschein, C., Androgenic and estrogenic activity in water bodies receiving cattle feedlot effluent in eastern Nebraska, USA. *Environ. Health Persp.* **2004,** *112*, 346-352.

92. Patel, M. S.; Peal, W. J., Acid-catalysed dehydration of 3-hydroxysteroids—III : The preparation of 3α- and 3β-methylcholesterol and some reactions of these compounds. *Tetrahedron* **1964,** *20*, 2511-2520.

93. Patel, M. S.; Peal, W. J., Acid-catalysed dehydration of 3-hydroxysteroids—II : The influence of solvents on the products of the reaction between hydrogen chloride and 3β-hydroxy-Δ5-steroids. *Tetrahedron* **1964,** *20*, 2499-2510.

94. De Marco, R.; Leggio, A.; Liguori, A.; Perri, F.; Siciliano, C., Transformations of 3-Hydroxy Steroids with Lewis and Anhydrous Protic Acids: The Case of Pregn-4-en-3β,17α,20β-Triol. *Chem. Biol. Drug Des.* **2011,** *78*, 269-276.

95. Ruelas, J. P.; Iriarte, J.; Kincl, F.; Djerassi, C., Steroids. XCVIII.1 Synthesis of Some 10β-Hydroxy-19-norsteroids. *J. Org. Chem.* **1958,** *23*, 1744-1747.

96. Kocovsky, P.; Baines, R. S., Stereoelectronically Controlled, Thallium(III)-Mediated C-19 Degradation of 19-Hydroxy Steroids. An Expedient Route to Estrone and its Congeners via 19-Nor-10.beta.-hydroxy Intermediates. *The J. Org. Chem.* **1994,** *59*, 5439-5444.

97. Canonica, S.; Kramer, J. B.; Reiss, D.; Gygax, H., Photoisomerization Kinetics of Stilbene-Type Fluorescent Whitening Agents. *Environ. Sci. Technol.* **1997,** *31*, 1754-1760.

98. La Clair, J. J.; Bantle, J. A.; Dumont, J., Photoproducts and Metabolites of a Common Insect Growth Regulator Produce Developmental Deformities in Xenopus. *Environ. Sci. Technol.* **1998,** *32*, 1453-1461.

99. Edhlund, B. L.; Arnold, W. A.; McNeill, K., Aquatic Photochemistry of Nitrofuran Antibiotics. *Environ. Sci. Technol.* **2006,** *40*, 5422-5427.

100. Makarova, M. A.; Williams, C.; Zamaraev, K. I.; Thomas, J. M., Mechanistic study of sec-butyl alcohol dehydration on zeolite H-ZSM-5 and amorphous aluminosilicate. *J. Chem. Soc. Faraday T.* **1994,** *90*, 2147-2153.

101. Skrdla, P. J.; Robertson, R. T., Investigation of alcohol dehydration by a cobalt(II) sulfate-promoted γ-alumina catalyst inside a gas chromatograph injection port. *J. Mol. Catal. A-Chem.***2003,** *194*, 255-265.

102. California Environmental Contaminant Biomonitoring Program (CECBP) Scientific Guidance Panel (SGP). *Synthetic Hormones in Animal Husbandry*, 2008. Available at: http://oehha.ca.gov/multimedia/biomon/pdf/120408synhormonesdoc.pdf.

103. Kjær, J.; Olsen, P.; Bach, K.; Barlebo, H. C.; Ingerslev, F.; Hansen, M.; Sørensen, B. H., Leaching of Estrogenic Hormones from Manure-Treated Structured Soils. *Environ. Sci. Technol.* **2007,** *41*, 3911-3917.

104. Blanco, M., M. Alcal, and M. Bautista, Pharmaceutical gel analysis by NIR spectroscopy: Determination of the active principle and low concentration of preservatives. *Eur. J. Pharm. Sci.*, **2008,** 33(4-5): p. 409-414.

105. Berry, D.J., Beran R.G., Plunkeft, M. J.,Clarke, L. A., Hung, W. T., The absorption of gabapentin following high dose escalation. *Seizure*, **2003,** 12(1): p. 28-36.

106. Burleson, D. J.; Penn, R. L., Two-Step Growth of Goethite from Ferrihydrite. *Langmuir* **2005,** *22*, 402-409.

107. Murray, J. W., The surface chemistry of hydrous manganese dioxide. *J. Colloid Interf. Sci.* **1974,** *46*, 357-371.

108. Wolf, D. C.; Dao, T. H.; Scott, H. D.; Lavy, T. L., Influence of Sterilization Methods on Selected Soil Microbiological , Physical, and Chemical Properties. *J. Environ. Qual.* **1989,** *18*, 39-44.

109. Yang, Y.; Hunter, W.; Tao, S.; Gan, J., Relationships between Desorption Intervals and Availability of Sediment-Associated Hydrophobic Contaminants. *Environ. Sci. Technol.* **2008,** *42*, 8446-8451.

110. Chiron, S., C. Minero, and D. Vione, Photodegradation Processes of the Antiepileptic Drug Carbamazepine, Relevant To Estuarine Waters. *Environ. Sci. Technol.*, **2006**. 40(19): p. 5977-5983.

111. Boenigk, J., A. Wiedlroither, and K. Pfandl, Heavy metal toxicity and bioavailability of dissolved nutrients to a bacterivorous flagellate are linked to suspended particle physical properties. *Aquat. Toxicol.*, **2005**, 71(3): p. 249-259.

112. Bouwer, E.J., McCarty, P. L., Bouwer, H., Rice, R. C., Organic contaminant behavior during rapid infiltration of secondary wastewater at the phoenix 23rd avenue project. *Water Res.*, **1984**, **18**(4): p. 463-472.

113. Torrents, A.; Stone, A. T., Hydrolysis of phenyl picolinate at the mineral/water interface. *Environ. Sci. Technol.* **1991,** *25*, 143-149.

114. Canonica, S., B. Hellrung, and J. Wirz, Oxidation of Phenols by Triplet Aromatic Ketones in Aqueous Solution. *J. Phys. Chem. A*, **2000**, 104(6): p. 1226-1232.

115. Jurgens, M.D., Holthaus, K. I., Johnson, A. C., Smith, J. L., Hetheridge, M., Williams, R.J., The potential for estradiol and ethinylestradiol degradation in English rivers, *Environ. Toxicol. Chem.*, **2002**, 21(3):480-8.

116. Kolodziej, E.P., T. Harter, and D.L. Sedlak, Dairy Wastewater, Aquaculture, and Spawning Fish as Sources of Steroid Hormones in the Aquatic Environment. *Environ. Sci. Technol.*, **2004,** 38(23): p. 6377-6384.

117. Ying, G. and R.S. Kookana, Degradation of Five Selected Endocrine-Disrupting Chemicals in Seawater and Marine Sediment. *Environ. Sci. Technol.*, **2003**, 37(7): p. 1256.

118. USDA, *Part I: Baseline Reference of Feedlot Management Practices, 1999;* National Animal Health Monitoring System #N327.0500; United States Department of Agriculture: Fort Collins, CO; http://www.aphis.usda.gov/animal_health/nahms/feedlot/downloads/feedlot99/Feedlot99_dr_PartI.pdf

119.   USDA, *Livestock Slaughter: 2011 summary*; National Agricultural Statistics Service ISSN: 0499-0544; United States Department of Agriculture, 2012

120.   Blazer, V.S.; Iwanowicz, L. R.; Henderson, H.; Mazik, P. M.; Jenkins, J. A.; Alvarez, D. A.; Young, J., A., Reproductive endocrine disruption in smallmouth bass (Micropterus dolomieu) in the Potomac River basin: spatial and temporal comparisons of biological effects. *Environ. Monit. Assess.,* **2012,** 184(7): p. 4309-34.

121.   Webster, J.P.; Kover, S. C.; Bryson, R. J.; Harter, T.; Mansell, D. S.; Sedlak, D. L.; Kolodziej, E. P., Occurrence of trenbolone acetate metabolites in simulated confined animal feeding operation (CAFO) runoff. *Environ. Sci. Technol.*, **2012, 46**(7): p. 3803-10.

122.   Durhan, E. J.; Lambright, C. S.; Makynen, E. A.; Lazorchak, J.; Hartig, P. C.; Wilson, V. S.; Gray, L. E.; Ankley, G. T., Identification of metabolites of trenbolone acetate in androgenic runoff from a beef feedlot. *Environ. Health Persp.* **2006,** *1*, 65-8.

123.   Parker, J.A.; Webster, J. P.; Kover, S. C.; Kolodziej, E. P., Analysis of trenbolone acetate metabolites and melengestrol in environmental matrices using gas chromatography–tandem mass spectrometry. *Talanta,* **2012,** 99(0): p. 238-246.

124.   Caldwell, D.J.; Mastrocco, F.; Anderson, P. D.; Lange, R.; Sumpter, J. P., Predicted-no-effect concentrations for the steroid estrogens estrone, 17beta-estradiol, estriol, and 17alpha-ethinylestradiol. *Environ. Toxicol. Chem.*, **2012,** 31(6): p. 1396-406.

125.   Williams, R.J.; Keller, V. D. J.; Johnson, A. C.; Young, A. R.; Holmes, M. G. R.; Wells, C.; Gross-Sorokin, M.; Benstead, R., A national risk assessment for intersex in fish arising from steroid estrogens. *Environ. Toxicol. Chem.,* **2009,** 28(1): p. 220-30.

126.   Boettcher, M., T. Kosmehl, and T. Braunbeck, Low-dose effects and biphasic effect profiles: Is trenbolone a genotoxicant? *Mutat. Res.*, **2011**, 723(2): p. 152-157.

127.   Mansell, D.S.; Bryson, R. J.; Harter, T.; Webster, J. P.; Kolodziej, E. P.; Sedlak, D. L., Fate of Endogenous Steroid Hormones in Steer Feedlots Under Simulated Rainfall-Induced Runoff. *Environ. Sci. Technol.*, **2011**, 45(20): p. 8811-8818.

128.   Falconer, I.R.; Chapman, H. F.; Moore, M. R.; Ranmuthugala, G., Endocrine-disrupting compounds: a review of their challenge to sustainable and safe water supply and water reuse. *Environ. Toxicol.*, **2006**, 21(2): p. 181-91.

129.   Iwanowicz, L.R.; Blazer, V. S.; Guy, C. P.; Pinkney, A. E.; Mullican, J. E.; Alvarez, D. A., Reproductive health of bass in the Potomac, U.S.A., drainage: part 1. Exploring the effects of proximity to wastewater treatment plant discharge. *Environ. Toxicol. Chem.*, **2009**, 28(5): p. 1072-83.

130.   Qu, S., E.P. Kolodziej, and D.M. Cwiertny, Phototransformation Rates and Mechanisms for Synthetic Hormone Growth Promoters Used in Animal Agriculture. *Environ. Sci. Technol.*, **2012**, 46(24): p. 13202-13211.

131. Lavado, R.; Loyo-Rosales, J. E.; Floyd, E.; Kolodziej, E. P.; Snyder, S. A.; Sedlak, D. L.; Schlenk, D., Site-Specific Profiles of Estrogenic Activity in Agricultural Areas of California's Inland Waters. *Environ. Sci. Technol.*, **2009**, 43(24): p. 9110-9116.

132. Scarth, J.P.; Clarke, A. D.; Teale, P.; Pearce, C. M., Comparative in vitro metabolism of the 'designer' steroid estra-4,9-diene-3,17-dione between the equine, canine and human: Identification of target metabolites for use in sports doping control. *Steroids*, **2010**, 75(10): p. 643-652.

133. Ho, P.C., Photooxidation of 2,4-dinitrotoluene in aqueous solution in the presence of hydrogen peroxide. *Environ. Sci. Technol.*, **1986**, 20(3): p. 260-267.

134. Zuo, Y., K. Zhang, and Y. Deng, Occurrence and photochemical degradation of 17α-ethinylestradiol in Acushnet River Estuary. *Chemosphere*, **2006**, 63(9): p. 1583-1590.

135. Forsgren, K.L.; Qu, S.; Cwiertny, D. M.; Schlenk, D., Trenbolone acetate metabolites promote ovarian growth and development in adult Japanese medaka(Oryzias latipes). In review, 2013.

136. Whidbey, C.M.; Daumit, K. E.; Nguyen, T. H.; Ashworth, D. D.; Davis, J. C. C.; Latch, D. E., Photochemical induced changes of in vitro estrogenic activity of steroid hormones. *Water Res.*, **2012**. 46(16): p. 5287-5296.

137. Leet, J.K., H.E. Gall, and M.S. Sepulveda, A review of studies on androgen and estrogen exposure in fish early life stages: effects on gene and hormonal control of sexual differentiation. *J. App. Toxicol.* **2011**, 31(5): p. 379-98.

138. Sellin Jeffries, M. K.; Conoan, N. H.; Cox, M. B.; Sangster, J. L.; Balsiger, H. A.; Bridges, A. A.; Cowman, T.; Knight, L. A.; Bartelt-Hunt, S. L.; Kolok, A. S., The anti-estrogenic activity of sediments from agriculturally intense watersheds: Assessment using in vivo and in vitro assays. *Aquat. Toxicol.*, **2011**, 105(1–2): p. 189-198.

139. Ahn, B. Y.; Kang, S. W.; Yoo, J.; Kim, W. K.; Bae, P. H.; Jung, J., Identification of estrogenic activity change in sewage, industrial and livestock effluents by gamma-irradiation. *Radiat. Phys. and Chem.*, **2012**, 81(11): p. 1757-1762.

140. Waller, C.L., D.L. Minor, and J.D. McKinney, Using three-dimensional quantitative structure-activity relationships to examine estrogen receptor binding affinities of polychlorinated hydroxybiphenyls. *Environ. Health Persp.*, **1995**, 103(7-8): p. 702-7.

141. Hemmer, M.J.; Cripe, G. M.; Hemmer, B. L.; Goodman, L. R.; Salinas, K. A.; Fournie, J. W.; Walker, C. C., Comparison of estrogen-responsive plasma protein biomarkers and reproductive endpoints in sheepshead minnows exposed to 17β-trenbolone. *Aquat. Toxicol.*, **2008**, 88(2): p. 128-136.

142. Dehennin, L.; Blacker, C.; Reiffsteck, A.; Scholler, R., Estrogen 2-, 4-, 6- or 16-hydroxylation by human follicles shown by gas chromatography-mass spectrometry associated with stable isotope dilution. *J. Steroid Biochem.*, **1984**, 20(1): p. 465-71.

143.   Gehm, B.D.; McAndrews, J. M.; Chien, P. Y.; Jameson, J. L.; Resveratrol, a polyphenolic compound found in grapes and wine, is an agonist for the estrogen receptor. *P. Natl. A. Sci.*, **1997**, 94(25): p. 14138-43.

144.   Pellissier, H.; M. Santelli, Chemical and Biochemical Hydroxylations of Steroids. A Review. *Org. Prep. Proced. Int.*, **2001**, 33(1): p. 1-58.

145.   Williamson, J.; D. Van Orden; J.P. Rosazza, Microbiological hydroxylation of estradiol: formation of 2- and 4-hydroxyestradiol by Aspergillus alliaceus. *Appl. Environ. Microb.*, **1985**, 49(3): p. 563-7.

146.   Medjakovic, S.; A. Jungbauer, Phytoestrogens and their Putative Effects on the Aryl Hydrocarbon Receptor. *Curr. Bio. Comp.*, **2011**, 7(3): p. 136-155.

147.   Görög, S. and É. Csizér, Analysis of steroids. XVI. Spectrophotometric determination of gestagenic hormones in the 3,5:diene form. *Z. Anal. Chem.*, **1971**, 254(2): p. 119-121.

148.   Figueroa, R.A.; MacKay,A. A., Sorption of Oxytetracycline to Iron Oxides and Iron Oxide-Rich Soils. *Environ. Sci. Technol.*, **2005**, 39(17): p. 6664-6671.

149.   Scheytt, T.; Mersmann, P.; Lindstädt, R.; Heberer, T., Determination of sorption coefficients of pharmaceutically active substances carbamazepine, diclofenac, and ibuprofen, in sandy sediments. *Chemosphere*, **2005**, 60(2): p. 245-253.

150.   ter Laak, T.L., W.A. Gebbink, and J. Tolls, Estimation of soil sorption coefficients of veterinary pharmaceuticals from soil properties. *Environ. Toxicol. Chem.*, **2006**, 25(4): p. 933-941.

151.   Stein, K.; Ramil, M.; Fink, G.; Sander, M.; Ternes, T. A., Analysis and Sorption of Psychoactive Drugs onto Sediment. *Environ. Sci. Technol.*, **2008**, 42(17): p. 6415-6423.

152.   Wu, C.; Spongberg, A.L.; Witter, J. D., Sorption and biodegradation of selected antibiotics in biosolids. *J Environ. Sci. Heal. A*, **2009**, 44(5): p. 454-461.

153.   Xia, K.; Bhandari, A.; Das, K.; Pillar, G., Occurrence and Fate of Pharmaceuticals and Personal Care Products (PPCPs) in Biosolids. *J. Environ. Qual.*, **2005**, 34(1): p. 91-104.

154.   Yamamoto, H.; Nakamura, Y.; Moriguchi, S.; Nakamura, Y.; Honda, Y.; Tamura, I.; Hirata, Y.; Hayashi, A.; Sekizawa, J., Persistence and partitioning of eight selected pharmaceuticals in the aquatic environment: Laboratory photolysis, biodegradation, and sorption experiments. *Water Res.*, **2009**, 43(2): p. 351-362.

155.   Jain, A.; Raven, K. P.; Loeppert, R. H., Arsenite and Arsenate Adsorption on Ferrihydrite: Surface Charge Reduction and Net OH- Release Stoichiometry. *Environ. Sci. Technol.*, **1999**, 33(8): p. 1179-1184.

156.   Schindler, P.W.; Gamsjäger,H., Acid — base reactions of the TiO2 (Anatase) — water interface and the point of zero charge of TiO2 suspensions. *Kolloid. Z. Z. Polym.*, **1972**, 250(7): p. 759-763.

157.   Carrasquillo, A. J.; Bruland, G. L.; MacKay, A. A.; Vasudevan, D., Sorption of Ciprofloxacin and Oxytetracycline Zwitterions to Soils and Soil Minerals: Influence of Compound Structure. *Environ. Sci. Technol.*, **2008**, 42(20): p. 7634-7642.

158.   Gu, C.; Karthikeyan, K. G., Interaction of Tetracycline with Aluminum and Iron Hydrous Oxides. *Environ. Sci. Technol.*, **2005**, 39(8): p. 2660-2667.

159.   Tolls, J., Sorption of Veterinary Pharmaceuticals in Soils: A Review. *Environ. Sci. Technol.*, **2001**, 35(17): p. 3397-3406.

160.   Cornell, R.M. and Schwertmann, U., The iron oxides: Structure, Properties, Reactions, Occurences and Uses, 2nd edition, 2003, Weinheim: Wiley-VCH.

161.   Strawn, D.G., Scheidegger, A. M.; Sparks, D. L., Kinetics and Mechanisms of Pb(II) Sorption and Desorption at the Aluminum Oxide−Water Interface. *Environ. Sci. Technol.*, **1998**, 32(17): p. 2596-2601.

162.   Hering, J. G., Interaction of Organic Matter with Mineral Surfaces, in *Aquatic Chemistry,*1995, American Chemical Society. p. 95-110.

163.   Leenheer, J.A., Chemistry of Dissolved Organic Matter in Rivers, Lakes, and Reservoirs, in Environmental Chemistry of Lakes and Reservoirs, 1994, American Chemical Society. p. 195-221.

164.   Shon, H. K.; Vigneswaran, S.; Snyder, S. A., Effluent Organic Matter (EfOM) in Wastewater: Constituents, Effects, and Treatment. Critical Reviews in *Environ. Sci. Technol.*, **2006**, 36(4): p. 327 - 374.

165.   Hari, A.C.; Paruchuri, R. A.; Sabatini, D. A.; Kibbey, T. C. G., Effects of pH and Cationic and Nonionic Surfactants on the Adsorption of Pharmaceuticals to a Natural Aquifer Material. *Environ. Sci. Technol.*, **2005**, 39(8): p. 2592-2598.

166.   Kibbey, T. C.; Paruchuri, R.; Sabatini, D. A.; Chen, L., Adsorption of Beta Blockers to Environmental Surfaces. *Environ. Sci. Technol.*, **2007**, 41(15): p. 5349-5356.

167.   Drewes, J. E.; Heberer, T.; Reddersen, K., Fate of pharmaceuticals during indirect potable reuse. *Water Sci. Technol.*, **2002**, 46(3): p. 73-80.

168.   Yu, J. T.; Bouwer, E. J.; Coelhan, M., Occurrence and biodegradability studies of selected pharmaceuticals and personal care products in sewage effluent. *Agr. Water Manage.*, **2006**, 86(1-2): p. 72-80.

169.   Philip, J.; Holcomb, I. J.; Fusari, S. A., Phenytoin, in *Analytical Profiles of Drug Substances*, F. Klaus, Editor 1984, Academic Press. p. 417-445.

170.   SCR PhysProp Database., 2009. Interactive physProp database demo. Available from: <http://www.srcinc.com/what-we-do/databaseforms.aspx?id=386>. Accessed March 26, 2011.

171.   Westerhoff, P.; Yoon, Y.; Snyder, S.; Wert, E., Fate of Endocrine-Disruptor, Pharmaceutical, and Personal Care Product Chemicals during Simulated Drinking Water Treatment Processes. *Environ. Sci. Technol.*, **2005**, 39(17): p. 6649-6663.

172. Anschutz, A. and Penn, R. L., Reduction of crystalline iron(III) oxyhydroxides using hydroquinone: Influence of phase and particle size. *Geochem. T.*, **2005**, 6(3): p. 60.

173. Hunter, R.J., Zeta potential in colloid science, 1981, London: Principles and ApplicationsAcademic Press.

174. Patil, K. M.; Bodhankar, S. L., Simultaneous determination of lamotrigine, phenobarbitone, carbamazepine and phenytoin in human serum by high-performance liquid chromatography. *J. Pharmaceut. Biomed.*, **2005**, 39(1–2): p. 181-186.

175. Zhu, L.; Chen, B., Interactions of Organic Contaminants with Mineral-Adsorbed Surfactants. *Environ. Sci. Technol.*, **2003**, 37(17): p. 4001-4006.